BINDING SERVICES
Tel +44 (0)29 2087 4949
Fax +44 (0)29 20371921
e-mail bindery@cardiff.ac.uk

Aspects of structural and functional assessment in open angle glaucoma

Ioanna Bourtsoukli

Doctor of Philosophy

School of Optometry and Vision Sciences

Cardiff University

2005

ProQuest LLC
789 East Eisenhower Parkway
P.O. Box 1346
Ann Arbor, MI 48106-1346

Acknowledgements

I would like to express my graditute to my supervisor, Prof John Wild for giving me the opportunity to work with him and for the inspiration of this thesis.

I am grateful to Mr James Morgan, Dr Gavin Powel, Dr Nick Sheen, Dr Adrian Jones and Dr Linda Kim; Mr Ejaz Ansari, Mr RajKumar and Mr Ian Cunliffe for their contribution to the research presented in this thesis; the staff at School of Optometry and Vision Sciences at Cardiff University for teaching and supporting me.

My heartfelt thanks to Dr Henning Tonsgaard for his guidance, optimism and constant support .

Special thanks to Miss Irene Passisi, Mrs Ping Ji and Mr Cameron Hudson for the friendship we established during my stay in Cardiff.

I wish to extend a very special note of appreciation to my dear friends, Miss Eleni Kotsomiti, Miss Irini Moutafi, Miss Goules Kotsomiti, Miss Kiriaki Georgopoulou, Miss Alexandra Kotsomiti, and Miss Ageliki Tjumi, for always believing in me.

I am indebted to my family for their moral and financial support throughout the years of my study.

Cardiff University

Aspects of structural and functional assessment in open angle glaucoma

Ioanna Bourtsoukli

Doctor of Philosophy

2005

Summary

Early detection of glaucoma is a prerequisite for effective management of the disease. The study was concerned with aspects of structural and functional assessment in open angle glaucoma. The major part of the study was concerned with the utilization of digital stereoscopic imaging of the optic nerve head in the detection of open angle glaucoma (OAG). Specifically, it addressed possible sources of variability that confound the diagnosis of glaucoma and are associated with the monoscopic, as opposed to stereoscopic, observation of the optic nerve head (ONH); the limited diagnostic value of the features of the peripapillary retina accompanying glaucomatous damage; and the between-observer variation in the subjective evaluation of the ONH. The study utilised a dataset of magnification corrected digital images from 51 normal individuals and from 113 patients with OAG. Misdiagnosis of glaucoma was associated with discrepancies in the evaluation of the rim area due to the monoscopic presentation of the ONH masking the presence of focal rim loss, otherwise evident with stereoscopic observation. The frequency and patterns of distribution of the alpha and beta peripapillary atrophy (PPA) were confirmed among normal and glaucomatous eyes but meaningful conclusions on the diagnostic value of PPA were hindered by the clinically broad criteria of this feature. Regression analysis of the global and sectorial rim areas for the discrimination of glaucomatous damage compared favourably with the subjective glaucoma diagnosis by expert observers.

The remaining part of the study was concerned with the evaluation of the Total and Pattern Deviation probability analysis in short-wavelength perimetry (SWAP). The material comprised the Humphrey Field Analyzer single field print-outs from standard automated perimetry (SAP) and from SWAP of 53 normal individuals; 18 patients with cataract, 22 with OHT and 55 with OAG. Focal visual field loss derived by SWAP was markedly less compared to SWAP indicating wider limits of normality for SWAP. Considerable caution should be exercised before the use of SWAP.

Contents

Chapter 1. Introduction **1**

1.1 Overview of the retinal structure 1

1.1.1 The retinal ganglion cells 3

1.1.2 The main neurotransmitters of the sensory and neural part of the retina 4

1.1.3 Glial cells 5

1.2 The inner retinal structure 10

1.2.1 The normal retinal nerve fibre layer 10

1.2.2 The crossing of the nerve fibres through the optic nerve head 12

1.2.3 The optic nerve 20

1.2.4 The ocular blood supply of the ONH and the retina 21

1.2.5 Physiologic peripapillary atrophy 34

1.2.6. Ageing of the retina 37

1.3 Glaucoma 40

1.3.1 Apoptotic pathways 40

1.3.2 Evidence of glaucomatous apoptotic death 42

1.3.3 Pathophysiology of glaucoma 44

1.3.4 Ocular hypertension as a risk factor for glaucoma 46

1.3.5 Normal tension glaucoma 47

1.3.6 Management of IOP levels in glaucoma patients. 48

1.4 The involvement of the retinal vasculature 49

1.4.1 The association of IOP and retrobulbar blood flow in glaucoma 49

1.4.2 Signs of vascular deficiency in glaucoma 50

1.5 The vascular theory 52

1.5.1 Ischaemic insults 52

1.5.2 Endothelium imbalance 52

1.5.3 Secondary degeneration 54

1.5.4 Excitotoxicity 54

1.5.5 Oxidative stress 55

1.5.6 Spreading depression 57

1.5.7 Genetic factors 58

1.5.8 Family history 58

1.6 Genes related to glaucoma 59

1.6.1 Stimulation of genes expression 60

1.6.2 Racial distribution of glaucomatous phenotypes 61

1.7 Structural changes in glaucoma 62

1.7.1 Degeneration of the nerve fibres 62

1.7.2 Neuroretinal rim loss: patterns of thinning 63

1.7.3 Glaucomatous cupping 65

1.7.4 Remodelling of the lamina cribrosa 65

1.7.5 Disc size as a factor for glaucomatous damage 66

1.7.6 The retinal vessels in glaucoma 67

1.7.7 Peripapillary atrophy 73

1.8 Neuroprotection 76

1.8.1 The debate of selective ganglion cell death in glaucoma 77

1.8.2 Are the surviving cells functional? 79

1.9 Perimetry 80

1.9.1 Stimulus intensity 80

1.9.2 Threshold light sensitivity 81

1.9.3 Threshold measurement programs 81

1.9.4 Humphrey STATPAC analysis package 83

1.9.5 The effect of stimulus size in the variability of threshold measurements 84

1.9.6 Visual field loss in glaucoma 85

1.9.7 Limitations of perimetry 85

1.10 Imaging 86

1.10.1 Fundus photography 86

1.10.2 Red free photography 87

1.10.3 Stereophotography 87

1.10.4 Confocal scanning laser topography 88

1.10.5 Optical coherence topography 95

1.10.6 Scanning laser polarimetry 97

1.10.7 Evaluation of the methods 98

Chapter 2. Rationale for research 100

2.1 Clinical evaluation of the threshold response in Short-Wavelength Automated Perimetry 100

2.2 The comparison of monoscopic and stereoscopic computer assisted planimetry in the evaluation of the normal and glaucomatous optic nerve head 103

2.3 Clinical evaluation of peripapillary atrophy in normal and glaucomatous eyes 106

2.4 Quantitative analysis of the neuroretinal rim for the discrimination of normal and glaucomatous discs 107

2.5 Logistics 109

Chapter 3. Clinical evaluation of the threshold response in Short-Wavelength Automated Perimetry **112**

3.1 Selective ganglion cell loss in glaucoma 112

3.2 Principles of SWAP testing 114

3.3 Swap in early detection of glaucoma 116

3.4 Sources of variability in light sensitivity with SWAP 117

3.5 Confidence limits for normality 118

3.6 Media opacities 118

3.7 Short-term fluctuation 120

3.8 Long-Term fluctuation 121

3.9 Fatigue effects 123

3.10 Determination of abnormality with SWAP 124

3.11 Aims of study 126

3.12 Methods 127

3.13 Examination Protocol 129

3.14 Analysis 131

3.15 Results 135

3.15.1 Within visits and between algorithm 135

3.15.2 Between visits within algorithm 152

3.16 Discussion 170

3.17 Limitations 175

3.18 Conclusion 178

Chapter 4. General Methodology **179**

4.1 Subjects characteristics 179

4.2 Examination protocol 180

4.3 Equipment 183

4.3.1 Digital stereoscopic planimetry system 183

4.3.2 Software features and functions 186

4.4 Planimetry 187

4.4.1 Stereoscopic image presentation 189

4.4.2 Monoscopic image presentation 190

4.4.3 Training module 191

4.5 Pilot studies for software accuracy and reproducibility testing 191

4.5.1 Reliability of planimetric estimates 192

4.5.2 Quantitative assessment of Peripapillary atrophy 193

4.6 Study cohorts 194

4.6.1 Subject classification procedure 194

4.6.2 Outcome of the final classification process 195

4.6.3 Demographics 196

4.7 Experimental design 197

4.7.1 The selection of images 197

4.7.2 Appointed observers 198

4.7.3 Observation consensus 199

4.7.4 Observation task 200

4.7.5 Training module 201

4.7.6 Assessments in stereo and mono 204

4.7.7 Time frame for observation 205

Chapter 5. The comparison of monoscopic and stereoscopic computer assisted planimetry in the evaluation of the normal and glaucomatous optic nerve head 206

5.1 Introduction 206

5.1.1 Comparison of stereoscopic and monoscopic imaging evaluations 208

5.1.2 Cameras of sequential and simultaneous image capture. 209

5.1.3 Stereo viewing systems 212

5.1.4 Interobserver variability in the assessment of stereo photography 214

5.2 Aims of study 219

5.3 Methods 219

5.3.1 Training sessions 221

5.3.2 Experimental procedure. 222

5.4 Results 223

5.4.1 Questionnaire data 224

5.4.2 Assessment times 230

5.4.3 Planimetry 232

5.4.4 Interobserver agreement 233

5.4.5 Glaucoma diagnosis 234

5.5 Discussion. 243

5.5.1 Planimetry measurements 243

5.5.2 Interobserver agreement 245

5.5.3 Glaucoma diagnosis 246

5.5.4 Possible limitations 248

5.6 Conclusion 250

Chapter 6. Clinical evaluation of peripapillary atrophy in normal and glaucomatous eyes 252

6.1 Peripapillary atrophy 252

6.2 Occurrence of PPA in normal and glaucomatous eyes 252

6.3 Speculations on the glaucomatous aetiology of PPA 253

6.4 Clinical observation of PPA in the course of glaucomatous damage 256

6.5 Distribution and quantification of PPA 257

6.6 Interobserver agreement for the evaluation of PPA 259

6.7 Correlation of PPA with other anatomical features in glaucomatous eyes 260

6.8 Peripapillary atrophy and visual field loss 260

6.9 Aims of study 261

6.10 Methodology 261

6.11 Results 265

6.11.1 Frequency of PPA 266

6.11.2 Quantification of PPA 268

6.11.3 Interobserver agreement 269

6.11.4 Distribution of PPA 270

6.11.5 Correlations of PPA with intrapapillary features 274

6.11.6 Association of PPA with the visual field indices 277

6.12 Discussion 282

6.12.1 PPA quantification and distribution 282

6.12.2 Association of PPA with the disc area 283

6.12.3 Association of PPA with the rim area 284

6.12.4 Association of PPA with the visual field loss 284

6.12.5 Interobserver agreement in the assessment of PPA 285

6.12.6 Possible limitations 286

6.13 Conclusions 288

Chapter 7. Quantitative analysis of the neuroretinal rim for the discrimination of normal and glaucomatous discs **289**

7.1 Introduction 289

7.1.1 The neuroretinal rim area 289

7.1.2 The ISNT rule 291

7.1.3 Glaucomatous rim loss 292

7.1.4 The neuroretinal rim measurement in glaucoma diagnosis 293

7.2 Aims of study 298

7.3 Methods 298

7.3.1 Quantitative analysis of the neuroretinal rim 299

7.3.2 Investigation of the diagnostic value of the ISNT rule 302

7.4 Results 303

7.4.1 Quantitative analysis of the neuroretinal rim 305

7.4.2 Global rim area quantitative analysis 308

7.4.3 Sectorial rim area quantitative analysis 312

7.4.4 Rim configuration 319

7.4.5 Evaluation of the disc shape 322

7.4.6 Quantification of the ISNT rule 323

7.5 Discussion 326

7.5.1 Quantification of the rim area 326

7.5.2 Diagnostic value of the global and sectorial rim analysis 327

7.5.3 Patterns of focal and diffuse glaucomatous rim loss 328

7.5.4 Possible limitations for the quantification of the rim area 329

7.5.5 The diagnostic value of the rim configuration 331

7.5.6 Possible limitations for the quantification of the sectorial rim width 332

7.6 Conclusion 334

Chapter 8 General conclusions and proposals for future work 336

8.1 General conclusions 336

8.1.1 Clinical evaluation of threshold response in Short-Wavelength Automated Perimetry 336

8.1.2 Comparison of monoscopic and stereoscopic computer assisted planimetry in the evaluation of the normal and glaucomatous optic nerve head 336

8.1.3 Clinical evaluation of peripapillary atrophy in normal and glaucomatous eyes 337

8.1.4 Quantitative analysis of the neuroretinal rim or the discrimination of normal and glaucomatous discs 338

8.2 Proposals for future work 338

8.2.1 Normative database of optic disc stereophotographs 338

8.2.2 Planimetry of retinal vessels for investigation of glaucomatous changes 339

8.2.3 Detection of glaucomatous progression with stereo chronoscopy and chronometry 340

Appendix I 341

Abstracts 372

References 374

Figures

1.1	A micrograph of the human retina in cross section	1
1.2	The "double hump" configuration of the RNFL at the ONH	12
1.3	Distribution of blood vessels on surface of the optic disc	21
1.4	Increased IOP and decreased OBF	49
3.1	The target presentation pattern with Program 30-2 and Program 24-2 respectively	132
4.1.	Z-screen monitor; The liquid crystal overly plate is mounted on a 21" high resolution monitor. The polarised glasses can be seen. Electronics for the control of the Z screen are mounted in the screen bezel.	184
4.2	Arrangement of the 72 sectors for R and L eye respectively	188
5.1	The subjective grading of the photographic quality of the images for the normal group by all three observers under stereoscopic examination.	226
5.2	The subjective grading of the photographic quality of the images for the glaucoma group by all three observers under stereoscopic examination	226
5.3	The subjective grading of the photographic quality of the images for the normal group by all three observers under monoscopic examination	227
5.4	The subjective grading of the photographic quality of the images for the glaucoma group by all three observers under monoscopic examination	227
5.4	The subjective grading of the assessment of the images for the normal group by all three observers under stereoscopic examination	228
5.6	The subjective grading of the assessment of the images for the glaucoma group by all three observers under stereoscopic examination	228
5.7	The subjective grading of the assessment of the images for the normal group by all three observers under monoscopic examination	229

5.8 The subjective grading of the assessment of the images for the glaucoma group by all three observers under monoscopic examination 229

5.9 The group mean disc and rim area measurements derived stereoscopically and monoscopically for 3 groups of glaucoma patients that were misdiagnosed with the monoscopic or the stereoscopic or by both methods, respectively, by each of the three observers 236

5.10 The optic disc appearance and the visual field probability analysis plots for a glaucoma patient that was misdiagnosed by all three observers under monoscopic examination. The black arrowhead indicates an inferior- nasal rim notch 238

5.11 The optic disc appearance and the visual field probability analysis plots for the L eye of a glaucoma patient that was misdiagnosed by all three observes under monoscopic examination. The black arrowhead indicates a superior-temporal rim notch 239

5.12 The group mean disc and rim area measurements derived stereoscopically and monoscopically for 3 groups of glaucoma patients with both optic disc damage and visual field defects that were misdiagnosed with the monoscopic or the stereoscopic or by both methods, respectively, by each of the three observers 242

6.1 The software interface and an example of an image that has been planimetrically assessed. 261

6.2 Computer display of a normal and a glaucomatous eye featuring PPA areas before and after they were planimetrically analysed by one of the observers 267

6.3 Graphical illustration of the distribution of the normal mean group sum of PPA area(mm^2), zone Alpha, as defined by the three observers 270

6.4 Graphical illustration of the distribution of the normal mean group sum of PPA area (mm^2), zone Beta, as defined by the three observers 271

6.5 Graphical illustration of the distribution of the glaucoma mean group sum of PPA area (mm^2), zone Alpha, as defined by the three observers 272

6.6 Graphical illustration of the distribution of the glaucoma mean group sum of PPA area (mm^2), zone Beta, as defined by the three observers 273

6.7 The distribution of the mean total rim area; Alpha and Beta PPA areas (mm^2) for the normal group, as averaged for the three observers across the 72 sectors around the ONH 274

6.8 The distribution of the mean total rim area; Alpha and Beta PPA areas (mm^2) for the glaucoma group, as averaged for the three observers across the 72 sectors around the ONH 274

6.9 Scatterplot of the mean total Alpha zone PPA area (mm^2) normalised for the global disc area (mm^2) within each eye and averaged across the three observers, against the MD indices across the normal group 277

6.10 Scatterplot of the mean total Beta zone PPA area (mm^2) normalised for the global disc area (mm^2) within each eye and averaged across the three observers, plotted against the MD indices across the normal group 278

6.11 Scatterplot of the mean total Alpha zone PPA area (mm^2) normalised for the global disc area (mm^2) within each eye and averaged across the three observers, against the PSD indices across the normal group 278

6.12 Scatterplot of the mean total Beta zone PPA area (mm^2) normalised for the global disc area (mm^2) within each eye and averaged across the three observers, against the PSD indices across the normal group 279

6.13 Scatterplot of the mean total Alpha zone PPA area (mm^2) normalised for the global disc area (mm^2) within each eye and averaged across the three observers, against the MD indices across the glaucoma group 280

6.14 Scatterplot of the mean total Beta zone PPA area (mm^2) normalised for the global disc area (mm^2) within each eye and averaged across the three observers, against the MD indices across the glaucoma group 280

6.15 Scatterplot of the mean total Alpha zone PPA area (mm^2) normalised for the global disc area (mm^2) within each eye and averaged across the three observers, against the PSD indices across the glaucoma group 281

6.16 Scatterplot of the mean total Beta zone PPA area (mm^2) normalised for the global disc area (mm^2) within each eye and averaged across the three observers, against the PSD indices across the glaucoma group 281

7.1 Scatterplot of the rim area values (mm^2) against the disc area (mm^2) values, as measured by observer 1 across the normal group 305

7.2 Scatterplot of the rim area values (mm^2) against the disc area (mm^2) values, as measured by observer2 across the normal group. 306

7.3 Scatterplot of the rim area values (mm^2) against the disc area (mm^2) values, as measured by observer3 across the normal group 307

7.4 Regression analysis of the rim area values (mm^2) against the disc area (mm^2) values, as measured by observer 1, across the normal group and glaucoma group 308

7.5 Regression analysis of the rim area values (mm^2) against the disc area (mm^2) values, as measured by observer 2 across the normal group and the glaucoma group 309

7.6 Regression analysis of the rim area values (mm^2) against the disc area (mm^2) values, as measured by observer 3 across the normal group and the glaucoma group 310

7.7 Frequency of the optic nerve sectors classed as abnormal for the perimetric glaucoma group 314

7.8 Frequency of the optic nerve sectors classed as abnormal for the preperimetric glaucoma group 315

7.9 The distribution of the group mean rim area across 12 sectors for the normal group and the total glaucoma group 320

7.10 The distribution of the group mean rim area across 12 sectors for the group of preperimetric glaucoma patients and the group of glaucoma patients with detectable visual field loss 321

7.11 Optic disc photographs showing the segments used to define the 10 and 30 degrees sectors for comparison of the Inferior (I), Superior (S), Nasal (N) and Temporal (T) sectors. 323

Tables

3.1 The numerical values that were utilised to represent the TD and PD probability percentages for the purpose of data analysis. 134

3.2 The group total number of tested locations matched to the TD probability scores with W-W perimetry and SWAP across all the normal subjects, at the second visit (visit 2). 136

3.3 The group total number of tested locations of the upper and lower field matched to the TD probability scores with W-W perimetry and SWAP, across all the normal subjects, at the second visit (visit 2). 136

3.4 The group total number of tested locations of the central and peripheral field matched to the TD probability scores with W-W perimetry and SWAP, across all the normal subjects, at the second visit (visit 2). 137

3.5 The group total number of tested locations matched to the PD probability scores with W-W perimetry and SWAP across all the normal subjects, at the second visit (visit 2). 138

3.6 The group total number of tested locations of the upper and lower field matched to the PD probability scores with W-W perimetry and SWAP, across all the normal subjects, at the second visit (visit 2). 138

3.7 The group total number of tested locations of the central and peripheral field matched to the PD probability scores with W-W perimetry and SWAP, across all the normal subjects, at the second visit (visit 2). 139

3.8 The group total number of tested locations matched to the TD probability scores with W-W perimetry and SWAP across all glaucoma patients at the second visit (visit 2). 140

3.9 The group total number of tested locations of the upper and lower matched to the TD probability scores with W-W perimetry and SWAP, across all glaucoma patients at the second visit (visit 2). 140

3.10 The group total number of tested locations of the central and peripheral field matched to the TD probability scores with W-W perimetry and SWAP, across all glaucoma patients at the second visit (visit 2). 141

3.11 The group total number of tested locations matched to the PD probability scores with W-W perimetry and SWAP across all glaucoma patients at the second visit (visit 2). 142

3.12 The group total number of tested locations of the upper and lower matched to the PD probability scores with W-W perimetry and SWAP, across all glaucoma patients at the second visit (visit 2). 142

3.13 The group total number of tested locations of the central and peripheral field matched to the PD probability scores with W-W perimetry and SWAP, across all glaucoma patients at the second visit (visit 2). 143

3.14 The group total number of tested locations matched to the TD probability scores with W-W perimetry and SWAP across all OHT patients at the second visit (visit 2). 144

3.15 The group total number of tested locations of the upper and lower field matched to the TD probability scores with W-W perimetry and SWAP, across all OHT patients at the second visit (visit 2). 144

3.16 The group total number of tested locations of the central and peripheral field matched to the TD probability scores with W-W perimetry and SWAP, across all OHT patients at the second visit (visit 2). 145

3.17 The group total number of tested locations matched to the PD probability scores with W-W perimetry and SWAP across all OHT patients at the second visit (visit 2). 146

3.18 The group total number of tested locations of the upper and lower field matched to the PD probability scores with W-W perimetry and SWAP, across all OHT patients at the second visit (visit 2). 146

3.19 The group total number of tested locations of the central and peripheral field matched to the PD probability scores with W-W perimetry and SWAP, across all OHT patients, at the second visit (visit 2). 147

3.20 The group total number of tested locations matched to the TD probability scores with W-W perimetry and SWAP, across all patients with cataract at the second visit (visit 2). 148

3.21 The group total number of tested locations of the upper and lower matched to the TD probability scores with W-W perimetry and SWAP, across all patients with cataract at the second visit (visit 2). 149

3.22 The group total number of tested locations of the central and peripheral field matched to the TD probability scores with W-W perimetry and SWAP, across all patients with cataract at the second visit (visit 2). 149

3.23 The group total number of tested locations matched to the PD probability scores with W-W perimetry and SWAP across all patients with cataract, at the second visit (visit 2). 150

3.24 The group total number of tested locations of the upper and lower field matched to the PD probability scores with W-W perimetry and SWAP, across all patients with cataract, at the second visit (visit 2). 151

3.25 The group total number of tested locations of the central and peripheral field matched to the PD probability scores with W-W perimetry and SWAP, across all patients with cataract, at the second visit (visit 2). 151

3.26 The group total number of tested locations matched to the TD probability scores with W-W perimetry at visit 2 and visit 3 respectively across all normal subjects. 152

3.27 The group total number of tested locations of the upper and lower field matched to the TD probability scores with W-W perimetry at visit 2 and visit 3 respectively, across all normal subjects. 153

3.28 The group total number of tested locations of the central and peripheral field matched to the TD probability scores with W-W perimetry scored at visit 2 and visit 3 respectively, across all normal subjects. 153

3.29 The group total number of tested locations matched to the TD probability scores with SWAP at visit 2 and visit 3 respectively, across all normal subjects. 154

3.30 The group total number of tested locations of the upper and lower field matched to the probability scores with SWAP at visit 2 and visit 3 respectively, across all normal subjects. 155

3.31 The group total number of tested locations of the central and peripheral field matched to the TD probability scores with SWAP at visit 2 and visit 3 respectively, across all normal subjects. 155

3.32 The group total number of tested locations matched to the PD probability scores at visit 2 and visit 3 respectively, with W-W perimetry across all normal subjects. 156

3.33 The group total number of tested locations of the upper and lower field matched to the PD probability scores with W-W perimetry at visit 2 and visit 3 respectively, across all normal subjects. 157

3.34 The group total number of tested locations of the central and peripheral field matched to the PD probability scores with W-W perimetry at visit 2 and visit 3 respectively, across all normal subjects. 158

3.35 The group total number of tested locations matched to the PD probability scores with SWAP at visit 2 and visit 3 respectively, across all normal subjects. 159

3.36 The group total number of tested locations of the upper and lower field matched to the PD probability scores with SWAP at visit 2 and visit 3 respectively, across all normal subjects. 159

3.37 The group total number of tested locations of the central and peripheral field matched to the PD probability scores with SWAP at visit 2 and visit 3 respectively, across all normal subjects. 160

3.38 The group total number of tested locations matched to the TD probability scores with W-W perimetry at visit 2 and visit 3 respectively, across all glaucoma patients. 161

3.39 The group total number of tested locations of the upper and lower field matched to the TD probability scores with W-W perimetry at visit 2 and visit 3 respectively, across all glaucoma patients. 161

3.40 The group total number of tested locations of the central and peripheral field matched to the TD probability scores with W-W perimetry at visit 2 and visit 3 respectively, across all glaucoma patients. 162

3.41 The group total number of tested locations matched to the TD probability scores with SWAP at visit 2 and visit 3 respectively across all glaucoma patients. 163

3.42 The group total number of tested locations of the upper and lower field matched to the TD probability scores with SWAP at visit 2 and visit 3 respectively, across all glaucoma patients. 163

3.43 The group total number of tested locations of the central and peripheral field matched to the TD probability scores with SWAP at visit 2 and visit 3 respectively, across all glaucoma patients. 164

3.44 The group total number of tested locations matched to the PD probability scores with W-W perimetry at visit 2 and visit 3 respectively across all glaucoma patients. 165

3.45 The group total number of tested locations of the upper and lower field matched to the PD probability scores with W-W perimetry at visit 2 and visit 3 respectively, across all glaucoma patients. 165

3.46 The group total number of tested locations of the central and peripheral field matched to the PD probability scores with W-W perimetry at visit 2 and visit 3 respectively, across all glaucoma patients. 166

3.47 The group total number of tested locations matched to the PD probability scores with SWAP at visit 2 and visit 3 respectively across all glaucoma patients. 167

3.48 The group total number of tested locations of the upper and lower field matched to the PD probability scores with SWAP at visit 2 and visit 3 respectively, across all glaucoma patients. 167

3.49 The group total number of tested locations of the central and peripheral field matched to the PD probability scores with SWAP at visit 2 and visit 3 respectively, across all glaucoma patients. 168

3.50 The between -algorithm, within visit differences across all study groups for W-W perimetry and SWAP. Each cell shows the mean number of abnormal points with W-W perimetry over the mean number of abnormal points with SWAP. 169

3.51 The between visit differences across all study groups for W-W perimetry. Each cell shows the mean number of abnormal point with visit 2 over the mean number of abnormal points with visit 3. 169

3.52 The between visit differences across all study groups for SWAP. Each cell shows the mean number of abnormal point with visit 2 over the mean number of abnormal points with visit 3. 170

3.53 The calculated ratio of the mean number of abnormal locations across the TD and PD maps for the normal group for W-W perimetry over the corresponding mean number of abnormal locations across the TD and PD maps for SWAP. 170

3.54 The ratio of the mean number of abnormal locations across the TD and PD maps for the normal group at visit 2 over visit 3, for W-W perimetry and SWAP respectively. 171

3.55 The ratio of the mean number of abnormal locations across the TD and PD maps for the glaucoma group for W-W perimetry over SWAP. 173

3.56 The ratio of the mean number of abnormal locations across the TD and PD maps for the glaucoma group at visit 2 over visit 3, for W-W perimetry and SWAP respectively. 173

3.57 The ratio of the mean number of abnormal locations across the TD and PD maps for the group of OHT patients for W-W perimetry over SWAP. 174

3.58 The ratio of the mean number of abnormal locations across the TD and PD maps across the group of cataract patients for W-W perimetry over SWAP. 175

4.1 The group mean and SD of certain biometric characteristics of the normal individuals 196

4.2 The group mean and SD of certain biometric characteristics of the OAG patients 197

4.3 The diagnosis of the glaucoma study group according to their visual field tests. The severity of visual field loss has been graded according with the Hodapp classification as modified by Litwak 197

4.4 The results of the TNO stereopsis test for all the observers, Including the expert ophthalmologist that was the primary observer for the dataset 199

4.5 The images of the training set given random ID numbers were presented stereoscopically and in the same order to all three observers 203

4.6 The random order of presentation for the images comprising the training set, as they were presented to all three observers in stereoscopic and monoscopic viewing respectively. 204

4.7 The selection of images and presentation order of the images within each group. 205

5.1 The group mean values and standard deviations for age, refractive status, corneal curvature and visual field indices for the 51 normal individuals and the 113 patients with glaucoma included in the study 223

5.2 The quality of the stereoscopic presentation of the images as evaluated by each of the three observers and expressed as percentage of the total number of images 224

5.3 The evaluation of the photographic quality as perceived by each observer under the stereoscopic and monoscopic examinations. The numbers of images appointed each of the four levels of quality are expressed in percentages 225

5.4 The evaluation of the difficulty of assessment for each image, as perceived by each observer under the stereoscopic and monoscopic examinations. 225

5.5 The mean time of assessment expressed in seconds for the four time periods corresponding to the alternate stereoscopic and monoscopic sessions 230

5.6 The total mean time of assessment for the stereo and mono assessment for the normal and glaucoma group, expressed in seconds 230

5.7 The mean and SD of the disc, the rim and the cup area measurements for the normal eyes, derived by stereoscopic and by monoscopic viewing as a function of observer 232

5.8 The mean and SD of the disc, the rim and the cup area Measurements for the normal eyes, derived by stereoscopic and by monoscopic viewing as a function of observer 232

5.9 The interobserver agreement on the disc and rim measurements derived from the monoscopic assessment for the normal and glaucoma group, as estimated by ICC (two way mixed effects model, absolute agreement) 233

5.10 The interobserver agreement on the disc and rim measurements derived from the stereoscopic assessment for the normal and glaucoma group, as estimated by ICC (two way mixed effects model absolute agreement). 234

5.11 The scores of sensitivity and specificity achieved by each of the three observers during stereoscopic and monoscopic examination, respectively. 235

5.12 The diagnostic precision achieved by each of the three observers during the stereoscopic and monoscopic examinations respectively. 235

5.13 The biometrical information and visual field indices for the two cases of glaucoma patients that were misdiagnosed under monoscopic observation. 240

5.14 The mean disc and mean rim area of the discs illustrated in figures 1:2 that correspond to the two cases of glaucoma patients that were misdiagnosed under monoscopic observation as measured by all three observer within the stereoscopic and monoscopic sessions. 240

5.15 The classification of the glaucoma study group according to their visual field tests. The severity of visual field loss has been graded according with the Hodapp classification as modified by Litwak. 241

5.16 The scores of sensitivity and specificity achieved by each of the three observers during stereoscopic and monoscopic examination. 243

5.17 The diagnostic precision achieved by each of the three observers during the stereoscopic and monoscopic examinations. 243

6.1 Group mean values and 1 SD for the age, refractive error and the visual field indices across the two study groups 262

6.2 Group mean parameters describing the optic disc shape, as evaluated by the expert observer, across the normal and glaucoma groups 265

6.3 Proportion of normal and glaucomatous eyes across the two study groups 266

6.4 The sum of PPA described as Alpha (α), Beta (β), and total areas (mm^2) averaged across the two study groups for each of the three observers 268

6.5 Planimetry results for the two study groups averaged for the three observers 269

7.1 Summary of the mean age; refractive error; visual field indices and group mean stereoscopic planimetry results for the normal and glaucoma group 300

7.2 Description of the disc segmentation for the sectorial quantitative analysis of the rim area into 12 sectors subtending 30 degrees 300

7.3 Summary of the mean age; refractive error; visual field indices and group mean stereoscopic planimetry results for the two subgroups of glaucoma patients, with and without visual field loss 301

7.4 Diagnostic scores for the three expert observers based on their subjective assessments 304

7.5 Diagnostic precision according to the quantitative analysis of the global neuroretinal rim and disc areas 311

7.6 Correlation coefficient (R^2) of the regression analysis of the segmental neuroretinal rim and disc areas across the 12 sectors for the total normal and total glaucoma group 312

7.7 Diagnostic precision calculated according to the quantitative analysis of the segmental neuroretinal rim and disc areas for the normal, the total glaucoma group, and the group of preperimetric glaucoma patients across the 12 sectors of the optic nerve 316

7.8 Diagnostic precision calculated according to the quantitative analysis of the segmental neuroretinal rim and disc areas for the normal, the total and preperimetric glaucoma group 318

7.9 Classification of glaucomatous discs according to the type of neuroretinal rim loss (diffuse / focal) as defined by the segmental rim analysis for each observer 319

7.10 The results of the disc shape analysis across the normal group and the glaucoma subgroups 322

7.11 Diagnostic outcome for the detection of glaucoma based on the rule I>S>N>T for the Inferior (I), Superior (S), Nasal (N), Temporal (T) for 10 and 30 degrees segments 324

7.12 Diagnostic outcome for the detection of glaucoma based on the rule I>S for the Inferior (I), Superior (S) for 10 and 30 degrees segments 325

Chapter 1 Introduction

One area of current research in glaucoma is concerned with the recognition of the earliest retinal structural damage secondary to the ganglion cell axonal death. While the mechanisms of injury and ganglion cell death have become more understandable, the aetiology of the disease is speculative and the need for better management remains essential. Tracing the primary glaucomatous changes with advanced imaging and psychometric evaluation techniques contributes to the understanding of the disease and provides guidance for the most effective application of proposed neuroprotection strategies.

1.1 Overview of the retinal structure

The retina has an estimated thickness of ¼ mm and consists of three layers of cells interlaced by two layers containing the synaptic neuronal processes made between the axons and dendrites of these neighbouring cell layers (Figure 1) (Dowling, 1987).

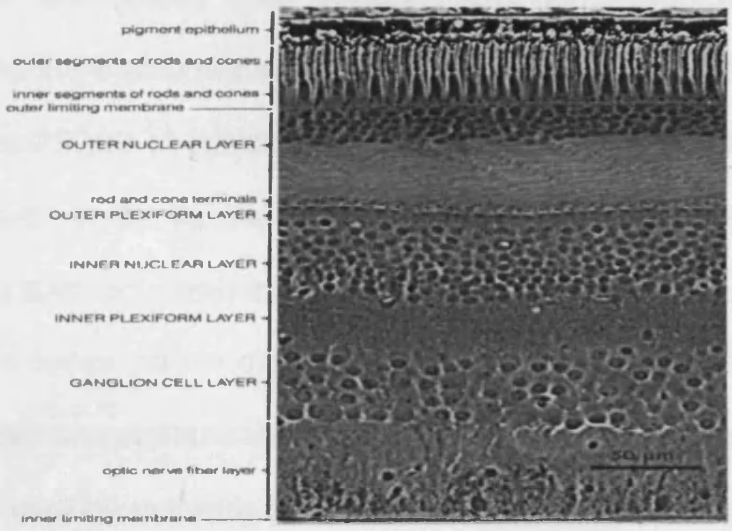

Figure 1. *A micrograph of the human retina in cross section (Dowling, 1987)*

The photoreceptors occupy the inner nuclear layer and a complex of bipolar horizontal and amacrine cells constitutes the outer nuclear layer. The synaptic processes between the rods and cones of one layer, with the bipolar and horizontal cells of the other layer, form, amongst them, the outer plexiform layer. Similarly, the bipolar cells together with the amacrine cells reach out with their dendrites to synapse with the ganglion cells' dendrites. The interconnections between the inner nuclear layer and the ganglion cells' layer compose the inner plexiform layer (Forrester, Dick *et al*, 1999; Ogden, 1994).

There are approximately 130.000,000 photoreceptors, including 6-7 million cones and rods that outnumber the cones 2:1 in the perifovea and reach a ratio of 30:1 outside the macula (Curcio, Sloan *et al*, 1990). The photoreceptors are located close to the outer retina, adjacent to the retinal pigment epithelium and its melanin-containing cells. The melanin molecules restore the light sensitive pigment of the photoreceptors when altered by the light absorption and absorb the excess light reaching the retina (Curcio, Millican *et al*, 2001). With a population ratio of 100:1 between the photoreceptors and ganglion cells axons, the visual stimuli is transferred across the retina from the layer of the stimulated photoreceptors to the ganglion cells' axons that form the nerve fibre layer. In the foveola the ganglion cells have a one-to-one relationship with the cones but in the periphery this relationship can be increased up to a ratio of 1:150 (Rodieck, 1998).

The nerve fibre layer as the most superficial layer of the neural retina is separated from the vitreous body by Müller cells that occupy the intracellular space and form the inner limiting membrane. Close to the nerve fibre bundles the large retinal blood

vessels are observed, being normally embedded within the nerve fibre layer (Hubel, 1988).

1.1.1 The retinal ganglion cells

There are 1 - 1.5 million ganglion cells in the retina assuming the highest concentration close to the fovea (35,000 cells/mm^2) and becoming more sparse in the periphery (250 cells/mm^2). Additionally, the ganglion cells in the fovea form seven layers but in the periphery they reduce to a single layer (Curcio & Allen, 1990). Currently, four types of ganglion cells have been identified in the retina: the midget, the parasol, the bistratified and the biplexiform ganglion cells. Among these types, the midget and the parasol ganglion cells are dominating the retina (Dacey & Petersen, 1992; De Lima Silveira, 2004; Kolb, Linberg *et al*, 1992; Rodieck, 1998).

Each type of ganglion cells has characteristic appearance in the retina and projects in specific parts of the lateral geniculate body that distinguish them into the parvo-cellular and magno-cellular portion. The midget ganglion cells have small bodies combined with thin axons and small dendritic fields and occupy predominately the fovea, comprising 70% of the total ganglion cell population (Curcio & Allen, 1990; De Lima Silveira, 2004). The midget ganglion cells have connections through the midget bipolar cells to the L- and M-cones. The parasol ganglion cells comprise 10% of the total ganglion cell population and have large bodies and thick axons connecting to the cones via the diffuse bipolar cells (Kolb *et al*, 1992). Conversely, the small bistratified ganglion cells have the same size of dendritic field as the parasol cells but they have thin axons and small bodies. They have a concentration of 400 cells/mm2 in the fovea but they can be very sparse in the periphery

(20cells/mm2) (Rodieck, 1998). Finally, the biplexiform ganglion cells are unique in the fact that they make direct connections to the photoreceptors (Mariani, 1982).

Astrocytic processes envelop the axons of every ganglion cell within the nerve fibre layer. Axons originating from neighbouring ganglion cells are put together in fibres with a diameter of, approximately 1μm and are finally arranged in bundles of fibres with a mean diameter of approximately 20 μm. Astrocytes cover and insulate the nerve fibres and a layer of tightly interconnected Müller cells encloses the bundles of fibres (Radius & Bade, 1981). Glial cells, namely astrocytes in combination with pericytes and microglia, are also seen to envelope the complex of retinal capillaries that are distributed in the same region, providing nourishment to the retinal ganglion cells.

1.1.2 The main neurotransmitters of the sensory and neural part of the retina

The neurotransmitter carrying the chemical signal from the photoreceptors to the bipolar cells and the ganglion cells is glutamate. All retinal cells may have neurotransmitter receptors and / or transporters on their membranes. One of the most common glutamate receptors is the NMDA ionergic receptor. Unless exposed to light, the photoreceptors constantly release glutamate that is attached to specialised receptors located on the membrane of the bipolar cells, allowing a variety of responses to different photoreceptors' input. For the same purpose, some of the bipolar cells may also carry inhibitory glutamate receptors.

Amacrine cells interact with bipolar and ganglion cells emitting the neurotransmitter y-aminobutyric acid (GABA) among a variety of other molecules that act as

neuromodulators within the inner plexiform plexus. Neuromodulators such as Nitric Oxide (NO) have been observed in the horizontal cells' interconnections at the inner nuclear layer and the inner plexiform layer. Interestingly, these factors are capable of influencing the neurons by diffusion and not only with the conventional way of interaction through synapses; therefore, they might exercise a rather widespread influence within the retinal circuitry.

Finally, Müller cells regulate synaptically released extracellular glutamate levels throughout the retina using specialised transporters (GLAST) that are exclusively localised on their membranes. They also regulate GABA release and remove k^+ from the synaptic surfaces within the neural retina (Marc, Jones *et al*, 2003). Overall, Muller cells provide the retinal neurons with direct metabolic support through the synthesis and storage of glycogen.

1.1.3 Glial cells

Several cell types, like the Müller cells, the microglia, the astrocytes and the pericytes are observed in the retinal layers, in close association with the ganglion cells and/ or the retinal vasculature. Müller cells have very close associations with the retinal neurons providing them with essential metabolic support through the production and storage of energy molecules. The processes of the Müller cells extend throughout most of the retinal layers. They are essential for the retinal homeostasis, removing ions and neurotransmitters that could upregulate the environment of the ganglion cells. Additionally they are seen to express neurotrophic factors such as brain-derived neurotrophic factors (BDNF), nerve growth factors (NGF) and glial-cell derived neurotrophic factors (GDNF) that on

demand, may replace the neuronal retrograde transport supply (Taylor, Srinivasan *et al*, 2003).

The glial cells that occupy the areas between the neural and vascular compartments of the retina form "glial limitans", which are composed of interconnecting astrocytes and microglia. This formation defines the outer margins of the perivascular space, which extends right after the endothelial lining of the vessels and usually includes the pericytes (Provis, 2001).

The parenchymal microglia and the vessel-associated microglia are the two categories of microglia cells observed in the retina. The parenchymal microglia are usually scattered in the retina, without known associations with the vasculature and lacking macrophage specialisation (Provis, Diaz *et al*, 1996). These cells are normally in a resting phase but are able to create antigens and also perform phagocytosis when subjected to appropriate stimulation. On the other hand, the microglia that are associated with the vessels bear macrophage markers and are particularly immunoresponsive. Besides immune surveillance and phagocytosis in the adult retina, it is proposed that during development of the retina microglia provide chemotactic guidance for the formation of the vessels of the vasculature.

In the developing human retina microglia are present in the nerve fibre layer, the ganglion cell layer, the inner plexiform layer and the outer plexiform layer (Diaz-Araya, Provis *et al*, 1995). In the adult retina the distribution and location of the microglia is not determined by the network of the blood vessels as suggested from

studies of the mammalian vascular retina compared to the avascular quail retina (Navascues, Moujahid *et al*, 1994).

Nerve degeneration, inflammation and / or trauma in the retina activate the microglia to initiate tissue defence mechanisms and even facilitate a regenerative process through production of microglia-suppressing factors (Thanos, Mey *et al*, 1993). Among their functions, the microglia also identify and remove injured or dying neurones. For this purpose, they may be redistributed within the retinal layers, accordingly. Both activated and not activated microglia express 'inducible Nitric Oxide Synthase' (iNOS), an enzyme that synthesises NO. The toxic effects of this molecule are useful for the macrophage activities of the microglia and may also act as a mediator for changes in the blood supply and neural activity. Microglia are known to secrete cytokines like tumour necrosis factor a (TNFa), through which they are mainly signalling other glial cells mainly for the purpose of maintaining their interconnections within the glial limitans. Cytokines also enable activated microglia in areas with retinal injury to attract other microglia for an effective widespread inflammatory response as well as to modulate the function of the neurones accordingly.

Finally, microglia are shown to be capable of producing enzymatic proteins closely associated with the lysosomes, the cathepsins. The lysosomes are the organelles acting as metabolic factories within the cells, therefore it is suspected that through the secretion of cathepsins, the microglia are co-operating with the RPE cells in maintaining a vital environment in the retina. Some cathepsins are also directly

associated with apoptosis through either direct or indirect pathways (Koike, Shibata *et al*, 2003).

Astrocytes are strongly associated with the vascularised retina. During development of the retinal vasculature, astrocytes control the expansion of the vessels, secreting vascular endothelial growth factor (VEGF). They divide and migrate across the retina depicting a pathway for the expansion of the vasculature (Sandercoe, Madigan *et al*, 1999). In the mature retina, astrocytes are known to provide very important structural support to the vessels. Degeneration of the astrocytes leads to overproduction of VEGF and detectable breaks in the glial limitans of the retinal arteries and veins. As expected, these sites of vascular degradation clinically correlate with sites of localised dilation of the vessels and incidence of leakage (Zhang & Stone, 1997).

Receptors in the membranes of the astrocytes act as sensors for environmental stimuli such as pressure and activate intracellular pathways that lead to changes in the morphology of the astrocytes, encourage their migration and proliferation and cause differential gene expression (Ledoux, Shen *et al*, 1998). With such activation, astrocytes are changed from polygonal to spindle shaped and may reallocate themselves within the retina. The migration activity of the astrocytes have been observed in the laboratory setting, where astocytic cells migrated as single cells repopulating a cell free area within the cell culture (Salvador-Silva, Aoi *et al*, 2004). Like microglia, astrocytes also express cytokines. They produce growth factors like the brain derived neurotrophic factor (BDNF) essential for the neurones and provide constant support to the endothelial vascular cells with VECF.

Experiments with cultures of animal brain neurons and astrocytes have demonstrated the ability of astrocytes to counteract the damage on neurons from reactive oxygen and nitrogen species. Activation of the NMDA receptors produces NO which reacts with O ions and further binds with proteins. As previously described, NO is a signalling molecule acting as a neurotransmitter and vasodilator, diffusing freely through cell membranes. The astrocytes scavenge NO and thereby protect the neurons from NMDA neurotoxicity through the glutathione system (Chen, Vartiainen *et al*, 2001). In fact, glutathione reacts with NO and it safely disposes in that way within the cell.

Astrocytes not only act as macrophages but they also sustain essential interactions with the other glial cells, the vasculature and the neurones. They are primarily responsible for the uptake of glutamate from the extracellular space through glutamate transporter proteins in their plasma membranes, maintaining a non-toxic environment in the retina and generally in the brain (Danbolt, 2001). In an over simplified description, glutamate is converted to glutamine and released in the extracellular space, in the vicinity of the neurons. Unlike glutamate, which can be quickly oxidised and bind with proteins and DNA molecules, glutamine is a stable and inactive biomolecule. Neurons are able to take up glutamine and reconvert it to glutamate with the purpose to use it either in their metabolism or as a transmitter.

Recent research present evidence of astroglial glutamate secretion (transport reversal) (Anderson & Swanson, 2000). Therefore, it is now established that astrocytes not only support the neurons but they are also able to interact with them and modulate their activity. Glutamate secretion from astrocytes is associated with

an increase of their intracellular Ca ions. In fact, waves of Ca ions are able to propagate within a number of astrocytes and stimulate glutamate secretion. It is known that bradykinin and prostaglandin can stimulate this Ca-dependent glutamate release.

The pericytes unlike the other two types of cells have a contractile function and a role in regulating the blood flow. They are only observed in mature vascular networks and not in newly formed capillary beds and they have the role of preserving vascular stability (Benjamin, Hemo *et al*, 1998). A large number of pericytes have been observed in the inner surface of the choriocapillaries and a relatively high number of pericytes per unit length is evident in the retinal microvascular bed (Anderson, 1996; Chakravarthy & Gardiner, 1999). Actually, the pericytes' coverage is greater for the retina than anywhere else in the brain, suggesting stricter regulation of the retinal capillaries (Provis, 2001).

1.2 The inner retinal structure

1.2.1 The normal retinal nerve fibre layer

Approximately 1.4 million ganglion cells whose axons are grouped in fibre bundles comprising the nerve fibre layer in the retina (Blumenthal & Weinreb, 2001). Although this approximation may be largely attributed to the differences in the methods employed for the evaluation of the retinal properties, there is also an element of physiologic anatomic variability. In prenatal phases some of the ganglion cells' axons undergo a process of degeneration (Provis, van Driel *et al*, 1985). This is based on the fact that in the retina and generally in the nervous system more neurons are produced than what would be required to serve a function. However,

the excess number of neurons is effectively removed as the ganglion cells that have failed to make productive interactions with target cells in the brain, initiate a self-destructive process that has been recognised as apoptotic death (Raff, Barres *et al*, 1993). Therefore, the genetically controlled procedure of apoptosis contributes if not accounts for the inherent variability seen in the number of ganglion cells beyond the stages of retinal development.

Within the retinal layers, the nerve fibres assume a characteristic distribution. The axons originated from the most peripheral retinal regions occupy the more superficial nerve fibre layers, the fibres from the nasal side of the macula follow a parallel route to the temporal area of the ONH forming the papillomacular bundle, while the rest of the fibres are spread radially, arching around the macula before entering the scleral canal (Minckler, 1980; Ogden, 1983). The retinal nerve fibres also have a special regional distribution with reference to their size: Thin, nerve fibres originate predominately from the region adjacent to the fovea and the thicker fibres originate in the periphery. The papillomacular bundle contains mostly small fibres and the nasal arcade includes mainly large fibres. As a general observation, all bundles increase in size as they approach the disc where more fibres are added to them (Ogden, 1984). Overall the inferior pole of the ONH shows the highest density of fibres and includes mainly fibres of small diameter (Sanchez, Dunkelberger *et al*, 1986).

In the peripapillary region, the retinal nerve fibre layer (RFNL) is thickest in the superior and inferior arcade regions than in the temporal and nasal sectors (Radius, 1980; Weinreb, Shakiba *et al*, 1995). This gives rise to the characteristic double

hump configuration of the RNFL as normally recorded with imaging techniques (figure 1.2). The RNFL is shown to get thinner with increasing distance from the optic nerve head (Varma, Skaf *et al*, 1996). Interestingly, Funaki and co-workers (1998) reported that the inferior RNFL was relatively thinner in larger optic discs, suggesting a redistribution of the RNFL thickness at the optic disc poles associated with the increasing size of the optic disc area (Funaki, Shirakashi *et al*, 1998). Interocular differences have been observed in normality, with the right eyes generally showing lower values for the RNFL thickness than the left eyes (Gherghel, Orgul *et al*, 2000).

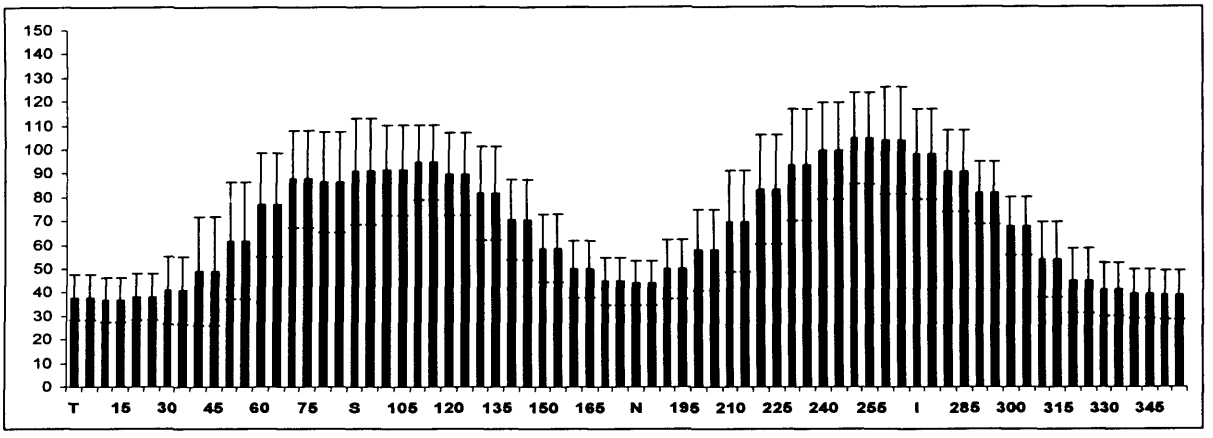

Figure 1.2 *shows the "double hump" configuration of the RNFL at the ONH. Graphical illustration based on estimates of the mean RNFL thickness from 11 healthy volunteers (range of refractive error: spherical equivalent = -5D to +2D), at a retinal circumference 1.75 DD away from the outer edge of the optic nerve head, as recorded by the GDx. Reproduction of published data reported in the study by lester, Tizte et al (2002).*

1.2.2 The crossing of the nerve fibres through the optic nerve head

The nerve fibres assemble at the ONH and within the optic disc area. Histological studies on primates and humans have reported a linear increase of the optic nerve fibre count with increased optic disc size (Jonas, Schmidt *et al*, 1992b; Quigley, Coleman *et al*, 1991b). Similarly, in vivo evaluation of the RNFL in normal subjects

with scanning laser polarimetry revealed increased RNFL thickness in relation to the disc area (Funaki *et al*, 1998). However, other quantitative results of the RNFL thickness once corrected for age revealed a large number of axons even in the smaller optic discs (Lachenmayr, Drance *et al*, 1991). Other studies also argue against the hypothesis that eyes with larger optic discs are likely to possess a higher nerve fibre count although, undeniably, the variability in the employed methods of the NFL evaluation has to be taken into account. The Confocal Scanning Laser Ophthalmoscopy Ancillary study to the Ocular Hypertension Treatment Study reported significantly larger optic discs for the group of African American than the other racial groups of participants but not a corresponding higher retinal nerve fibre layer thickness, as quantified by the Heidelberg Retina Tomograph (Zangwill, Weinreb *et al*, 2004b).

Several factors have been suggested to have an influence on the optic disc configuration. Measurements of the scleral ring of Elschnig in adult normal eyes revealed an element of anatomical inter-individual variability that must be affecting the disc and cup size (Jonas, Zach *et al*, 1989c). Age, markedly influences the size of the disc during the first years of life (while the globe is developing) but cross-sectional studies among healthy subjects of more than 40 years of age (Varma, Tielsch *et al*, 1994) and less than 40 years of age (Rudnicka, Frost *et al*, 2001) respectively, agreed that age was not a determinant of the disc parameters.

According to the findings of the Rotterdam study males are likely to have bigger discs than females, which could be possibly attributed to the difference in the average body weight between men and women (Ramrattan, Wolfs *et al*, 1999).

Moreover, significant variability in the measurements of the optic disc topography among healthy participants has been associated with racial features and population studies have consistently indicated that optic discs tend to be larger in Afro-Caribbean than in Caucasian populations. The mean optic disc was found approximately 12% larger in black race than in white race participants of a population based sample (Varma *et al*, 1994). A recent study revealed marked differences in the appearance of the optic nerve head among OHT patients of Caucasian, African and Asian descent, primarily associated with the differences in optic disc size (Zangwill *et al*, 2004b).

Larger size optic discs are a known feature of highly myopic eyes, as optic discs seem to stretch and develop parallel to the myopic stretching of the retina. Among high myopic eyes of more than -8.00 dioptres, disc size was strongly associated with refraction and axial length (Jonas, Gusek *et al*, 1988a). Generally, axial length was found to be the most important predictor of size for most of the optic disc parameters (Rudnicka *et al*, 2001).

It terms of shape, the optic disc is normally vertically oval. The vertical diameter of the disc was estimated in normal population to be about 9% larger than the horizontal one (Jonas, Gusek *et al*, 1988c). Interestingly, male subjects have discs with similar vertical diameter but larger horizontal diameter than the discs of female subjects (Quigley, Brown *et al*, 1990). Furthermore, histological post-mortem measurements of the optic disc in eyes from black and white race human donors suggested that, while the horizontal disc diameter was similar between the two groups, the optic discs from black donors had a greater vertical diameter than the

white donors (Varma *et al*, 1994). A larger index of ovalness has been associated with longer axial length and larger disc area in a population study among healthy Japanese (Chihara & Chihara, 1994; Chihara, Liu *et al*, 1997). The disc shape becomes more variable in high myopic eyes and compared to emetropic eyes, discs of normal highly myopic eyes were reported to be not only significantly larger but also more ovally configured and more oblique (Jonas & Papastathopoulos, 1995). Additionally, disc shape varies in eyes with very steep or flat corneal curvatures as there is a tendency in such eyes for the relative orientation of the disc to correlate with the axis of corneal astigmatism (Jonas & Grundler, 1997a).

Tilted discs are a normal congenital variation in the optic disc appearance that have been attributed a high index of ovalness (Jonas & Grundler, 1997a). The tilted disc syndrome is a non-hereditary bilateral condition associated with the abnormal closure of the embryonic fissure and resulting into the oblique insertion of the optic disc into the globe (Sowka & Aoun, 1999). The disc appears oval shaped and obliquely oriented, usually towards the nasal side. In addition, the superotemporal portion of the disc is usually elevated while the inferonasal portion appears displaced posteriorly (Brodsky, 1994). Perimetric evaluation of tilted discs have associated them with a widespread visual field defect that may be more pronounced superotemporally, suggesting that tilted discs may include in all quadrants fewer axons than an average normal optic disc (Brazitikos, Safran *et al*, 1990). Among normal eyes, tilted discs have been strongly associated with high myopia and high corneal astigmatism (Hyung, Kim *et al*, 1992). Eyes with tilted discs have demonstrated the surprising association of longer than average axial length with however average size of the optic disc area (Chihara & Chihara, 1994).

1.2.2.1 The neuroretinal rim

After gradually sloping over the sides of the scleral canal, the nerve fibres interweave with each other forming the neuroretinal rim before they disappear into the deeper retinal layers on their way to exit the globe. The rim area is highly correlated with the retinal nerve fibre capacity; therefore, it remains controversial whether there is a lot of inter-individual variability in the size of the normal rim associated with smaller or bigger numbers of nerve fibres. It has been suggested that the rim area is correlated with the optic disc area with larger optic discs having a large neuroretinal rim. However, normal macrodiscs were not associated with relatively larger NRR areas (Jonas *et al*, 1989c; Jonas *et al*, 1992b). Moreover, the comparative large disc size of the African over the Caucasian volunteers in the Baltimore population study was associated with relatively small rim areas and this disparity increased with increasing disc size (Varma *et al*, 1994), contradicting a recent inter-racial study, which reported that the discs of African Americans OHT patients, planimetrically analysed with the HRT, were statistically significant larger and included equally large rim areas, compared to the discs of the other racial groups (Zangwill *et al*, 2004b). Budde and colleagues (2000) showed that the rim size was found to correlate with disc size regionally (Budde, Jonas *et al*, 2000).

The retinotopical arrangement of the axons within the RNFL is consequently reflected upon the composition of the neuroretinal rim band. Namely, the papillomacular bundle forms the temporal rim, the nasal fibres reach the nasal rim, and the fibres from the superior and inferior distant retina converge on the superior and inferior rim, respectively. Also within all parts of the rim axons originating from

the peripheral retina lie closer to the disc margins than the axons from closer sources.

A distinct pattern of the neuroretinal rim band configuration has been identified in normal eyes, usually described as the ISNT rule: the rim thickness is biggest in the inferior sector of the disc, followed by the superior, the nasal and the temporal disc areas (Jonas *et al*, 1988c). In morphometrically analysed normal optic discs with vertically oval shape the rim was estimated to be significantly wider at the disc poles while the inferior part was significantly wider than the superior. As expected, the smaller circumference of the most vertically oval discs at the poles was associated with relatively greater neuroretinal rim estimates in the same regions (Jonas *et al*, 1988a). It is noted that the rim shape does not change with disc size (Jonas & Budde, 2000).

1.2.2.2 The cup

The optic cup describes the excavation within the disc area not occupied by nerve fibres. The cup is normally oval, with its horizontal diameter almost 7.7% longer than the vertical diameter (Jonas *et al*, 1988c). It is noted that no racial variability has been reported for the cup shape (Girkin, McGwin *et al*, 2005; Zangwill, Weinreb *et al*, 2004a). Conversely, cup size is positively correlated to the optic disc size. Large discs tend to have large optic cups and small discs with an area of less than 1.6-1.8 mm^2 may even appear with no cupping, although there is substantial inter-individual variability concerning these features (Jonas, Nguyen *et al*, 1989a). The depth of the cup depends primarily on the anatomical configuration of the scleral canal and is further affected by the process of the development, as well as the

regression, of the hyaloid artery and its glial sheath, normally occurring shortly after birth (Apple, Rabb *et al*, 1982). Interestingly, although cup depth correlated with disc size in all comparative studies between normal eyes of different racial background using the HRT (Girkin *et al*, 2005; Zangwill *et al*, 2004a), once the analysis was corrected for disc size a deeper maximum cup depth was reported for the group of participants with African descent, thereby highlighting a possible racial aspect in the normal variability that describes the cup formation (Girkin *et al*, 2005).

1.2.2.3 The lamina cribrosa

The optic cup includes a structure of perforated connective tissue, the lamina cribrosa. The bundles of fibres enter the septa of the lamina cribrosa at the laminar region of the anterior optic nerve and weave their way through the sclera tissue. The lamina cribrosa is constructed from bundles of collagen and glial tissue that form oval to round compartments. Overlying plates of connective tissue and glial elements create the lamina plexus. This structure secures the appropriate arrangement of the nerve bundles within the optic nerve head by including them in pores of various diameters analogous to the bundle diameters. It is assumed that the cup is formed from ganglion cell axons degenerated during the embryonic phase after failing to reach the optic nerve. Moreover, given the existence of empty pores in the middle of the laminar structure it can be speculated that the lamina cribrosa is actually formulated before the cup.

The axons follow an almost direct path through the lamina cribrosa, although there is evidence of a small percentage of axons with slightly deviated routes, passing randomly from the peripheral and more central parts of the laminar pores (Morgan,

Jeffery *et al*, 1998). A complex system of retinal and choroidal capillaries is also distributed within the perforated structure of the lamina cribrosa nourishing the nerve fibres.

The septum is thinnest and larger pores are observed at the superior and inferior quadrants of the lamina cribrosa including the fibre bundles with the larger diameters (Quigley, Adicks *et al*, 1981). Histological studies have shown that within the lamina cribrosa, the highest density of fibres is observed in the infero-temporal sector while the larger bundles of fibres are mainly included in the supero-nasal sector (Mikelberg, Drance *et al*, 1989). Research on primates has also revealed that within the lamina cribrosa there is regional variability in the density of the structural elements i.e. the connective tissue and glial cells. According to Radius and Bade (1981) the nasal quadrant of all regions within the optic disc has the highest proportion of connective tissue and is consistently thicker than the temporal quadrant. Additionally, the laminar tissue is increased in the more peripheral parts of the lamina cribrosa than the central portion (Radius & Bade, 1981).

In normal eyes, the central laminar region is more posteriorly located than the more peripheral regions, giving to the lamina cribrosa a U-shaped configuration (Quigley, Hohman *et al*, 1983). This central area possesses elastic properties that facilitate a pronounced displacement of the optic disc tissues under mechanical stress that could be resulted from fluctuations in the intraocular pressure or even external head injuries. The plasticity of the optic nerve head through the lamina cribrosa has been demonstrated in vivo when acute elevation of the IOP by suction in healthy eyes resulted in a reversible displacement of the lamina and increase of the cup depth

accordingly (Azuara-Blanco, Harris *et al*, 1998). The physiologic high inter-individual variability describes the variable flexibility of the laminar structure (Levy, Crapps *et al*, 1981). Comparison of the anatomical structure of the lamina cribrosa between healthy individuals of various racial background revealed some variations in the pore number and overall size of the structure but did not show differences in the proportion of connective tissue that would suggest a compromise of the structural integrity (Dandona, Quigley *et al*, 1990).

1.2.3 The optic nerve

At the retrolaminar region, sheaths of myelin constructed by oligodendro-glial cells cover the optic nerve fibres therefore appearing with a whitish colour instead of the transparent appearance they have within the retina. Myelination of the nerve fibres precedes the inclusion of the nerve fibre bundles in meninges and the formation of the optic nerve. The optic nerve transfers the input received by the retinal ganglion cells to specialised areas of the brain. The optic nerve measures about 1mm whilst running through the sclera on its way to exit the globe. Nerve fibres from both eyes are rearranged at the optic chiasm so that each optic nerve carries a combination of visual stimuli, derived from both eyes. Via the optic nerves, the ganglion cells' axons project to target areas at the lateral geniculate nucleus of the thalamus, which, in turn, are connected with the visual cortex of the brain, where specialised centres are responsible for the visual processing.

1.2.4 The ocular blood supply of the ONH and the retina

The blood supply of the ONH originates from the ophthalmic artery and it is delivered through the central retinal artery (CRA) and the posterior cilliary arteries (PCAs) (figure 1.3).

The CRA enters the ONH approximately 1cm behind the globe and remains confined in an envelope of connective tissue until it emerges at the optic disc. The PCAs pierce the sclera close to the optic nerve trunk and give rise to a network of short posterior cilliary arteries (sPCAs), forming the circle of Zinn-Haller at the scleral plane and connecting to the microvasculature within the pia matter (figure 1.3) (Hayreh, 1996).

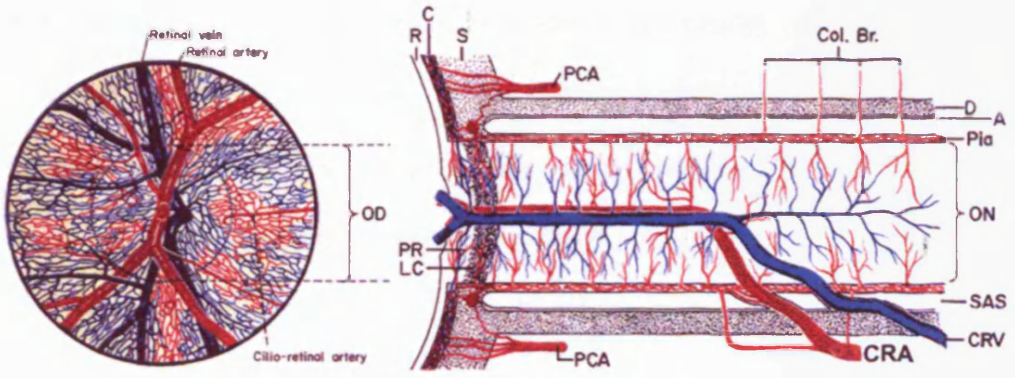

Figure 1.3 *Distribution of blood vessels on surface of the optic disc and the retina for the left eye and within the blood supply of the optic nerve (Hayreh, 1974).*

The nerve fibre layer at the anterior of the optic nerve head and the peripapillary retina receives blood supply from the retinal arterioles, branches of the central retinal artery (Hayreh, 1996). The retinal capillaries at the optic disc margins extend radially to supply the neuroretinal rim without any contribution from the choroidal

circulation (Zhao & Xu, 1987). Anastomosis exists between the retinal capillaries and the capillary plexus of the prelaminar region. Occasionally, branches of the PCAs, the cilioretinal arteries emerge from the prelaminar region to contribute to the circulation at the retinal level. Considerable inter-individual normal variability describes the number, size and distribution of these arteries. A positive correlation between disc size and the number of cilioretinal arteries has been reported by Jonas *et al* (1988), while Hayreh (1963) investigated the incidence of PCAs around the ONH, estimating up to 5 PCAS (Hayreh, 1963; Jonas *et al*, 1988a). Hayreh (1990) highlighted the importance of the retinal areas outside the distribution region of the PCAs. It was suggested that these areas, described as "watershed" areas, were regions of poor circulation and could be implicated in ischaemic conditions (Hayreh, 1990).

The prelaminar region, where the fibres bend into the scleral canal, is exclusively supplied by the posterior cilliary arteries (Onda, Cioffi *et al*, 1995). Vascular casting studies have previously suggested the involvement of the peripapillary choroid in the vasculature of the prelaminar region, however haemodynamic studies clarified that the short posterior arteries run through the choroidal layer without any anastomosis with the choriocapillaries (Hayreh, 1996). Both the CRA and the peripapillary choriocapillaries are not playing a role in the supply of this region.

Branches from the short posterior cilliary arteries and from the circle of Zinn-Haller supply directly, or via the pial circulation, the laminar regions. The lamina cribrosa includes a dense capillary bed that does not receive any input from the central retinal artery. It was initially speculated that the circle of Zinn-Haller, a circular

arterial anastomosis, is part of the choroidal vasculature, but it was finally revealed that it is situated at the scleral level and, most importantly, that it is separate from the choroidal circulation (Hayreh, 1996). The circle of Zinn-Haller shows considerable structural variation and has been reported to be incomplete or even absent in some eyes (Zhao & Li, 1987). The non-myelinated ONH, at the prelaminar and laminar region, appears to have rich blood flow and intense tissue activity, comparable with the grey matter of the brain.

The retrolaminar region is mainly supplied by the pial system, vessels surrounding the optic nerve. Branches of the circle of Zinn-Haller are shown to extend to the most anterior parts of this region. Most importantly, the retrolamina is likely to receive direct supply from the CRA (Hayreh, 1996).

The circulation of the anterior optic nerve is served by rich capillary beds confluent within all four anatomical regions of the optic nerve: the retinal capillaries of the nerve fibre region are interconnected with the capillaries of the prelaminar region, which then expand with a different arrangement to the laminar region and finally, they are distributed in the retrolaminar region. It was initially speculated that these interconnections of the capillaries along the anterior optic nerve play some protective role against regional ischaemic episodes (Anderson, 1970), but more recent studies conclude the opposite (Hayreh, 1996).

The arterial vessels penetrate the inner retina, and normally remain embedded in the nerve fibre layer, confined within the structural glial tissue. There are three capillary networks rising from the retinal arterioles, intercommunicating between

them and distributing along three different parts of the retina. One capillary bed runs within the nerve fibre layer and the ganglion cells; a second one exists within the inner nuclear layer and finally, there is a superficial network distributed around the disc and along the temporal superior and inferior retinal vessels.

While the retinal arteries deliver the blood supply to the inner retina, the choroid supplies the outer retina. Upon entering the sclera, the short posterior arteries comprise the choroidal arteries which give rise to a rich bed of capillaries, the choriocapillaries. The capillaries of the anterior optic nerve do not anastomose with the choriocapillaries. There is actually only a small involvement of the peripapillary choroid in the circulation of the ONH, that occurs through small connections of the prelaminar vascular outflow to the choroidal veins (Hayreh, 1996).

The blood flow in the retina is generally lower than in the choroid. Moreover, the retinal and optic nerve head vessels, unlike the choroidal vessels, do not show autonomic intervention beyond the lamina cribrosa. Also the retina has Müller cells and astrocytes that extend over large areas and maintain close spatial relationship with the vessels. Interestingly, all retinal and choroidal capillaries share a unique characteristic that determines their behaviour to circulatory stimuli, their lack of precapillary sphincters. These are valves that ensure that not all capillaries are simultaneously perfused and their action is normally determined by the metabolically needs of the hosting tissue (Henkind, 1967).

1.2.4.1 The retinal vessels

The central retinal artery and the central retinal vein have been described manifesting eccentrically within the disc, usually at the upper nasal quadrant in normal eyes, with the central retinal vein always situated temporally to the retinal artery (Jonas & Fernandez, 1994). As the vessels branch into large numbers of very small capillaries across the retina and the ONH, the retinal vessels show a monotonic decrease in diameter, which becomes more prominent with increase in the distance from the optic nerve head (Mitchell, Smith *et al*, 1997). The retinal arterioles have significantly wider diameters at the inferior-temporal ONH border, followed by the superior-temporal region, the superior-nasal region and finally the inferior-nasal region (Jonas & Hayreh, 1999). This pattern of vessel distribution complies with the density distribution of the retinal nerve fibre and it is therefore assumed that it reflects the nutritional needs across the retina. Rassam *et al* (1996) measuring the regional retinal blood flow reported higher values in the temporal versus the nasal retina, but the same blood flow in the superior versus the inferior retina (Rassam, Patel *et al*, 1994). Similarly, baseline measurements of vessel diameters from 20 healthy volunteers revealed that the temporal vessels were larger than the nasal, with no differences identified between the superior and inferior retina (Jean-Louis, Lovasik *et al*, 2005). After all, the temporal retina is larger than the nasal and most importantly, it contains the highly metabolic area of the macula.

From observations of the normal vasculature, there is evidence that the retinal vessel diameter undergoes temporal changes, occurring in association with the cardiac circle. It is suggested that the arteries are maximally dilated in mid-systole

and attenuated towards end-diastole, undergoing an overall diameter change of 3.5%. Conversely, there is a 4% increase of the IOP with early systole, resulting in passive reduction of the venular diameter. Venular diameter is then increased in diastole undergoing a diameter change estimated to be of 4.82% at its largest. In addition, the retinal vasculature exhibits vasomotion which is the spontaneous contraction and relaxation that the small arterioles show in a cyclical fashion. Although the frequency of those movements is still unknown in the retinal tissue, it has been estimated that the mean change induced in arteries and veins by vasomotion is 3.71% and 2.61% respectively (Knudtson, Klein *et al*, 2004).

The vascular reactivity of arteries and veins has been studied in the normal retina, inducing artificial disturbances based on the blood pressure (BP) (Blum, Bachmann *et al*, 1999); or the IOP (Nagel, Wilser *et al*, 2002); or the metabolic modulation of the retina by inhalation of oxygen or carbon dioxide (Jean-Louis *et al*, 2005) and also with flickering light provocation of (Formaz, Riva *et al*, 1997; Nagel & Vilser, 2004). The arteries, compared to veins, have different reactivity to the same metabolic stimulation in the normal retina. Experimentally induced hyperoxia triggered a wider amplitude of vasoconstriction in veins (reporting a group mean change across all retinal quadrants of 14.45 % compared to baseline), than in arteries (reporting a group mean change of 9.15% across all retinal quadrants compared to baseline (Jean-Louis *et al*, 2005).

Moreover, there is contradictory evidence that the vascular responses may vary between different regions of the retina. Greater vessel reactivity to oxygen was reported for the arteries and veins in the temporal than in the nasal retinal sector

(Kiss, Polska *et al*, 2002). However, examination of healthy eyes, in vivo, with the Retinal Vessel Analyzer (RVA), while investigating the increased or decreased delivery of agents like O_2 and CO_2 within the retinal tissue, revealed the same degree of vasoconstriction for arteries and veins, respectively, across all retinal areas (Jean-Louis *et al*, 2005).

The importance of vessel size in vessel reactivity has yet to be determined. Polak and colleagues (2000) did not find changes of vasoreactivity among the peripapillary arteries before and after the first bifurcation (Polak, Schmetterer *et al*, 2002; Schmetterer & Polak, 2001). However, model microcirculation calculations surprisingly suggested that small vessels would be expected to undergo larger diameter changes (Berthold, Riemer *et al*, 2002). Other clinical studies investigating vessels with a range of baseline diameter also didn't identify such behaviour (Nagel & Vilser, 2004). Attempting to explain their findings, the authors speculated that the very small arterioles, with a diameter of 20 to 30 micrometers, respond differently to stimulation because they seem to behave similarly to the precapillary sphincters in the retina.

Furthermore, no relationship has been identified between the degree of dilation and constriction that a given vessel, may demonstrate once stimulated. Actually, many studies inducing vessel dilation in healthy retinas observed that at the end of the normal subsequent constriction response, the vessels were likely to assume diameters below their baseline measured diameter at the start of the experiment (Nagel & Vilser, 2004; Polak *et al*, 2002). This is a result of an overshooting regulatory response and we can speculate that the type of stimulation as well as the

size of the vessel examined is likely to give variable results. Therefore, the amplitude of arterial reaction is a more important parameter to be evaluated than the maximum dilation achieved.

1.2.4.2 Autoregulation

Since the retina lacks autotonomic intervention, autoregulation is the mechanism that keeps the blood flow stable through the retinal vessels, despite large fluctuations in IOP (Johnson, 1986). The vascular perfusion pressure of the optic nerve is defined as the mean local arterial pressure minus the IOP. Based on this relationship, an increase in the IOP would decrease the perfusion pressure and, in turn, stimulate a drop in vascular resistance, thereby maintaining an unchanged blood flow. Varying degrees of autoregulation influence the blood flow in the retina, the choroid and through the optic nerve (Delaey & Van de Voorde, 2000). Different tissues appear to possess different amounts of autoregulation and the autoregulatory control mechanisms also vary between the type and size of vessels (Buckley, Hadoke *et al*, 1997).

The blood flow in the retina and the optic nerve head is regulated by alteration of the arteriole vascular resistance and is determined by the perfusion pressure, the resistance of vessel diameter and vascular blood velocity. The diameter of the vessels depends on the contractile state of their smooth muscle cells and pericytes, which is regulated by neurotransmitters, circulating vasoactive substances, or local metabolic and endothelium derived substances. Within a tissue, the number of simultaneously perfused capillaries depends on the metabolic needs of the tissue and is controlled by the precapillary sphincters, acting like mechanical valves.

However, considering that the choroidal and retinal arterioles do not have such sphincters, modifications of the vascular diameter occurs simultaneously in the whole ocular arteriolar system. A myogenic-based autoregulation mechanism is activated via changes in the systemic arterial pressure and/or the IOP. Ocular perfusion pressure is equal to the arithmetic difference between the mean arterial pressure and the intraocular pressure readings. Therefore, rise or fall of the perfusion pressure results normally in constriction and dilation of the arterioles, respectively, modulated by the autoregulation system. Moderate variations in perfusion pressure create a variation in the transmural pressure difference that acts as a stimulus of the myogenic mechanism of autoregulation changing the vascular resistance. Increased IOP or reduced arterial pressure causes reduction of the transmural pressure difference. In turn, the activity of pacemaker cells on the arteriolar wall is reduced, which reduces the arteriolar tone and, as a final result, reduces the vascular resistance (Alm, 1993). Autoregulation becomes disabled outside a limited range of perfusion levels. Analytically, experimental studies have suggested that autoregulation still functions when there is a 41% increase of the systemic pressure or when the IOP increases above 27-30 mmHg (Robinson, Riva *et al*, 1986). Such changes are equivalent to a decrease of the mean retinal perfusion pressure down to 50% (Riva, Grunwald *et al*, 1986) The autoregulatory function of the retina is actually a balance between myogenic and metabolic mechanisms. The metabolic based mechanism of autoregulation is controlled by factors of the retinal metabolism like retinal-tissue PO_2, PCO_2, and PH, which are metabolic products aiming to respond to the metabolic needs of the retinal tissue.

Vasoactivity of the terminal arterioles is controlled by the vascular endothelium cells, which translate the mechanicals signals produced by the physical force of the blood flow into biochemical signals, thereby initiating a response of the vessels via the autoregulation mechanism. Reduction or increase in the blood pressure and perfusion pressure mediates constriction or dilation, respectively. The chemical agents produced by the endothelium cells are classified as vasodilators and vasoconstrictors and may mediate autoregulative vasomotor function for the macro and micro-vasculatures of the retina (Hayreh, 1996). Prostacyclin and nitric oxide act as the main vasodilators in the retina. Nitric oxide is formed by L-arginine with the contribution of a series of enzymes, like nitric oxide synthase (NOS) 1, 2, 3. It's synthesis can be stimulated by bradykinin (Meyer, Flammer *et al*, 1993). It seems that the endothelium continuously produces nitric oxide and maintains the ophthalmic circulation in a constant dilated state.

Endothelial-derived vasoactive agents mediating constriction are the endothelins (endothelin-1, -2, -3) and angiotensin-II. Endothelins act via the endothelin receptors A and B, which are situated at the vascular smooth muscle and the vascular endothelial cells, respectively. Angiotensin II is synthesised in the endothelial cells by agiotensin-I with the action of an enzyme that is also capable of inactivating bradykinin (Jonas & Hayreh, 1999).

The vascular tone depends upon a balance between the endothelial vasodilators and vasoconstrictors. Therefore, reduced formation of vasodilators would result in vasoconstriction and vice versa. Calcium antagonists are able to enhance the effects of nitric oxide and inhibit those of endothelin-1 (Ferro & Webb, 1997).

Similarly, vasoactive products released by activated platelets, like serotonin, can attenuate vasodilatation or reverse vasoconstriction.

There is differentiation in the production of endothelium-derived agents, depended on the size of the vessels and on the physiology of the tissue. Studies on the human retinal artery have demonstrated the prevalence of nitric oxide and endothelin, among the vasoactive agents (Haefliger, Flammer *et al*, 1992). The release of nitric oxide can be mediated in all vessels, but greater sensitivity to bradykinin is particularly associated with decreasing vascular diameter. Also, Synthase-3, which catalyses nitric oxide production, has been observed only in the small blood vessels of the prelaminar region of the optic nerve head (Neufeld, Hernandez *et al*, 1997). Wide distribution of NOS has also been observed in the human choroid indicating that nitric oxide regulates both retinal and choroidal circulation (Flugel, Tamm *et al*, 1994).

A similar aspect of specialisation has been observed in the activity of the vasoconstrictors. Endothelin-1 and serotonin induced smaller contractions to the ophthalmic artery than to one of its branches, the cilliary artery (Haefliger, Flammer *et al*, 1993). Angiotensin-II receptors are present in the rat retinal arterioles and ONH capillaries; angiotensin-II produced either locally or leaking from the choroid, must therefore be employed in the autoregulation at those regions. Factors such as age, health and medication may be additional determinants for autoregulation (Ferraridileo, Davis *et al*, 1991).

1.2.4.3 The retinal blood barrier

The reduced permeability between the ocular vasculature with the retina and aqueous humour creates the blood retinal barrier (BRB). Like the vessels of the brain, the vasculature in the retina maintains less permeability to a variety of blood-born molecules, favouring a strict regulation of the retinal microenvironment. The BRB is composed by the endothelium of the blood cells and the retinal pigment epithelium with the additional contribution of the cilliary processes that regulate the chemicals transported across the vitreous (Cunha-Vaz, 2004).

The vessels are acquiring their blood barrier properties by their "glial limitans". The vessels may demonstrate barrier properties because of the tight junctions formed between their endothelial cells, and also by expressing specific enzymes and molecular transporters. The barrier properties expressed by the capillaries are also strongly associated to various factors in their local environment and are mainly attributed to the contractibility of the pericytes that are abundant on their walls. Different layers of the retina show various degrees of permeability, e. g. the choroid demonstrates high permeability, but in the retina the barrier features are more prominent, although both tissues receive their blood supply from the ophthalmic artery. It has been reported that highly vascularised areas of the retina generally demonstrate more permeability than areas with less blood supply (Cunha-Vaz, 2004). The astrocytes in the inner vascular plexus and the Müller cells in the outer vascular plexus have been recognised as factors for the formation and maintenance of the BRB (Tout, Dreher *et al*, 1993) Moreover, the retinal microglia in association with the macroglia are thought to influence the permeability of the vascular endothelium (Provis, 2001).

The tight junctions interconnecting the cells of the RPE layer are also responsible for the restricted permeability to blood components. The RPE cells are capable of producing various cytokines which in turn interact with glial cells, therefore influencing possible inflammatory responses in the retina and the maintenance of the blood vessels (Provis, 2001). Experiments on animal RPE tissue in vitro have demonstrated the production of cytokine TNF-a from RPE cells. Furthermore, it has been also observed that TNF-a is capable of triggering the RPE cells to produce nitric oxide (NO) as RPE cells also bear cytokine receptors. It is noted that specifically the RPE-derived NO is associated with the integrity of the tight junctions between the RPE cells, therefore effecting their BRB contribution (Holtkamp, Kijlstra *et al*, 2001).

Additionally, it has been shown that high concentration of glucose may trigger the RPE cells to produce vascular endothelial growth factor (VEGF). Interestingly, when injected in the vitreous of healthy animals, both cytokines like TNF-a and growth factors like VEGF, were observed to initiate a breakdown of the BRB (Luna, Chan *et al*, 1997).

Finally, the aqueous humour serves metabolic purposes for the ocular tissues without vascular supply and has a high concentration in antioxidants, free amino acids, growth factors and proteins. There is active transport of substances from the vitreous to the RPE and the vessels of the retina. As demonstrated by experiments with fluorescence, the penetration of substances from the blood supply towards the vitreous is very low but is likely to be reversed in pathologic conditions associated with circulatory abnormalities (Cunha-Vaz & Maurice, 1967). On the other hand,

there are no existent barriers preventing diffusion of molecules from the extracellular space of the retina into the vitreous.

1.2.5 Physiologic peripapillary atrophy

The area around the optic nerve head, referred as the peripapillary area, may exhibit specific features described with the term "peripapillary atrophy" (PPA). Nevarez and his colleagues (1988) described the features of peripapillary retina as the result of misalignment between the boundaries of the three tissues that form the scleral canal: the epithelium, the choroid and the sclera (Nevarez, Rockwood *et al*, 1988). At the disc margins, the neuroectoderm folds inwards to form the RPE with its outer layer and the retinal neural tissue with its inner layer. The alignment of this fold with the disc margins may be occasionally unsuccessful resulting in regions adjacent to the disc with a double layer or even an absence of RPE tissue. The formation of a double layer of the RPE appears as a highly pigmented region (Fantes & Anderson, 1989). Additionally, the pigment of the RPE tends to show a gradual fading as it approaches the disc margins and the position of the fold emphases the irregular appearance of the peripapillary area. Some times the pigment epithelium shows more than pigmentation irregularities forming areas described as chorioscleral crescents. In such areas, the retinal pigment epithelium is retracted from the disc margin and the choroid is thinned out or even absent, revealing a part of the underlying sclera. The anatomical basis for this malformation is also thought to lie in the formation of neuroectoderm during the embryonic phase of the optic nerve. The twin study in Australia has actually demonstrated the congenital nature of the PPA (Healey, 2004).

A misalignment of the tissues is likely to occur from ocular stretching as seen in tilted and myopic discs (Fantes & Anderson, 1989). The crescents in tilted disc syndrome are usually located in the inferonasal region, accompanying the characteristic inferonasal tilting of the discs (Apple *et al*, 1982). In myopic eyes PPA areas usually expand concentrically around the optic disc margins.

Grey crescents are pigmented crescents that are observed within the scleral lip and are included in the rim area. These kind of crescents have been associated with the morphology of the normal optic nerve head in populations of black subjects (Shields, 1980) and recently by the Reykjavik Eye Study (Wang, Damji *et al*, 2003). While their histological nature is speculative, referring to accumulation of melanin that extends in the deeper layers of the lamina cribrosa, there are associations of their presence with the most temporal location of the disc, with the presence of PPA, but not with age and myopia.

PPA can also be considered a feature of the normal ageing retina. The accumulated lipofuscin in the ageing retina interacts with the retinal pigment epithelium (RPE) melanin molecules, promoting pigmentation irregularities (Boulton & Dayhaw-Barker, 2001) To a certain extent, normal ageing may also lead to localised chorioretinal degeneration (Curcio, Saunders *et al*, 2000).

1.2.5.1 Normal distribution of PPA

PPA expands concentrically around the ONH and can be classified into two zones. Alpha zone refers to the area of peripapillary atrophy that exhibits irregular pigmentation and Beta zone refers to the area where the pigmentation irregularities

are replaced by whitish areas of absent or destroyed tissue, which allows visibility of the choroidal vessels and the sclera. Beta zone is the area most adjacent to the optic disc margins and it is in sequence with Alpha zone without distinct borders to separate their extent (Jonas & Naumann, 1989). The classification of PPA into Alpha zone and Beta zone assists the optic nerve head assessment, but also reflects the severity of atrophy. The two zones exhibit different prevalence in the normal eye, with Alpha zone being more prominent and Beta zone being rare. The distribution, pattern and extent of the PPA are generally symmetrical between the eyes positively correlated with optic disc size and the axial eye length. Alpha zone may appear more marked in normal eyes, while the Beta zone is mainly present as a myopic crescent. Alpha zone develops radially, with preferential expansion in the direction of the temporal disc border followed by the nasal disc border (Jonas & Naumann, 1989).

Conversely, Beta zone has a more uniform and symmetrical distribution profile (Jonas & Naumann, 1989; Jonas, Fernandez *et al*, 1992a). The inter-individual variability that characterises the development of the two zones is congenital, dependent upon the anatomical variations described previously and influenced by factors of gender and race. This latter aspect particularly applies to Alpha zone, which is frequently observed in heavily pigmented eyes and is therefore more prevalent in dark skin races. The prevalence of both Alpha and Beta zones increase with increasing age, particularly that of Beta zone (Jonas & Königsreuther, 1994).

1.2.6 Ageing of the retina

With age, in all cells there is a greater shift towards accumulation of lipofuscin. Lipofuscin is metabolic waste formed through the incomplete turnover of cellular components that are either damaged or redundant. Lipofuscin is predominately produced in the lysosomes, while there is evidence that lipofuscinigenesis is possible in the glial cells and may also result from damaged or dying cells when accumulated within the extra cellular matrix. Within the ocular tissues, greater amounts of lipofuscin have been observed in the RPE cells that degrade the photoreceptor outer segments. When in high concentrations, lipofuscin, which is formed though the process of structural renewal of the normal cell, may encourage cellular function impairment. Thus, cellular deposits of lipofuscin contribute to the age-related functional decline and potentially the manifestation of pathological conditions (Brunk & Terman, 2002). Therefore, regulation of the toxic lipofuscin molecules is imperative and is likely to be achieved through cell division. However, experiments have suggested that lipofuscin is not undegradable, as previously thought, but, on the contrary, it can be normally exocytocised from the cells where it is formed and also be recycled within the normal tissue of the central nervous system. Lipofuscin formed within the ageing neurons would be normally transferred to glial cells, which if not able to degrade it, they safely dispose it though the blood supply to other tissues specialised for this process (Katz, Rice *et al*, 1999). Therefore, lipofuscin accumulation in pathologic conditions associated with ageing would possibly result from the interrupted disposal rate rather than the excess production of the molecule.

1.2.6.1 Structural changes in the ageing neural retina

Age-related loss of ganglion cells has been reported to range from no significant decline to loss of 400.000 of a 1.648 million axons in a life span of 70 years. The number of nerve fibres decrease with increasing age, with an estimated mean loss of 4000 fibres per year and it has been proposed that there is selective susceptibility of the smaller optic nerve fibres to the normal ageing process (Jonas *et al*, 1992b). More recent studies have reported that the density of the ganglion cell layer decreases with age, especially in the region outside the macula. Surprisingly, degradation of the myelin sheath of the ganglion cells axons, but not of the nerve fibres, was seen in the monkey. In support of the histological findings a number of clinical studies utilising different imaging techniques have identified diffuse RNFL thinning at the peripapillary retina in ageing eyes (Jonas *et al*, 1989a; Jonas & Dichtl, 1996).

Studies have estimated an annual decline of the rim area ranging between 0.28% and 0.39% in subjects aged 30-70 years, by both computer assisted planimetry and scanning laser ophthalmoscopy (Garway-Heath, Wollstein *et al*, 1997). Surprisingly, other studies did not report similar changes of the rim size (Moya, Brigatti *et al*, 1999; Ramrattan *et al*, 1999). For this discrepancy, it is important to take into account that the available knowledge is based only upon the reports of cross-sectional and not longitudinal studies. The considerable inter-individual variability could actually result in misleading conclusions. Moreover, there is speculation that even if the overall volume of the rim is relatively stable, there might be an age related change of the rim tissue consistency, with the glial component increasing and compensating for the loss of the neural component.

1.2.6.2 The ageing vasculature

Flowmetry studies on retrobulbar vessels, retinal and choroidal perfusion have revealed a negative correlation between ocular perfusion levels and ageing. Groh and colleagues reported a significant decrease of the retinal blood flow with a rate of 8% per decade (Groh *et al*, 1996).

Histological findings have associated ageing with vascular alterations at the optic nerve head leading to reduced perfusion (Dolman, McCormick *et al*, 1980). Additionally, ageing was associated with a significant decrease of blood flow at the nasal and temporal rim area (8% and 4% per decade, respectively) among optic nerve heads from normal subjects of various age groups (Boehm, Koeller *et al*, 2005). The findings of this study were based upon laser Doppler-Flowmeter measurements and the increased resistance of the vascular bed at the neuroretinal rim was indicative of reduced vessel diameter and/or decreased density of the capillaries. It was speculated that the underlying factor for these changes must have been the altered autoregulative mechanisms in the ageing optic nerve head rather than the age related thinning of the retinal nerve fibre layer affecting the density of the vasculature or the accuracy of the blood flow measurements.

1.2.6.3 Ageing and retinal disease

The extent to which particular anatomical and physiological changes in the healthy elderly eye, as well as their momentum, predispose to specific visual deficits, remains unresolved. However, to date, the leading causes of blindness worldwide have a higher incidence among the elderly (Faubert, 2002).

1.3 Glaucoma

Glaucoma describes a group of neuropathies with similar phenotypes resulting from apoptosis of the retinal ganglion cells and leading to a characteristic visual field constriction (Coleman, 1999). Different pathways of damage have been identified, targeting the axon of the neurons with often a face of secondary degeneration following the primary assault and inducing a widespread damage on both the axon and soma of the effected ganglion cells. The characteristic structural changes at the optic nerve head observed in the resulting neuropathy may be accompanied by irregularities in IOP levels (Distelhorst & Hughes, 2003). Histologically, the identification of glaucomatous pathology, before pronounced visual field loss has occurred, can be made upon the event of accelerated apoptotic death of the ganglion cells (Quigley, Nickells *et al*, 1995).

1.3.1 Apoptotic pathways

Apoptosis is a mechanism of cell death identified in all tissues and in all stages of life. The apoptotic procedure is strictly genetically controlled and usually observed in isolated cells. In the nervous system, apoptotic neuronal loss has been observed as a normal function that clears spare tissue cells during development and selectively removes cells that compromise the tissue performance in the mature retina (Jacobson & McCarthy, 2002). The apoptotic procedure is characterised by the shrinking volume of the dying cells that are rapidly phagocytosised by neighbouring cells of the same type and/or macrophages without accompanying inflammation of the hosting tissue (Weber, Kaufman *et al*, 1998). The expression of a number of genes associated with apoptosis can be mediated through various intracellular pathways that to some extent have not been completely elucidated.

The caspases are a cascade of enzymes that act as definitive apoptotic factors. However, one of the indirect pathways towards apoptosis involve, excess intracellular Ca^{2+}, initiated by the upregulation of the glutamate receptors (Laabich, Li *et al*, 2001).

A very distinct difference of apoptosis from the other most common type of cell death called necrosis, is that the cells' organelles and membranes are not rapidly degraded and released in the intracellular space, instead they are enveloped and neatly disposed within the bodies of the phagocytosis cells (Weber *et al*, 1998). Conversely, necrosis demonstrates DNA fragmentation at the primary stages and degradation of the other cytoplasmic organelles with special reference to the mitochondria during the more advanced stages of the process. This causes disruption of the tissue homeostasis resulting in activation of the immune system. Necrotic cells also seem to undergo cytoplasmic swelling before the degradation of their outer membranes (Jacobson & McCarthy, 2002).

Although different, apoptotic and necrotic cell death seem linked in many ways. It has been shown that necrosis may be already in process for some cells while other cells of the same tissue are about to enter an apoptotic phase. Therefore, it is possible that the same stimuli can activate both destructive pathways with a time difference that could be possibly attributed to differences in the susceptibility of the cells against acute disturbance or to secondary chemical chain reactions that create widespread and less acute tissue changes. Furthermore, it has been reported that in cases of rapid apoptotic death where the tissue cannot efficiently dispose the apoptotic bodies, some cells undergo necrosis (Wyllie, 1992).

1.3.2 Evidence of glaucomatous apoptotic death

Glaucomatous neuropathies have been exclusively associated with apoptosis of the retinal ganglion cells as demonstrated from experimental glaucomatous damage on primates through axotomy and post-mortem examination of human glaucomatous eyes (Quigley *et al*, 1995). Various chemicals, known as apoptotic markers were identified in cultures of neuronal cells from acute glaucoma animal models (Agar, Yip *et al*, 2000) and also from experimental work with chronic hypertensive animal models (Laquis *et al*, 1998). Tezel and colleagues (2000) experimented with glaucoma-like stimuli inducing IOP elevation and ischaemia and demonstrating apoptotic death of the neurones (Tezel, Dorr *et al*, 2000).

Researchers have even proposed the concurrence of apoptosis and necrosis in glaucomatous damage. Glaucomatous retinal damage seems possible in many ways, such as intraocular pressure disruption, optic nerve axotomy, ischaemia and/ or hypoxia, which could allow different pathways of cell death to be simultaneously activated. Not surprisingly, both in necrosis and apoptosis the ROS agents, the calcium ions, and generally the membrane channels, hold an important role. Vorwerk and colleagues (1999) demonstrated that a small or larger extent of glutamate receptors' stimulation by exposure to N-methyl-D-aspartate (NMDA) on cultured retinal ganglion cells was likely to trigger a characteristic apoptotic intracellular pathway or a rapid irreversible necrotic-like cell death, respectively (Vorwerk *et al*, 1999). The work by Tezel, Yang *et al* (2004) also demonstrated ganglion cell damage though a cascade of events slightly different to the classic procedures of apoptotic death. Their experiments on cultures of animal ganglion cells showed that when exposed to TNF-a and/or hypoxia, ganglion cells underwent

mitochondrial dysfunction associated with the release of cytochrome c and apoptosis inducible factor (AIF), but at the same time, they experienced a caspase-independent pathway of cell death, based on the over-production of free radicals (Tezel, Trinkaus *et al*, 2004).

The genetically controlled mechanism of apoptosis is likely to favour the characteristic specialisation seen in all neurodegenerative diseases, affecting certain types of neurons in the CNS. Recent research advancements have implicated apoptosis in the destructive pathways of many neurodegenerative diseases. Apoptotic death is proposed as the end stage of neurons in glaucoma but also in Alzheimer's, Parkinson's and Huntington's disease. However, the progression course of all the above pathologies is rather extended, contradicting the rapid mechanism of apoptosis as it has already been observed in the nervous system. While the pathogenesis of all the above pathologic conditions is still under research, it is strongly suggested that apoptosis in neurodegenerative diseases occurs for the targeted neurons through more complex pathways of damage (Kanazawa, 2001).

However, it is important to consider that our knowledge on apoptotic death procedures is primarily based on animal glaucoma models; therefore, the findings might not be applicable in the human retina. Moreover, glaucomatous damage manifested over a chronic pathology as seen in the human eye, is likely to occur through different pathways.

1.3.3 Pathophysiology of glaucoma

The intraocular pressure (IOP) represents the pressure of aqueous humour within the eye and is determined by the Goldman equation, as a balance between the rate of aqueous humour production, the facility of aqueous humour outflow and the levels of episcleral venous pressure. Normal values of IOP range between 10 and 21 mmHg. Additionally, within individuals there is a normal fluctuation in IOP levels throughout the day with higher readings in the early morning hours. Diurnal variation in IOP is dependent on the circadian rhythm and usually lies within the range of 4 mmHg. There is a normal slight increase of IOP with ageing. This could be associated with the age-related decline in the number of trabecular endothelial cells. Also, the pore size of the trabecular meshwork decreases linearly with age, as it relates to the tension sustained by the cilliary muscle that is gradually lost (Saccà, Rolando *et al*, 1998). However, changes of intraocular pressure induced either by a decrease of the outflow or more rarely, with increase of the episcleral venous pressure are traditionally associated with glaucomatous pathology.

1.3.3.1 Increased intraocular pressure

The first theory approaching the pathogenesis of glaucoma described the pure mechanical impact of increased intra-ocular pressure (IOP), usually associated with the disease, on the retinal properties (Radius & Bade, 1981). Elevated IOP produces strain on the retinal tissue, with the optic nerve head (ONH) being the most susceptible structure and, therefore, more likely to be the site of the resultant damage. This damage can be mainly traced to the scleral part of the ONH and in, particular, to the lamina cribrosa. While the hydrostatic pressure at the prelaminar part is equal to the intraocular pressure, there is a gradual decrease of the pressure

within the lamina cribrosa, reaching the level of the intracranial pressure at the most posterior parts of the lamina and the retrolaminar section. When the IOP becomes upregulated, the difference in pressure on either side of the lamina cribrosa causes the lamina sheaths to collapse, damaging the adjacent nerve fibres. Experimental and clinical observations have demonstrated structural changes induced in the optic nerve head by IOP elevation (Burgoyne, Crawford Downs *et al*, 2005; Quigley, Brown *et al*, 1991a).

The anatomical changes in the ONH are not only associated with the loss of the ganglion cells axons. It has been observed that astrocytes may become activated by IOP elevation and start a migration process that is responsible for the rearrangement of the extracelular matrix in the ONH (Hernandez, 2000; Morgan, 2000). Furthermore, there is enhanced glial composition of elastin specifically triggered by the IOP elevation and not observed in ONH damage by axotomy that further compromises the structural integrity of the axons in the laminar region (Pena, Netland *et al*, 1998).

The structural changes triggered by increased IOP levels, constitute impairment of the axoplasmic transport for the involved ganglion cells. Failure of the retrograde transport results in the obstructed supply of the brain derived neurotrophic factors along the ganglion cells' axons (Hayreh, March *et al*, 1979). Neuronal signalling factors play an important role in the development and survival of the axons and when the axons are injured these factors are blocked out. Under this condition, the CNS transmits an injury signal that induces an intensive inflammatory response in the retina followed by the apoptotic death of the ganglion cells. Upregulation of

neurotrophins and their receptors in the retinal cells, proceeding ganglion cell death was recently demonstrated under ocular hypertensive conditions (Levin & Gordon, 2002).

Finally, the misalignment of the tissues from the over-stretching of the retina under the mechanical forces in action, may result in failure of the blood retinal barrier at the already weak position of the disc borders (Neufeld & Gachie, 2003). This gives free access to the retina to various substances from the choroidal layer. Without the filtering function of the RPE cells, these agents can just leak from the choroid and disturb the balance of the neuronal environment, encouraging secondary degeneration. Additionally, experiments have demonstrated that transient increase of the IOP is unlikely to create ischaemic damage and cause loss of nerve fibres. In one of the most recent studies, healthy optic nerve heads were imaged in vivo with the GDx after they were subjected to a pressure of 100mmHg for 45 sec and no alteration of the RNFL thickness was detected (Iester, Tizte *et al*, 2002).

1.3.4 Ocular hypertension as a risk factor for glaucoma

Subjects exhibiting statistically increased IOP, without accompanying pathological cupping and/ or visual field defects in the retinal nerve fibre layer, are described as ocular hypertensive (Jonas & Königsreuther, 1994). Ocular hypertension (OHT) has been long regarded as a risk factor for glaucoma. Longitudinal studies have reported the development of glaucomatous damage in ocular hypertensive eyes within a follow up period of 10 years (Tuulonen & Airaksinen, 1991). Although, it is only an estimated 10% of the ocular hypertensive patients that progress to glaucoma there are significant associations between the IOP levels and the

likelihood of glaucomatous damage development (Quigley, Enger *et al*, 1994; Rasker, vandenEnden *et al*, 1997).

1.3.5 Normal tension glaucoma

A considerable population of glaucoma patients suffer from normal tension glaucoma (NTG) accounting for 33 % of the total OAG population, according to one of the most recent population studies undertaken in Italy (Bonomi, Marchini *et al*, 1998). It has been speculated that NTG has a similar vascular aetiology and has been associated with migraine symptoms and vasospasm (Gasser & Flammer, 1987). Yamazaki (1997) detected in NTG patients a retrobulbar circulation abnormality which did not seem to apply to OAG patients with elevated IOP readings (Yamazaki & Drance, 1997). Similarly, significantly slower choroidal haemodynamics were demonstrated in NTG patients compared to normal ocular hypertensive and other OAG patients (Duijm, van den Berg *et al*, 1997). Patients with NTG have also demonstrated a remarked diurnal variation of IOP caused primarily by alterations in the blood pressure. Furthermore, visual field deterioration in NTG and HTG patients was reported under low or extreme fluctuating blood pressure BP despite good IOP control (Graham & Drance, 1999).

Highlighting a different aspect of the unique relationship between IOP and NTG patients, recent studies have reported significantly decreased average central corneal thickness (CCT) in NTG patients, compared to other OAG and OHT patients. Therefore, it is widely speculated that the IOP measurements in NTG patients are generally underestimated (Emara, Tingey *et al*, 1999).

1.3.6 Management of IOP levels in glaucoma patients

The prevalence of glaucoma increases as a function of the magnitude of the elevated IOP and of the fluctuation in IOP. The visual impairment project (Lee, Mukesh *et al*, 2003) revealed the association of increased risk in development of open angle glaucoma (OAG) with both increased IOP and age. While there is considerable inter-individual variability in the magnitude of the IOP that may result in glaucomatous damage, it is evident that OAG and NTG suspects with pronounced IOP elevation show a higher susceptibility (Jonas, Grundler *et al*, 1998b). The most recent longitudinal follow-up studies clearly record the association of a relatively higher IOP that may even be within the so-called normal levels, with progression of OAG and NTG patients (Palmberg, 2002). On the other hand, glaucoma animal models have suggested that IOP induced damage may be significantly correlated with the highest achieved IOP elevation rather than a prolonged exposure time of moderate IOP disruption, at least in some types of glaucomatous damage (Chauhan, Pan *et al*, 2002).

Individually designed treatments for IOP control are proposed as the most effective approach for management of the disease (Palmberg, 2002). In conclusion, IOP monitoring is strongly recommended for all OHT and OAG patients (Spaeth, Lucy *et al*, 2000) although according to some epidemiological studies the role and control of IOP in the progression of glaucoma remains equivocal (Tezel, Siegmund *et al*, 2001). However, it is argued that this is more an issue of the achievable IOP lowering, as recent research findings speculate that the level of tolerance to IOP once the laminar structures have exceeded their threshold of elasticity after prolonged exposure to high IOP levels, is likely to be very low, therefore IOP

treatment might need to be tailored at levels that are much lower than normal (Burgoyne, 2004).

1.4 The involvement of the retinal vasculature

1.4.1 The association of IOP and retrobulbar blood flow in glaucoma

Both increased IOP and decreased ocular blood flow (OBF) were found to be equally important predictive factors for glaucoma progression (figure 1.4) (Satilmis, Orgul *et al*, 2003). Also posterior ocular blood flow (POBF), which refers to the blood flow in the choroid and the anterior optic nerve head supplied by the posterior cilliary vessels and accounting for approximately 80% of the total ocular blood flow, was found to have significant negative correlations with IOP in treated OAG patients with moderate to severe damage (Hitchings, 1991).

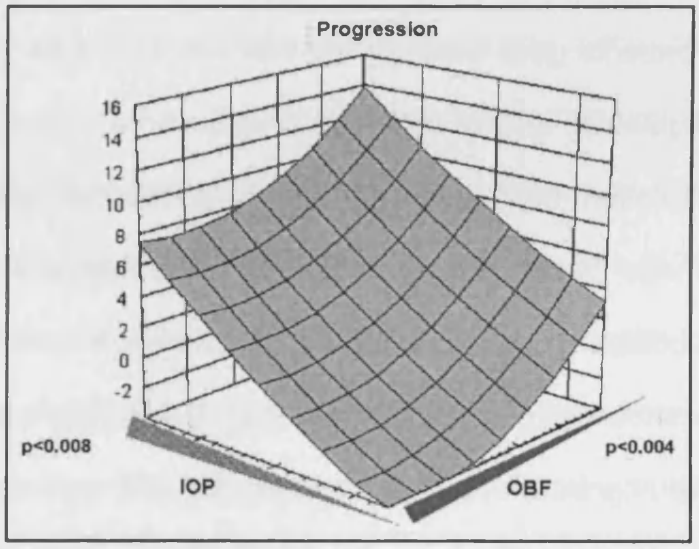

Figure 1.4 *shows the increased IOP and decreased OBF as important predictive factors for glaucoma progression (Satilmis et al, 2003).*

Conversely, glaucoma patients with a diurnal IOP curve not exceeding a level of 21mmHg, demonstrated altered retrobulbar blood flow parameters, such as

increased resistance in the central retinal artery, which correlated with an exaggerated nocturnal fall of systemic blood pressure (Gherghel, Orgul *et al*, 2001). Similarly, Tokunaga, Kashiwagi *et al* (2004) identified progression of visual field loss in both NTG and HTG patients, over a period of 4 years, that was associated not only with recordings of nocturnal blood pressure (BP) decline greater than 20% of baseline, but also with a very slight nocturnal fluctuation of less than 10%. Hence, glaucomatous damage seemed associated generally with the degree of deviation from the physiologic variation in blood pressure (Tokunaga, Kashiwagi *et al*, 2004).

1.4.2 Signs of vascular deficiency in glaucoma

A number of clinical studies have strongly suggested the involvement of the vasculature in glaucomatous damage. Reduced retinal blood supply that was identified in OHT patients gave some of the first indications for the involvement of deficient blood regulation in the aetiology of glaucoma (Trew & Smith, 1991). Compromised circulation has been reported in correlation with the degree of glaucomatous damage (Broadway, Nicolela *et al*, 1999; Rankin, Drance *et al*, 1996) and irregular retrobulbar circulation at the ONH region was more marked in advanced glaucomatous stages (Liu, Chiou *et al*, 1999). The association of OAG with conditions like migraine, systemic hypertension and coronary disease further supports this relationship (Klein, Klein *et al*, 1993). Moreover, a comparative study between groups of normal subjects, OHT and OAG patients have recently demonstrated statistically significant blood flow alterations in glaucoma patients followed by the OHT patients (Hafez, Bizzarro *et al*, 2003).

Glaucomatous damage may also be specifically associated with disturbance of the choroidal circulation. Histological studies in end-stage glaucoma eyes have identified altered choroidal vessels both in density and diameter (Spraul, Lang *et al*, 2002). Finally, NTG patients have been associated with defective retrobulbur velocities recorded by flowmetry that seemed likely to involve the deeper retinal layers as structural changes of the retinal vessels were not present (Plange, Remky *et al*, 2003).

Direct involvement of the vascular system is suggested by the higher prevalence of haemorrhages and retinal vein occlusions in glaucomatous eyes (Sonnsjo & Krakau, 1993). Moreover, central retinal vein occlusion (CRVO) has been strongly linked to open angle glaucoma (OAG) (Beaumont & Kang, 2002).

Recent studies indicate that reduced capillary blood flow in the retina and in parts of the ONH may also occur in elderly subjects without glaucomatous pathology. Taking into consideration that glaucoma is predominately an age-related disease with an estimated prevalence increasing sharply over the age of 70 (Tielsch, Katz *et al*, 1991), it is likely that vascular deficiency, which appears to accompany the ageing retina, has a determinant role in glaucoma pathogenesis. Not surprisingly, earlier studies have recorded a prevalence of generalised circulatory abnormalities of the retrobulbar vessels in senile sclerotic discs (Nicolela, Walman *et al*, 1996). Age-induced changes in the retrobulbar haemodynamics in healthy individuals were found comparable to vascular changes associated with glaucoma (Harris, Harris *et al*, 2000). Furthermore, it has been reported that a decrease in the blood flow at the neuroretinal rim, the lamina cribrosa and other parts of the retina, becomes more

apparent with advancing age (Embleton, Hosking *et al*, 2002). Moreover, there is an association of haemorrhages to generalised vascular diseases and to age progression (Grodum, Heijl *et al*, 2002).

1.5 The vascular theory

1.5.1 Ischaemic insults

The pressure-induced retinal stretching and deepening of the optic cup identified by the mechanical theory is also likely to significantly compress the retinal blood vessels. Not surprisingly, vein occlusions that are associated with OAG are usually occurring at the optic disc margins, where the vessels undergo considerable mechanical strain as they change planes and the intravenous pressure is at it's lowest level, increasing the regional susceptibility to IOP elevation (Beaumont & Kang, 2002). In the biocellular level, ischaemic insults stimulate neurotransmission and may depolarise the membranes of the ganglion cells, encouraging an unrestricted transport of water molecules and ions from the extracelular matrix. The resulting swelling of the ganglion cells is thought to exert compression of the ganglion axons at their crossing through the lamina cribrosa structure (Osborne, Ugarte *et al*, 1999; Osborne, Melena *et al*, 2001; Osborne, Casson *et al*, 2004).

1.5.2 Endothelium imbalance

It is speculated that in the primary stages of glaucomatous pathogenesis, the combined action of contracting and dilating agents that serve the retinal autoregulation system becomes disrupted. Anderson (1983) proposed that retinal stretching could challenge the integrity of the retinal barrier around the optic nerve head, resulting into dilating agents from the choroidal circulation leaking into the

retina and altering the autoregulation mechanisms (Anderson, 1983). Imbalances of the endothelium generally suggest the failure of the retinal blood barrier. Not surprisingly, upregulation of the endothelial derived relaxing and contracting factors has been postulated to be important for the development of various other ocular vascular disorders besides glaucoma, such as diabetes.

Finally, with reference to the role of IOP in glaucoma, it is important to take into account the fact that normal autoregulatory mechanisms can function optimally only within certain levels of IOP (Robinson *et al*, 1986). Therefore, it can be speculated that the endothelium imbalance occurs secondary to the high IOP levels. However, other pathological pathways independent of IOP elevation cannot be excluded. Experiments on rabbits have demonstrated a mediated apoptosis by the imbalance of the vasoactive agents resulting from the application of a vasoconstrictor agent, endothelin-1 (Oku, Sugiyama *et al*, 1999). Similarly, research on human eyes showed that glaucomatous ONHs had abnormally high concentration of the enzymes (synthase 1, 2, 3) that are known to be involved in the synthesis of the vasodilator nitric oxide (Neufeld *et al*, 1997). Other studies have directly associated glaucomatous damage with abnormalities of the L-arginine/nitric oxide system (Schmetterer & Polak, 2001). These findings are also confirmed by in vivo vasoreactivity testing of glaucoma patients compared to healthy volunteers. A defect in the mediated release of vasodilators at the retinal arteries has been observed in NTG patients (Henry, Newby *et al*, 1999) and impairment of the vasoconstriction agents in POAG patients was evident from the decreased sensitivity and reactivity of their retinal vessels to pressure stimuli, after mediation of a short-term IOP elevation (Buckley, Hadoke *et al*, 2002).

1.5.3 Secondary degeneration

It has become more widely accepted that glaucomatous stimuli may eventually trigger the apoptotic death of ganglion cells that haven't been injured directly. Factors that normally support the cells can become upregulated under pathological conditions causing widespread damage and delayed death of the neurons after the occurrence of the glaucomatous attack, a secondary degeneration. Besides the metabolic changes in the retina caused by direct injury of the neurons there are more gradual changes that are likely to be initiated through complex intracellular pathways, leading to apoptosis. The concept of a prolonged phase of sickness for the neurons, implicating intracellular mechanisms of aging, oxidative stress and excitotoxicity, altered gene expression and reduced protein production is actually proposed for most of the neurodegenerative diseases (Kanazawa, 2001), including glaucomatous neuropathies (Dreyer, 1998; Luo, Heidinger *et al*, 2001).

1.5.4 Excitotoxicity

Increased extracelular concentrations of the neurotransmitter glutamate activates both NMDA and non-NMDA receptors on the surface of the neurons and initiates a process of depolarisation of their membranes leading to increased influx of Ca^{2+}. As an immediate result, mitochondrial calcium overload stimulates the release of cytochrome-c and leads to apoptosis. Furthermore, as a secondary effect from the large increases in intracellular calcium, there is altered enzymatic activity, triggering more apoptotic cascades (Choi, 1988). Glutamate release is associated with ischaemic episodes in the brain. This glutamate is likely to be from neurons and not the glial cells.

Experimental and clinical findings have associated IOP deregulation with increased levels of glutamate and ganglion cell death (Quigley, 1995; Quigley *et al*, 1995). IOP elevation or increase of intravitreal glutamate concentration induced experimentally in animal models resulted in excitotoxic ganglion cell loss (Vorwerk, Gorla *et al*, 1999a; Vorwerk, Naskar *et al*, 1999b). Moreover, increased concentration of glutamate was detected in the vitreous humor of glaucoma patients (Dreyer, 1998). Given the relatively unobstructed transport of molecules between vitreous humour and the retina, these findings are indicative of failure of the retinal blood barrier, secondary glutamate excitotoxity in the retina and have direct implications on the progression of the ganglion cells death.

Conversely, vitreal glutamate elevation could be associated with the concurrent disruption of the glutamate transporters and their receptors, as demonstrated in cultured neurons from human glaucomatous retinas (Naskar, Vorwerk *et al*, 2000). In such case, neuronal apoptotic death is actually a defensive neuronal response, aiming to limit the influence of excess extracellular glutamate over their intracellular mechanisms.

1.5.5 Oxidative stress

Oxidative stress implies the enhanced intracellular concentration of free radicals and cellular oxidants like nitric oxide (NO) that mainly results in changes of the permeability features of the cellular membranes. In turn, increased membrane permeability causes further oxidation of various intracellular biomolecules. The regulation of free radicals and the selective molecular exchanges with the extracelular matrix is imperative for the neuronal activity. Oxidative stress generally

disturbs the function of the intracellular organelles through excess formation of free radicals and may induce blockage of active transports from the cellular membranes, leading to continuous Ca^{2+}influx. Increased concentration of intracellular calcium initiates apoptosis through the mitochondrial upregulation and could also alter the enzymes that would normally convert the intracellular oxidants into harmful compounds (Weinreb & Levin, 1999).

Studies of cultured rat retinal ganglion cells showed that nitric oxide ions, when in large concentrations in the culture environment, encouraged apoptosis (Morgan, Caprioli *et al*, 1999). When cultured under hydrostatic pressure, activated astrocytes and microglia expressed iNOS while ganglion cells expressed cNOS intracellularly. However, the high concentrations of BDNF secreted by activated glial cells was capable of upregulating the nitric oxide synthase activity inside the neurones (Samdani, Dawson *et al*, 1997; Samdani, Newcamp *et al*, 1997). In axotomised animal optic nerves glial cells expressed NO and damaged the neurones before apoptosis was observed (Koeberle & Ball, 1999). Similarly, astrocytes activated by raised IOP stimulation initiated NO production leading to ganglion cell death (Hernandez, 2000; Morgan, 2000).The generation of excess reactive oxygen species (ROS) are presumably increasing the peroxidation of fatty and/or nucleic acids and eliminating the protein cross-linking. Normally the cell has a defence system consisting of enzymes like superoxide dismutase (SOD), catalysing the conversion of superoxide radicals (O_2^-) to hydrogen peroxide (H_2O_2), which finally metabolises into water molecules with the contribution of other enzymes. It is imperative that all the above enzymatic activities are functional within the cell otherwise there is a risk of lipid peroxidation and oxidative stress. Moreno *et*

al (2004) demonstrated a significant decline of the antioxidant defence system activity in rat retinas that were modelling experimental glaucoma induced by increase of IOP over a longer period of time (Moreno, Campanelli *et al*, 2004). Alternatively, excess generation of ROS might simply overcome the cell's defensive capacity. It is noted that free radicals diffuse easily across cell membranes and they can induce a widespread effect on the cells. Oxidative stress augments lipofuscin production and in reverse, high lipofuscin accumulation may initiate oxidative stress and apoptosis (Brunk & Terman, 2002). Oxidative stress may also result from reperfusion after ischaemia (Osborne *et al*, 2004). It is noted that highly vascularized tissues such as the ONH and peripapillary areas are markedly susceptible to such ischaemic episodes.

1.5.6 Spreading depression

Microglia and astrocytes when activated in the CNS are able to encourage widespread retinal cell damage, described as glial depression. During depression, the regional glial cells, transmit chemical messages to the surrounding neural tissue that insult has occurred and cause the activation of more distal glial cells. This has been described as Ca waves, based on the increase of Ca intracellularly within astrocytes, associated with ATP production and even release of glutamate. Experimental and clinical studies have reported the migrating behaviour of activated glial cells and have associated them with glaucomatous sites of injury, demonstrating glial depression in the retina. Comparative observation of glaucomatous and normal optic nerve heads, identified microglial cells relocated in increased numbers around the scleral canal and the folds of lamina cribrosa, presumably trying to support the blood retinal barrier and save the neurons

(Neufeld, 1999; Neufeld & Gachie, 2003). It is speculated that spreading depression places additional energy demands on the already stressed retinal cells, encouraging them to undergo apoptosis (Osborne *et al*, 2001).

1.5.7 Genetic factors

Glaucomatous pathogenesis has been associated with failure of vital metabolic connections and generalised toxic insult for the neural ganglion cells attributed to mechanical and vascular factors. However, not all types of ischaemia and IOP fluctuation mediate the same degree of damage or they can certainly not always establish glaucomatous pathology, suggesting that genetic mechanisms also underlie the primary glaucomatous aetiology.

1.5.8 Family history

Glaucoma patients are very often showing signs of inherent susceptibility suggesting that there are genetic factors predisposing to glaucoma. Actually, about 33% of the cases of glaucoma involve first-degree relatives (parents, siblings or children) of glaucoma patients (Vernon, 1991). The Barbados family study investigated the prevalence of glaucoma among the members of 207 families and reported that 1:4 of all glaucoma patients' siblings were either OAG patients or suspects, regardless of their age (Leske, Nemesure *et al*, 2001). Similarly, the visual impairment project recognised an almost threefold increased risk for glaucoma among individuals with positive family history, ranking this factor as the strongest besides age (Weih, Mukesh *et al*, 2001a). Moreover, 40 % of the participants in the Ocular Hypertensive treatment study, across all racial groups, reported a family history of glaucoma (Zangwill *et al*, 2004a). However, it is still

inconclusive whether positive family history in glaucoma predisposes ocular hypertensive patients to glaucomatous progression. To the contrary, it has been speculated that up to a certain age, ocular hypertension may suggest an increased tolerance to elevated IOP and act as a protective factor against glaucomatous damage (Quigley *et al*, 1994).

The prevalence of glaucoma within a family is used to identify glaucoma suspects and is one of the most useful clues in discriminating glaucoma from other neuropathies. Current knowledge supports the assumption that at least a subset of glaucoma may have a genetic basis while factors such as IOP fluctuation and ageing further determine the development of glaucomatous damage. Family history has an inverse correlation with age progression especially after the age of 70 years (Budde & Jonas, 1999) and strong associations with IOP elevation (Klein, Klein *et al*, 2004; Weih *et al*, 2001a; Weih, Nanjan *et al*, 2001b).

1.6 Genes related to glaucoma

Although not all glaucomatous phenotypes seem to follow a clear Mendelian pattern of inheritance there are already six loci with an autosomal dominant character identified to cause glaucoma. Genetic predilection has been implicated in primary congenital glaucoma, juvenile-onset OAG and late-onset OAG. One of the widely recognised genes related to glaucoma is expressing the protein myocilin and called MYOC or TIGR. Myocilin has been traced within the ganglion cells axons and the astrocytes at the level of the optic nerve head, is produced in high concentrations within the trabecular meshwork and can be also secreted into the aqueous humour (Clark, Steely *et al*, 2001). The non-digestible mutants of this myocilin cause

congestion in cultures of trabecular meshwork endothelial cells and although the blockage of the filters along the trabecular outflow pathway could be the mechanism of action of these proteins in glaucoma, the role of myocilin glaucoma pathogenesis remains elusive (Jacobson, Andrews *et al*, 2001). Nevertheless, myocilin glaucoma seems strongly associated with high levels of intraocular pressure. There are 33 known mutations of the Myocilin gene accounting for approximately 2 to 4 % of adult onset glaucoma cases worldwide. However, the frequency of these mutations differs considerably within populations of different ethnic background (Herndon, Challa *et al*, 2003).

Another gene linked with glaucoma is the OPA1 gene encoding for the protein optineurin that is also expressed by the trabecular meshwork tissue cells. Recent findings reveal that this gene is actually neuroprotective, increasing the outflow facility to counteract the IOP elevation. Both IOP elevation and TNFa could trigger the expression of this gene in human tissue cultures (Vittitow & Borras, 2002). Interestingly, normal tension glaucoma has been associated with mutations of the OPA1 gene and the encoded altered proteins cause impairment of the mitochondrial function (Buono, Foroozan *et al*, 2002).

1.6.1 Stimulation of genes expression

It has been suggested that genes associated with glaucoma are more likely to determine the response of the tissues in the event of an insult, than to interfere with the normal regulatory mechanisms. This is demonstrated by the finding that at the trabecular meshwork, which is the tissue mainly responsible for the IOP maintenance, short periods of elevated pressure levels mediated the suppression of

a range of genes and the expression of previously silent genes, including some of the genes already linked with glaucoma (Borras, 2003). Similarly, heat shock proteins which are a cellular protection mechanism against stress stimuli were also observed to be upregulated in glaucoma (Wax & Tezel, 2002).

Furthermore, differential expression of random genes under conditions such as glaucoma may coincidentally activate apoptotic pathways. Changes of the cell metabolism and increased or decreased production of certain gene products may be responsible for the replication of a message for apoptosis initiation (Nickells, 1999). Altered gene expression has recently been observed in ischaemic retinal cells. Under hypoxia, the cells express the hypoxia-inducible factor 1a (HIF1a) which stimulates the expression of various genes that are meant to facilitate the survival of the cell under the given conditions. Among these genes are those encoding for VEGF, INOs and proteins that increase oxygen delivery. Considering HIF1a a reliable indicator of hypoxia, experiments on glaucomatous and normal retinal tissue have provided evidence of the ischaemic status associated with glaucomatous damage. High concentration of HIF1a was traced in the ganglion cell' s axons and the glial cells of the ONH region, as well as in glial cells at deeper retinal layers, of glaucomatous eyes with moderate damage (Tezel & Wax, 2004).

1.6.2 Racial distribution of glaucomatous phenotypes

Racial differences in the prevalence of glaucoma also suggest an underlying genetic predisposition. For example, studies on the incidence of glaucoma in Japan that recorded an association of the disease with increasing age and decreasing IOP, contrast with the findings of population studies in the western word (Shiose,

1990). Moreover, there is a marked prevalence of OAG among African Americans compared to Caucasians that however does not correspond with the presence of different IOP levels (Sommer, Tielsch *et al*, 1991). In support of this, the development of glaucoma has been estimated to be 4-16 times more frequent in the black race associated with earlier onset in whites, 92% have OAG over 8% with ACG, while for people with African descent this ratio is 150/1. The analogy is reversed in the Chinese population where ACG is the most common type of glaucoma, almost three times more prevalent than POAG. Surprisingly, pigmentary glaucoma occurs predominately among Caucasians (Wormald, Basauri *et al*, 1994).

1.7 Structural changes in glaucoma

1.7.1 Degeneration of the nerve fibres

The RNFL thickness is significantly decreased in glaucoma patients, followed by OHT subjects compared to age-matched normal subjects (King, Bolton *et al*, 2000). The RNFL undergoes diffuse and/or localised damage. The pattern of RNFL thinning vary between NTG patients and other OAG patients (Matsuno, Kurimoto *et al*, 2001) and is not restricted in the areas corresponding to visual field defects (Matsumoto, Shirato *et al*, 2003). Diffuse damage manifesting as generalised thinning of the NFL can be identified via the increased visibility of the vessels. Conversely, localised RNFL damage is usually situated close to, or in touch with the temporal optic disc borders. This type of loss however becomes obvious when more than half of the NFL thickness is lost. It has been suggested that wedge shaped localised NFL defects are likely to occur in areas of diffuse RNFL thinning and conversely that localised defects expand to highlight areas of diffuse damage (Sommer *et al*, 1991). Wedge shaped NFL defects usually seen in patients with

arcade field damage, are characteristic features of glaucomatous pathology (Jonas & Xu, 1994).

1.7.2 Neuroretinal rim loss: patterns of thinning

The degeneration of nerve fibres becomes evident at the ONH as thinning of the neuroretinal rim. From histological analysis of human glaucomatous optic nerve heads, Quigley and colleagues (1981) reported that early cupping is actually a manifestation of nerve fibre loss and not a result of rearrangement and/or damage of the neuroretinal rim glial component (Quigley *et al*, 1981). In glaucoma, the reduction in the neuroretinal rim may initially show a diffuse mode and/ or regional preferences. Pederson and Anderson (1980) reported a symmetrical expansion of the cup, appearing round in ocular hypertensive eyes progressing to glaucoma before visual field loss (Pederson & Anderson, 1980). A cross sectional study including normal, hypertensive and glaucomatous eyes with visual field loss showed a significant reduction of the rim width at the poles and possibly at the temporal horizontal direction among the glaucoma eyes compared to the normal group. However, no significant findings were identified for the ocular hypertensive group (Jonas *et al*, 1998b). As a general observation, rim loss starts predominately in the temporal inferior sector, followed by the temporal superior, the temporal horizontal and finally the nasal sector. In the more advanced stages, the rim loss is rather generalised, with the nasal region affected last (Jonas, Fernandez *et al*, 1993). Eyes with displaced central vessel trunk also exhibit this sequence of neuroretinal rim loss (Jonas & Fernandez, 1994). It is likely that any region of the optic disc may be affected at a given time but the location of most pronounced rim loss varies with the severity (Jonas, Budde *et al*, 1999b). Observations on

preperimetric glaucomatous eyes concluded that the total neuroretinal rim area was the best discrimination planimetric variable, suggesting that in early stages of glaucoma the loss is uniformly occurring in all sectors. Other studies also agree that diffuse patterns of rim loss are more common than focal changes (Emdadi, Zangwill *et al*, 1998; Garway-Heath & Hitchings, 1998).

The most distinct patterns of glaucomatous optic disc damage are associated with recognised patterns of rim thinning (Budde, Jonas *et al*, 1999). For example, focal glaucoma exhibits localised loss of neuroretinal rim occurring at the poles, while the remaining rim appears relatively intact. Commonly, for glaucomatous myopic eyes rim thinning occurs mainly temporarily, inferiorly and/or superiorly (Broadway *et al*, 1999). Diffuse rim loss has been demonstrated in OAGs in strong association with advanced age. These cases are usually described as senile sclerotic glaucoma and are concurrent with concentric cup enlargement (Broadway *et al*, 1999; Jonas & Xu, 1993). As the disease advances, it becomes more difficult to recognise distinct patterns in the development of glaucomatous damage (Jonas, Bergua *et al*, 2000; Jonas & Budde, 2000). Given the pattern of progression of the visual filed loss, early changes must occur in the upper nasal part of the ONH and end changes occur in the inferior temporal region (Jonas *et al*, 1999b). However, it has been suggested that there might be a strong bias from the observation of the visual field loss that leads us to think that the rim is lost mainly superiorly and inferiorly to the disc.

Neuroretinal rim loss evident in non-glaucomatous neuropathies is also associated with changes of colour and is predominately occurring with a characteristic sectorial pattern (Fournier, Damji *et al*, 2001).

1.7.3 Glaucomatous cupping

Attenuation of the neuroretinal rim results in an increase of the cup size. Because of the horizontally shaped cup situated in a vertically oval, the cup to disc ratio is normally bigger for the horizontal meridian and smallest for the vertical meridian. Therefore, the enlargement of the cup is evident when the former relationship is reversed (Jonas & Naumann, 1989; Jonas *et al*, 1989c; Jonas & Budde, 2000). Large discs usually exhibit bigger cups, which may be susceptible to glaucomatous enlargement (Burk, Rohrschneider *et al*, 1992; Jonas & Grundler, 1997a). A vertical elongation of the cup is an early sign of glaucomatous damage, described with the cup to disc ratio at that meridian. However, enlargement of the cup area over time is a characteristic feature of various developing optic neuropathies.

1.7.4 Remodelling of the lamina cribrosa

The morphological changes at the cup are associated with a compression of the lamina cribrosa, which bows posteriorly. The inherent elasticity of the lamina cribrosa structure is decreased in glaucoma patients, although this could also be partly attributed to ageing (Azuara-Blanco *et al*, 1998). It is suggested that the bowing of the lamina cribrosa may compromise the nutrition of the rim, as that assumes a longer distance from the vessel trunk. Larger glaucomatous discs would favour a more pronounced displacement of the lamina cribrosa (Jonas *et al*, 1999b). Moreover, advanced glaucoma is associated with the loss of supportive

collagen tissue and distension of the lamina cribrosa pores (Miller & Quigley, 1988). The displacement of the laminar plates that may accompany these structural changes is likely to obstruct the normally direct route of the axons through the lamina cribrosa (Morgan *et al*, 1998) and increase their susceptibility to compression. Interestingly, histological observations suggest that the remodelling of the lamina cribrosa continues to take place even when there is not a notable progression of glaucomatous damage (Tezel *et al*, 2004).

1.7.5 Disc size as a factor for glaucomatous damage

Jonas (1991) first suggested that glaucomatous susceptibility was not related to the optic disc size (Jonas, Gusek *et al*, 1991). Small ONHs are susceptible to glaucoma (Jonas *et al*, 1992b; Quigley *et al*, 1991b) but larger glaucomatous discs would favour a more pronounced displacement of the lamina cribrosa and the central vessel trunk (Jonas *et al*, 1999b). Not surprisingly, a considerable overlap of disc measurements was reported between normal and glaucomatous populations (Caprioli, 1992). Similarly, recent investigations reveal that glaucomatous damage, as it is depicted upon the ONH configuration in African and White Americans, may be variable but is independent of the racial difference in disc size (Girkin, McGwin *et al*, 2003). Conversely, investigations of the mechanical behaviour of the ONH structure reveal that IOP induced stress would be more severe on optic discs with larger diameter (Burgoyne *et al*, 2005).

Moreover, for the subgroup of glaucoma patients that damage has primarily a vascular aetiology it is worth noting that smaller sized glaucomatous optic discs have been correlated with increased arterio-venous passage (AVP) times, alleged

to depict venous outflow obstruction (Arend, Remky *et al*, 2002). Nevertheless, glaucomatous eyes with larger myopic discs have been also associated with findings of reduced retrobulbar circulation (Nemeth, Michelson *et al*, 2001).

1.7.6 The retinal vessels in glaucoma

Retinal vessels are thought to influence the susceptibility of the retinal nerve fibres to glaucomatous damage as they provide them with nutritional support and possibly act as an element of additional anatomical support within the ONH structure. Within the NFL it is speculated that the vessels may protect the nerve fibres from the mechanical forces and even the various metabolical changes associated with glaucomatous pathogenesis at the retinal plane, simply by inducing local elevation of the nerve fibres (Chihara & Honda, 1992). Furthermore, it is controversial whether the presence of cillioretinal arteries could be an additional protective parameter against the progression of damage especially in the temporal ONH region (Lee & Schwartz, 1992) or they have a rather insignificant influence in glaucomatous progression (Budde & Jonas, 2003a, 2003b).

Baring of the vessels is a common feature of the glaucomatous retina. This is a direct result of the gradual thinning of the nerve fibre layer and possibly a combined degeneration of the glial component of the vasculature, allowing the vessels to have a more distinct appearance than usual: they are normally embedded in the nerve fibre layer and enveloped by the glial limitans. Prominent appearance of the vessels is also observed at the optic nerve head with the additional feature of vessels hanging unsupported over the disc area. This effect is described as bayoneting of

the vessels and is increasingly apparent in correlation to the degree of thinning of the underlying rim area.

Furthermore, glaucomatous optic nerve head configuration can be associated with a characteristic displacement of the central vessels' trunk, towards the superonasal quadrant. It is suggested that this rearrangement, favoured in larger optic discs, can be attributed to the glaucomatous remodelling of the lamina cribrosa and has direct implications on the blood supply of the rim area and the peripapillary retina (Jonas & Fernandez, 1994).

1.7.6.1 Structural abnormalities of the vessels

The immediate disruption of the vasculature becomes evident in the appearance of the involved vessels. The vessel maintenance is generally adjusted to the nutritional demands of the tissues, thus damage to the ganglion axons and death of the ganglion cells in neuropathies has a shrinking effect on the supporting vasculature. Changes in vessel density in the involved tissues are also likely to be accompanied by other structural alterations. Vessel disturbance may assume a number of appearances with constricted and/or dilated segments of the vessels in various combinations and in different locations. Changes in the vessel configuration are observed under ischaemic and atrophic conditions in the retina such as occlusions of the large blood vessels, the CRA and/or the PCAs. Ocular pathological conditions are likely to induce ischaemic episodes at the ONH while, systemic vascular abnormalities target the choroid and subsequently influence the blood flow within the adjacent retinal tissues. Such ischaemic lesions in the choroid

or the retina are likely to involve the arteries rather than the veins and may show a permanent or transient profile (Hayreh, 1996).

Arteriolar calibre changes are described by different terms according to the characteristics of the involved vessels. A single sequence of a narrow segment followed by a distinctively wider segment along the vessel body is described as focal narrowing (Pedersen, Grunkin *et al*, 2000). Constriction of the vessels adjacent to the disc margins is termed proximate constriction and a repeated appearance of narrow segments followed by wider segments along the vessel can be referred to as beading of the vessels. Vascular tortuosity is a combination of dilation and serpentine appearance of the vessels. In this condition, radial stretching of the blood vessel causes dilation and the serpentine path occurs because of longitudinal stretching. The tortuosity of the vessels may be focal when occurring only in a small region of retinal blood vessels, or it may involve the entire retinal vascular tree. Finally, vasospasm refers to the condition of general constriction and occurs when the vessels are stretched (Hayreh, Pe'er *et al*, 1999). Traction of the retinal arterioles can be concurrent to the collapse of the lamina cribrosa in migraine.

Oedema accumulated in and around the vessel wall may temporally produce narrowing of the blood column (Hayreh, 1996), whereas scarring and fibrosis of the vessel wall induces a permanent localised vessel narrowing (Pedersen *et al*, 2000). CRA occlusion is associated with irregular narrowing of the retinal arterioles that may appear more severe because of an accompanying oedema of the retina. However, this finding is associated with the early stages of the occlusion and the

arteriole diameter returns to normal as soon as the CRA is enclamped. In this case, the visual field loss is also a transient result (Hayreh, 1999).

Several studies have reported changes of vessels' appearance accompanying glaucomatous damage, although there are speculations that those observations actually were artefacts due to localised retinal swelling (Hayreh, 1996; Hayreh *et al*, 1999). Rader and colleagues (1994) have observed proximal constriction of the peripapillary retinal arterioles and generalised narrowing among NTG patients (Rader, Feuer *et al*, 1994). Glaucomatous and non-glaucomatous optic neuropathy has been implicated in the occurrence of focal narrowing and general constriction, with higher prevalence among NTG patients (Papastathopoulos & Jonas, 1995). Proximal constriction of the peripapillary retinal arterioles has been also observed in ocular hypertensive patients, correlating with the magnitude of the peripapillary atrophy and the severity of field loss in those patients that progressed to glaucoma (Rankin *et al*, 1996). Considerable changes of the diameter of the temporal vein were noted in OAG patients (Lee, Uhm *et al*, 1998). Focal narrowing was associated with rim thinning and progression of glaucomatous damage (Papastathopoulos & Jonas, 1999). Finally, generalised vascular constriction was observed within areas of peripapillary atrophy corresponding to visual field loss in OAG patients (Hall, Andrews *et al*, 2001).

Interestingly, glaucoma animal models resulting from induced IOP elevation do not demonstrate retinal blood vessels' abnormalities (Cioffi, 2001; Sawada & Neufeld, 1999). Of course, the use of animal models in glaucoma studies is debatable, as acute induced damage cannot adequately represent the slow progressive

mechanisms usually seen in the disease (Goldblum & Mittag, 2002). However, the findings by Neufeld (1999) could also compliment the hypothesis that glaucomatous pathogenesis is likely to be associated with vascular changes occurring in the deeper retinal layers (Neufeld, 1999).

It has been recently suggested that changes of the retinal vasculature at the capillary bed are likely to be responsible for NTG pathology since reduced velocities occur in the retrobulbar vessels without apparent structural abnormality (Arend *et al*, 2002). The regulatory function of the capillary bed in glaucoma has been largely overlooked by previous studies, as attention has been placed almost exclusively on the large vessels. Not surprisingly, the choroid demonstrates arteriolar narrowing in correlation with conditions of high systolic blood pressure. Furthermore, choroidal circulation is probably the first site of damage in systemic hypertension and hypertensive choroidopathy, as demonstrated from experiments on spontaneously systemically hypertensive rats that identified prominent narrowing and tortuosity of the choriocapillaries (Bhutto & Amemiya, 2002). Moreover, the large concentration of pericytes in the choriocapillaries seems likely to stimulate mechanisms of the autoregulation system. It is suggested that the choroidal vasoconstriction mediated mainly by the pericytes, leads to acute ischaemia that may become chronic both in systemic hypertension and in diabetes (Hurcomb, Wolffsohn *et al*, 2001).

Focal narrowing of the retinal arterioles can also occur in other systemic diseases. Both in arteriosclerosis and diabetes mellitus, the changes in the vessels diameter is believed to be indicative of the risk level of the vascular disease. Similarly, venous beading and fluctuation of the vein diameter are strongly correlated with

disease progression in diabetic retinopathy (Pedersen *et al*, 2000). The retinal vessel diameters are directly influenced by retinal oxygenation and vasodilation is an indicator of the hypoxic state of the retina. Progressive vasodilation has been associated with progressive diabetic retinopathy and following laser photoagulation the vessels were seen to constrict, reflecting the improvement of the oxygenation (Stefansson, Landers *et al*, 2005). The ageing retina shows less prominent, but similar, vascular changes to those observed in hypertension and diabetes (Pedersen *et al*, 2000). Comparative studies between healthy subjects have also demonstrated a decreasing vasoconstriction of the arterioles with increase in age (Blum, Scherf *et al*, 2001).

1.7.6.2 Haemorrhages

Impaired circulation is a causative factor for haemorrhagic episodes in the retina. Haemorrhages may accompany vasospasm and occlusion of the CRA, associated with various pathologic conditions. Moreover, haemorrhages can result from the mechanical stretching and rupture of the vessels, likely to occur in tessellated retinas. They are usually developed at the infero-temporal or supero-temporal disc margins and are flame-shaped. Haemorrhages are transient in nature, usually absorbed by the retina within 2 to 6 weeks after their occurrence. For this, they are difficult to be assessed and only a minor number is successfully recorded in population screening. Haemorrhages are recognised as risk factors for glaucoma (Jonas & Hayreh, 1999). They are specifically associated with NTG pathology and recent findings have reported negative associations of haemorrhages with high IOP levels and therefore with cases of pressure dependent glaucomatous damage (Soares, Artes *et al*, 2004).

Haemorrhages are spatially significantly correlated with existent rim notches and RNFL defects (Sugiyama, Tomita *et al*, 1997b). Haemorrhagic episodes are usually sited at the optic nerve quadrants that have the most prominent glaucomatous damage (Hayakawa, Sugiyama *et al*, 1998; Law, Choe *et al*, 2001; Sugiyama, Tomita *et al*, 1999). It is also postulated that the occurrence of haemorrhages corresponds to locations where the rim is still intact but subsequently rim notches are developed (Jonas & Fernandez, 1994; Law *et al*, 2001).

Haemorrhages are an acute expression of atrophy developed at the ONH and may develop in neuropathies besides glaucoma. However, different rates of occurrence have been recognised, with the highest relative frequency observed among the glaucomatous population (Hayakawa *et al*, 1998; Sugiyama, Tomita *et al*, 1997a; Sugiyama *et al*, 1997b; Sugiyama *et al*, 1999). A variety of factors predispose to the occurrence of haemorrhages, including gender and racial classification. Haemorrhages are prevalent in women and are strongly associated with age progression both in pathologic conditions and also among healthy individuals (Healey, Mitchell *et al*, 1998; Sugiyama *et al*, 1999).

1.7.7 Peripapillary atrophy

The peripapillary chorioscleral crescents become more visible with glaucomatous RNFL loss but they may also represent acquired atrophy of the retinal pigment epithelium, the choroid or combination of them. In pathologic conditions such as glaucoma, the retinal pigment epithelial cells are decreasing in number (Curcio *et al*, 2000; Panda & Jonas, 1992). A number of conditions have been associated with

the aetiology of PPA , including a congenital anatomic variation at the peripapillary retina and myopic retinal changes as well as factors more specific to glaucoma

In glaucoma, both zone Alpha and zone Beta are relatively enlarged and more prevalent than in the normal eye. This has been demonstrated from experimentally induced glaucomatous damage on animal models (Hayreh *et al*, 1999). Zone Alpha is distributed around the optic disc in a manner similar to the normal eye but because of the relative enlargement the zone becomes more distinct and the differences between the two zones are particularly apparent on the nasal side (Jonas, Budde *et al*, 1999a; Jonas & Budde, 2000). In comparison to Zone Alpha, Zone Beta is more reproducible (Park, Park *et al*, 2001; Uchida, Ugurlu *et al*, 1998). Zone Beta is usually present in glaucomatous eyes and has a uniform distribution around the ONH (Uhm, Lee *et al*, 1998). It exhibits considerable differences in size between the various glaucoma groups (Jonas *et al*, 1999a). Highly myopic glaucomatous eyes show an increased prevalence of scleral crescents that contribute to the atrophic appearance of the peripapillary region (Dichtl, Jonas *et al*, 1996). Discrimination between glaucomatous and healthy eyes cannot be achieved by the observation of Zone Alpha, alone. The high inter-individual variation in the normal appearance means that the zone can only be effectively assessed on an individual basis over the follow-up period.

PPA seemingly reflects the degree of glaucomatous damage. The extent of peripapillary atrophy increases with increase in the extent of ONH cupping as expressed in terms of the C/D ratio (Jonas *et al*, 1992a) and with a decrease in the neuroretinal rim width (Emdadi *et al*, 1998; Jonas & Grundler, 1997a; Park, Tomita

et al, 1996b). Zone Beta is associated with a mostly concentric loss of rim width and both zones show a spatial correlation with the sectors exhibiting the most marked rim loss.

The PPA is also strongly correlated with functional loss. Zones Alpha and Beta correspond to relative and absolute scotomata, respectively. The correlation with visual field loss is greater for zone Beta. The presence and location of zone Beta corresponds to the extent of focal visual loss (Emdadi, Kono *et al*, 1999; Tezel *et al*, 2000).

PPA shows different prevalence and distribution within the different types and subtypes of glaucomatous damage (Jonas & Xu, 1993; Jonas & Budde, 2000). This variation is probably due in part to the different mechanisms of pathogenesis activated in the different types of glaucoma. Overall, PPA has been frequently observed in NTG patients and, unlike other glaucomatous features, PPA expansion and progression does not correlate with higher IOP levels, further supporting the vascular component of the aetiology of PPA (Sugiyama *et al*, 1997b). Interestingly, PPA is more frequent among OHT patients that subsequently develop glaucomatous damage (Stewart, Connor *et al*, 1995). Additionally, PPA has strong associations with selected phenotypic appearances of glaucomatous damage. As previously described, crescents of PPA are a common feature of myopic and/ or tilted glaucomatous eyes. In senile glaucoma, areas of PPA are usually expanding evenly around the ONH and discs that demonstrate a concentric enlargement of the cup are also reported to have small areas of PPA (Broadway *et al*, 1999; Nicolela & Drance, 1996; Nicolela, Drance *et al*, 2001).

PPA has been specifically associated with the progressive stages of glaucoma. Follow-up studies on ocular hypertensive patients that subsequently develop glaucoma reveal the gradual enlargement of the PPA (Tezel, Kolker *et al*, 1997a; Tezel, Kolker *et al*, 1997b). However, enlargement is an aspect of PPA only seen in glaucoma; whereas in normal eyes and in other neuropathies the PPA area is quite stable over time. Recent studies emphasise the ability of PPA to assist the differentiation of glaucoma from other neuropathies. Glaucoma-like discs (GLD), likely to be misdiagnosed as NTG because of the common intrapapillary appearance of the two conditions, may be discriminated due to their remarked differences in the extent of PPA (Park *et al*, 2001). Similarly, the ONH in Anterior ischaemic optic neuropathy may show cupping of the disc and rim loss but enlargement of the PPA hasn't been observed at any stage of the disease (Hayreh & Jonas, 2001).

1.8 Neuroprotection

Neuroprotection is the concept of medical treatment applied directly to the retina and to the optic nerve thereby preventing or counteracting the apoptotic process of the ganglion cells. Neuroprotective methods could optimally act as a shield for cell groups and structures that demonstrate high sensitivity and/or susceptibility to IOP elevation and/or ischaemia. For the degenerating retina, substances that block key chemical reactions of the apoptotic metabolism could prevent cell death (Nickells, 1999; Osborne *et al*, 1999). Studies have identified the potential in glial derived neurotrophic factors (GDNF) to increase the impaired expression of glutamate transporters in excitotoxic environment and regulate the increased intracellular glutamate levels, sparing the neurons (Naskar *et al*, 2000). Other therapeutic

procedures address the conditions of secondary degeneration of the ganglion cells (Hartwick, 2001; Vorwerk *et al*, 1999b).

1.8.1 The debate of selective ganglion cell death in glaucoma

Early histological findings on human glaucomatous eyes and primates have demonstrated a selected loss of large diameter optic nerve fibres throughout all portions of the optic nerve. However, the results of this study and other similar histological studies have been strongly questioned on the basis of structural changes and shrinkage of the ganglion cells that occurs before apoptosis (Glovinsky, Quigley *et al*, 1991a; Glovinsky, Quigley *et al*, 1991b; Quigley, Sanchez *et al*, 1987).

Findings by Vickers and colleagues (1995) have also highlighted inconsistencies between the ganglion cell population appearing to degenerate in the retina and the representation of the population at the lateral geniculate nucleus (Vickers, Schumer *et al*, 1995). Although loss of the larger axons was documented at the level of the retina fibres (Vickers *et al*, 1995), non selective loss for both large and small axons was demonstrated at the level of the lateral geniculate nucleus in the monkey glaucoma model (Vickers, Hof *et al*, 1997).

Results from studies on automated perimetry and electrophysiology suggest early functional deficits in glaucoma involving both the M or P cell pathways (Graham, Drance *et al*, 1996; Harwerth, Carter-Dawson *et al*, 2004; Yucel, Zhang *et al*, 2003).

Although glaucoma does not seem to affect selectively some ganglion cells populations, it is still evident that some ganglion cells may undergo apoptosis in earlier rather than later stages of glaucomatous damage. Quigley (1998) proposed that a proportionally bigger assault for the large nerve fibres might be encouraged purely by reasons of regional vulnerability that the ONH structures might be showing, with specific reference to the anatomical variance of optic disc size and the anatomy of the lamina cribrosa (Quigley, 1998). On the other hand, ocular hypertensive mouse eyes undergoing glaucomatous damage revealed a pattern of preferential nerve axon loss, at the superior and inferior poles of the ONH, however predominately affecting the axons of the superior portion (Mabuchi, Aihara *et al*, 2004). This was an interesting finding given that the mouse eyes lack a lamina cribrosa structure.

There are also some speculations of selective glaucomatous loss referring to ganglion cells undergoing phases of secondary degeneration and how they might be showing different possibilities for survival in a state of sickness after encountering the initial glaucomatous assault with regards to their size. It was reported that NMDA mediated toxicity resulted in more pronounced damage in ganglion cells with relatively longer axons and larger bodies (Vorwerk *et al*, 1999a). Similarly, glutamate induced excitotoxicity on cultured pig retinal ganglion cells demonstrated both large and small neurone death over a prolonged period of time, with however greater effects on the larger retinal ganglion cells (Wehrwein, Thompson *et al*, 2004).

Assumptions of differences between the neurons that selectively survive for shorter or longer periods of time compared to the neurons that undergo immediate apoptosis (Luo *et al*, 2001; Osborne *et al*, 1999). A recent study has suggested that different degrees of damage in glaucoma animal models subjected to similar procedures may be attributed to different levels of autoimmune response, that can be activated within the retinal ganglion cells as an inbuilt neuroprotective mechanism against glutamate upregulation accompanying the glaucomatous assault (Osborne *et al*, 2004).

1.8.2 Are the surviving cells functionable?

It is known that degeneration of the retina encourages a remodelling of the cells and rewiring of the retina, leaving the cells appearing active when tested electrophysiologically, but without a meaningful function (Marc & Jones, 2003; Marc *et al*, 2003). Moreover, there is electrophysiological evidence on glaucomatous ganglion cells being compromised functionally while the accompanying structural damage is very early and cannot be detected on the ONH. However, when the ganglion cells die because of axotomy and subsequent deprivation from neurotrophic factors it is unknown if the initiated apoptotic procedures can be reversed and it is yet to be seen if retinal ganglion cell can possible regenerate the injured axons and re-establish their connection with the brain. Moreover, it is still unclear if neuroprotective strategies were to be successful, the surviving cells would be functional. A recent clinical study suggested that successful restoration of IOP levels in glaucoma patients with very early stages of damage resulted in sparing the neurons as demonstrated by improvement of their electrophysiology recordings (Ventura & Porciatti, 2005).

1.9 Perimetry

Visual dysfunction may be assessed by clinical perimetry methods. These methods involve the subjective measurement of differential light sensitivity across the visual field. Kinetic perimetry employs a stimulus of constant size and intensity that moves with the optimal rate of 4 degrees per second at the boundaries of the visual field, from non-seeing to seeing areas (Johnson & Keltner, 1987). This technique is however not sensitive to early localised depressions. Conversely, static perimetry utilises a stationary stimulus of constant size with variable intensity measuring the visual threshold at a specific location of the visual field.

1.9.1 Stimulus intensity

A stimulus with a brightness of 1 log unit is 10 times brighter than the background, (a stimulus of 2 log units is x100). Brightness is usually expressed with decibel units. For conversion, 1dB = 0.1 log units. Smaller decibel measurement relates to greater stimulus brightness. When stimuli of great brightness are employed for the visual field testing, retinal sensitivity is rather low.

There is a choice of six sizes of stimuli used in perimetry, known as Goldmann size stimuli, ranging from the smallest Goldmann size 0, to the largest Goldmann size V stimuli. The diameter of a given Goldmann stimulus is twice that of the immediate smaller one. Goldmann size III is the default size for the white-on-white (W-W) perimetry which is using a white stimulus presented on a white background, as performed with the Humphrey Field Analyser. The Goldmann size III covers an area of 4mm2 that subtends 30.71 min of arc (0.471 degrees) onto the retina, at a viewing distance of 30cm and has been chosen to be the standard presentation

because it is known to be less effected than smaller size stimuli by optical defocus (Heijl, 1985), while it shows equal variability of threshold sensitivities with the bigger size stimuli within a retinal eccentricity of 30 degrees (Gilpin, Stewart *et al*, 1990).

1.9.2 Threshold light sensitivity

Perimetry measures the differential light sensitivity against a constant background illumination. The visual threshold at a given location is defined as the luminance of a stimulus that is just perceived, or that is seen only 50% of the times it is presented. The Humphrey perimeters use the bracketing strategy to measure visual threshold: At a given location stimuli light intensity is increased with 4dB steps until the patient gives the first positive response. Then the intensity decreases with 2dB steps until the patient does not respond. Therefore, the threshold light value is verified twice with a measurement resolution of 1dB.

1.9.3 Threshold measurement programs

Computerised perimetry is performed by a variety of visual field measurement programs. Some of them investigate the central 30 degrees field and measure thresholds at approximately 76 locations with a 6 Degrees resolution. Bebie *et al* (1976) first described the fluctuation that can be seen in visual field thresholds distinguished in short term fluctuation (STF) and long term fluctuation (LTF) (Bebie, Fankhauser *et al*, 1976). Short term fluctuation, (STF), is the variation in responses that occurs over the performance of a single test. It is a combination of the instability of the tested threshold, a measurement error and variable levels of cooperation or attentiveness shown by the patient.

One component of the short term fluctuation is the variability of the patients' responses as shown by the variability of threshold measurements at a limited number of test locations that are selectively measured twice. The SF or RMS is the square root of the variance of these double determinations and the higher the value the greater this patients' response variability for a given location of the visual field. Test locations that are double determined during the course of a single visual field testing and happen to lie along the edge of a scotoma are likely to result in an increased SF.

The variability of responses in normal individuals is known to be greater in the periphery than in the central visual field (Haas, Flammer *et al*, 1986). Consequently, within the statistical maps that compare the measured threshold values with age matched scores, the difference should be greater in the periphery than in the central field in order to consider the findings significantly different. Patients with glaucomatous field loss have demonstrated increased STF compared to normal subjects while glaucoma suspects (OHTs) had intermediate values of STF, lying between the glaucoma and the normal scores (Flammer, Drance *et al*, 1984).

Long term fluctuation (LTF) is the variation in responses that occurs over the performance of a repeated test. Homogeneous LTF is a unidirectional change in sensitivity occurring throughout the entire visual field, while heterogeneous LTF refers to different directions of change in sensitivity at different visual field locations. Knowledge of the magnitude of LTF for an individual is very useful for the interpretation of a series of visual field examinations in follow up examinations. LTF can be a confounding factor for the elucidation of visual field changes caused by

glaucoma using perimetry. Both STF and LTF are weakly correlated to each other but one cannot possibly be predicted by the other. Differential light sensitivity decreases with age at a constant rate and varies across the visual field increasing towards the more central locations (Flammer *et al*, 1984).

1.9.4 Humphrey STATPAC analysis package

The Humphrey STATPAC analysis package provides statistical summary indices of the visual field, that compare the measured threshold values across the visual field to a database of corresponding values derived from a large normal population. Statistical variables help to numerically define early functional loss (Flammer, Drance *et al*, 1985).

The average of all the measured thresholds across all the tested visual field locations is the mean sensitivity (MS). The average difference between the measured thresholds and similar scores derived from a database of age-matched subjects is expressed as the mean defect (MD). Although MD is influenced by localised field defects, it is most sensitive to diffuse depression of the visual field. Values of the MD statistically associated with normal limits range between -2dB to 2dB.

The GHT (Glaucoma Hemi Threshold) is a statistical indicator of any difference in sensitivities between the two vertical hemifields, thus showing asymmetry across the horizontal meridian.The spatial scatter of the measured thresholds is expressed by the PSD, which uses the standard deviation as a measure of variability (in dB).

The PSD indices when corrected for the STF define a new variable, the CPSD. This adjusted parameter is most sensitive to localised defects.

The presentation of the results derived with the Humphrey perimeter include a numeric display of the measured light threshold values; a display of the difference of the measured thresholds from the normal values of the database (total deviation); a graphic greyscale representation of these values; a display of the spatial variability in the threshold values which is adjusted for the overall sensitivity of the field (pattern deviation) and a set of probability plots that correspond to the total and pattern deviation maps and show the probability of the measured threshold values to be statistically different from normal.The numeric threshold maps can demonstrate localised defects and the comparative threshold plots are useful in detecting more diffuse depression of the visual field. Total deviation describes the height of the hill of vision, highlighting the array of differences of measured thresholds compared to the values from age-corrected normal subjects of the instrument's database. Pattern deviation incorporates a software correction function that takes into account the amount of sensitivity reduction that has occurred throughout the tested locations and removes that effect presenting the shape of the visual field and allowing focal defects to be readily identified. Probability analysis extrapolates the total and pattern deviation to the normal population.

1.9.5 The effect of stimulus size in the variability in threshold measurements

Large stimuli are associated with decreased variability. This is attributed to a greater likelihood of small stimuli to be degraded by the effect of refractive error

and/ or existing media opacities. Moreover, the effect of spatial summation which is greater in the peripheral than the central field might account for the reduced variability observed when smaller size stimuli are used to test central field locations (Anderson & Patella, 1999). Similarly, a reduced number of stimulated receptive fields have been suggested to account for the SF, LF and normal inter-individual variability associated with smaller stimulus sizes testing areas of damage.

1.9.6 Visual field loss in glaucoma

A gradual diminution of sensitivity generates relative scotomata that develop into absolute scotomata. The first obvious visual consequence of glaucoma is visual constriction. Visual field loss in glaucoma follows a characteristic pattern of damage resulting from defects of the retinal nerve fibre layer (RNFL).

1.9.7 Limitations of perimetry

Factors like refraction, artefacts, fatigue and the age variation influence the results of visual field testing. Also, the lengthy examination perimetric procedures are not optimal for screening purposes. Finally, it is a technique that is largely dependent on the patient's performance both in terms of speed of their response and also in terms of how well they have understood the instructions they were given. The subjective nature of perimetry is also enhanced by the fact that visual field integrity is evaluated by comparisons with a normative database of sensitivity levels across the visual field. Perimetry is applicable for early, moderate and advanced damage by glaucoma and when evaluating a single test it is particularly valuable when previous reference of perimetric performance for the same patient exists. It is

speculated that the VFT pattern in glaucoma is biased because of limited examined locations and the size of stimulus tested over the period of a single examination.

1.10 Imaging

Compared to perimetry, investigation of glaucomatous damage with imaging techniques appears more appropriate. Firstly, the reduction in differential light sensitivity as evaluated by perimetry does not correlate with the numbers of retinal ganglion cell loss, with almost 40% of ganglion cells being lost prior to the occurrence of a visual field defect (Quigley, Addicks *et al*, 1982). Additionally, the structural changes may not be associated with ganglion cell loss but be attributable to the reorganisation of the extracellular matrix or laminar position, therefore not necessarily resulting in visual field damage (Chauhan, McCormick *et al*, 2001). Finally, the relative scale of measurement for visual field progression is coarser than that for ONH progression (Chauhan *et al*, 2001; Harwerth, Crawford *et al*, 2002).

1.10.1 Fundus photography

Photographic techniques record the overall appearance of the RNFL; investigating areas of increased vessel visibility and disruption of the nerve fibre bundles that appear as dark striations. At the ONH, optic disc size, the vertical cup to disc ratio, the neuro-retinal rim width, the appearance of the lamina cribrosa, the position of the vessel trunk and the integrity of the vessels are all points of interest. Equally important, is the configuration of the peripapillary area that may show signs of atrophy.

1.10.2 Red free photography

When photographed the fibres appear like bright striations within darker areas. This image is the result of the reflected light on the nerve fibre bundles structure and at the same time, the light absorption by the retinal pigment epithelium (Kaufman & Mittag, 1994). Red free monochromatic RNFL photographs highlight the RNFL texture and the outlines of the small retinal vessels, normally embedded under the nerve fibres. The degree to which the vessels are visible shows the degree of their coverage by the nerve fibres and give an indirect indication of the NFL thickness at any given location. (Blumenthal & Weinreb, 2001).

1.10.3 Stereophotography

Stereophotography involves images captured by stereoscopic cameras, acquiring a pair of images simultaneously. The two images are fused into one when suitably viewed, with the assistance of projectors or computerised systems. Stereophotography will be discussed extensively in Chapter 5.

Planimetry refers to the part of this method that uses stereo photographs to produce one-dimensional measurements of the ONH structure. It involves the demarcation of the ONH properties on the stereophotographs and the measurements of the features. The procedure may be manually performed or by using computer technology.

The use of stereophotography in detecting the structural changes of a patient's ONH overtime is termed "chronoscopy". Chronoscopy is based on the sequential presentation of the stereoimages. This method is shown to increase the sensitivity

of discrimination between normal and glaucomatous eyes. However, the stereo viewer still demonstrates a big specificity as it allows a more detailed examination (Barry, Eikelboom *et al*, 2000).

1.10.4 Confocal scanning laser topography

A scanning laser tomograph (HRT) uses the confocal scanning laser optical principle, combined with sequential multi-layer imaging. The fundus is scanned with a small beam of laser light (670nm) projected through a pinhole and the light reflected from the retinal surface of interest is collected by a detector that blocks all signals outside the set focal plane. A series of two-dimensional images produced by the scanning across the retina at different focal planes give rise to a layered three-dimensional image. The HRT computes 32 consecutive images derived at 32 equidistant depths with a resolution of 256 x 256 pixels.

The operator inputs the refractive correction of the examined eye expressed as a mean sphere value and may customise the scan depth and field of view (10, 15 or 20 degrees) for the HRT topography scan. The scaling factors of the HRT images have been evaluated with a model eye (Janknecht & Funk, 1994) and the measurements were found comparable to in vivo measurements of the retinal properties as obtained during vitrectomies (Bartz-Schmidt, Thumann *et al*, 1999). A quality control system evaluates the acquired mean topographic images automatically. The acquisition of 3 quality scans that are averaged in a mean 3D topography image of the ONH for analysis has been proved to give more reproducible pixel topographic measurements (Weinreb, Lusky *et al*, 1993).

The HRT II was introduced in 1999 as an advanced version of the HRT. It has a fixed field of view of 15 degrees, automatically sets the scan depth depending on the disc depth and acquires a series of 16 to 64 plane scans of 384 x 384 pixels each. Also it acquires three consecutive scans and controls each scan for brightness determining the quality of the final images. Furthermore, it has an internal fixation point for the examined eye, as opposed to the external target used in HRT, is slightly faster in acquiring the images and has a lower commercial price making it more approachable for clinical use.

Both planimetric and volumetric measurements of the optic disc are available with the HRT method. The instrument estimates the global disc, rim and cup areas; the maximum cup depth and cup volume; the cup to disc areas ratio; the rim volume and segmental rim areas distributed in six sectors: superior temporal (45°); superior nasal (45°); inferior temporal (45°); inferior nasal (45°); temporal (90°) and nasal (90°).

For the differentiation between the rim and the cup areas of the ONH images, HRT utilised a fixed reference plane which was positioned 320 μm below the estimated mean retinal height of the examined eye but in HRT II this reference plane is defined by the mean contour line for the disc margin. HRT II has a set reference plane at 50 μm below the 350-360 degrees segment of the disc margin, in correspondence with the rather unchangeable in glaucoma papilomacular bundle and in a depth that is larger than two standard deviations of the average segment height reproducibility as estimated for glaucoma eyes.

Independent of the reference profile, the HRT II provides a graphical presentation of the retinal surface height profile along the disc contour line and estimates the "height variation contour" as the difference in the most elevated and most depressed part of the contour line. In addition, it computes the "mean retinal nerve fibre layer thickness" which is the mean height difference between the standard reference plane and the height profile along the contour line.

The obtained measurements are simultaneously analysed with classification techniques incorporated in the HRT and HRT II respectively. The HRTC classification is a software-provided discriminant analysis formula of the HRT expressing a linear combination of the rim volume, cup shape and height variation contour measures and the age factor (Mikelberg, 1995). The examined eyes scoring negative values with this classification are classified as abnormal (lester, Mochi *et al*, 1997).

The HRT II has incorporated the Moorefield's' analysis which is age and disc size corrected. All sectors are evaluated in comparison with a normal database using Moorfields' regression before classified as normal, borderline or glaucomatous. For every rim sector, there is an actual and a predictive value of size estimated. The predictive value of the sectorial rim is estimated according to the subject's age and the overall size of the disc area, determining the final classification of the disc. The Moorfields' regression Analysis (MRA) compares the log of the measured neuroretinal rim area with the predicted age-corrected and disc size adjusted rim area derived from a normative database (Wollstein, Garway-Heath *et al*, 1998). For each eye, MRA is evaluated both globally and regionally for the temporal superior

(46-90), nasal superior (91-135), nasal (136-225), nasal inferior (226-270), temporal inferior (271-315) and temporal (316-45) sectors, respectively. If the measured log rim area is lower than the software specified 99.9% cut-off, based on healthy eyes, for the entire disc or for any of the regions, the eye is classified as abnormal.

Add-on software packages have been used in conjunction with the HRT principal software enabling the assessment and evaluation of areas in the peripapillary retina and macula. Specialised custom software has been used for the evaluation of the peripapillary atrophy (Park *et al*, 1996b) providing estimates of the total atrophic area, the angular extent and radial extent describing this area; the maximum distance away from the disc margin that the atrophic area expands to and the maximum disc radius corresponding to this location.

The use of the mean of three images to obtain the topographic measurements has been applied in most studies involving the HRT creating more objective measurements (Weinreb *et al*, 1993). Errors of measurement may manifest from the normal variability in pupil size of the examined patients and the appropriate adjustment of the reference plane for the images (Orgul, Croffi *et al*, 1997). It was shown that the HRT was more reproducible for non-dilated than for dilated pupils (Mikelberg, 1993), but Zangwill *et al* (1997) reported that dilation did not change the results when examining eyes with media opacities where dilation would have been a benefit (Zangwill, Berry *et al*, 1997). This effect was however questioned on the basis that the larger aperture of the light beam also increases the risk of misalignment between the focal properties of the instrument and the observed retina (Orgul *et al*, 1997).

HRT, when compared to manual planimetry, was found to underestimate the disc area and overestimate the rim area in both normal and glaucomatous ONHs (Jonas, Mardin *et al*, 1998c). HRT results seem affected by the disc size as large discs were classified as glaucomatous although their fields were normal and small discs with recordable field loss were graded as normal (Mardin, Horn *et al*, 1999). Wollstein and his coworkers (2000) used linear regression to account for the relationship of rim and disc area improving the detection of early glaucoma and ranking HRT as successful as the evaluation of stereoscopic optic disc photographs (Wollstein, Garway-Heath *et al*, 2000a). The scleral rim can be difficult to assess from the reflectivity and topographic HRT images, being a source of variability for the demarcation of the disc boundaries. Hatch *et al* (1999) reported an interobserver variability for the operator defined disc margins (Hatch, Flanagan *et al*, 1999). Therefore, for more reproducible contour line definition the HRT operator viewed the corresponding stereoscopic images whilst attempting to outline the disc margins (Iester, Mikelberg *et al*, 2001).

The instrument may also give false measurements of the rim area. Actually, the reference plane is used as a topographic cut-off, defining the structures below the plane as the cup and the structures above the plane as the neuroretinal rim. Among other factors, the variability in the rim size can be also attributed to the fact that the HRT method cannot identify tissue differences so it is likely that the blood vessels are included in the rim area and give higher estimates of the rim area than photograph planimetry (Dichtl *et al*, 1996; Jonas, Budde *et al*, 1998a).

When used to assess PPA, the HRT exhibits large variability in measurements compared with planimetric results obtained by stereo-photographs. The reproducibility for Zone Beta is better than for the Zone Alpha but accuracy is likely to be compromised when defining the inner borders of Zone Beta in ONHs with a broad scleral ring.

Mardin *et al* (1999) suggested that the combination of quantitative parameters in the form of discriminant analysis facilitates glaucoma detection with the HRT (Mardin *et al*, 1999). However, the discriminant analysis model showed different performance among discs with glaucomatous visual field damage but different glaucomatous disc appearances such as focal ischaemic discs, myopic discs, senile sclerotic discs, and discs with generalized cup enlargement highlighting the superiority of expert clinical optic disc evaluation over computer methods (Broadway, Drance *et al*, 1998). Similarly, Kesen *et al* (2002) estimated that diagnosis by clinical impression based on VFTs, IOP and the optic disc appearance was a more specific method compared to HRTC automated discrimination analysis (Kesen, Spaeth *et al*, 2002). As the authors suggested, the limited performance of the HRT may be attributed to the fact that the formula does not include key importance features such as focal rim loss.

The HRT is known to give poor visibility of disc haemorrhages but it shows great potential to detect changes over time (Kono, Jonas *et al*, 1999a). Hatch and colleagues (1999) suggested that the HRT is rather useful to detect follow up change than actually determine abnormality by comparison to a normal dataset

(Hatch *et al*, 1999). In follow up examinations the contour line is exported from the initial image (Roff, Hosking *et al*, 2001).

The progression analysis adjusts the follow up images for differences in quality. The baseline contour line is exported to the mean topographic images (MTI) of the follow up examinations. From each available MTI 384 x 384 clusters of 4 x 4 adjacent pixels are combined to form superpixels. A probability map displays a magenta coloured superpixel to indicate reduction of the topographic height compared with the baseline examination at a probability of $p>0.05$ and a green coloured superpixel to indicate elevation with a probability of $p<0.05$. Confirmed change is present when the significance value associated with the topographic height within a given superpixel is less than $p<0.05$ in a cluster of 20 superpixels for 3 consecutive sets of follow up images (Chauhan, Blanchard *et al*, 2000; Chauhan *et al*, 2001).

For the use of HRT in longitudinal studies it is worth considering the effects of disc compliance, likely to be modulated by IOP levels and the severity of glaucomatous disease, on the reproducibility of the reference plane and therefore of the obtained measurements (Tan, White *et al*, 2004).

Shape modelling allows the classification of the images by the HRT without using the contour lines (Swindale, Stjepanovic *et al*, 2000). The proposed technique is based on parametric mathematical modelling of the ONH shape and model parameters that produce the greatest degree of similarity between the model and

the image. These parameter values sufficiently describe the ONH morphology and can be used for the further morphologic analysis.

1.10.5 Optical coherence topography

With the optical coherence tomograph (OCT) two-dimensional topographic images of a thin optical slice of tissue may be obtained. The instrument provides higher resolution images than SLO utilising low coherence light. Low coherence interferometry generates a cross section of the retina, based on the different reflectivity of the retinal layers. Therefore, it provides information of the contour and thickness of the retinal properties and generates a colour-coded image of the retina. The measurements are based on the estimation of the delay between transmission and reflection on the observed structures. OCT can identify tissues of various structures and composition. For this, it analyses the polarisation of the reflected light and can potentially use many wavelengths of light. The relationship of the location of the high reflectance retinal layer that lies just under the inner retina to the measurements of the thickness of the RNFL is determined by computer algorithm (Schuman, Hee *et al*, 1995).

OCT provides tomographic images taken at different radial planes through the ONH and peripapillary region. The OCT instrument gives an estimation of the thickness of the RNFL as extracted from the lowest and the highest point of the measured profile and has identified the different thickness of the NFL between the temporal-nasal and inferior-superior disc margins. While the RNFL and the choroid are well visualised, the cup can also be examined very clearly. At the ONH, the OCT estimates the cup and disc diameters (*m) and the cup and rim areas (*m²). For

glaucoma detection, it uses circular scans around the optic nerve or radial scans through the optic nerve head (Huang, Swanson *et al*, 1991; Schuman *et al*, 1995). OCT may also give information on the anterior chamber of the eye. OCT generates the profile of the anterior chamber and estimates the dimension of the anterior chamber, the thickness and curvature of the cornea.

A big advantage of OCT is that, unlike other instruments, it doesn't use a reference plane. In comparison with the results from perimetry, OCT indications of RNFL thinning are in full agreement with recorded visual field defects and observed notches of the rim. The correspondence with the C/D ratio exists only for small and for big cups and provides equivocal results for medium sized discs (Huang *et al*, 1991; Schuman *et al*, 1995). OCT is considered ideal for both early diagnosis and quantitative monitoring. Unlike SLO and SLT, the retinal section subjected to observation is not limited by the size of the pupil or by ocular aberrations.

Latest studies suggest that OCT measurements, when compared to the results of histological studies, appear to underestimate the overall retinal thickness. At the ONH region, it gives the variation of the sectors, measuring a thicker layer at the poles of the disc and a minimum RNFL at the temporal side, but it shows an incorrect tendency to record a greater RNFL thickness at the superior than at the inferior pole. However, OCT exhibits high reproducibility when it assesses the entire retinal thickness rather than just the RNFL (Jones *et al*, 2001). More recent studies on the OCT reproducibility also demonstrate the effectiveness of the instrument in estimating the RNFL thickness (Funaki, Shirakashi *et al*, 2002).

Using OCT for quantitative evaluation of the ONH is not recommended. There is poor definition of the disc margins, arbitrarily taken at the termination of the pigment epithelium. However, comparison of cup to disc ratio estimates by expert observers with the OCT, with biometry and planimetry revealed that the cup area as assessed by the photographic methods could correlate well with the OCT calculated cup margins when defined half way down the cup excavation. There is an obvious problem with tilted discs and unlike photos the vessels configuration while dipping in the cup excavation is not available to assist cup definition. The OCT in comparison to red-free photography has higher diagnostic accuracy but is an inadequate method when differentiating ocular hypertensive and glaucoma suspects from normal (Soliman, van den Berg *et al*, 2002a; Soliman, de Jong *et al*, 2002b).

1.10.6 Scanning laser polarimetry

Scanning laser polarimetry (SLP) is a confocal laser ophthalmoscope with a polarization modulator, a cornea polarization compensator and a polarization detection unit. It uses a polarized laser (780nm) and directs light against the retina. The RNFL rotates the light that reaches it and disturbs its polarization from that initially arranged by the modulator. The degree of rotation corresponds to the RNFL thickness. The detection unit measuring the amount of light that is retarded when reflected back from the retina estimates the thickness of the RNFL. The less retardation recorded, the thinner is the assessed RNFL. The modulator is used to adjust the laser's state of polarization and the corneal polarization compensator neutralizes the polarizing properties of the cornea and the lens. In the scanning laser polarimeter (GDx), it is considered that the light is reflected mainly from the

outer margin of the retina, the RNFL is assumed the main source of interruption for the polarization and this interruption is also considered uniform. Depth resolution is based on assumptions about the optical properties of the retinal tissues; therefore, the GDx provides an indirect way of measuring the RNFL. The suspected inadequacy of the polarization compensator also reduces the credibility of the instrument.

It was shown that GDx overestimates the thickness of the RNFL around the ONH, when there is PPA. Errors of this kind could be avoided if the thickness of the temporal side was considered the standard value. Nevertheless, the various sizes of the ONH are another important source of measurement errors. Measuring the thickness of the RNFL can give only a rough approximation of the nerve fibre count. The IOP level and the cardiac pulsation influence the disc topography; therefore, all instruments assessing the ONH would show a compromised performance (Funaki *et al*, 2002).

1.10.7 Evaluation of the methods

All quantitative methods exhibit difficulty in distinguishing the normal appearance from that of early glaucomatous and sometimes even moderate glaucomatous damage. Assessment of advanced glaucomatous ONH gives higher rates of success. The study of the evaluation of the structural measurements of RNFL obtained both with scanning laser polarimetry and with the OCT concluded that both methods provided consistent information for the RNFL thickness but were unable to differentiate between normals and ocular hypertensives (Hoh, Aung *et al*, 2002). However, the attenuated RNFL thickness was highly correlated with visual

function in glaucomatous eyes. In the most recent comparative study on all the imaging methods, the qualitative assessment of stereo-photographs was regarded to be a more accurate method than the quantitative methods of CSLO, SLP and OCT in diagnosing early to moderate glaucomatous damage (Greaney, Hoffman *et al*, 2002). It was also suggested that the performance of the quantitative methods was considerably improved when all techniques were used in combination.

Chapter 2 Rationale for research

This thesis was a continuation of studies undertaken by the group concerned with the evaluation of the SWAP algorithm compared to W-W perimetry with reference to factors influencing the within subject and between subject variability of the threshold response. Previous studies of Short Wavelength Automated Perimetry (SWAP) included the optimisation of stimulus parameters (Hudson, Wild *et al*, 1993), the effect of light scatter, ocular media absorption and macular pigment (Moss & Wild, 1994; Moss, Wild *et al*, 1995; Wild & Hudson, 1995), the learning effect in normal subjects (Wild & Moss, 1996) and the short term and long term variability of the threshold estimates (Hutchings, Hoskins *et al*, 2001; Wild, Cubbidge *et al*, 1998).

Previous research within the School was also concerned with the investigation of structural changes by stereophotography and planimetry of the ONH in patients with Open Angle Glaucoma (OAG) using computerised imaging (Sheen, 2002).

2.1 Clinical evaluation of threshold response in Short-Wavelength Automated Perimetry

Specialised perimetric algorithms isolating the function of sparsely represented ganglion cell types in the normal retina are alleged to successfully investigate early functional deficits associated with retinal pathology. SWAP identifies the under-sampling of the SWS ganglion cells and several studies have shown that this technique delineates visual field abnormality earlier than conventional perimetry testing (Heron, Adams *et al*, 1988; Johnson & Nelson-Quigg, 1993; Johnson,

Brandt *et al*, 1995; Polo, Abecia *et al*, 2001; Sample, Boynton *et al*, 1988; Wild, Moss *et al*, 1995).

The subjective nature of perimetry permits psychophysical variability that confounds the detection of the earliest response alteration from cells affected by glaucoma. Standard automated perimetry is considered the gold standard for the newer perimetric algorithms, given the longevity of the technique and the knowledge of it's performance. The threshold estimates are dependent upon the within- and between-examination variability (Heijl, Lindgren *et al*, 1987b; Heijl & Lund, 1987). SWAP induces a greater fatigue effect than W-W perimetry due to the longer examination duration with the full threshold program and the learning effects associated with the task are persistent long after the third examination (Searle, Wild *et al*, 1991b), Research within the group (Hutchings *et al*, 2001; Wild *et al*, 1995) and from other investigators (Kwon *et al,* 1998) has reported that the commercially available SWAP demonstrates great between-subject normal variability, approximately 1.9 to 2.7 times greater than for W-W perimetry, depending on the effect of media opacities (Wild *et al*, 1998). Also, long-term fluctuation (LF) and short-term fluctuation (SF) have been reported to be greater for normal subjects in SWAP than in W-W perimetry (Blumenthal, Sample *et al*, 2000b; Hutchings *et al*, 2001).

Reduction in light transmission is predominantly due to age-related changes to the crystalline lens, influencing the performance of SWAP (Hudson *et al*, 1993; Johnson, Adams *et al*, 1988; Sample, Esterson *et al*, 1988; Sample, Esterson *et al*, 1989; Savage, Haegerstrom-Portnoy *et al*, 1993).

Observations by the group suggest that SWAP has increased confidence limits for normality, that hinder the detection of abnormality with the technique because the reduction in sensitivity required to indicate abnormality will be greater than for W-W perimetry (Wild *et al*, 1998).This effect is seen in conjunction with the reduced dynamic range of the instrument with SWAP, which arises from the high luminance background and the low transmission of the short-wavelength stimulus.

The statistical analysis package SWAPPAC, incorporated in the HFA and supporting the commercially available SWAP also undermines abnormality (Wild, 2001). It is noted that previous studies have defined abnormality for SWAP without considering the influence of the normal variability, whilst demonstrating the superiority of the technique against conventional perimetry for glaucoma detection (Sample & Weinreb, 1992). An investigation of SWAP performance using the total and pattern deviation probability maps of SWAPPAC, demonstrated the under-estimation of the presence of glaucomatous defects (Soliman *et al*, 2002b).

A third generation of perimetric algorithms (SITA) is currently considered for SWAP. SITA SWAP has reduced average examination duration, increased dynamic range and smaller between-subject variability compared to Full-Threshold SWAP (Bengtsson, 2003; Bengtsson & Heijl, 2003). However, the SITA algorithm uses a strategy to estimate the threshold values based on the frequency of seeing function. Thus, SITA SWAP like Full-Threshold SWAP is also likely to show limitations when delineating abnormality compared to W-W perimetry.

This study is a clinical observational study of the performance of SWAP compared to W-W perimetry across various study groups including normal volunteers, glaucoma and OHT patients, and patients with cataract.

2.2 The comparison of monoscopic and stereoscopic computer assisted planimetry in the evaluation of the normal and glaucomatous optic nerve head

Photography of the optic disc is one of the most traditional methods used to record the appearance of the optic nerve head in a clinical setting and stereoscopic systems have been always considered optimal for the observation of the ONH in glaucoma, providing realistic representation of the 3D ONH structure and thereby, a better estimation of glaucomatous cupping. Clinical subjective diagnosis with stereoscopic photos was ranked as superior against automated diagnosis with the HRT, and more accurate than the discrimination ability of other automated methods evaluating NFL (Greaney *et al*, 2002; O'Connor, Zeyen *et al*, 1993).

There are currently available systems that combine digital stereoscopic view with custom computer programmes that enable planimetry for glaucoma research (Barry *et al*, 2000; Burgoyne *et al*, 2005; Morgan, Sheen *et al*, 2005b; Parkin, Shuttleworth *et al*, 2001; Sheen, Morgan *et al*, 2004; Shuttleworth, Khong *et al*, 2000; Sung, Bhan *et al*, 2002; Yogesan, Barry *et al*, 1999a). However, in clinical settings the use of stereo photography has been degraded mainly because of practical difficulties of the technique, without overlooking the relatively higher cost of the stereo viewing systems compared to monoscopic devises. As a consequence, monoscopic examination has been used in clinical practice and in large clinical trials to determine the presence of glaucomatous optic neuropathy (Heijl, Leske *et al*, 2002;

Spry, Spencer *et al*, 1999; Watkins, Panchal *et al*, 2003; Wolfs, Ramrattan *et al*, 1999). Moreover, the demand for widespread screening of glaucoma has encouraged the idea of telemedicine applications and has highlighted the practical limitations of currently available imaging techniques incorporating stereophotography.

Several studies have undertaken the task of comparing different imaging techniques in order to investigate the compatibility of their results. Clinical decisions as well as topographical ONH measurements are shown to be variable when derived by ophthalmoscopy, stereophotography, scanning laser ophthalmoscopy or other semi-automated imaging systems respectively (Correnti, Wollstein *et al*, 2003; Ikram, Borger *et al*, 2002). Although it is widely speculated that the difference in performance between the various techniques, is heavily attributed to their monoscopic or stereoscopic features it is yet to be elucidated if the stereoscopic viewing mode can be associated with more reliable results.

Digital imaging is becoming available at low cost and is expected to play a significant role and screening for a number of eye diseases. Fundus film based stereophotography is the golden standard for the evaluation of the retina but given the technological changes, research is already exploring the efficiency of digital non stereoscopic images for diagnostic purposes. Telemedicine systems currently proposed for the improvement of the eye care services, facilitating communication between clinicians and glaucoma screening services, can operate particularly fast using monoscopic digital images under compression (Constable, Yogesan *et al*, 2000). Digital systems are currently evaluated for the screening of glaucoma

(Constable *et al*, 2000), diabetic retinopathy and AMD (Somani, Tennant *et al*, 2005). It has been suggested that increased image resolution can improve the performance of digital imaging over photography, but the stereoscopic aspect of imaging is seemingly important for the diagnosis of some pathological appearances. The sufficiency of imaging techniques utilising monoscopic viewing is not fully determined for glaucoma diagnosis and progression, despite the obvious practical benefits for shared eye care. A more widespread clinical application of stereo systems can be realised given the increasingly affordable costs of stereo cameras and stereo-viewing devises. Moreover, there is an increase of available computing power which enables storage, processing, display and even electronic transfer of image stereopairs as quick and efficient as that of monoscopic images (Lee, Shin *et al*, 2000). However, before investing in this technology, it is important to further investigate if stereoscopic images convey more diagnostic information in glaucoma than monoscopic images and to investigate if new computer assisted planimetry systems, evaluating advanced quality fundus images, could perform equally well utilising monoscopic presentation.

Research within the group has been concerned with the improvement of stereoscopic presentation, comparing the stereoscopic quality between images of different cameras and evaluating the comfortable use and good stereo perception achieved with the more advanced technology of available stereo viewers over manual mirror based systems (Sheen, 2002). This study evaluated the development of a custom computer program for quantitative analysis of the ONH in a semi-automated fashion. The first issue that was addressed was the rapid and

cost-effective clinical presentation of true colour fundus images under stereoscopic conditions.

Since stereo and mono presentation of fundus photography for glaucoma diagnosis and planimetry is one of the aspects that need to be investigated towards the optimisation of the imaging techniques, this study undertook the task to compare between stereoscopic and monoscopic presentation of the optic nerve head with a method of image presentation where the analysis tools have been standardised. This comparison was concerned with the accuracy of planimetry and the sensitivity for subjective diagnosis of glaucoma by a panel of expert observers that assessed 51 normal and 113 glaucoma ONH images.

2.3 Clinical evaluation of peripapillary atrophy in normal and glaucomatous eyes

This study was motivated by the growing knowledge on the mechanisms of the pathogenesis of the disease, as well as the additional demands for early detection of glaucoma with respect to the effective application of neuroprotection therapies (Quigley, 1995).

Peripapillary atrophy is one of the anatomical variables describing glaucoma abnormalities. Histological studies have speculated that the PPA areas constitute precursors of the defective autoregulative mechanisms associated with glaucoma. Moreover, PPA areas in glaucomatous eyes have been identified as sites of glial activation (Neufeld, 1999; Neufeld & Gachie, 2003) and lipofuscin accumulation (Lammer, Link *et al*, 2005). PPA has a dynamic involvement in the earliest (Stewart *et al*, 1995; Tezel *et al*, 1997a; Tezel *et al*, 1997b) and also the progressive stages

of the disease (Tezel *et al*, 2000; Uchida, Ugurlu *et al*, 1997; Uchida *et al*, 1998; Uchida, Yamamoto *et al*, 1999).

However, clinically the significance of PPA is limited for the discrimination of glaucoma (Jonas *et al*, 2000; Jonas, 2005). PPA could serve the purposes of early detection of glaucoma and be the primary site of neuroprotective management in glaucoma. However PPA is clinically overlooked because of the difficulty of assessment, associated with high interobserver variability.

It was hypothesised that assessment of the ONH with computer assisted planimetry could provide an accurate description of the presence, the extent and severity of PPA. The study described in Chapter 6 was involved with the identification and quantification of areas of peripapillary atrophy in order to elucidate clinical correlations of the presence and extent of PPA with other established features of glaucomatous damage.

2.4 Quantitative analysis of the neuroretinal rim for the discrimination of normal and glaucomatous discs

Diagnostic tools for glaucoma that allow automated decisions can be useful in cross sectional screening for the disease. Digital imaging technologies have been developed that quantify the optic disc structure and facilitate the discrimination of normal and glaucomatous discs. However, quantitative evaluation of the ONH parameters by planimetry is often limited by observer variation that may impair the diagnosis, and/or the detection of the disease progression (Zeyen, Raymond *et al*, 1992). While the combined evaluation of more than one optic disc variable

improves the diagnostic precision of an imaging technique, the rim area alone is usually one of the best predictors, achieving high scores of sensitivity and specificity. The rim area is a useful indicator of the presence of glaucoma but there is an overlap of rim size between normal and glaucomatous groups, that is partly attributed to the correlation between the rim and disc size (Caprioli, 1992; O'Connor *et al*, 1993). A normal range of rim values in a given healthy population can be defined by the prediction intervals of the regression line describing the relation between the rim and optic disc areas (Caprioli, Sears *et al*, 1987). Discriminant functions incorporated in automated imaging techniques evaluate topographic rim measurements derived from healthy eyes and produce promising results for glaucoma detention (Mardin *et al*, 1999; Wollstein *et al*, 2000a; Wollstein, Garway-heath *et al*, 2000b). The HRT incorporates a quantitative analysis (Moorfields Regression analysis) based on the global and regional rim values with a reported diagnostic precision that was found to compare favourably with the subjective glaucoma diagnosis by expert observers. The statistical results highlight the deviation of the neuroretinal rim areas from the normative database and may assist clinical judgments.

Stereoscopic planimetry relies on stereoscopic clues to identify the most superficial limits of the cup slope and the technique has the highest sensitivity for early preperimetric glaucoma (Caprioli, 1992). Stereoscopic digital planimetric systems have shown improved performance for the rim definition. Semi-automated techniques generate magnification corrected estimates of the ONH topography and can provide rather reproducible results in the hands of experienced and/ or well trained observers (Morgan, Sheen *et al*, 2005a). This study aimed to perform a

quantitative analysis of the neuroretinal rim area based on normative data derived with a stereoscopic digital planimetry system and investigate the sensitivity of this method for glaucoma discrimination.

Within the clinical setting, subjective evaluation of the rim configuration is also one of the guidelines usually employed to assist glaucoma diagnosis. Morphometric analysis of the rim area from eyes of a healthy population identified a rather distinct pattern in the rim configuration that was proposed to have a clinical value in the detection of eyes with glaucomatous optic neuropathy (Jonas, Gusek *et al*, 1988d). This parameter of rim shape that has gained considerable empirical value over the recent years is known as the ISNT rule. This rule proposes that for normal optic discs the distribution of the rim size would be expected to be wider inferiorly, superiorly, nasally and finally temporally. Although the rule has been promoted for the clinical discrimination of glaucomatous discs, it has not been reproduced with quantitative assessment of the optic nerve head using modern imaging techniques. Moreover, it is yet to be determined if the ISNT rule yields any accuracy when applied to identify eyes with early glaucomatous damage. The aims of this study were extended to determine the efficacy of the ISNT rule for the detection of glaucoma based on digital stereoscopic optic disc analysis.

2.5 Logistics

Delays were encountered in the collation of the clinical details and examination results of the normal subjects and glaucoma patients that comprised the study groups for the studies described in Chapter 5 and Chapter 6 of this thesis. A large database of normal subjects and patients with either OHT or glaucoma had

attended a series of imaging and perimetry examinations over the course of previous research within the school. These data were subjected to a painstaking procedure of re-evaluation and selection according to optimised clinical criteria as described in Chapter 4, before being considered for inclusion. Data from a total number of 300 eyes were initially examined for their eligibility for inclusion in the present study.

The programming of the software used for the stereoscopic imaging studies posed considerable delays involving a series of tests and unpredicted time frames for necessary reprogramming. It was only when the software was granted a satisfactory quality that it was released for use in the experimental procedures described in chapter 4. Unfortunately, some of the software add-on programmes, which were planned to be developed for the present study in order to enable more sophisticated investigation of the retinal features, were not finalised on time, thereby severing the design and purposes of this thesis.

The clinicians that volunteered to perform the clinical assessments of this study were ophthalmologists with special interest on glaucoma detection, that had years of working experience within the British health system. The procedure of their recruitment was determined by the fact that the research project was undertaken in Cardiff University and it involved a considerable amount of experimental work from their behalf, over a limited period of time. The investment in an additional computer-assisted system for stereoscopic image presentation enabled the recruitment of a clinician that was based in Birmingham where they also performed all their observations. All three volunteer clinicians had to overcome the practical difficulties

associated with the long hours of the experiment and had to complete their experimental work in parallel with their daily clinical practice. Thus, most of the sessions were scheduled over the weekends and during holidays and were facilitated by the possibility of 24-hour access to the School premises. Each observer assessed 210 images, in stereoscopic and monoscopic view respectively.

Comparison of the perimetry algorithms described in Chapter 3 was based on data independently collected at Cardiff and Aston University throughout research undertaken under the supervision of Professor JM Wild. The various study groups had been recruited using standardised examination procedures and all acquired visual field tests met the same reliability criteria. These data were analysed together, as the ensuing larger sample sizes would increase the power of the subsequent statistical analysis. However, since the perimetry results are not available in electronic format, it was required that all necessary data obtained from the visual field printouts; namely the probability scores across the Total Deviation and Pattern Deviation maps were manually computed into Excel spreadsheets before their analysis, as described in Chapter 3. Overall, this procedure involved 410 visual field tests.

Chapter 3 Clinical evaluation of the threshold response in Short-Wavelength-Automated-Perimetry

3.1 Selective ganglion cell loss in glaucoma

Retinal ganglion cells comprise the magnocellular (M), the parvocellular (P) visual pathways and the least known koniocellular (K) pathway, in which they are categorized according to the anatomical arrangement of their neural synapses in the lateral geniculate nucleus (LGN). The M-pathway includes the parasol ganglion cells that have relatively large receptive fields, are more sensitive to low spatial frequency and high temporal frequency, and generally give a similar type of response to all wavelengths of light. The M-cells synapse in the M layers of the LGN and constitute about 10% of the total number of ganglion cells (Shapley & Perry, 1986). The P-pathway consists of the midget ganglion cells which have small receptive fields; are more sensitive to high spatial frequency; are less sensitive to high temporal frequency stimuli and are responsive to chromatic information (Callaway, 1998; Lennie, 1980; Merigan & Maunsell, 1993). The P-cells account for the 80% of the total number of retinal ganglion cells , and synapse in the P layers of the LGN (Shapley & Perry, 1986). Merigan and Maunsell (1993) suggested that the M- and P-cell pathways have specialized, but also overlapping, detectors and functions.

The koniocellular (K) pathway consists of the small bistratified ganglion cells and accounts for the remaining 10% of the total number of ganglion cells. It is alleged that the K- cell pathway exerts a modulating role over the activity of the M-cell and P-cell pathways (Callaway, 1998; Lennie, 1980; Merigan & Maunsell, 1993). The K-

cells project to specified layers within the LGN and it is speculated that they are involved in colour vision, object recognition and visual resolution (Casagrande, 1994; Hendry & Reid, 2000).

The P-pathway emerges from three types of cones, namely the LWS, the MWS cones and the SWS cones. The LWS and MWS cones mediate the red and green channels while the SWS cones give rise to the blue channel (De Valois, Webster et al, 1986). The SWS cones are the least of all types of cones approximating 5-10% of the total population of cones (Calkins, 2001; Curcio, Allen et al, 1991). The SWS pathway includes the S cones, S-cone bipolar cells and the bistratified midget ganglion cells (Dacey & Lee, 1994; Dacey, 2000; De Monasterio, Schein *et al*, 1981).

The SWS cones are absent from the centre of the fovea with a distribution that peaks at approximately 1.5° retinal eccentricity and declines until approximately 7 to 8° retinal eccentricity (Volbrecht, Nerger et al, 2000). Unlike the MWS or LWS cone pathways the SWS cones do not contribute to the achromatic (luminance) pathway (Eisner & MacLeod, 1980) and exhibit a narrower luminance response range which suggests that the SWS cones saturate, while the MWS and LWS cones maintain some sensitivity (Cho, Poulsen et al, 2000; Dacey, 2000).

Glaucoma is associated with damage to all chromatic pathways, reducing the numbers of each of the SWS, MWS and LWS ganglion cells. However, it has been speculated that the SWS cones might be the most vulnerable of all cone types under conditions of hypoxia and ischaemia because they exhibit higher metabolic

requirements (Holopigian, Seiple et al, 1997; Kono, Chi et al, 1996; Yamamoto, Kamiyama et al, 1996). Also, the ganglion cells mediating the SWS pathway have a larger diameter than the ones mediating the medium-wavelength sensitive (MWS) and long-wavelength sensitive (LWS), which is in agreement with histological studies that have identified preferential damage of the larger ganglion cells by glaucoma (Quigley, 1994a).

Glaucomatous damage affecting the MWS and LWS pathways occurs at the retinal level, within the ganglion cell and/or the nerve fibre layer, producing focal defects as well as diffuse visual field loss (Chauhan, Mohandas et al, 1993; Henson, Artes et al, 1999). However, the location of damage along the SWS pathway has not been clearly established (Drasdo, Aldebasi et al, 2001). The SWS ganglion cells are fewer in number and sparsely populated, thereby functional defects associated with this pathway will manifest earlier than the others as a result of the under-sampling or minimal overlap of the SWS ganglion cell receptive fields. Therefore psychophysical tests designed to isolate the SWS mechanism would seem to detect a selective loss in function (rather than a selective loss of ganglion cell type) for this pathway. This concept constitutes the hypothesis of the 'reduced redundancy' (Johnson, 1994; Lynch, Johnson *et al*, 1997).

3.2 Principles of SWAP testing

Stiles (1939) succeeded in isolating the SWS mechanisms using specific stimulus conditions, namely a blue stimulus with a peak wavelength approximating the peak response of the SWS cones, presented on a high luminance yellow background. While the high luminance yellow background suppresses the responses of the

MWS and LWS cones, as well as rod activity, the SWS cone activity is effectively isolated (Stiles, 1939).

SWAP employs this technique to evaluate the sensitivity of the SWS cones towards the detection of visual field loss in glaucomatous, OHT and glaucoma suspect eyes (Demirel & Johnson, 2000). The magnitude of SWS isolation is strongly dependent upon the stimulus and background characteristics of the SWAP program. As the peak wavelength of the stimulus filter decreases, SWS isolation increases, at the cost of an increase in OMA and a reduction in the dynamic range of the perimeter (Hudson *et al*, 1993; Vetrugno, Quaranta *et al*, 2000). Sample and colleagues demonstrated that a narrowband blue stimulus ensured SWS pathway isolation (Delgado, Nguyen et al, 2002; Sample & Weinreb, 1992) and was less susceptible to shifts of the peak retinal wavelength due to OMA (Sample, Johnson et al, 1996). When a stimulus filter with a broader spectral transmission was used there was some stimulation of the MWS pathway and hence, incomplete isolation of the SWS pathway (Sample & Weinreb, 1990; Sample, Taylor et al, 1993), although the dynamic range of the perimeter was increased (Adams, Johnson *et al*, 1991; Hudson *et al*, 1993; Johnson *et al*, 1988; Johnson, Adams *et al*, 1993; Johnson & Casson, 1995; Moss & Wild, 1994; Vetrugno *et al*, 2000; Wild & Hudson, 1995). Consequently, the stimulus for the commercially available SWAP for the HFA is set to be a narrowband 440 nm filter (27 nm half-peak width) (Sample et al, 1996). The default stimulus for SWAP comprises a Goldmann size V (1.74° diameter) blue stimulus presented with a 200msec duration, since maximum isolation of the SWS pathway is possible with a 2° diameter stimulus and maximal temporal summation is achieved at a stimulus duration of 200msec (King-Smith, Grigsby *et al*, 1994).

3.3 SWAP in early detection of glaucoma

The blue-yellow channel was shown to be affected in patients with OHT or with early glaucoma (Felius, de Jong et al, 1995; Greenstein, Halevy et al, 1996; Harwerth, Smith III et al, 1999; Harweth, Carter-Dawson et al, 1999). It has been suggested that SWAP can detect the presence of visual field loss at an earlier stage than W-W perimetry (Delgado *et al*, 2002; Heron *et al*, 1988). Longitudinal studies on glaucoma suspects showed the presence of visual field loss with SWAP prior to W-W perimetry, by at least three to five years (Johnson & Nelson-Quigg, 1993). Similarly, visual field loss by W-W perimetry was identified subsequently to defects with SWAP among OHT patients that progressed to glaucoma (Casson, Johnson et al, 1993; Delgado et al, 2002), with a ratio of two out of five cases (Wild *et al*, 1995). Overall, high-risk OHT patients have been associated with an increased prevalence of visual field loss with SWAP (Johnson & Casson, 1995; Polo *et al*, 2001).

Patients with glaucoma demonstrated a significant loss of SWS function throughout the central visual field (Heron et al, 1988) and showed wider and/or deeper early visual field defects with SWAP than with W-W perimetry (Adams et al, 1991; Delgado et al, 2002; Johnson et al, 1993; Sample & Weinreb, 1992; Wild & Hudson, 1995). Several studies also suggest that glaucoma patients with stable visual fields by standard W-W perimetry would show visual field progression with SWAP (Delgado et al, 2002; Johnson et al, 1993; Sample & Weinreb, 1992). Moreover, the baseline SWAP defect is larger than the W-W defect in glaucomatous eyes with progressive W-W field loss (Casson et al, 1993; Johnson et al, 1993; Sample & Weinreb, 1992). However, no advantage is gained from using SWAP to quantify

extensive areas of visual field damage in moderate to advanced glaucoma (Demirel & Johnson, 2000). In such cases SWAP has a limited performance because of the reduced dynamic range of the technique compared to W-W perimetry. It is estimated that the maximum stimulus brightness for SWAP with the HFA is 65asb (20.6cdm^{-2}) compared to 100.000asb (3183cdm^{-2}) for W-W perimetry.

Moreover, reduction in the SWS isolation suggests that in the areas with deep defects the stimulus may be detected by the MWS and LWS channels, which are always active for W-W perimetry. SWAP is therefore more suited for the investigation of any extension in the area of existing field loss and for the examination of patients with OHT and patients with early W-W field loss. For more advanced visual field defects, the extent of visual field deficit would be similar between the two techniques (Hart, Silverman et al, 1990; Wild & Hudson, 1995).

3.4 Sources of variability in light sensitivity with SWAP

The normal age-related decline in the light sensitivity is attributed to age related changes in the retina associated with the foveal cone photo-pigment (Kilbride, Hutman et al, 1986; Van Norren & Van Meel, 1985), the photoreceptor density (Farber, Flannery et al, 1985; Gartner & Henkind, 1981), the ganglion cell density (Balazsi, Rootman *et al*, 1984; Dolman *et al*, 1980) and the number of cortical cells (Scheibel, Lindsay et al, 1975). However, normal age-related reductions in sensitivity have been reported to be greater for the SWS channel than for both the MWS and LWS channels, with a rate of approximately 0.3dB per decade (Johnson et al, 1988). Sensitivity slopes of 1.5 dB to 2.2 dB per decade have been measured for the commercially available SWAP (Wild *et al*, 1998).

Visual field locations with increased eccentricity show a greater rate of sensitivity decline relative to the more central field, when evaluated with SWAP, particularly in the region of the superior nasal field (Johnson et al, 1988; Sample, Irak et al, 1997). This greater variability for SWAP is more noticeable at increased eccentricities and with increased age but is evident in all stimulus locations for SWAP compared to W-W perimetry (Wild & Hudson, 1995; Wild, Hutchings et al, 1997) as the shape of the FOS curve in SWAP is flatter than that for w-w perimetry (Bigun, Choy et al, 2001).

3.5 Confidence limits for normality

The between-individual variation in the normal threshold at each stimulus location using the commercially available SWAP is, on average, 2.7 times greater for SWAP than for W-W perimetry and approximately 1.9 times greater after correction for OMA was applied (Wild et al, 1998). As a result of the increased variability, the reduction in sensitivity required to indicate abnormality for SWAP is proportionately greater than for W-W perimetry, thereby confounding the detection of field loss with SWAP.

3.6 Media opacities

The absorption of visible wavelengths, the scattering of light, and defocus resulting from opacities within the cornea, crystalline lens or vitreous reduce stimulus contrast and thereby attenuate the threshold. Increasing media opacity with age complicates the detection of progressive glaucomatous visual field loss (Bengtsson, Lindgren et al, 1997). Many studies have reported that cataract causes a diffuse loss of sensitivity with automated static perimetry (Budenz, Feuer *et al*, 1993; Curcio *et al*, 1991; Guthauser & Flammer, 1988; Purcell & Stewart, 1988). A

discolouration of the layers within the lens occurs with aging and leads to an increase in light absorption and a reduction in the effective level of light reaching the retina.

Absorption is wavelength dependent and preferentially attenuates the shorter wavelengths (Delgado et al, 2002; Vetrugno et al, 2000). For conventional white-on-white perimetry, both the stimulus and background are affected. Also, the SWS stimulus shows a preferential absorption by the ocular media (Delgado et al, 2002; Johnson et al, 1988; Johnson & Casson, 1995; Wild & Hudson, 1995; Wild et al, 1998). Ocular media absorption (OMA) exhibits large between-individual variability in the normal eye, particularly for the older age groups (Delgado *et al*, 2002; Johnson *et al*, 1988; Savage *et al*, 1993; Siik, Airaksinen *et al*, 1991). Reduced transmission of the SWS stimulus due to OMA leads to a reduction in the height of the hill of vision. Normal variability increases as a result of the within- and between-subject variations in OMA (Vetrugno et al, 2000), the variable influence of intraocular light scatter which is exaggerated in eyes with cataract (Moss & Wild, 1994), as well as, due to the between-subject variation in the density of macular pigment (Wild & Hudson, 1995). Not surprisingly, the between-subject normal variability of the threshold estimate with SWAP is reduced when the effect of the OMA is accounted for (Wild et al, 1998).

Light absorption is considered to attenuate the conventional perimetric response less than light scatter (Bettelheim & Ali, 1985; Greve, 1980). Light scatter describes the dispersion of a point source of light as it passes through the ocular media. It is the main cause of visual loss in cataract (Philipson, 1969) and is subdivided into

stray light reaching the retina (forward light scatter) and light reflected away from the crystalline lens (backward light scatter). Forward light scatter due to lens opacities is thought to be one of the causes of image degradation (Bettleheim & Chylack, 1985; Wood, Wild *et al*, 1989). Cataract has been found to be highly correlated with forward light scatter (Dengler-Harles, Wild et al, 1990), producing an overall reduction in sensitivity as the degree of light scattering is increased (Dengler-Harles et al, 1990; Moss & Wild, 1994; Vetrugno et al, 2000). Diffuse reduction in sensitivity by simulated light scatter resulted in equal depression of both normal and abnormal areas of the visual field (Budenz et al, 1993). However, it can be difficult to separate the effect of cataract from advanced field loss using the Total and Pattern Deviations as light scatter might initiate a response from a larger area of the retina, thereby resulting in higher sensitivity (Purcell & Stewart, 1988). This assumption is further supported by the fact that in pseudophakic eyes where light scatter is absent, the stimuli falls upon a smaller area of the retina and brighter stimuli are required in order to elicit a response.

Cataracts influence both W-W perimetry and SWAP, as the degree of light scatter shows little dependency on the wavelength of incident light (Whitaker, Steen *et al*, 1993). The reduction in sensitivity, especially for the posterior sub-capsular type cataracts (Moss & Wild, 1994; Vetrugno et al, 2000) has been shown to be far greater for SWAP than for W-W perimetry (Kassoff, Kassoff *et al*, 2001).

3.7 Short-term fluctuation

The short-term fluctuation (SF) represents the variation associated with the within-subject and within-examination response (Bebie *et al*, 1976; Flammer *et al*, 1984). It

is based upon the variation of sensitivity values at given locations in the field that are determined twice within the course of a single examination and is dependent upon the strategy used to estimate the threshold (Bebie et al, 1976; Flanagan, Hrynchak et al, 1999; Weber & Klimaschka, 1995). Short-term fluctuation can also be influenced by the reliability parameters, i.e. the number of fixation losses and the false positive or false negative rates. The HFA obtains double determinations of threshold at each of ten locations across the visual field and SF is known to vary with eccentricity, being up to 27% greater at the four peripheral points than at the six most central locations with W-W perimetry (Heijl *et al*, 1987b). Also, SF is increased at locations that lie along the border of the blind spot (Haefliger & Flammer, 1989). For W-W perimetry stimulus sizes less than the Goldmann size III have been associated with larger SF (Gilpin *et al*, 1990), but SF is unaffected by changes in stimulus duration (Pennebaker, Stewart et al, 1992).

Studies on different samples of normal eyes have shown that SF for SWAP was greater than for W-w perimetry by 21% (Wild & Hudson, 1995) or 24% (Wild et al, 1998). Moreover, increased SF was identified among glaucoma patients with similar magnitude for W-W perimetry and SWAP (Delgado et al, 2002).

3.8 Long-Term Fluctuation (LF)

The Long-term Fluctuation (LF) is the variability in threshold over a series of examinations after accounting for the SF, possible learning effects and the age factor (Bebie *et al*, 1976; Blumenthal, Sample *et al*, 2000a; Blumenthal *et al*, 2000b; Flammer *et al*, 1984). The LF includes the variability that affects equally all tested locations, referred to as Homogenous LF (LF_{HOM}) and the variability that is different

for specific locations, described as the Heterogeneous LF (LF_{HET}) (Hutchings, Wild *et al*, 2000). The LF_{HOM} might represent the fluctuation of Mean Sensitivity or Mean Defect/Deviation over time and the LF_{HET} describes the variation in localised areas of the field (Zulauf, Caprioli et al, 1991). The LF has also been expressed in terms of a single component either as the variance (dB^2), the Standard Deviation (dB) or as the range (dB) of repeated thresholds (Boeglin, Caprioli et al, 1992) over two or more examinations (Blumenthal et al, 2000b; Boeglin et al, 1992; Heijl, Lindgren et al, 1992; Katz & Sommer, 1987). The calculation of LF is limited to the central field and doesn't take into account the fluctuation in the periphery. There is an equivocal relationship of LF with increasing stimulus eccentricity in normals (Heijl *et al*, 1987b; Rutishauser & Flammer, 1988) and in glaucoma patients (Boeglin et al, 1992; Zulauf et al, 1991). It has also been suggested that the magnitude of the LF may be underestimated when the visual field examinations are performed within short periods of time (Boeglin et al, 1992), but at all occasions, LF has to be considered when classifying consecutive visual fields as stable or progressive.

In patients with glaucoma the LF was found greater for SWAP compared to W-W perimetry almost by 107% using the HFA (Kwon, Park et al, 1998). Similarly, the group mean LF, defined as the standard deviation of the thresholds derived with HFA and the full Threshold algorithm, across three successive examinations was 23% greater than that for W-W perimetry in patients with stable glaucoma (Blumenthal et al, 2000b). The classically defined LF was also found to be larger for SWAP compared to W-W perimetry in glaucoma suspects and at a smaller proportion, among glaucoma patients, thereby rendering the identification of

progressive visual field loss more difficult when evaluating SWAP than W-W perimetry (Hutchings *et al*, 2001).

3.9 Fatigue Effects

The outcome of visual field can be influenced by the fatigue effect that is apparent in all groups of in normal patients (Hudson, Wild *et al*, 1994; Searle *et al*, 1991b), in patients with OHT (Hudson et al, 1994; Wild, Searle et al, 1991) and in patients with glaucoma (Heijl & Drance, 1983; Johnson et al, 1988). As the duration of the examination increases, sensitivity declines (Heijl & Drance, 1983; Hudson et al, 1994; Johnson et al, 1988). The fatigue effect within an examination leads to a general reduction in sensitivity in the normal eye up to 2.5dB (Hudson et al, 1994; Johnson et al, 1988) and becomes more pronounced with examination durations greater than 5 minutes (Marra & Flammer, 1991). The mean overall within examination reduction in sensitivity due to fatigue was estimated to be 3dB in glaucoma patients (Johnson et al, 1988) and 2.2dB in OHT patients (Hudson et al, 1994).

It has been suggested that the order in which the eyes are tested in a visual field examination needs to be taken into account, as the fatigue effect was smaller for the eye examined first in normal subjects (Searle et al, 1991b). For the same reason the fatigue effect is more evident in the most peripheral stimulus locations, of the tested central field locations (Hudson et al, 1994; Johnson et al, 1988). Throughout the course of the examination the patients may become progressively less responsive and as a result the central stimulus locations show normal sensitivity while locations tested later seem to have depressed sensitivity (Gauthier,

Tarr et al, 1999). The effects of fatigue over the visual field examination are intensified among glaucoma patients and they are distinctly greater in areas of the visual field that are adjacent to or within a focal defect (Heijl & Drance, 1983).

SWAP testing with stimulus size V exhibited greater examination duration by 15% when compared to W-W perimetry using stimulus size III, for normal subjects (Wild et al, 1998). The longer examination duration for SWAP is likely to be a result of the increased difficulty of the detection task it involves (Wild et al, 1998). Fatigue may be minimised by utilising shorter threshold algorithms, such as the Swedish Interactive Threshold Algorithm standard (SITA Standard) (Bengtsson *et al*, 1997; Wild, Pacey *et al*, 1999). The modified SITA algorithm for SWAP has already been tested but is yet to be available clinically (Bengtsson & Heijl, 2000). Using the mean examination duration of two visits, examination duration with the Full Threshold algorithm was 11.8 min but the duration with SITA SWAP was reduced to 3.6 min (Bengtsson & Heijl, 2000).

The extended examination time with SWAP relative to W-W perimetry is a practical disadvantage for the technique and undoubtedly increases the effects of patient fatigue over the threshold estimates.

3.10 Determination of abnormality with SWAP

A major limitation associated with the use of SWAP in the clinical setting is the magnitude of normal variability inherent with this technique. Given the increased physiologic variability of the threshold with SWAP it would not be appropriate to define abnormality by the deviation of the threshold from normal levels (Flammer *et*

al, 1984; Heijl *et al*, 1987b). However, previous studies have defined abnormality for SWAP in terms of deviations in absolute values of sensitivity relative to a small cohort of normal individuals that was matched to the glaucoma group, without considering the influence of the threshold variability (Sample & Weinreb, 1992). Alternatively, abnormality with SWAP had been analysed based upon deviations in the height of the visual field from the age-corrected normal value rather than on deviations in shape (Delgado et al, 2002).

In clinical practice, the evaluation of single visual fields relies on the calculation of points that are significantly depressed in the pattern deviation plot. The pattern deviation approach can effectively remove generalised visual field defects. It is common knowledge that the prolonged duration of the test with SWAP and the learning effect which is persistent long after the third examination decrease the retinal sensitivity with this technique (Searle et al, 1991b). This is particularly important for the examination of glaucoma since increased generalised depression of the field may lead to underestimation of focal loss (Wild & Moss, 1996).

Wild and colleagues, that evaluated the sensitivity and specificity of SWAP for glaucomatous field loss using the total and pattern deviation probability maps, did show that short term fluctuation was larger with SWAP and that the variability of retinal sensitivity was greater for SWAP than in W-W perimetry (Wild et al, 1995). However, they did not provide a statistical comparison of the two techniques based on the plot maps. Similar results were obtained by Soliman et al (2002),that compared the scores of significantly depressed points in the pattern deviation plot as evaluated by conventional W-W perimetry and SWAP using the commercially

available analysis packages incorporated in the HFA. The study concluded that SWAP was the least sensitive method, as it failed to express the expected point depression in normals and underestimated the defects both in glaucoma and OHT patients (Soliman *et al*, 2002a).

It has been suggested that the confidence limits for normality as defined with the commercially available SWAP statistical package are wider than for STATPAC, thereby the level of depression required to score the same probability in the pattern deviation plot map is greater in SWAP than in W-W perimetry (Soliman et al, 2002a; Wild, 2001). Narrower normal threshold limits would result in more sensitive probability analysis maps (Bengtsson, 2003). This is an additional limitation for SWAP in the delineation of abnormality and progressive field loss.

3.11 Aims of study

This study is a clinical investigation of the commercially available SWAP algorithm in comparison to the standard examination with W-W perimetry, based on the probability analysis maps across various normal and abnormal visual field tests. We described the measurement error by each algorithm on a group of normal subjects and subsequently, we compare the level of depression evident in the pointwise TD and PD analysis for a group of patients with ocular hypertension; a group of patients with glaucoma and a group of patients with cataract. We also explore the within-algorithm between-visits long-term fluctuation associated with each perimetry test across all various study groups.

3.12 Methods

The visual fields data obtained within previous research studies were re-evaluated. Parts of these data were derived from a dataset of normal subjects', glaucoma and ocular hypertensive patients that was established during a PhD study conducted by Hancock (2000) (Hancock, 2000). This dataset included 18 normal subjects, 33 glaucoma patients and 22 ocular hypertensive patients. Another part of the data analysed in this study were derived from the dataset of normal subjects and glaucoma patients that was established during a PhD study conducted by Kim (2003) (Kim, 2003). This dataset comprised of 35 normal subjects (14 males) and 22 patients with OAG (12 males). Finally, the visual field data from a group of 18 cataract patients had been part of the a PhD study undertaken by Cubbidge (1997) (Cubbidge, 1997).

The normal subjects had been randomly recruited from the Optometry Clinics at Aston and/or Cardiff University and the patients with OAG and ocular hypertension had been recruited from the Eye Clinic of Birmingham, Heartlands Hospital and/or from the Cardiff Eye Unit, University Hospital of Wales. The patients with cataract were recruited at the Eye Clinic of Birmingham, Heartlands Hospital.
The studies had received approval by the Aston University Human Science Ethical Committee; the Birmingham Heartlands Research and Ethics Committee and/or the Bro Taf Local Research Ethics Committee, Cardiff.

The inclusion criteria for the normal, OHT and OAG patients had been as follows: in either eye, a visual acuity of 6/9 or better, distance refractive error of less than or equal to 5 dioptres mean sphere and less than 2.5 dioptres cylinder, lenticular

changes not greater than NC2.0, NO2.0, C1.0 or P1.0 by LOCS III (Chylack, Wolfe *et al*, 1993), IOP level of less than 22 mm Hg, normal ONH appearances, open angles, no history of congenital colour vision defect, no medication known to affect the visual field, no previous ocular surgery or trauma, no history of diabetes mellitus or other ocular disorder. All glaucoma patients had no history of ocular disorder other than glaucoma. The patients were required to have demonstrated a consistently raised pre-therapy IOP of 22mmHg or greater and they had undergone at least one automated static threshold visual field examination using W-W perimetry prior to inclusion in the study. The diagnosis of glaucoma in the designated eye had been based upon the appearance of the optic nerve head as assessed by a consultant ophthalmologist experienced in glaucoma (IAC or JEM) and upon the presence of visual field loss characteristic of glaucoma by W-W perimetry (JMW). All glaucoma patients had experience of W-W perimetry but were naïve to SWAP perimetry.

The diagnosis of the OHT patients had been based upon the normal appearance of the optic nerve head as assessed by a consultant ophthalmologist (IAC) and upon the normal results of visual field testing with W-W perimetry using the full threshold algorithm and programs 30-2 or 24-2 of the HFA (JMW). These patients had initially presented with either an IOP reading greater than 24mmHg; or an IOP reading greater than 22mmHg and a vertical CDR greater than 0.5 units; or an IOP reading greater than 22mmHg, a CDR less than 0.5 units and family history of glaucoma. From the cohort of OHT patients, 16 individuals were already receiving anti-glaucoma medication that was unchangeable for the period of the study in

reference. All patients were naïve to SWAP perimetry but had experience of W-W perimetry.

All patients with cataract were otherwise normal (see inclusion criteria for normal) but were scheduled to undergo cataract surgery within a period of the next 2 months. The diagnosis of cataract and referral for cataract surgery was based on the investigation of lenticular changes greater than NC2.0, NO2.0, C1.0 or P1.0 by LOCS III (Chylack *et al*, 1993).

Perimetry was performed according to standardized procedures. The distance refractive correction, in the form of a full aperture trial lens, together with any near correction appropriate for the viewing distance of the perimeter bowl, was used for each Program. The non-tested eye was occluded with an opaque patch. In addition to the standard Heijl-Krakau technique, fixation was monitored continuously with the gaze tracker and viewed by the video monitor. All visual fields for the normal group, using stimulus size III for W-W perimetry and using stimulus size V for SWAP, met the inclusion criteria for reliability, namely, less than 20% fixation losses. All visual fields for the normal group for W-W perimetry and SWAP met the inclusion criteria for the false-response catch trials, namely: less than 33% false negative and less than 33% false positive catch trials.

3.13 Examination protocol

The normal subjects, the patients with glaucoma and the OHT patients recruited by Hancock (2000) had attended for two visits only. Each visit consisted of two sessions. At one session, one randomly assigned eye of each of the 18 normal

subjects, the designated eye of each of the 33 glaucoma patients and the 18 OHT patients underwent an examination with Program 24-2 and the Full Threshold algorithm using conventional W-W perimetry and stimulus sizes III and at the other session, the subjects and patients underwent an examination with Program 24-2 using SWAP and the Full Threshold algorithm using the standard stimulus size V. The two sessions were separated by a rest period of 10 minutes. The order of the sessions within a visit was randomized for each subject but held constant between sessions over each of the two visits. The visits were each separated by an interval of approximately 14 days and the same protocol was followed throughout both visits.

The normal subjects and patients with glaucoma recruited by Kim (2004) had attended for three visits. Each visit consisted of two sessions. At one session, one randomly assigned eye (22 right eyes) of each of the 35 normal subjects and the designated eye (13 right eyes) of each of the 22 glaucoma patients underwent an examination with Program 30-2 and the Full Threshold algorithm using conventional W-W perimetry and stimulus sizes III and at the other session, the subjects and patients underwent an examination with Program 30-2 using SWAP and the Full Threshold algorithm using the standard stimulus size V. The two sessions were separated by a rest period of 45 to 60 minutes. The order of the sessions within a visit was randomized for each subject but held constant between sessions over each of the three visits. The visits were each separated by approximately weekly intervals and were carried out within a maximum period of 8 weeks. The same protocol was followed throughout all three visits.

The 18 cataract patients that were recruited by Cubbidge (1997) attended for two visits before their scheduled cataract surgery (Cubbidge, 1997). In each visit they performed both W-W perimetry and SWAP using the full threshold algorithm and programs 30-2 or 24-2 of the HFA. W-W and SWAP perimetry was performed at two visits postoperatively.

Only 11 patients were able to attend for the two follow up visits after the surgical procedure. The same protocol was followed at the preoperative and postoperative examinations.

3.14 Analysis

The first visits were considered to be a familiarization period for the study and the results were discarded prior to data analysis, in order to reduce the influence of the learning effect. The results for left eyes were converted into right eye format and the visual field locations immediately above and below the blind spot were excluded from the analyses.

The 30-2 presentation pattern includes all the test locations of the 24-2 pattern plus an additional outer rim of 22 locations (Figure 3.1). In order to make all available datasets compatible, these additional peripheral locations were removed from all the W-W and SWAP perimetry data derived with the 30-2 target presentation pattern, so that the analysis was based on the same 54 test locations across all evaluated visual field tests.

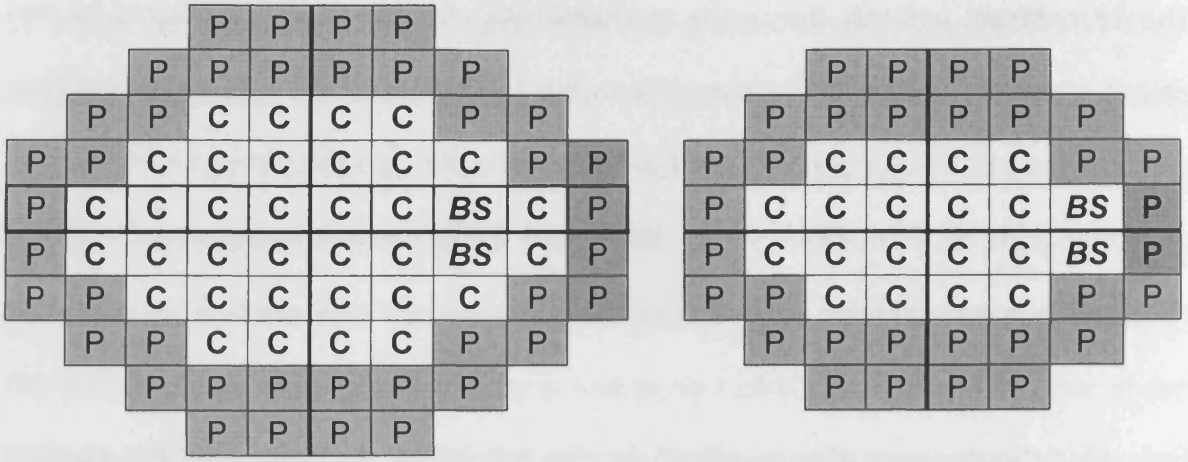

Figure 3.1. *The target presentation pattern with Program 30-2 and Program 24-2 respectively. Program 30-2 tests 22 peripheral locations (highlighted locations) that are not included in the 24-2 pattern. The letters P and C represent the peripheral and central locations respectively; (BS stands for the locations representing the physiologic blind spot).*

For the re-evaluation of the visual fields only the Total Deviation and Pattern Deviation probability analysis was used. The calculation of age-corrected confidence limits for normality used in the height (HFA Total Deviation) and shape (HFA Pattern Deviation) probability analysis is based upon the between-individual normal variability of the threshold estimate at each stimulus location, as described for a normative dataset. Probability plots illustrate the statistical likelihood of the measured value at any given location lying within the range associated with the age-corrected normal value. The HFA uses the STATPAC software program that provides probability plots based upon empiric data (Heijl et al. 1991). The HFA normative database for the full threshold algorithm is compiled from the visual field data of one eye of each individual at the third perimetric examination based on the assumption that at after three examinations with W-W perimetry the majority of the learning effect has been overcome (Searle *et al*, 1991b). Similarly, a normal database of SWAP fields has been used for the calculation of the commercially

available version of Humphrey STATPAC for SWAP perimetry (Zeiss-Humphrey Systems). However little knowledge is available from published sources on the characteristics of this dataset.

The deviation between the measured sensitivity and the age-matched normal value is determined at each stimulus location and is displayed as the Total Deviation plot. The associated levels of statistical probability (<5%, <2%, <1% and <0.5%) are displayed as the Total Deviation probability map. As the probability symbol darkens, the measured value of sensitivity becomes less likely to lie within the normal range. For example, a value of p<0.5% indicates that the deviation from the age-corrected normal value at that given location would be found in less than 0.5% of the normal population. The Pattern Deviation values are determined from the Total Deviation values when adjusted for the General Height, which is the age-corrected total deviation value corresponding to a location of the field that is not affected by localised damage, thereby incorporating only the effects of generalised depression and long term fluctuation (Anderson & Patella, 1999). The effect of diffuse generalised depression in sensitivity that may result from uncorrected refractive errors, small pupils or media opacities is effectively removed at the Pattern deviation analysis, unmasking the areas of localized defects. The differences from the normal at each location are plotted on a numerical Pattern Deviation plot and are represented in the Pattern Deviation probability plot. The Pattern deviation values represent the shape of the visual field rather than the height.

The TD and PD symbols of the statistical analysis maps were translated into values and were computed. The conversion of the probability percentages into numerical values is shown in table 3.1.

Probability percentage	Within normality	<5%	<2%	<1%	<0.5%
Numerical value	0	2	5	10	20

Table 3.1. *The numerical values that were utilised to represent the TD and PD probability percentages for the purpose of data analysis.*

The visual field data obtained with W-W perimetry and stimulus size III and SWAP and stimulus size V were analysed for the second and third visit when available. The difference in TD and PD values for each algorithm across all study groups was expressed with the total number of locations exhibiting a specific combination of recordings within each group.

The between algorithm differences in the total and pattern deviation probability levels at each stimulus location at visit 2 were expressed with 5x 5 contingency tables for each pair of algorithms across all study groups. Identical analysis was undertaken for the within – algorithm and between-visit differences, based on the results derived at the second and third visit.

The difference between the number of locations lying above and bellow the diagonal of the contingency table represent the difference in probability scores between the two algorithms for the same locations, while the numbers on the diagonal line of the table refer to the locations were both algorithms scored the same probability. Similarly, the number of locations lying above and below the

diagonal of the contingency table represent the difference in probability scores between the two visits for the same locations when tested with the same algorithm.

The total number of locations above and below the diagonal was expressed as a proportion of the total number of tested locations across each study group. The between-algorithm within-visit and the within-algorithm between-visit comparisons were also based on the total number of locations with the same score of TD and PD probability values.

For evaluation of the W-W perimetry and SWAP outcomes as a function of test location, the adjusted TD and PD scores were tabulated separately for the upper and lower hemifield locations, as defined by the middle line at the 24-2 presentation target. The TD and PD scores were also tabulated separately for the central and peripheral field locations of the 24-2 presentation target as presented in figure 3.1.

3.15 Results

3.15.1 Within visits and between algorithm

The cohort comprised 53 normal subjects. The differences in the group mean TD probability values between the two types of perimetry across all locations as determined at the second visit are shown in tables 3.2 – 3.4.

TD						
W-W						
SWAP	%	0	<5	<2	<1	<0.5
	0	2474	61	11	6	1
	<5	51	8	0	2	0
	<2	18	1	0	0	1
	<1	7	0	0	0	0
	<0.5	9	0	0	0	0
W-W more significant (%)						4
SWAP more significant (%)						3
W-W similar to SWAP (%)						93

	Locations
W-W: TD = 0	2559
Overestimated by SWAP: TD > 0	85
SWAP: TD = 0	2553
Overestimated by W-W: TD > 0	79

Table 3.2 *The group total number of tested locations matched to the TD probability scores with W-W perimetry and SWAP across all the normal subjects, at the second visit (visit 2). Summary tables give the proportions of the tested locations that are more depressed with the one and/or the other algorithm and the total number of locations lying within the normal confidence limits when tested with W-W perimetry that are overestimated by SWAP and vice versa, for all the normal subjects at the second visit (visit 2).*

TD Upper Hemifield							TD Lower Hemifield					
W-W							W-W					
SWAP	%	0	<5	<2	<1	<0.5	%	0	<5	<2	<1	<0.5
	0	1247	29	6	3	1	0	1227	32	5	3	0
	<5	22	7	0	1	0	<5	29	1	0	1	0
	<2	8	0	0	0	0	<2	10	1	0	0	1
	<1	1	0	0	0	0	<1	6	0	0	0	0
	<0.5	0	0	0	0	0	<0.5	9	0	0	0	0
W-W more significant (%)						3	W-W more significant (%)					3
SWAP more significant (%)						2	SWAP more significant (%)					4
W-W similar to SWAP (%)						95	W-W similar to SWAP (%)					93

Table 3.3 *The group total number of tested locations of the upper and lower field matched to the TD probability scores with W-W perimetry and SWAP, across all the normal subjects, at the second visit (visit 2). Summary tables give the proportions of the tested locations that are more depressed with the one and/or the other algorithm.*

TD Central Field							TD Peripheral Field						
W-W							W-W						
SWAP	%	0	<5	<2	<1	<0.5	%	0	<5	<2	<1	<0.5
	0	1194	30	9	3	1	0	1280	31	2	3	0
	<5	23	4	0	0	0	<5	28	4	1	2	0
	<2	3	0	0	0	0	<2	14	1	0	0	1
	<1	2	0	0	0	0	<1	5	0	0	0	0
	<0.5	3	0	0	0	0	<0.5	6	0	0	0	0
W-W more significant (%)						3	W-W more significant (%)						3
SWAP more significant (%)						2	SWAP more significant (%)						4
W-W similar to SWAP (%)						94	W-W similar to SWAP (%)						93

Table 3.4 *The group total number of tested locations of the central and peripheral field matched to the TD probability scores with W-W perimetry and SWAP, across all the normal subjects, at the second visit (visit 2). Summary tables give the proportions of the tested locations that are more depressed with the one and/or the other algorithm.*

The two algorithms perform similarly when describing the height of the hill of vision across the normal group with the same score for 94% of the tested locations and having a similar measurement error as represented by the number of locations above and below the diagonal (table 3.4). For the central field locations (table 3.4) the number of points scored outside the normal limits are more with W-W (43 locations) than SWAP (31 locations) that could be an indication of underestimation by SWAP. In the periphery however, SWAP exceeded W-W scores by a number of 14 locations (table 3.4).

The differences in the group mean PD probability values between the two types of perimetry across all locations as determined at the second visit, are shown in tables 3.5 – 3.7.

PD						
W-W						
SWAP	%	0	<5	<2	<1	<0.5
	0	2489	54	11	10	3
	<5	47	4	0	0	1
	<2	11	1	0	0	0
	<1	8	0	0	0	0
	<0.5	11	0	0	0	0
W-W more significant (%)						3
SWAP more significant (%)						3
W-W similar to SWAP (%)						94

	Locations
W-W: PD = 0	2566
Overestimated by SWAP: PD > 0	77
SWAP: PD = 0	2567
Overestimated by W-W: PD > 0	78

Table 3.5 *The group total number of tested locations matched to the PD probability scores with W-W perimetry and SWAP across all the normal subjects, at the second visit (visit 2). Summary tables give the proportions of the tested locations that are more depressed with the one and/or the other algorithm and the total number of locations lying within the normal confidence limits when tested with W-W perimetry that are overestimated by SWAP and vice versa, for all the normal subjects at the second visit (visit 2).*

PD Upper Hemifield							PD Lower Hemifield					
W-W							W-W					
SWAP	%	0	<5	<2	<1	<0.5	%	0	<5	<2	<1	<0.5
	0	1259	26	5	4	1	0	1230	28	6	6	3
	<5	21	3	0	0	0	<5	26	1	0	0	1
	<2	2	1	0	0	0	<2	9	0	0	0	0
	<1	1	0	0	0	0	<1	7	0	0	0	0
	<0.5	2	0	0	0	0	<0.5	8	0	0	0	0
W-W more significant (%)						3	W-W more significant (%)					3
SWAP more significant (%)						2	SWAP more significant (%)					4
W-W similar to SWAP (%)						95	W-W similar to SWAP (%)					93

Table 3.6 *The group total number of tested locations of the upper and lower field matched to the PD probability scores with W-W perimetry and SWAP, across all the normal subjects, at the second visit (visit 2). Summary tables give the proportions of the tested locations that are more depressed with the one and/or the other algorithm.*

As expected, the two algorithms perform similarly when describing the shape of the hill of vision across the normal group (table 3.5). The measurement error is also similarly between the two techniques among the locations of the upper and lower hemifield, the central and most peripheral region of the field (table 3.7).

PD Central Field							PD Peripheral Field					
		W-W						W-W				
SWAP	%	0	<5	<2	<1	<0.5	%	0	<5	<2	<1	<0.5
	0	1195	23	9	6	1	0	1294	31	2	4	2
	<5	26	1	0	0	0	<5	21	3	0	0	1
	<2	5	1	0	0	0	<2	6	0	0	0	0
	<1	0	0	0	0	0	<1	8	0	0	0	0
	<0.5	5	0	0	0	0	<0.5	6	0	0	0	0
W-W more significant (%)						3	W-W more significant (%)					3
SWAP more significant (%)						3	SWAP more significant (%)					3
W-W similar to SWAP (%)						94	W-W similar to SWAP (%)					94

Table 3.7 *The group total number of tested locations of the central and peripheral field matched to the PD probability scores with W-W perimetry and SWAP, across all the normal subjects, at the second visit (visit 2). Summary tables give the proportions of the tested locations that are more depressed with the one and/or the other algorithm.*

The cohort comprised of 55 glaucoma patients. The group mean TD probability values as measured with the two techniques at the second visit are shown in tables 3.8 – 3.10.

TD						
W-W						
SWAP	%	0	<5	<2	<1	<0.5
	0	1638	132	76	63	91
	<5	73	36	23	25	59
	<2	28	13	9	9	90
	<1	12	5	5	8	81
	<0.5	18	8	4	7	237
W-W more significant (%)						24
SWAP more significant (%)						6
W-W similar to SWAP (%)						70

	Locations
W-W: TD = 0	1769
Overestimated by SWAP: TD > 0	131
SWAP: TD = 0	2000
Overestimated by W-W: TD > 0	362

Table 3.8 *The group total number of tested locations matched to the TD probability scores with W-W perimetry and SWAP across all glaucoma patients at the second visit (visit 2). Summary tables give the proportions of the tested locations that are more depressed with the one and/or the other algorithm and the total number of locations lying within the normal confidence limits when tested with W-W perimetry that are overestimated by SWAP and vice versa, for all glaucoma patients at the second visit (visit 2).*

TD Upper Hemifield							TD Lower Hemifield					
W-W							W-W					
SWAP	%	0	<5	<2	<1	<0.5	%	0	<5	<2	<1	<0.5
	0	836	68	30	14	25	0	802	64	46	49	66
	<5	41	23	14	21	38	<5	32	13	9	4	21
	<2	11	11	5	7	69	<2	17	2	4	2	21
	<1	3	2	1	2	58	<1	9	3	4	6	23
	<0.5	0	2	1	2	91	<0.5	18	6	3	5	146
W-W more significant (%)						25	W-W more significant (%)					22
SWAP more significant (%)						5	SWAP more significant (%)					7
W-W similar to SWAP (%)						70	W-W similar to SWAP (%)					71

Table 3.9 *The group total number of tested locations of the upper and lower matched to the TD probability scores with W-W perimetry and SWAP, across all glaucoma patients at the second visit (visit 2). Summary tables give the proportions of the tested locations that are more depressed with the one and/or the other algorithm.*

TD Central Field							TD Peripheral Field					
W-W							W-W					
SWAP	%	0	<5	<2	<1	<0.5	%	0	<5	<2	<1	<0.5
	0	770	61	40	31	61	0	867	71	36	32	30
	<5	29	16	13	11	22	<5	45	18	10	14	37
	<2	10	5	0	3	26	<2	19	8	9	6	64
	<1	6	3	2	3	39	<1	6	2	3	5	42
	<0.5	5	6	1	3	154	<0.5	13	2	3	4	84
W-W more significant (%)						23	W-W more significant (%)					24
SWAP more significant (%)						5	SWAP more significant (%)					7
W-W similar to SWAP (%)						72	W-W similar to SWAP (%)					69

Table 3.10 *The group total number of tested locations of the central and peripheral field matched to the TD probability scores with W-W perimetry and SWAP, across all glaucoma patients at the second visit (visit 2). Summary tables give the proportions of the tested locations that are more depressed with the one and/or the other algorithm*

The depressed locations in the TD probability plot maps are markedly less with SWAP than W-W perimetry. At the TD plot for the glaucoma group 18% of all locations which scored within the normal limits for SWAP are depressed by W-W perimetry, while only 7% of all normal locations for W-W were depressed for SWAP (table 3.9). The difference between the algorithms as a function of the total number of depressed locations with SWAP being more insensitive of the two techniques, is more prominent among the upper than the lower hemifield locations and marginally more in the periphery than the central regions.

The group mean PD probability values for the glaucoma group as measured with the two techniques at the second visit are shown in tables 3.11 – 3.13.

PD						
W-W						
SWAP	%	0	<5	<2	<1	<0.5
	0	1894	99	65	35	116
	<5	78	17	9	11	56
	<2	30	12	5	7	44
	<1	18	2	3	4	55
	<0.5	36	6	8	6	134
W-W more significant (%)						18
SWAP more significant (%)						7
W-W similar to SWAP (%)						75

	Locations
W-W: PD = 0	2056
Overestimated by SWAP: PD > 0	162
SWAP: PD = 0	2209
Overestimated by W-W: PD > 0	315

Table 3.11 *The group total number of tested locations matched to the PD probability scores with W-W perimetry and SWAP across all glaucoma patients at the second visit (visit 2). Summary tables give the proportions of the tested locations that are more depressed with the one and/or the other algorithm and the total number of locations lying within the normal confidence limits when tested with W-W perimetry that are overestimated by SWAP and vice versa, for all glaucoma patients, at the second visit (visit 2).*

PD Upper Hemifield							PD Lower Hemifield					
W-W							W-W					
SWAP	%	0	<5	<2	<1	<0.5	%	0	<5	<2	<1	<0.5
	0	941	51	39	22	53	0	953	48	26	13	63
	<5	35	12	7	9	42	<5	43	5	2	2	14
	<2	12	6	3	4	31	<2	18	6	2	3	13
	<1	3	0	1	2	37	<1	15	2	2	2	18
	<0.5	3	1	3	3	55	<0.5	33	5	5	3	79
W-W more significant (%)						21	W-W more significant (%)					15
SWAP more significant (%)						5	SWAP more significant (%)					10
W-W similar to SWAP (%)						74	W-W similar to SWAP (%)					75

Table 3.12 *The group total number of tested locations of the upper and lower matched to the PD probability scores with W-W perimetry and SWAP, across all glaucoma patients at the second visit (visit 2). Summary tables give the proportions of the tested locations that are more depressed with the one and/or the other algorithm.*

PD Central Field							PD Peripheral Field					
		W-W						W-W				
SWAP	%	0	<5	<2	<1	<0.5	%	0	<5	<2	<1	<0.5
	0	897	50	27	15	50	0	1000	51	38	19	64
	<5	32	8	3	7	21	<5	45	9	6	4	35
	<2	10	5	3	4	16	<2	19	7	2	3	28
	<1	6	0	0	3	24	<1	13	1	3	2	31
	<0.5	17	5	5	3	109	<0.5	17	1	3	3	26
W-W more significant (%)						16	W-W more significant (%)					20
SWAP more significant (%)						6	SWAP more significant (%)					8
W-W similar to SWAP (%)						78	W-W similar to SWAP (%)					72

Table 3.13 *The group total number of tested locations of the central and peripheral field matched to the PD probability scores with W-W perimetry and SWAP, across all glaucoma patients at the second visit (visit 2). Summary tables give the proportions of the tested locations that are more depressed with the one and/or the other algorithm.*

The mean number of abnormal points in the PD probability maps is greater for W-W perimetry than SWAP, referring to 11% of the total number of tested locations. It is noted that 14% of all locations fall within the limits of normality by SWAP but are depressed with W-W while 8 % of the locations are only depressed by SWAP (table 3.11). The two algorithms show the biggest differences in sensitivity in the upper hemifield (table 3.12) and SWAP scores less points in the PD maps relatively to W-W perimetry for the peripheral than the more central regions (table 3.13).

The cohort comprised 22 OHT patients. The group mean TD probability values as measured with the two techniques at the second visit, are shown in tables 3.14 – 3.16.

TD						
W-W						
SWAP	%	0	<5	<2	<1	<0.5
	0	925	40	16	13	9
	<5	26	2	2	3	3
	<2	8	1	4	2	5
	<1	5	2	2	5	12
	<0.5	2	0	3	2	8
W-W more significant (%)						10
SWAP more significant (%)						5
W-W similar to SWAP (%)						85

	Locations
W-W: TD = 0	966
Overestimated by SWAP: TD > 0	41
SWAP: TD = 0	1003
Overestimated by W-W: TD > 0	78

Table 3.14. *The group total number of tested locations matched to the TD probability scores with W-W perimetry and SWAP across all OHT patients at the second visit (visit 2). Summary tables give the proportions of the tested locations that are more depressed with the one and/or the other algorithm and the total number of locations lying within the normal confidence limits when tested with W-W perimetry that are overestimated by SWAP and vice versa, for all OHT patients at the second visit (visit 2).*

TD Upper Hemifield							TD Lower Hemifield					
W-W							W-W					
SWAP	%	0	<5	<2	<1	<0.5	%	0	<5	<2	<1	<0.5
	0	473	23	8	9	2	0	452	17	8	4	7
	<5	2	1	1	1	0	<5	24	1	1	2	3
	<2	2	0	0	1	4	<2	6	1	4	1	1
	<1	0	1	1	1	11	<1	5	1	1	4	1
	<0.5	0	0	2	0	7	<0.5	2	0	1	2	1
W-W more significant (%)						11	W-W more significant (%)					8
SWAP more significant (%)						1	SWAP more significant (%)					8
W-W similar to SWAP (%)						88	W-W similar to SWAP (%)					84

Table 3.15. *The group total number of tested locations of the upper and lower field matched to the TD probability scores with W-W perimetry and SWAP, across all OHT patients at the second visit (visit 2). Summary tables give the proportions of the tested locations that are more depressed with the one and/or the other algorithm.*

TD Central Field							TD Peripheral Field					
W-W							W-W					
SWAP	%	0	<5	<2	<1	<0.5	%	0	<5	<2	<1	<0.5
	0	442	20	10	7	6	0	483	20	6	6	3
	<5	15	1	0	2	2	<5	11	1	2	1	1
	<2	3	0	0	0	3	<2	5	1	4	2	2
	<1	1	0	0	2	6	<1	4	2	2	3	6
	<0.5	0	0	1	2	5	<0.5	2	0	2	0	3
W-W more significant (%)						11	W-W more significant (%)					9
SWAP more significant (%)						4	SWAP more significant (%)					5
W-W similar to SWAP (%)						85	W-W similar to SWAP (%)					86

Table 3.16. *The group total number of tested locations of the central and peripheral field matched to the TD probability scores with W-W perimetry and SWAP, across all OHT patients at the second visit (visit 2). Summary tables give the proportions of the tested locations that are more depressed with the one and/or the other algorithm*

Across the OHT group, the measurement error with W-W perimetry was greater than for SWAP involving 78 and 41 points respectively within the summary probability map (table 3.14). The W-W algorithm scored 7.5 times more abnormal points than SWAP across the upper hemifield (table 3.15); 2.5 more locations within the central region and 1.7 more locations within the peripheral field (table 3.16). For the locations of the lower hemifield the two algorithms are different for the same percentage of locations (8%) (table 3.15).

The group mean PD probability values for the OHT patients as measured with the two techniques at the second visit, are shown in tables 3.17 – 3.19.

PD						
W-W						
SWAP	%	0	<5	<2	<1	<0.5
	0	983	20	6	1	2
	<5	28	4	3	3	8
	<2	14	0	1	2	7
	<1	1	2	0	0	4
	<0.5	5	2	3	0	1
W-W more significant (%)						5
SWAP more significant (%)						5
W-W similar to SWAP (%)						90

	Locations
W-W: PD = 0	1031
Overestimated by SWAP: PD > 0	48
SWAP: PD = 0	1012
Overestimated by W-W: PD > 0	29

Table 3.17. *The group total number of tested locations matched to the PD probability scores with W-W perimetry and SWAP across all OHT patients at the second visit (visit 2). Summary tables give the proportions of the tested locations that are more depressed with the one and/or the other algorithm and the total number of locations lying within the normal confidence limits when tested with W-W perimetry that are overestimated by SWAP and vice versa, for all OHT patients, at the second visit (visit 2).*

PD Upper Hemifield							PD Lower Hemifield					
W-W							W-W					
SWAP	%	0	<5	<2	<1	<0.5	%	0	<5	<2	<1	<0.5
	0	488	15	3	0	2	0	495	5	3	1	0
	<5	9	1	2	3	8	<5	19	3	1	0	0
	<2	3	0	1	2	7	<2	11	0	0	0	0
	<1	0	1	0	0	4	<1	1	1	0	0	0
	<0.5	1	0	0	0	0	<0.5	4	2	3	0	1
W-W more significant (%)						8	W-W more significant (%)					2
SWAP more significant (%)						3	SWAP more significant (%)					7
W-W similar to SWAP (%)						89	W-W similar to SWAP (%)					91

Table 3.18. *The group total number of tested locations of the upper and lower field matched to the PD probability scores with W-W perimetry and SWAP, across all OHT patients at the second visit (visit 2). Summary tables give the proportions of the tested locations that are more depressed with the one and/or the other algorithm.*

PD Central Field							PD Peripheral Field						
		W-W						W-W					
SWAP	%	0	<5	<2	<1	<0.5	%	0	<5	<2	<1	<0.5
	0	478	11	4	0	0	0	507	9	2	1	2
	<5	7	1	2	1	2	<5	21	3	1	2	6
	<2	6	0	1	1	4	<2	6	0	0	1	3
	<1	0	0	0	0	4	<1	1	2	0	0	0
	<0.5	3	2	1	0	0	<0.5	2	0	2	0	1
W-W more significant (%)						5	W-W more significant (%)						5
SWAP more significant (%)						4	SWAP more significant (%)						6
W-W similar to SWAP (%)						91	W-W similar to SWAP (%)						89

Table 3.19. *The group total number of tested locations of the central and peripheral field matched to the PD probability scores with W-W perimetry and SWAP, across all OHT patients, at the second visit (visit 2). Summary tables give the proportions of the tested locations that are more depressed with the one and/or the other algorithm.*

From the summary PD map (table 3.17), it is apparent that the algorithms demonstrate a similar measurement error when evaluating the shape of the hill of vision across the OHT group. SWAP however, overestimated a total number of 48 locations that were normal by W-W perimetry, as opposed to 29 locations that were only abnormal with SWAP. The hemifield analysis shows that W-W describes almost 3 times more abnormal points than SWAP in the upper field, but this relationship is reversed for the lower hemifield locations where W-W and SWAP score 10 and 41 abnormal locations, respectively (table 3.18). The differences between the algorithms are less for the peripheral locations but the measurement error between W-W and SWAP is 3:2 for the locations of the central region (table 3.19).

The cohort comprised of 18 patients with cataract. The group mean TD probability values as measured with the two techniques at the second visit are shown in tables 3.20 – 3.22.

		TD				
		W-W				
	%	0	<5	<2	<1	<0.5
SWAP	0	409	101	46	41	31
	<5	24	26	14	11	23
	<2	16	15	9	7	20
	<1	6	5	6	9	10
	<0.5	8	12	8	6	37
W-W more significant (%)						34
SWAP more significant (%)						12
W-W similar to SWAP (%)						54

	Locations
W-W: TD = 0	463
Overestimated by SWAP: TD > 0	54
SWAP: TD = 0	628
Overestimated by W-W: TD > 0	219

Table 3.20. *The group total number of tested locations matched to the TD probability scores with W-W perimetry and SWAP, across all patients with cataract at the second visit (visit 2). Summary tables give the proportions of the tested locations that are more depressed with the one and/or the other algorithm and the total number of locations lying within the normal confidence limits when tested with W-W perimetry that are overestimated by SWAP and vice versa, for all patients with cataract , at the second visit (visit 2).*

Across the patients with cataract, W-W perimetry described more depressed locations than SWAP. The difference in the performance between the two algorithms is also evident from the fact that 35% of all tested locations were scored as normal with SWAP but showed decreased sensitivity with W-W perimetry In contrast only 4 % of the locations identified as normal by W-W perimetry were depressed by SWAP (table 3.21).

TD Upper Hemifield							TD Lower Hemifield						
	W-W							W-W					
SWAP	%	0	<5	<2	<1	<0.5	%	0	<5	<2	<1	<0.5
	0	219	71	24	19	15	0	190	30	22	22	16
	<5	15	19	6	2	8	<5	9	7	8	9	15
	<2	6	11	5	3	3	<2	10	4	4	4	17
	<1	2	1	3	5	2	<1	4	4	3	4	8
	<0.5	1	0	1	2	7	<0.5	7	12	7	4	30
W-W more significant (%)						34	W-W more significant (%)						34
SWAP more significant (%)						9	SWAP more significant (%)						14
W-W similar to SWAP (%)						57	W-W similar to SWAP (%)						52

Table 3.21 *The group total number of tested locations of the upper and lower matched to the TD probability scores with W-W perimetry and SWAP, across all patients with cataract at the second visit (visit 2). Summary tables give the proportions of the tested locations that are more depressed with the one and/or the other algorithm.*

TD Central Field							TD Peripheral Field						
	W-W							W-W					
SWAP	%	0	<5	<2	<1	<0.5	%	0	<5	<2	<1	<0.5
	0	171	51	28	20	28	0	238	50	18	21	3
	<5	4	7	5	3	19	<5	20	19	9	8	4
	<2	3	6	3	2	10	<2	13	9	6	5	10
	<1	4	3	4	5	9	<1	2	2	2	4	1
	<0.5	4	5	3	2	33	<0.5	4	7	5	4	4
W-W more significant (%)						41	W-W more significant (%)						28
SWAP more significant (%)						9	SWAP more significant (%)						15
W-W similar to SWAP (%)						50	W-W similar to SWAP (%)						57

Table 3.22 *The group total number of tested locations of the central and peripheral field matched to the TD probability scores with W-W perimetry and SWAP, across all patients with cataract at the second visit (visit 2). Summary tables give the proportions of the tested locations that are more depressed with the one and/or the other algorithm*

Overall, more points of the TD map were shown to be depressed by W-W perimetry than SWAP. This was a consistent finding across the upper and lower hemifield and when the central and peripheral regions of the field were evaluated separately. W-

W recorded 3.6 times more locations than SWAP being outside the normal limits across the upper hemifield (table 3.21) and the difference between the two algorithms was exacerbated among the most central locations (table 3.22).

The group mean PD probability values as measured with the two techniques for the cataract patients at the second visit are shown in tables 3.23 – 3.25.

PD						
	W-W					
	%	0	<5	<2	<1	<0.5
SWAP	0	698	44	14	18	8
	<5	57	10	5	4	2
	<2	12	2	2	2	1
	<1	7	0	2	0	0
	<0.5	9	3	0	0	0
W-W more significant (%)						11
SWAP more significant (%)						10
W-W similar to SWAP (%)						79

	Locations
W-W: PD = 0	783
Overestimated by SWAP: PD > 0	85
SWAP: PD = 0	782
Overestimated by W-W: PD > 0	84

Table 3.23 *The group total number of tested locations matched to the PD probability scores with W-W perimetry and SWAP across all patients with cataract, at the second visit (visit 2). Summary tables give the proportions of the tested locations that are more depressed with the one and/or the other algorithm and the total number of locations lying within the normal confidence limits when tested with W-W perimetry that are overestimated by SWAP and vice versa, for all patients with cataract, at the second visit (visit 2).*

PD Upper Hemifield							PD Lower Hemifield						
	W-W							W-W					
SWAP	%	0	<5	<2	<1	<0.5	%	0	<5	<2	<1	<0.5
	0	375	26	6	9	3	0	323	18	8	9	5
	<5	16	1	4	2	0	<5	41	9	1	2	2
	<2	3	0	2	2	0	<2	9	2	0	0	1
	<1	0	0	0	0	0	<1	7	0	2	0	0
	<0.5	1	0	0	0	0	<0.5	8	3	0	0	0
W-W more significant (%)						12	W-W more significant (%)						10
SWAP more significant (%)						4	SWAP more significant (%)						16
W-W similar to SWAP (%)						84	W-W similar to SWAP (%)						74

Table 3.24 *The group total number of tested locations of the upper and lower field matched to the PD probability scores with W-W perimetry and SWAP, across all patients with cataract, at the second visit (visit 2). Summary tables give the proportions of the tested locations that are more depressed with the one and/or the other algorithm.*

PD Central Field							PD Peripheral Field						
	W-W							W-W					
SWAP	%	0	<5	<2	<1	<0.5	%	0	<5	<2	<1	<0.5
	0	312	24	8	9	5	0	384	21	6	9	3
	<5	29	8	4	3	2	<5	28	3	1	1	0
	<2	6	2	1	2	1	<2	6	0	1	0	0
	<1	5	0	1	0	0	<1	2	0	1	0	0
	<0.5	7	3	0	0	0	<0.5	2	0	0	0	0
W-W more significant (%)						13	W-W more significant (%)						9
SWAP more significant (%)						12	SWAP more significant (%)						8
W-W similar to SWAP (%)						75	W-W similar to SWAP (%)						83

Table 3.25. *The group total number of tested locations of the central and peripheral field matched to the PD probability scores with W-W perimetry and SWAP, across all patients with cataract, at the second visit (visit 2). Summary tables give the proportions of the tested locations that are more depressed with the one and/or the other algorithm.*

In the summary PD probability W-W perimetry and SWAP exceed each other on a similar percentage of the total number of tested locations (table 3.23). With reference to the percentage of locations being depressed with each algorithm, W-W perimetry appears effected by cataract considerably more than SWAP in the upper

hemifield. Surprisingly the score is reversed for the locations of the lower hemifield where SWAP scores 1.6 more abnormal locations than W-W (table 3.24).

3.15.2 Between visits within algorithm

The within algorithm between visits analysis was based upon the results obtained at the second and third visit from 35 normal subjects and 22 glaucoma patients only that had attended for a third examination with W-W and SWAP perimetry.

The group mean TD probability values as measured with W-W perimetry at two consecutive visits across the normal group, are shown in tables 3.26 – 3.27.

TD						
W-W visit 2						
W-W visit 3	%	0	<5	<2	<1	<0.5
	0	1616	39	6	6	2
	<5	50	4	0	2	0
	<2	9	1	0	0	0
	<1	8	2	0	0	0
	<0.5	5	0	0	0	0
Visit 2 more significant						3
Visit 3 more significant						4
Visit 2 similar to Visit 3						93

	Locations
W-W visit 2: TD = 0	1688
Overestimated on visit 3 by W-W: TD > 0	72
W-W visit 3: TD = 0	1669
Overestimated on visit 2 by W-W: TD > 0	53

Table 3.26 *The group total number of tested locations matched to the TD probability scores with W-W perimetry at visit 2 and visit 3 respectively across all normal subjects. Summary tables give the proportions of the tested locations that are more depressed at the one and/or the other visit and the total number of locations lying within the normal confidence limits when tested at visit 2 that are overestimated at visit 3 and vice versa, for all the normal subjects tested with W-W perimetry.*

W-W perimetry appears more sensitive at the third visit, with 19 locations appearing normal for visit 2 although depressed at visit 3 (table 3.26). Also the numbers of depressed points below 0.1% is increased from 8 to 13.

TD Upper Hemifield							TD Lower Hemifield						
	W-W visit 2							W-W visit 2					
W-W visit 3	%	0	<5	<2	<1	<0.5	%	0	<5	<2	<1	<0.5
	0	803	22	2	3	1	0	811	17	4	3	1
	<5	26	2	0	1	0	<5	24	2	0	1	0
	<2	5	1	0	0	0	<2	5	0	0	0	0
	<1	4	1	0	0	0	<1	5	1	0	0	0
	<0.5	4	0	0	0	0	<0.5	1	0	0	0	0
Visit 2 more significant						3	**Visit 2 more significant**						3
Visit 3 more significant						5	**Visit 3 more significant**						4
Visit 2 similar to Visit 3						92	**Visit 2 similar to Visit 3**						93

Table 3.27 *The group total number of tested locations of the upper and lower field matched to the TD probability scores with W-W perimetry at visit 2 and visit 3 respectively, across all normal subjects. Summary tables give the proportions of the tested locations that are more depressed at the second and/or the third visit.*

TD Central Field							TD Peripheral Field						
	W-W visit 2							W-W visit 2					
W-W Visit 3	%	0	<5	<2	<1	<0.5	%	0	<5	<2	<1	<0.5
	0	764	18	5	2	1	0	852	21	1	4	1
	<5	30	3	0	1	0	<5	20	1	0	1	0
	<2	7	1	0	0	0	<2	2	0	0	0	0
	<1	4	2	0	0	0	<1	4	0	0	0	0
	<0.5	2	0	0	0	0	<0.5	3	0	0	0	0
Visit 2 more significant						3	**Visit 2 more significant**						3
Visit 3 more significant						5	**Visit 3 more significant**						3
Visit 2 similar to Visit 3						92	**Visit 2 similar to Visit 3**						94

Table 3.28 *The group total number of tested locations of the central and peripheral field matched to the TD probability scores with W-W perimetry scored at visit 2 and visit 3 respectively, across all normal subjects. Summary tables give the proportions of the tested locations that are more depressed at the second and/or the third visit with the same algorithm.*

From the group mean probability values, it is apparent that the measurement error with W-W perimetry is increased at the third visit (table 3.28). The number of depressed points at visit 2 compared to visit 3 is similar for the upper and lower hemifield. As a function of eccentricity, the locations with depression increase by twelve new entries at visit 3 across the central field but the results remain the same for the locations of the most peripheral region. The group mean TD probability values as measured with SWAP at two consecutive visits across the normal group, are shown in tables 3.29 – 3.31.

TD						
SWAP visit 2						
SWAP visit 3	%	0	<5	<2	<1	<0.5
	0	1610	36	11	5	4
	<5	33	16	4	0	2
	<2	10	4	5	2	1
	<1	4	0	0	0	2
	<0.5	1	0	0	0	0
Visit 2 more significant						4
Visit 3 more significant						3
Visit 2 similar to Visit 3						93

	Locations
SWAP visit 2: TD = 0	1658
Overestimated on visit 3 by SWAP: TD > 0	48
WW visit 3: TD = 0	1666
Overestimated on visit 2 by W-W: TD > 0	56

Table 3.29 *The group total number of tested locations matched to the TD probability scores with SWAP at visit 2 and visit 3 respectively, across all normal subjects. Summary tables give the proportions of the tested locations that are more depressed at one and/or the other visit and the total number of locations lying within the normal confidence limits when tested at visit 2 that are overestimated at visit 3 and vice versa, for all the normal subjects tested with SWAP.*

For the SWAP algorithm visit 3 shows an improvement of depressed locations at all probability levels. For example, at a probability level of 0.5%, visit 3 scored only one

depressed location in the TD map, as opposed to a total number of 4 locations exhibiting this level of depression for visit 2.

TD Upper Hemifield							TD Lower Hemifield						
SWAP visit 2							SWAP visit 2						
SWAP visit 3	%	0	<5	<2	<1	<0.5	%	0	<5	<2	<1	<0.5
	0	807	17	4	0	0	0	803	18	7	5	4
	<5	22	9	2	0	0	<5	12	7	2	0	2
	<2	6	3	2	1	0	<2	4	1	3	1	1
	<1	2	0	0	0	0	<1	2	0	0	0	2
	<0.5	0	0	0	0	0	<0.5	1	0	0	0	0
Visit 2 more significant						3	**Visit 2 more significant**						5
Visit 3 more significant						4	**Visit 3 more significant**						2
Visit 2 similar to Visit 3						93	**Visit 2 similar to Visit 3**						93

Table 3.30 *The group total number of tested locations of the upper and lower field matched to the probability scores with SWAP at visit 2 and visit 3 respectively, across all normal subjects. Summary tables give the proportions of the tested locations that are more depressed at the second and/or the third visit with the same algorithm.*

TD Central Field							TD Peripheral Field						
SWAP visit2							SWAP visit 2						
SWAP visit 3	%	0	<5	<2	<1	<0.5	%	0	<5	<2	<1	<0.5
	0	789	22	3	2	1	0	821	14	8	3	3
	<5	11	2	2	0	1	<5	22	14	2	0	1
	<2	3	0	0	0	0	<2	7	4	5	2	1
	<1	3	0	0	0	1	<1	1	0	0	0	1
	<0.5	0	0	0	0	0	<0.5	1	0	0	0	0
Visit 2 more significant						4	**Visit 2 more significant**						4
Visit 3 more significant						2	**Visit 3 more significant**						4
Visit 2 similar to Visit 3						94	**Visit 2 similar to Visit 3**						92

Table 3.31 *The group total number of tested locations of the central and peripheral field matched to the TD probability scores with SWAP at visit 2 and visit 3 respectively, across all normal subjects. Summary tables give the proportions of the tested locations that are more depressed at the second and/or the third visit with the same algorithm.*

The difference between the two visits is wider for the lower hemifield locations where a total of 23 locations became normal at visit 3. A smaller extent of improvement of the TD points is apparent across the central region (table 3.30) and is more present at the upper hemifield (table 3.31) where the total number of depressed points was reduced at visit 3 by 14 and 9 locations, respectively. In contrast, SWAP has similar scores between visits for the locations of the most peripheral regions (table 3.31).

The group mean PD probability values as measured with W-W perimetry at two consecutive visits, across the normal group, are shown in tables 3.32 – 3.34.

PD						
W-W visit 2						
W-W visit 3	%	0	<5	<2	<1	<0.5
	0	1629	35	5	10	3
	<5	33	5	1	0	0
	<2	15	2	0	0	0
	<1	6	0	1	0	1
	<0.5	4	0	0	0	0
Visit 2 more significant						3
Visit 3 more significant						3
Visit 2 similar to Visit 3						94

	Locations
W-W visit 2: PD = 0	1687
Overestimated on visit 3 by W-W: TD > 0	58
W-W visit 3: PD = 0	1682
Overestimated on visit 2 by W-W: TD > 0	53

Table 3.32 *The group total number of tested locations matched to the PD probability scores at visit 2 and visit 3 respectively, with W-W perimetry across all normal subjects. Summary tables give the proportions of the tested locations that are more depressed at one and/or the other visit and the total number of locations lying within the normal confidence limits when tested with W-W perimetry at visit 2 that are overestimated at visit 3 and vice versa, for all the normal subjects.*

The PD maps for the two consecutive visits across the normal group reveal 6 new locations being depressed for visit 3 while normal at visit 2, although as a proportion of the total number of tested locations the two visits appear equally sensitive. In comparison, to the TD plot the PD analysis reduced the difference between the results derived by the two visits but visit 3 remained marginally more sensitive than visit 2.

PD Upper Hemifield							PD Lower Hemifield					
	W-W visit 2							W-W visit 2				
W-W visit 3	%	0	<5	<2	<1	<0.5	%	0	<5	<2	<1	<0.5
	0	817	17	3	4	1	0	811	18	3	6	2
	<5	14	3	0	0	0	<5	20	1	1	0	0
	<2	8	2	0	0	0	<2	7	0	0	0	0
	<1	2	0	0	0	0	<1	4	0	1	0	1
	<0.5	4	0	0	0	0	<0.5	0	0	0	0	0
Visit 2 more significant						3	**Visit 2 more significant**					4
Visit 3 more significant						3	**Visit 3 more significant**					4
Visit 2 similar to Visit 3						94	**Visit 2 similar to Visit 3**					93

Table 3.33 *The group total number of tested locations of the upper and lower field matched to the PD probability scores with W-W perimetry at visit 2 and visit 3 respectively, across all normal subjects. Summary tables give the proportions of the tested locations that are more depressed at the second and/or the third visit with the same algorithm.*

PD Central Field							PD Peripheral Field					
		W-W visit 2						W-W visit 2				
W-W visit 3	%	0	<5	<2	<1	<0.5	%	0	<5	<2	<1	<0.5
	0	775	17	3	6	0	0	854	18	2	4	3
	<5	23	2	1	0	0	<5	10	3	0	0	0
	<2	7	2	0	0	0	<2	8	0	0	0	0
	<1	2	0	1	0	1	<1	4	0	0	0	0
	<0.5	0	0	0	0	0	<0.5	4	0	0	0	0
Visit 2 more significant						3	**Visit 2 more significant**					3
Visit 3 more significant						4	**Visit 3 more significant**					3
Visit 2 similar to Visit 3						93	**Visit 2 similar to Visit 3**					94

Table 3.34 *The group total number of tested locations of the central and peripheral field matched to the PD probability scores with W-W perimetry at visit 2 and visit 3 respectively, across all normal subjects. Summary tables give the proportions of the tested locations that are more depressed at the second and/or the third visit with the same algorithm.*

The PD maps for the two consecutive visits across the normal group reveal 6 new locations being depressed for visit 3 while normal at visit 2. All but one from a total of 6 locations that were depressed only at visit 3 are identified within the central region of the field (table 3.34) and the upper hemifield (table 3.34). Therefore the algorithm appeared most reproducible between visit 2 and 3 among the locations of the most peripheral region and at the lower hemifield (table 3.33).

The group mean PD probability values as measured with SWAP, at two consecutive visits across the normal group, are shown in tables 3.35 – 3.37.

PD						
SWAP visit 2						
SWAP visit 3	%	0	<5	<2	<1	<0.5
	0	1662	23	8	4	6
	<5	20	4	1	0	0
	<2	6	4	1	2	1
	<1	4	0	0	1	2
	<0.5	1	0	0	0	0
Visit 2 more significant						3
Visit 3 more significant						2
Visit 2 similar to Visit 3						95

	Locations
SWAP Visit 2: PD = 0	1693
Overestimated on visit 3 by SWAP: PD > 0	31
W-W Visit 3: PD = 0	1703
Overestimated on visit 2 by SWAP: PD > 0	41

Table 3.35 *The group total number of tested locations matched to the PD probability scores with SWAP at visit 2 and visit 3 respectively, across all normal subjects. Summary tables give the proportions of the tested locations that are more depressed at the one and/or the other visit and the total number of locations lying within the normal confidence limits when tested with SWAP at visit 2 that are overestimated at visit 3 and vice versa, for all the normal subjects.*

PD Upper Hemifield							PD Lower Hemifield					
SWAP visit 2							SWAP visit 2					
SWAP Visit 3	%	0	<5	<2	<1	<0.5	%	0	<5	<2	<1	<0.5
	0	834	12	1	0	0	0	828	11	7	4	6
	<5	13	2	0	0	0	<5	7	2	1	0	0
	<2	4	2	1	1	0	<2	2	2	0	1	1
	<1	3	0	0	0	2	<1	1	0	0	1	0
	<0.5	0	0	0	0	0	<0.5	1	0	0	0	0
Visit 2 more significant						2	**Visit 2 more significant**					4
Visit 3 more significant						3	**Visit 3 more significant**					1
Visit 2 similar to Visit 3						95	**Visit 2 similar to Visit 3**					95

Table 3.36 *The group total number of tested locations of the upper and lower field matched to the PD probability scores with SWAP at visit 2 and visit 3 respectively, across all normal subjects. Summary tables give the proportions of the tested locations that are more depressed at the second and/or the third visit with the same algorithm.*

PD Central Field							PD Peripheral Field					
SWAP visit 2							SWAP visit 2					
SWAP visit 3	%	0	<5	<2	<1	<0.5	%	0	<5	<2	<1	<0.5
	0	811	14	5	0	3	0	851	9	3	4	3
	<5	4	1	0	0	0	<5	16	3	1	0	0
	<2	0	1	0	0	0	<2	6	3	1	2	1
	<1	0	0	0	0	0	<1	4	0	0	1	2
	<0.5	1	0	0	0	0	<0.5	0	0	0	0	0
Visit 2 more significant						3	**Visit 2 more significant**					3
Visit 3 more significant						1	**Visit 3 more significant**					3
Visit 2 similar to Visit 3						96	**Visit 2 similar to Visit 3**					94

Table 3.37 *The group total number of tested locations of the central and peripheral field matched to the PD probability scores with SWAP at visit 2 and visit 3 respectively, across all normal subjects. Summary tables give the proportions of the tested locations that are more depressed at the second and/or the third visit with the same algorithm.*

SWAP perimetry based on the PD analysis showed that light sensitivity improved at Visit 3 with 12 more locations showing scores within normal limits, although initially depressed at visit 2 (table 3.35). The difference between the two visits was maximal for the lower hemifield locations, where 31 locations were depressed at visit 2 but only 13 remained abnormal at visit 3 (table 3.36). The total number of affected locations reduced to half across the central region by the third visit but there was a very small increase of depressed peripheral locations (table 3.37).

The group mean TD probability values as measured with W-W perimetry at two consecutive visits across the glaucoma patients, are shown in tables 3.38 – 3.40.

TD						
W-W visit 2						
W-W visit 3	%	0	<5	<2	<1	<0.5
	0	716	38	21	10	12
	<5	39	13	2	7	12
	<2	13	6	5	2	14
	<1	4	9	3	8	6
	<0.5	12	6	7	10	125
Visit 2 more significant						11
Visit 3 more significant						10
Visit 2 similar to Visit 3						79

	Locations
W-W visit 2: TD = 0	784
Overestimated on visit 3 by W-W: TD > 0	68
W-W visit 3: TD = 0	797
Overestimated on visit 2 by W-W: TD > 0	81

Table 3.38 *The group total number of tested locations matched to the TD probability scores with W-W perimetry at visit 2 and visit 3 respectively, across all glaucoma patients. Summary tables give the proportions of the tested locations that are more depressed at the one and/or the other visit and the total number of locations lying within the normal confidence limits when tested with W-W perimetry at visit 2 that are overestimated at visit 3 and vice versa, for all the glaucoma patients.*

TD Upper Hemifield							TD Lower Hemifield					
W-W visit 2							W-W visit 2					
W-W visit 3	%	0	<5	<2	<1	<0.5	%	0	<5	<2	<1	<0.5
	0	358	21	8	2	4	0	358	17	13	8	8
	<5	21	9	1	1	8	<5	18	4	1	6	4
	<2	7	5	0	0	7	<2	6	1	5	2	7
	<1	0	5	3	3	4	<1	4	4	0	5	2
	<0.5	2	1	4	3	73	<0.5	10	5	3	7	52
Visit 2 more significant						10	**Visit 2 more significant**					12
Visit 3 more significant						9	**Visit 3 more significant**					11
Visit 2 similar to Visit 3						81	**Visit 2 similar to Visit 3**					77

Table 3.39 *The group total number of tested locations of the upper and lower field matched to the TD probability scores with W-W perimetry at visit 2 and visit 3 respectively, across all glaucoma patients. Summary tables give the proportions of the tested locations that are more depressed at the second and/or the third visit with the same algorithm.*

TD Central Field							TD Peripheral Field						
W-W visit 2							W-W visit 2						
W-W visit 3	%	0	<5	<2	<1	<0.5	%	0	<5	<2	<1	<0.5
	0	336	20	7	8	5	0	379	17	13	2	7
	<5	14	6	2	4	4	<5	24	9	0	4	8
	<2	4	1	2	1	9	<2	9	5	3	1	6
	<1	1	5	1	5	4	<1	3	4	2	3	2
	<0.5	7	3	5	3	71	<0.5	5	3	2	7	54
Visit 2 more significant						12	**Visit 2 more significant**						10
Visit 3 more significant						8	**Visit 3 more significant**						11
Visit 2 similar to Visit 3						80	**Visit 2 similar to Visit 3**						79

Table 3.40. *The group total number of tested locations of the central and peripheral field matched to the TD probability scores with W-W perimetry at visit 2 and visit 3 respectively, across all glaucoma patients. Summary tables give the proportions of the tested locations that are more depressed at the second and/or the third visit with the same algorithm.*

Overall, light sensitivity is seemingly improved at visit 3. Across the total number of tested locations with W-W for the glaucoma group, visit 3 appears to score less depressed points than visit 2. This change refers to 15 locations (table 3.38), of which 10 locations belong to the lower hemifield (table 3.39). Moreover, the difference between the second and third visit is more prominent across the central region of the field than the most peripheral locations (table 3.40).

The group mean TD probability values measured with SWAP across the glaucoma group, at two consecutive visits, are shown in tables 3.41 – 3.43. Across the glaucoma group, visit 2 with SWAP is associated overall with greater number of depressed locations than visit 3 (table 3.41).

TD						
SWAP visit 2						
SWAP visit3	%	0	<5	<2	<1	<0.5
	0	740	50	10	4	2
	<5	38	30	16	7	2
	<2	19	9	26	4	11
	<1	3	4	4	22	8
	<0.5	8	1	3	9	70
Visit 2 more significant						10
Visit 3 more significant						9
Visit 2 similar to Visit 3						81

	Locations
SWAP visit2: TD = 0	808
Overestimated on visit 3 by SWAP: TD > 0	68
W-W visit 3: TD = 0	806
Overestimated on visit 2 by SWAP: TD > 0	66

Table 3.41. *The group total number of tested locations matched to the TD probability scores with SWAP at visit 2 and visit 3 respectively across all glaucoma patients. Summary tables give the proportions of the tested locations that are more depressed at the one and/or the other visit and the total number of locations lying within the normal confidence limits when tested with SWAP at visit 2 that are overestimated at visit 3 and vice versa, for all glaucoma patients.*

TD Upper Hemifield							TD Lower Hemifield					
SWAP visit 2							SWAP visit 2					
SWAP visit 3	%	0	<5	<2	<1	<0.5	%	0	<5	<2	<1	<0.5
	0	360	24	6	0	0	0	380	26	4	4	2
	<5	21	24	11	4	1	<5	17	6	5	3	1
	<2	11	4	19	1	2	<2	8	5	7	3	9
	<1	1	2	2	17	5	<1	2	2	2	5	3
	<0.5	3	0	2	6	24	<0.5	5	1	1	3	46
Visit 2 more significant						10	**Visit 2 more significant**					11
Visit 3 more significant						9	**Visit 3 more significant**					8
Visit 2 similar to Visit 3						81	**Visit 2 similar to Visit 3**					82

Table 3.42. *The group total number of tested locations of the upper and lower field matched to the TD probability scores with SWAP at visit 2 and visit 3 respectively, across all glaucoma patients. Summary tables give the proportions of the tested locations that are more depressed at the second and/or the third visit with the same algorithm.*

TD Central Field							TD Peripheral Field					
SWAP visit 2							SWAP visit 2					
SWAP visit 3	%	0	<5	<2	<1	<0.5	%	0	<5	<2	<1	<0.5
	0	364	27	3	1	1	0	376	23	7	3	2
	<5	17	5	7	4	1	<5	20	26	9	3	1
	<2	7	3	3	0	6	<2	12	6	23	4	5
	<1	3	3	2	11	6	<1	0	1	2	11	2
	<0.5	5	0	3	5	41	<0.5	3	1	0	3	29
Visit 2 more significant						11	**Visit 2 more significant**					10
Visit 3 more significant						9	**Visit 3 more significant**					8
Visit 2 similar to Visit 3						80	**Visit 2 similar to Visit 3**					81

Table 3.43. *The group total number of tested locations of the central and peripheral field matched to the TD probability scores with SWAP at visit 2 and visit 3 respectively, across all glaucoma patients. Summary tables give the proportions of the tested locations that are more depressed at the second and/or the third visit with the same algorithm.*

The performance of Visit 2 and visit 3 is very similar for the locations across the upper hemifield but there is a change of 15 locations across the lower hemifield (table 3.42). The improvement noted at visit 3 has a similar magnitude among the central and peripheral locations (table 3.43).

The group mean PD probability values as measured with W-W perimetry across the glaucoma patients, at two consecutive visits are shown in tables 3.44 – 3.46.

PD						
W-W visit 2						
W-W visit 3	%	0	<5	<2	<1	<0.5
	0	808	29	17	5	12
	<5	26	11	1	1	10
	<2	12	4	2	1	8
	<1	10	1	1	5	8
	<0.5	15	5	2	8	98
Visit 2 more significant						8
Visit 3 more significant						8
Visit 2 similar to Visit 3						84

	Locations
W-W visit 2: PD = 0	871
Overestimated on visit 3 by W-W: PD > 0	63
W-W visit 3: PD = 0	871
Overestimated on visit 2 by W-W: PD > 0	63

Table 3.44 *The group total number of tested locations matched to the PD probability scores with W-W perimetry at visit 2 and visit 3 respectively across all glaucoma patients. Summary tables give the proportions of the tested locations that are more depressed at the one and/or the other visit and the total number of locations lying within the normal confidence limits when tested with W-W perimetry at visit 2 that are overestimated at visit 3 and vice versa, for all glaucoma patients.*

PD Upper Hemifield							PD Lower Hemifield					
W-W visit 2							W-W visit 2					
W-W visit 3	%	0	<5	<2	<1	<0.5	%	0	<5	<2	<1	<0.5
	0	380	14	10	3	8	0	427	15	7	2	4
	<5	12	6	1	0	6	<5	14	4	0	1	4
	<2	6	3	2	1	6	<2	6	2	0	0	2
	<1	5	1	1	5	6	<1	5	0	0	0	3
	<0.5	2	2	1	3	66	<0.5	13	3	1	5	32
Visit 2 more significant						10	**Visit 2 more significant**					7
Visit 3 more significant						7	**Visit 3 more significant**					9
Visit 2 similar to Visit 3						83	**Visit 2 similar to Visit 3**					84

Table 3.45 *The group total number of tested locations of the upper and lower field matched to the PD probability scores with W-W perimetry at visit 2 and visit 3 respectively, across all glaucoma patients. Summary tables give the proportions of the tested locations that are more depressed at the second and/or the third visit with the same algorithm.*

PD Central Field							PD Peripheral Field					
W-W visit 2							W-W visit 2					
W-W visit 3	%	0	<5	<2	<1	<0.5	%	0	<5	<2	<1	<0.5
	0	386	12	7	2	6	0	422	17	10	3	6
	<5	11	6	0	0	3	<5	15	5	1	1	7
	<2	7	1	2	1	5	<2	5	3	0	0	3
	<1	5	0	1	2	6	<1	5	1	0	3	2
	<0.5	6	5	0	5	49	<0.5	9	0	2	3	49
Visit 2 more significant						8	**Visit 2 more significant**					9
Visit 3 more significant						8	**Visit 3 more significant**					8
Visit 2 similar to Visit 3						84	**Visit 2 similar to Visit 3**					83

Table 3.46. *The group total number of tested locations of the central and peripheral field matched to the PD probability scores with W-W perimetry at visit 2 and visit 3 respectively, across all glaucoma patients. Summary tables give the proportions of the tested locations that are more depressed at the second and/or the third visit with the same algorithm.*

According to the PD map, the W-W algorithm performs similarly for the two visits across the glaucoma group. The widest differences between the results of the two visits involve the locations of the upper hemifield where the numbers of scores between visit 2 and visit 3 have a ratio of 3:2. From the proportion of depressed locations it appears that visit 3 underestimates the defects in the upper hemifield, at all ranges of probability scores, but identifies more depression in the lower hemifield (table 3.45). W-W perimetry appears very reproducible among the central field locations but in the periphery visit 3 scores 7 less depressed points than visit 2 across the total glaucoma group.

The group mean PD probability values measured with SWAP for the glaucoma group at two consecutive visits are shown in tables 3.47 – 3.49.

PD						
SWAP visit 2						
SWAP visit 3	%	0	<5	<2	<1	<0.5
	0	848	46	6	11	9
	<5	35	16	16	3	3
	<2	6	9	8	6	2
	<1	3	2	4	10	4
	<0.5	6	3	3	3	38
Visit 2 more significant						10
Visit 3 more significant						7
Visit 2 similar to Visit 3						83

	Locations
SWAP visit 2: PD = 0	898
Overestimated on visit 3 by SWAP: TD > 0	50
W-W visit 3: PD = 0	920
Overestimated on visit 2 by SWAP: TD > 0	72

Table 3.47. *The group total number of tested locations matched to the PD probability scores with SWAP at visit 2 and visit 3 respectively across all glaucoma patients. Summary tables give the proportions of the tested locations that are more depressed at the one and/or the other visit and the total number of locations lying within the normal confidence limits when tested with SWAP at visit 2 that are overestimated at visit 3 and vice versa, for all glaucoma patients.*

PD Upper Hemifield							PD Lower Hemifield					
SWAP visit 2							SWAP visit 2					
SWAP visit 3	%	0	<5	<2	<1	<0.5	%	0	<5	<2	<1	<0.5
	0	416	26	1	2	0	0	432	20	5	9	9
	<5	19	9	9	2	0	<5	16	7	7	1	3
	<2	4	9	7	6	1	<2	2	0	1	0	1
	<1	3	1	4	7	1	<1	0	1	0	3	3
	<0.5	2	2	1	3	15	<0.5	4	1	2	0	23
Visit 2 more significant						9	**Visit 2 more significant**					11
Visit 3 more significant						9	**Visit 3 more significant**					5
Visit 2 similar to Visit 3						82	**Visit 2 similar to Visit 3**					84

Table 3.48. *The group total number of tested locations of the upper and lower field matched to the PD probability scores with SWAP at visit 2 and visit 3 respectively, across all glaucoma patients. Summary tables give the proportions of the tested locations that are more depressed at the second and/or the third visit with the same algorithm.*

PD Central Field							PD Peripheral Field					
SWAP visit 2							SWAP visit 2					
SWAP visit 3	%	0	<5	<2	<1	<0.5	%	0	<5	<2	<1	<0.5
	0	416	15	2	3	6	0	435	29	4	8	3
	<5	13	6	4	1	2	<5	22	9	12	2	1
	<2	2	1	3	2	1	<2	4	8	5	4	1
	<1	3	1	2	4	2	<1	0	1	2	6	2
	<0.5	6	3	0	2	28	<0.5	0	0	3	1	10
Visit 2 more significant						7	**Visit 2 more significant**					12
Visit 3 more significant						6	**Visit 3 more significant**					7
Visit 2 similar to Visit 3						87	**Visit 2 similar to Visit 3**					81

Table 3.49. *The group total number of tested locations of the central and peripheral field matched to the PD probability scores with SWAP at visit 2 and visit 3 respectively, across all glaucoma patients. Summary tables give the proportions of the tested locations that are more depressed at the second and/or the third visit with the same algorithm.*

According to the probability analysis for the SWAP algorithm 29 locations returned to normal at visit 3 suggesting that here was an overestimation of the level of depression at visit 2 (table 3.47). Light sensitivity is improved by 44% for the locations of the lower hemifield, and by 16% in the peripheral regions of the visual field. Moreover, Visit 3 is associated with similar number of abnormal locations to visit 2 within the upper hemifield and for the most central region.

The summary of the results for the within visit between algorithms differences across all study groups is presented in table 3.50.

Group		W-W / SWAP				
		global	upper	lower	central	periphery
Normal	TD	82 / 86	40 / 31	42 / 55	43 / 31	40 / 54
	PD	79 / 78	36 / 27	44 / 50	39 / 37	40 / 41
Glaucoma	TD	649 / 173	344 / 74	305 / 99	307 / 70	342 / 105
	PD	497 / 199	295 / 67	202 / 132	217 / 83	279 / 112
OHT	TD	105 / 51	60 / 8	45 / 43	56 / 22	49 / 29
	PD	56 / 55	46 / 14	10 / 41	29 / 19	27 / 34
Cataract	TD	304 / 106	153 / 39	151 / 64	175 / 38	129 / 68
	PD	98 / 92	52 / 20	46 / 72	58 / 52	41 / 39

Table 3.50 *The between -algorithm, within visit differences across all study groups for W-W perimetry and SWAP. Each cell shows the mean number of abnormal points with W-W perimetry over the mean number of abnormal points with SWAP.*

The summary of the results for the between-visit differences across all study groups is presented in table 3.51 for the W-W perimetry and in table 3.52 for SWAP.

Group		W-W LF (visit 2 / visit 3)				
		global	upper	lower	central	periphery
Normal	TD	55 / 75	29 / 41	26 / 36	27 / 46	28 / 29
	PD	55 / 61	25 / 30	31 / 32	28 / 35	27 / 26
Glaucoma	TD	124 / 109	56 / 51	68 / 58	64 / 54	60 / 64
	PD	92 / 84	55 / 36	38 / 49	42 / 41	50 / 43

Table 3.51 *The between visit differences across all study groups for W-W perimetry. Each cell shows the mean number of abnormal point with visit 2 over the mean number of abnormal points with visit 3.*

Group		SWAP LF (visit 2 / visit 3)				
		global	upper	lower	central	periphery
Normal	TD	66 / 52	24 / 33	43 / 20	31 / 17	34 / 35
	PD	47 / 35	16 / 22	31 / 13	12 / 6	25 / 29
Glaucoma	TD	114 / 98	54 / 52	60 / 46	56 / 48	59 / 48
	PD	106 / 77	48 / 48	58 / 26	38 / 33	66 / 41

Table3.52. *The between visit differences across all study groups for SWAP. Each cell shows the mean number of abnormal point with visit 2 over the mean number of abnormal points with visit 3.*

3.16 Discussion

For the normal group the two algorithms exhibited the same magnitude of measurement error overall across the field within the TD probability maps.

Group		W-W / SWAP				
		global	upper	lower	central	periphery
Normal	TD	0.95	1.29	0.76	1.39	0.74
	PD	1.01	1.33	0.88	1.10	1.00

Table 3.53. *The calculated ratio of the mean number of abnormal locations across the TD and PD maps for the normal group for W-W perimetry over the corresponding mean number of abnormal locations across the TD and PD maps for SWAP.*

However, the separate analysis of the central and peripheral locations have revealed measurement differences between the tests, that result in underscoring of TD points in the central region by SWAP and a surprising increase of abnormal locations with the same test within the most peripheral region. This is in agreement with research on normal variability with SWAP that compared to standard perimetry incorporates a wider range of values to describe normality, therefore locations that are scored as abnormal with W-W are likely to remain within the normal limits for

SWAP (Wild et al, 1998). The increased sensitivity of the algorithm across the most peripheral locations could be associated with a learning effect that would be expected to be more apparent in the periphery than the central region. It was also noted that SWAP was more depressed in the lower than the upper hemifield locations which contradicts previous reports on the normal hill of vision with SWAP which suggested that the technique is more sensitive within the inferior field (Sample, 1997). However, as expected, the evaluation of the shape of the normal field by the PD analysis with SWAP compared well to W-W perimetry without indications of any variability associated with eccentricity.

		W-W				
Normal Group		global	upper	lower	central	periphery
Visit2 / Visit3	TD	0.73	0.70	0.72	0.59	0.96
	PD	0.90	0.84	0.97	0.80	0.96

		SWAP				
Normal Group		global	upper	lower	central	periphery
Visit2 / Visit3	TD	1.27	0.73	2.15	1.83	0.97
	PD	1.34	0.73	2.38	2.00	4.31

Table 3.54 *The ratio of the mean number of abnormal locations across the TD and PD maps for the normal group at visit 2 over visit 3, for W-W perimetry and SWAP respectively.*

The between visits within algorithm analysis across the normal group for SWAP further supports the presence of a learning effect, as visit 3 was associated with improvement of sensitivity. The apparent decrease in abnormal locations is seen markedly across the central field but in the periphery the SWAP results appear unchanged. This is likely to be the combined effect of a learning effect with an enhanced fatigue effect at these locations. It is known that the results of the visual

field examinations are influenced by the learning effect and by the decline in performance due to fatigue (Moss, 1993). Moreover, the peripheral locations are subjected to fatigue effects more than the central locations, because they are examined later in the course of a single examination. Fatigue could counteract the impact of learning for the tested locations and lead to improvement of sensitivity when within any given follow up examination the learning effect is greater than the fatigue effect or when an increase in the learning effect coincides with a constant fatigue effect. The influence of fatigue on the magnitude of learning has been investigated for W-W perimetry (Hudson *et al*, 1994; Searle, Shaw *et al*, 1991a; Wild *et al*, 1991) where in the majority of cases, the learning process is completed after the initial two examinations (Weber, Dannheim *et al*, 1990; Wild *et al*, 1991). However, for SWAP the learning effect is still present beyond the third visit (Kim, 2002). Moreover, SWAP is associated with a detection task of increased difficulty compared to W-W perimetry that leads to longer examination duration and the results are subjected to greater fatigue effects (Wild *et al*, 1998). The improvement of sensitivity with SWAP on the follow up visit as shown by the TD values was also regionally dependent, being greater in the superior than the inferior hemifield, as previously seen in the study by Wild and Moss (1996). Finally, it can be assumed that the between-visits comparisons with SWAP for the PD analysis were also subjected to the variability of height due to the learning effect that was not entirely removed from the TD values after correction for the Mean Height abnormality.

By contrast, the between-visits results for the total deviation probability analysis with W-W perimetry showed a marked increase of abnormal points at the 3rd visit However this change didn't involve the peripheral locations, although there are

previous reports associating the improvement in sensitivity with W-w perimetry with this region, in normal subjects and glaucoma patients (Heijl & Bengtsson, 1996; Searle *et al*, 1991a; Wild, Dengler-Harles *et al*, 1989).

The mean number of abnormal points as described in the TD and PD probability plot maps was less for SWAP than W-W perimetry, across the upper and lower hemifield, as well as the central and peripheral locations for the glaucoma group.

		W-W / SWAP				
Group		global	upper	lower	central	periphery
Glaucoma	TD	3.75	4.65	3.08	4.38	3.26
	PD	2.50	4.40	1.53	2.60	2.50

Table 3.55*.The ratio of the mean number of abnormal locations across the TD and PD maps for the glaucoma group for W-W perimetry over SWAP.*

		W-W				
Glaucoma Group		global	upper	lower	central	periphery
Visit2/Visit3	TD	1.14	1.09	1.17	1.18	0.94
	PD	1.09	1.53	0.77	1.02	1.16

		SWAP				
Glaucoma Group		global	upper	lower	central	periphery
Visit2/Visit3	TD	1.16	1.03	1.30	1.17	1.23
	PD	1.37	1.00	2.23	1.15	1.61

Table 3.56. *The ratio of the mean number of abnormal locations across the TD and PD maps for the glaucoma group at visit 2 over visit 3, for W-W perimetry and SWAP respectively.*

This is contradicting previous research suggesting that SWAP is more sensitive than W-W perimetry among early glaucoma patients (Sample *et al*, 1993; Wild,

1997). The results however are in agreement with the work by Soliman and colleagues (2002) that compared the PD statistical analysis of the analysis packages by HFA for the two techniques (Soliman *et al*, 2002b). This result is associated with the lower inter-individual variability with W-W standard perimetry that describes a smaller range for normal age-adjusted values and therefore shallower depressions are needed in W-W fields for statistical and clinical significance. Moreover, it is important to consider that the glaucoma group investigated in this study included patients with different levels of damage but SWS pathway isolation is present only with mild focal loss corresponding to 12-14 dB dépth of depression (Demirel & Johnson, 2000). Thus, patients with a pre-existing glaucomatous visual field loss deeper than the degree of SWS isolation would not benefit from the SWAP examination and such areas of the visual field would be more appropriately examined with conventional W-W perimetry. The wider confidence limits and the magnitude of SWS isolation for SWAP limit the range over which SWAP defects can be detected and monitored (Wild, 2001) and as a consequence W-W perimetry appears to be the most sensitive of the two algorithms.

As expected, the results from the OHT group give a similar impression to the analysis of the normal group.

Group		W-W / SWAP				
		global	upper	lower	central	periphery
OHT	TD	2.06	7.50	1.05	2.54	1.69
	PD	1.02	3.29	0.24	1.53	0.80

Table 3.57.*The ratio of the mean number of abnormal locations across the TD and PD maps for the group of OHT patients for W-W perimetry over SWAP.*

Group		W-W / SWAP				
		global	upper	lower	central	periphery
Cataract patients	TD	2.87	3.64	2.36	4.60	1.90
	PD	1.06	2.60	0.64	1.00	1.00

Table 3.58. *The ratio of the mean number of abnormal locations across the TD and PD maps across the group of cataract patients for W-W perimetry over SWAP.*

Although the SWS stimulus is preferentially absorbed by cataract (and would be expected that SWAP is associated with more depressed locations than W-W, since the general height reduction attributable to the magnitude of lenticular absorption increases as the wavelength of the stimulus decreases (Hudson et al, 1993; Kim, Kim et al, 2001; Savage et al, 1993), this relationship is reversed in our results as a consequence of the wider limits of normality associated with SWAP in conjunction with the smaller dynamic range of the technique (Wild, 2001).

3.17 Limitations

Potential differences between perimetry techniques in the Total deviation and in the Pattern Deviation values may arise from the differences in their algorithms or from the differences in the given normative databases. Ideally, a normative database common to all algorithms should be utilised in any between algorithm evaluations.

This study compared the Full Threshold algorithm for W-W perimetry and SWAP. However, the two tests don't share the same database. Moreover, while the database for W-W perimetry is well explored there is no formal documentation describing the database associated with SWAP. These differences in the normal databases for the HFA will be inherent in the analyses of the Total and Pattern Deviation probability tables. It is almost impossible to conduct a thorough perimetric examination analysis without the implications of this difference in normal databases affecting the results.

The comparison between the two algorithms based on the probability scores might not be able to reflect the complete range of differences in the depth of focal loss across the glaucoma group, as identified by each technique, because each probability symbol covers a particular range of defect depths. The variability between the two algorithms, for the same probability score, is further affected by the differences in the dynamic range of the perimeter for each technique. The comparison of SWAP with W-W perimetry, based on the probability values, is certainly influenced by the reduced dynamic range for SWAP arising from the high luminance background and the low transmission of the short-wavelength stimulus (Wild, 2001). Moreover, due to the wider confidence limits for SWAP, it is argued that the current methods for defining focal loss with W-W perimetry may not be equally applicable for SWAP. The inherent variability for the threshold response for SWAP across the central field may impair the adjustment in the general height (GH index). As a consequence, the variability can be transferred to the PD values (Andersson, Åsman et al, 2001).

It is also important to consider that the probability values within each cell are not independent of those of other cells. As a consequence, the format of the contingency table can be influenced by one or more anomalous or outlying visual fields from one or more individuals. Correction for the contribution of multiple locations with high probability levels derived from a single individual to the summary contingency tables, could probably be accounted for with statistical adjustment of the data for the frequency of probability levels within each individual set of data. However, the use of the probability analysis is optimal for the pointwise analysis because it takes into account the effects of age, eccentricity and defect depth. Moreover, interpretations are facilitated from the between-visit within-algorithm pointwise analyses, where the comparison of probability analysis can reveal the within-individual differences for each algorithm according to the difference in pointwise deviations from each respective normal database.

The effect of limited dynamic range by SWAP compared to W-W perimetry due to the high luminance of the background and the reduced transmission of the stimuli renders SWAP less suitable than W-W perimetry to investigate glaucomatous damage of moderate to advanced levels (Wild, 2001). Therefore, the results of the glaucoma group analysis are influenced by the number of cases at different stages of glaucoma included in the cohort.

Among the patients with cataract, the TD and PD analysis assumes that cataract reduces the height of the visual field uniformly. However, the magnitude of the height attenuation varies as a function of the type and location of the cataract.

Thus, the statistical evaluation of patients with cataract might be limited due to the variability in the General Height.

Finally, at all cases, caution should be exercised when evaluating these results because of the limited size of the study groups.

3.18 Conclusion

This is the first cross sectional study that compares SWAP with standard W-W perimetry on the basis of the probability analysis maps available with the HFA. The main outcomes of this comparison are firstly that there is a learning effect with SWAP which is present irrespective of any prior experience with W-W perimetry and persistent at the third visit. Secondly, it became obvious that the normal variability incorporated in SWAPPAC leads to underestimation of the magnitude of the statistical significance both of the TD and of the PD values compared to W-W perimetry, thereby compromising the current technique in the investigation of OHT and POAG.

Chapter 4 General Methodology

4.1 Subjects characteristics

The study utilized the image of the optic nerve head from one eye, designated at random, of each of 58 normal subjects and of each of 113 patients with glaucoma. The images had been acquired in two previous studies (Sheen, 2002). Each image had been digitised from a 35mm colour photographic transparency.

The two studies had been undertaken at Cardiff School of Optometry and Vision Sciences according to robust protocols. The selection of subjects and patients prior to ONH imaging had conformed to rigid inclusion criteria. All individuals had received a routine ophthalmic examination to determine their eligibility for entry into either previous study. The examination had comprised determination of refractive error; assessment of distance visual acuity; applanation tonometry; slit lamp bio-microscopy; gonioscopy; indirect ophthalmoscopy through a dilated pupil; and threshold perimetry.

Normal subjects had been recruited from the academic and administrative staff of Cardiff University and from the spouses and friends of those patients with glaucoma participating in the study. The patients with open angle glaucoma had been recruited from the glaucoma clinics at the Cardiff Eye Unit, University Hospital of Wales (UHW). Each volunteer had been informed about the nature of the study and the consent form had been signed in accordance with the guidelines of the Ethical Committee of the Bro Taf Health Authority.

The exclusion criteria for the normal subjects comprised a history of intra-ocular or visual pathway disease; no previous ocular surgery or trauma; a family history of glaucoma; diabetes or a family history of diabetes; systemic medication known to affect the eye; a distance refractive error greater than 5.00 dioptres and/or greater than 3.50 dioptres cylinder in the designated eye; visual acuity of worse than 6/12 in the designated eye; intraocular pressures greater than 21mmHg; narrow angles (Grade ii or smaller); an anterior segment abnormality in the designated eye, including cataract, considered likely to prevent ocular photography of the optic nerve head; an abnormal appearance of the optic nerve head; and an abnormal fundal appearance.

The exclusion criteria for the patients with open angle glaucoma comprised previous ocular surgery or trauma; diabetes or a family history of diabetes; a distance refractive error greater than 5.00 dioptres sphere (DS) and/or greater than 3.50 dioptres cylinder (DC) in the designated eye; visual acuity of worse than 6/12 in the designated eye; narrow angles (Grade ii or smaller); an anterior segment abnormality in the designated eye, including cataract, considered likely to prevent ocular photography of the optic nerve head; and an abnormal fundal appearance other than that attributable to glaucoma.

4.2 Examination protocol

All individuals attended for one or two visits at which they underwent the following procedures. Refractive error in the designated eye had been determined either by retinoscopy and subjective monocular refraction or by automated objective refraction with the Topcon KR-7500 Autokerato-refractometer (Topcon Instruments,

Japan). Keratometry readings along the two principal meridians had been obtained with the Topcon KR-7500 Autokerato-refractometer. Visual acuity had been recorded through the optimum refractive correction or through the current spectacles using a standard internally illuminated Snellen chart at 6m.

All individuals had undergone standard automated perimetry using either the Humphrey Field Analyser 740 or 750 (Carl Zeiss Meditech, Dublin, CA) with Program 24-2 and the SITA Standard or SITA Fast algorithm. Refractive correction, in the form of full aperture trial lenses, appropriate for the viewing distance of the perimeter bowl had been used for each patient. The non-examined eye had been occluded with an opaque patch. Fixation had been continuously monitored with the Heijl-Krakau technique and with the gaze tracker. All examinations had met the inclusion criteria for reliability.

All fields had been evaluated in a masked fashion by an expert (JMW) experienced in the evaluation of threshold standard automated perimetry. The severity of the visual fields exhibiting glaucomatous damage had been defined in terms of the classification system of Hodapp and colleagues (1993) and modified for use with Program 24-2 and the SITA Standard algorithm by Litwak (2001) (Hodapp, Parrish II *et al*, 1993). This system describes the severity of loss in terms of the Mean Deviation visual field index and in terms of the number, severity and proximity to fixation of the Pattern Deviation probability symbols.

A series of three high quality scans of the optic nerve head had been obtained for each patient, through pupils dilated either with topical 1% Tropicamide and 2.5%

Phenylephrine HCl (Chauvin Pharmaceuticals, Romford, Essex, England), using the 10 degrees field of view of the Heidelburg Retina Tomograph. A mean topography image was calculated with the HRT software version 2.01, on which the contour line of the disc margin had been outlined by the operator. The stereoscopic images of the optic nerve head for the corresponding patient had been available to assist the demarcation of the contour line. The standard reference plane for the measurements had been placed 50 mm posterior to the mean height of the demarcated disc margin, on the temporal segment between 350 and 360 degrees. The angular range of measurement had been specified for 30 degrees and the total area had been calculated by the stereo-metric measure function of the HRT software.

All patients had also undergone simultaneous stereo-photography of the optic nerve head with the Nidek-3Dx camera (Nidek Corporation, Aisako, Japan). For each eye, a double true colour 15^0 image centred on the optic disc was captured on a single 35mm frame of a slide film (Kodak Elite ASA 200 or Kodak Elite Chrome ISO 200). Three simultaneous sets of images were obtained for each individual.

The biometric, visual field and image data had been acquired either at one visit (29 normal volunteers and 57 glaucoma patients) or at two visits separated by a maximum of one week (25 normal volunteers and 56 glaucoma patients). In all cases the imaging data had been obtained after the perimetric testing either after the acquisition of the biometric data in a single visit or at the second of the two visits.

The optimum quality image pair for each individual obtained with the Nidek-3DX camera (Nikon Corp., Tokyo, Japan) had been digitised in high resolution (1250-1395 pixels, 24 bits/pixel) using the Nikon LS-2000 digitiser (Image acquisition with the Nidek 3DX camera is described in chapter 5.1.2). After digitisation the R and L images of each stereo pair had the same size and were true colour BMP images. In later stages, all images were converted from a BMP into a JPG format which retained image resolution but reduced with the application of a loss compression function, the required computer process time and computer storage space.

The best quality image pair was selected for the study. Image quality was determined on the basis of uniformity of contrast and equality of illumination. The images had not been subjected to any software enhancement, equalisation or any other image manipulation technique and were therefore representative of the quality of images usually obtained in a clinical setting. An experienced ophthalmologist (JEM) graded the photographic and stereoscopic presentation for all sets of images and verified their adequacy before inclusion in the study.

4.3 Equipment

The imaging technique employed in the study for the diagnostic and planimetric evaluation of the ONH images is a computer assisted stereoscopic system supported by custom-made software.

4.3.1 Digital stereoscopic planimetry system

Analytically, two PC computers coupled with 19-inch flat screen monitors (High Colour 16bi; 1280 x1024; G400, Sony Corporation, Mizunami, Japan) and fitted

with specialised graphics card were used for the study. The stereo presentation was enabled by a monitor Z-screen (Stereo graphics Corporation, San Rafael, California) fitted on each computer monitor (Figure 4.1).

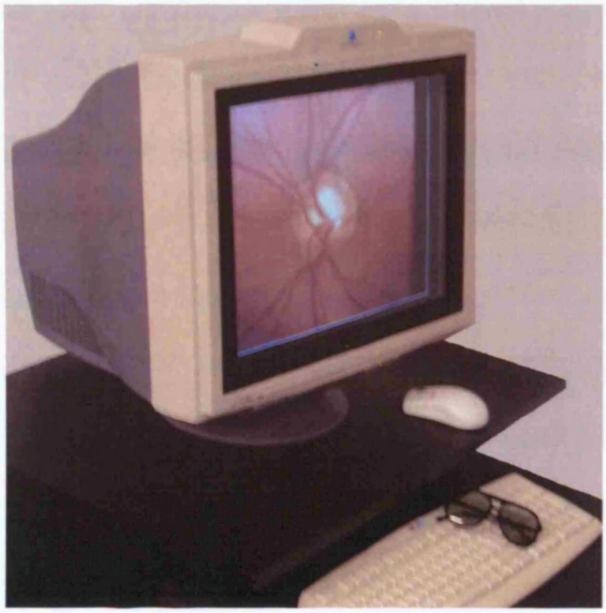

Figure 4.1 *Z screen monitor; the liquid crystal overly plate is mounted on a 21" high resolution monitor. The polarised glasses can be seen on the keyboard. Electronics for the control of the Z screen are mounted in the screen bezel.*

Stereoscopic displays use computer technology to create three-dimensional depth perception based on two-dimensional images and are designed to provide realistic representations of visual information when viewing complex three-dimensional structures such as the optic nerve head. Stereoscopic viewing is possible by creating different perspective views of an object and presenting them seperately to the right and left eye of the observer. The two different perspective views are presented on the computer monitor at a refresh rate of at least 120 Hz i.e. approximately 60 Hz for each view thus, exceeding the critical fusion frequency of the human eye (Ali & Amir, 1991). The two views, one for the left and one for the

right eye, are separated by means of a signal generated by the computer in order to identify the on-screen images as left and right.

To create the three-dimensional depth perception the two views must be separated by a selection device. The selection device used in this study was a combination of a Z-screen which is an electronically controlled polarisation modulation panel and a set of passive polarising eyewear (StereoGraphics Corporation, San Rafael, California, USA). The Z-screen is a liquid crystal display (LCD) and electronically controlled to change the polarisation characteristics of the light passing through it. A controller unit in the Z-screen activates the panel in synchrony with the computer generated signal that separates the left and right views. The passive polarising filters in the eyewear allow only the correct perspective view to reach each eye thereby creating the three-dimensional depth perception.

The custom software supporting the image presentation was initially written by James. E. Morgan in Object Pascal, Borland Delphi 4.0 and was developed with the work of Dr. Gavin Powell, a computer programming expert. Primary versions of the software were utilised in previous studies undertaken at the School (Sheen, 2002) but the software operations underwent multiple modifications over the last 3 years until shaped according to the needs of the current study. The final version of the software is adjusted for a real time stereo image composition and presentation, involves sophisticated functions for a reliable and reproducible planimetric evaluation and has incorporated a statistical analysis package that enhances the diagnostic expediency of the technique.

4.3.2 Software features and functions.

4.3.2.1 Magnification factors

The custom software operates with Microsoft Windows 2000 which is principally compatible with the graphics card and has incorporated the camera settings for the Nidek 3Dx as suggested by Rudnicka and colleagues (2001) (Rudnicka *et al*, 2001). The algorithms used for the magnification correction of the images were derived from the work of Garway-Heath and colleagues (1998) namely, the estimation of the magnification formula is based on the keratometry and refraction settings of the examined eye (Garway-Heath, Rudnicka *et al*, 1998b). This magnification formula is sufficient for ocular refraction of less than 7 dioptres. The system has been calibrated according to a model eye without taking into account the individual axial length as a scaling factor. The information of the axial length had not been available for the subjects of the dataset but all eyes with refractive error of more than 5 dioptres (Dpt) were excluded from the study. While viewed, the images are adjusted to a set presentation frame and the operator is able to apply custom magnification ranging from 0,5 to 100x.

4.3.2.2 Parallax effect

The double cursor shaped as a star point has a 3D appearance. Increased or decreased disparity between the two mono cursors, would increase or decrease the apparent depth of the cursor in stereoview. With the stereoscopic viewing the cursor is subjectively set at different levels and can be visualised at various depths within the three-dimensional structure of the ONH.

The parallax effect describes the errors introduced when the drawing cursor lies on a different plane than the structures been demarcated. The double cursor is optimally positioned at the plane of the scleral canal when defining the margins of the disc, the areas of atrophy at the peripapillary retina or even the sloping cup boundaries. When the cursor appeared as a single line while viewed through the Z screen both with and without the circular polarisation filters it was positioned on the surface of the 2D images in monoscopic viewing and approximately on the surface of the computer monitor in stereoscopic viewing.

4.4 Planimetry

The control panel on screen allows the operator to decide upon the order of the assessment. Areas of interest are demarcated by operator demarcation points interconnected by colour coded lines. The data points describing the disc and the cup area are fitted on a Bergier curve, determining amongst them the rim area.

Demarcations are performed similarly for the intrapapillary and parapapillary features. The zonal differentiation of the peripapillary atrophy depends on the operators' discretion ability but overlapping demarcated areas of atrophy that had been given different zonal classification are always registered as alpha type atrophy. In the event that there is an overlap to some extent between two areas classified as Alpha and Beta area respectively, the software automatically registers the overlapping segment in the Alpha wider area of atrophy.

The software provides an estimation of the demarcated features of the ONH and the retina in digital units and also in measurements of area (mm^2). The centre of

gravity of the operator defined cup area is used as a reference point that enables the mapping of all data points applied on the image for a given assessment. All area estimations are derived from the calculated distance of every data point to the cup's centre. Through the cup's centre the optic disc area and the parapapillary area is divided in 72 sectors of 5 degrees. The first sector describes the measurements between 0 - 5 degrees of direction around the ONH and always corresponds to the temporal region of the ONH for both eyes (figure 4.2). The software provides the global measurements and a sectorial analysis of the areas demarcated by the operator both in number of pixels and in surface measurements (mm^2). All intrapapillary and peripapillary features are evaluated in segments of 5 degrees around the ONH while the measurements may also be given in 30 and 45 degrees sectors, enabling comparisons with other planimetry data.

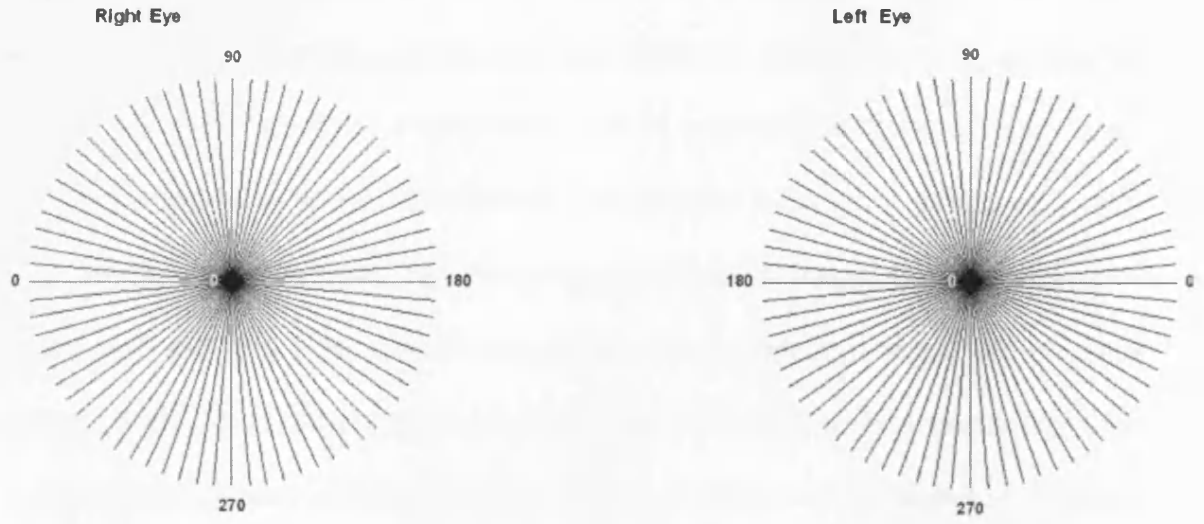

Figure 4.2 *Arrangement of the 72 sectors for R and L eye respectively.*

As part of the planimetric assessment of the ONH, the software explores the aspect of disc shape and the ONH's spatial position. For this analysis the maximum and the minimum diameter of the disc is estimated and by convention, these meridians are always perpendicular to each other. Also with depth adjustments of the data points demarcating the disc an estimation of the spatial position of the optic disc on the retinal plane can be made. The results of the disc shape analysis are shown graphically during the assessment Appendix I.

4.4.1 Stereoscopic image presentation

The initial version of the software produced stereoscopic viewing of the images through the interlaced method. A vertical synchronisation unit compresses each stereo pair to half of its original height and the R and L image are combined to a single interlaced image. The interlaced image contains the same number of lines from each of its component images, the R and L image of the stereo pair. The alternate lines of the new image are rapidly displayed to either the right or the left eye of the operator with the use of the circular polarised glasses, creating a stereo presentation. The refresh rate of the image is set to a level that allows the operator to perceive a single stereoscopic image at all times. However, the stereoscopic image resulting with the interlaced method may include only half of the information contained in the original images. It is therefore argued that the lost photographic information compromises the quality of the final image.

The Quad- buffer method has been put forward as a better stereoscopic method where two sets of the same image stereo pair flicker with a frequency rate that exceeds the fusion frequency of the human eye. Stereoscopic view is created by

the presentation of the two images that had been photographed from slightly different angles. In order to overcome problems with the downloading time that each image requires, two stereo-pairs of the same eye flicker and alternate before the operators' eyes. It is noted that the produced stereo images retain the full amount of photographic information recorded in the component images and at all times, the operator has a single stereoscopic view of each retinal image (Lipton, 2002).

A TCG file is a custom format file that automatically uncompresses the JPG files when first viewed within the program. This file determines the reading process for the file and the sequence of the colour triplets (RGB to BGR).

The images for each stereo pair need to be aligned with each other so they can combine in a three dimensional presentation. The disparity between the images is optimally set to a minimum, making the stereo-pair appear almost as a single image when viewed without the use of the polarization filters. Changes in the disparity of the images may induce excess stereo effects and create discomfort for the operator within short time of use. For the observation procedure, all images were aligned to the minimum disparity for optimal stereo presentation. The alignment code and therefore the image disparity were permanently stored for each presentation in an attempt to improve the image stereo presentation.

4.4.2 Monoscopic image presentation

The software can be used effectively without the input from the stereo-viewer. This enables the operator to select between the stereoscopic or monoscopic

presentation of the images. Each image pair is effectively perceived in stereo when viewed through the Z screen with the simultaneous use of the circular polarisation filters. Without the use of these filters, the apparent monoscopic view of the images is blurred. However, by activating the monoscopic software mode, the stereo viewer is disabled and only one image from each stereo pair becomes available on screen. By convention, the image registered as Right in each image pair is always displayed monoscopically. Using either the monoscopic or the stereoscopic software setting, each image can be assessed in both viewing conditions and the measurements are recorded in separate files clearly referencing the type of viewing mode activated for each assessment.

4.4.3 Training module

A teaching module was incorporated in the initial version of the software making available an expert's assessment and facilitating comparisons from non-expert operators. The operators could improve their assessment guided by the expert's estimates of the cup/disc ratios that readily available to them (Sheen, 2002). While the latest software version doesn't include the training module it incorporates a similar function: every assessment is personalised before being stored allowing multiple assessments of the images to be stored and enabling the representation of all planimetry assessments on demand. Therefore, the software may still be used for training purposes but it can also be applied to expert observers.

4.5 Pilot studies for software accuracy and reproducibly testing

Several pilot studies were conducted to assist the development of the software. These pilot studies primarily aimed to ensure the accurate evaluation of the retinal

properties, neutralised by the magnification correction formula, which was registered in the software code.

4.5.1 Reliability of planimetric estimates

The evaluation of the magnification correction formula registered in the software code and the determination of the accuracy of the measurements acquired with the stereoscopic computerised method, were performed using the HRT planimetry measurements as the golden standard. The cross evaluation of the computerised planimetry results with the HRT planimetry software was based on the disc size as the most reproducible feature of the ONH. The study by Sheen (2002) first evaluated the compatibility of the two techniques. The stereo photographs from 54 normal subjects and 52 glaucoma patients were evaluated by three experienced ophthalmologists and compared with the HRT scans for the same patients obtained within the same examination visit. The disc boundaries on the HRT were outlined by a single operator (NJS) with simultaneous presentation of the stereo photographs for higher precision. This study suggested a good agreement between the assessments performed with the two techniques.

A second evaluation on the reproducibility of the stereoscopic computerised method was performed with the stereoscopic assessment of the dataset on two occasions by the expert ophthalmologist (JEM).

Similar planimetry procedures were performed regularly on samples of the database during the software development. The investigation with the pilot studies

also ensured consistency of the measurements between different versions of the software, for both global areas and sectorial measurements.

4.5.2 Quantitative assessment of peripapillary atrophy

A double set of measurements was initially available for the areas registered as peripapillary atrophy. The two different estimates of the areas of interest were based on the calculation of the area within the operator defined boundaries and also derived by an automated software function that modified the true area boundaries and extended them to the disc margins. The later normalised peripapillary areas in fact included the scleral canal width at the given direction. The peripapillary atrophy area estimates were available in both pixels and mm^2 and were arranged in 5-degrees sectors. Considering that the areas of atrophy progress from the Alpha to the Beta zone, an automated software function was developed allowing adjacent PPA areas to be registered as continuous. Further to connecting the existent boundaries of the demarcated areas there was a provision made in the program so that the segments of "healthy" tissue between the adjacent areas of atrophy would be also classified as Alpha and included in the measurement.

This function showed some resemblance to the custom-made HRT add-on software utilised in previous studies on the peripapillary atrophy (Park *et al*, 2001). Although it would facilitate comparisons between the two software programs it soon became apparent that the automatic shape analysis of the peripapillary areas was randomly subjected to errors when the true area boundaries were modified and adjusted to the optic disc margins. Moreover, the measurements included the scleral canal width that can not be considered uniform. Therefore, it was not possible to detect

the accuracy of the measurements for the modified PPA areas and control for random code errors.

4.6 Study cohorts

For the purposes of the current study both normal subjects and glaucoma patients were classified taking into account the optic disc appearance. The visual field tests were also evaluated and the final classification was based on the compatible results between the two diagnostic techniques, allowing for structural changes to be present without field defects but not for the opposite.

4.6.1 Subject classification procedure

An expert ophthalmologist (JEM) viewed all fundus images stereoscopically and monoscopically on two separate occasions, being masked to the true identity of the subjects. Conversely, an expert perimetrist (JMW) evaluated the visual fields for all subjects, twice. Both experts made a 'two-forced-choice' classification of the images and fields either as normal or glacomatous. There was a three months interval between the two image presentations and almost a year between the two fields' assessments for each subject. Contradictory results either between the two disc evaluations or between the disc and visual field classification were resolved with a third presentation and field evaluation from the experts, shortly after their second attempts.

For the images and visual fields that were assessed three times, the final classification was made based on two out of three consistent decisions from either of the experts. The optic disc appearance was considered more reliable than the

field's status; therefore, the classification was based primarily on the imaging diagnosis when the perimetry results suggested normal performance or a borderline sensitivity loss. Images and fields of glaucoma patients without field loss and of all the normal subjects with borderline or abnormal glaucoma hemifield test (GHT) were also evaluated three times. Furthermore, the images of all the subjects that were described as difficult to be classified accurately on the grounds of optic disc appearance alone also underwent a third evaluation before being excluded from the analysis.

4.6.2 Outcome of the final classification process

The final classification of the two study groups resulted in 11 subjects, that were described as normal at recruitment, to be finally included in the glaucoma patients cohort. The expert ophthalmologist (JEM) repeatedly identified glaucomatous optic disc features for these patients.

On the other hand, 12 subjects described as glaucoma patients at recruitment were not included in the final glaucoma cohort. Two normal tension glaucoma (NTG) patients with normal visual fields and without ever being treated for glaucoma, were included in the final normal cohort; one NTG patient with normal visual fields was repeatedly diagnosed as normal by imaging but was already receiving medication so had to be excluded from all groups; eight glaucoma patients without visual field loss were repeatedly classified as normal by imaging and were finally considered as OHT patients; one glaucoma patient with definite glaucomatous field loss that was repeatedly classified as normal by imaging was finally excluded.

From 26 subjects recruited from the previous studies as ocular hypertensive (OHT) patients without glaucomatous discs and visual field loss, thirteen subjects were classified as definitely normal by imaging; nine subjects were classified as early glaucoma patients and four subjects were described as glaucoma suspects. By the end of the classification process the dataset consisted of 21 OHT subjects. This group included the 13 subjects that were initially recruited as OHT and also the eight glaucoma patients that were repeatedly found to have normal ONH appearance and normal fields but were already under IOP lowering treatment.

4.6.3 Demographics

The group of normal individuals comprised 34 female and 20 male. The mean age was 59.44 years (SD=10.57; range 40 to 76 years). The general characteristics of the cohort are summarised in table 4.1.

	Normal (N= 54)	
Parameter	Mean	SD
Age (years)	59.44	10.57
Sphere (Dpt)	0.62	2.00
Cylinder (Dpt)	-0.59	0.66
Mean Refractive Error (Dpt)	0.33	1.98
K 1 (mm)	7.70	0.24
K 2 (mm)	7.64	0.26
MD (dB)	-0.10	1.45
PSD	1.95	1.12

Table 4.1 *The group mean and SD of certain biometric characteristics of the normal individuals.*

The patients with OAG comprised 61 females and 52 males. The mean age was 65.02 years (SD = 10.46; range 38 to 84 years). The general characteristics of the

cohort are summarised in table 4.2. It is noted that 51 OAG patients had being receiving IOP lowering medication and 1 patient had had trabeculectomy in both eyes.

	Glaucoma (N=113)	
Parameter	Mean	SD
Age (years)	65.42	10.49
Sphere (Dpt)	0.86	1.80
Cylinder (Dpt)	-0.74	0.73
Mean Refractive Error (Dpt)	0.49	1.83
K 1 (mm)	7.79	0.26
K 2 (mm)	7.77	0.28
MD (dB)	-4.33	5.48
PSD	4.92	3.74

Table 4.2 *The group mean and SD of certain biometric characteristics of the OAG patients.*

	Visual Field Diagnosis							
	Severity of Damage							
Glaucoma Patients	EARLY-Normal N=37		MILD N=24		MODERATE N=22		ADVANCED N=30	
	MEAN	SD	MEAN	SD	MEAN	SD	MEAN	SD
MD (dB)	-0.42	1.76	-2.19	1.49	-4.08	1.90	-10.89	6.36
PSD	1.97	1.30	2.79	1.07	5.20	1.79	9.93	2.87

Table 4.3 *The diagnosis of the glaucoma study group according to their visual field tests. The severity of visual field loss has been graded according with the Hodapp classification as modified by Litwak.*

4.7 Experimental design

4.7.1 The selection of images

The selection of images for observation included 210 images which corresponded to the total number of subjects recruited by the two previous studies undertaken at School of Optometry & Vision Sciences (Sheen, 2002).

The dataset of images subjected to observation was larger than the dataset of normal volunteers and glaucoma patients finally included in the analysis (54 normal subjects and 113 OAG patients). Within the additional images we report the cases of 2 normal volunteers and 7 glaucoma patients that were only partly assessed stereoscopically and/or monoscopically by the three observers, due to random errors with the operation of the software resulting into unsaved data files; the images from 21 OHT patients; 10 images that were excluded on the grounds of their difficulty to be correctly diagnosed by imaging only and the images of 2 glaucoma patients that had borderline refractive errors with respect to the inclusion criteria set for this study.

4.7.2 Appointed observers

Three experienced ophthalmologists with fellowship in glaucoma were appointed with the assessment of the dataset of images from the two study cohorts, using the custom software. Two of the appointed observers (KR and EAA) were recruited from the University Hospital of Wales and the third observer (IAC) was recruited from Birmingham and Midlands Eye Centre.

None of the observers (KR, EAA, and IAC) were involved in the recruitment of the volunteers, the primary examination procedure or the classification of the subjects in the cohorts and were at all times masked to the true identity of the volunteers. For the statistical analysis each observer was given an ID number ranging from 1 to 3.

All observers had stereo-acuity better than 40 seconds of arc as evaluated with the TNO stereopsis test at the recommended distance of 40 cm (table 4.5).

Observer	Code	Secs of Arc
JEM	Ob Expert	15
KR	Ob 1	15
EAA	Ob 2	30
IAC	Ob 3	15

Table 4.4 *The results of the TNO stereopsis test for all the observers, including the expert ophthalmologist that was the primary observer for the dataset.*

All observers were completely naive to the software operations prior to the study. However, one of the observers (EAA) had previously used an early version of the software as part of a previous study undertaken at Cardiff University (Sheen, 2002).

4.7.3 Observation consensus

The description of the intapapillary and peripapillary features of the ONH as applied for all planimetry assessments was agreed between all observers as follows:

- The margins of the disc corresponded with the inner circumference of the scleral canal.
- The optic cup was determined by it's contour and not according to the changes in colour of reflectance. The margins of the cup were chosen to correspond with the points where the sloping cup walls met the plane of the disc surface, at the level of the scleral canal. In other words, the cup was demarcated in the position where the rim was first shown to deviate at the back, using the kinking of the vessels as a landmark feature. The

configuration even of the smallest retinal vessels is a useful clue for the demarcation of the disc inner boundaries. The retinal plane was chosen to be the depth where all measurements were performed.

- The peripapillary atrophy was classified into Alpha or Beta zones. The areas of Alpha zone were identified by morphological features such as irregularities of hypo- and / or hyper-pigmentation in the peripapillary retina combined with subtle thinning of the chorioretinal layer. Conversely, Beta zone areas was featuring apparent retinal pigment epithelium loss and atrophy of the choriocapillaris, usually bordering with areas of Alpha zone of atrophy and expanding relatively closer to the scleral ring of Elschnig than Alpha zone (Jonas *et al*, 1989a).

4.7.4 Observation task

For the assessment of each image, the observers were principally requested to demarcate the areas of interest and keep a written record of the features they observed. Furthermore, they were asked to score on a 4 point scale of inadequate, sufficient, quite good and excellent the photographic quality of the image dataset when viewed both in stereoscopic and monoscopic setting. In addition, all observers scored on a 3 point scale of poor, good and very good the stereoscopic presentation of the images.

The observers also had to make a subjective assessment of the optic nerve head configuration and make a diagnosis of glaucomatous damage. This decision was based on standard clinical criteria, which included loss of physiological rim shape and cupping, presence of focal thinning (notching) and/or disc margin

haemorrhage(s) (Jonas *et al*, 1999b). Signs of peripapillary atrophy were considered additional features of the glaucomatous appearance but not representative of glaucoma.

All images were classified in two main groups: images with normal ONH and images with glaucomatous damage. For the images that the observers were reluctant to make a definite diagnosis solely by the ONH appearances they were given the option to register them as suspicious before making a forced diagnosis as normal or glaucomatous.

Finally, the observers subjectively scored all images according to their overall degree of difficulty for diagnosis by imaging techniques only, using a four point scale of easy, moderately difficult, difficult and very difficult (Appendix I)

4.7.5 Training module

All observers were introduced to the set of equipment employed for the study and were also provided with a manual describing in detail the custom-made software operations (the manual is presented in the appendix). In order to avoid mishandling of both the hardware and the software, a training module was set up to run individually for each of the observers, in the beginning of the assessments. The observers were given a set of 18 ONH images that were only used for training purposes and were not part of the image database used for the main study. The images used for training were initially acquired for the purposes of the two previous studies undertaken at Cardiff University but were derived from individuals that hadn't been able to follow the complete examination protocol. As a consequence,

no record of the refraction errors, intraocular pressures and/or repeated visual field tests could be retrieved for these volunteers.

The images comprising the training set were planimetrically assessed as well as graded for their quality of appearance and diagnostic difficulty by an ophthalmologist and glaucoma consultant (JEM) who was experienced in the software operations. For this purpose, they were viewed stereoscopically and the 18 ONHs were finally classified into a subgroup of 5 normal and 13 glaucomatous as diagnosed by imaging techniques only.

The images of the training set were representative of the quality of images acquired in a clinical setting and covered the range of photographic and stereoscopic presentation observed in images of the main dataset.

The training module delivered to all three observers was organised in two parts which were both undertaken within a period of one week. For the first part of the training session the observers viewed the 18 training images stereoscopically and could selectively refer to the expert's assessment for the same images. The expert's assessments were recalled on the stereo-viewing system before or after the observers' assessment. The procedures followed in the introductory training session are described in table 4.6.

Training Module Part 1

Training Images	Assessment Task
10, 11 and 12	Trial assessments.
13, 14, 16, 17 and 19	Expert's assessment of the images is displayed before the the observers' assessment.
20, 22, 23, 24 and 25	Expert's assessment is displayed after the observers' assessment.
26, 27, 28, 29, and 30	Complete assessment without reference to the expert's assessment.

Table 4.5 *The images of the training set given random ID numbers were presented stereoscopically and in the same order to all three observers.*

The expert's assessment demonstrated the level of precision that is feasible once the operator is experienced in the software function. It is noted that JEM had acquired a substantial experience on the software functions and his planimetric results on the disc and cup areas had shown good agreement with the corresponding HRT measurements demonstrated by studies undertaken with the primary versions of the software.

In the second part of the training session, the observers were asked to make a complete assessment of the training set immediately before proceeding with the observation of the images in the main dataset. The 18 images of the training set were presented with a new random order which remained the same for all three observers (table 4.7). Each observer assessed all images within a single session without any reference to the expert's assessment. Overall, each observer had to assess the training set twice: shortly before the first stereoscopic assessment and the first monoscopic assessment of the main dataset using the stereoscopic and monoscopic settings of the software, respectively.

Training Module Part 2																	
ORDER																	
1st	2nd	3rd	4th	5th	6th	7th	8th	9th	10th	11th	12th	13th	14th	15th	16th	17th	18th
IMAGE ID																	
19	26	29	24	20	13	28	23	22	25	12	14	30	17	27	11	16	10

Table 4.6 *The random order of presentation for the images comprising the training set, as they were presented to all three observers, in stereoscopic and monoscopic viewing respectively.*

The training module provided the observers with a good understanding of the methods employed in the study and controlled the influence of their learning process over the computed procedures on the assessment of the images in the main database. Whilst assessing the training set, the observers exercised their "hand and eye" coordination and increased their accuracy levels to a satisfactory standard. Finally, the training procedures enabled the observers to make an estimation of the time needed for the completion of their task.

4.7.6 Assessments in stereo and mono

The observation task included a stereoscopic and a monoscopic assessment of the same dataset of images, following the same observation procedure. For this purpose, the 210 images selected for observation were initially arranged in two groups, Group 1 and Group 2, each including 100 and 110 images, respectively. Each group of images was assessed by all three observers, both stereoscopically and monoscopically. Two of the observers (Observer 1 and Observer 2) assessed the images in the same random order, while the third observer (Observer 3) was presented with the images arranged in reversed order. However, all observers

alternated their observations between the two viewing modes in similar fashion (table 4.7).

	A	B	B	A
Viewing mode	Stereoscopic	Monoscopic	Monoscopic	Stereoscopic
	Group 1	**Group 2**	**Group 1**	**Group 2**
Presentation Order	1→100	101→210	1→100	101→210
Reversed Presentation Order	100→1	210→101	100→1	210→101

Table 4.7 *The selection of images as arranged in two groups: Group 1 included 100 images with ID numbers ranging from 1 to 100 and was assessed first stereoscopically (A) and then monoscopically (B) by all three observers; Group 2 included 110 images with ID numbers from 101 to 210 and was assessed first monoscopically (A) and then stereoscopically (B) by all three observers. The presentation order of the images within each group remained the same for two of the observers (Observer 1 and 2) and was reversed for the assessments of the third observer (Observer 3).*

4.7.7 Time frame for observation

Two PC based systems coupled with stereo-viewer Z screens, having the same hardware and software specifications were used so that the assessments of all three observers could be performed within the same period of time. The observation procedure was subjected to the availability of time for each volunteer observer, their physical strength and dedication to the project. Never the less, all observers succeeded to complete all the parts of the study within a two months period of time.

Chapter 5 Comparison of monoscopic and stereoscopic computer assisted planimetry in the evaluation of the normal and glaucomatous optic nerve head

5.1 Introduction

Stereo-photography in ophthalmology is predominately employed for the diagnosis of glaucoma. It involves the acquisition of a pair of images, from slightly different angles, that can be viewed appropriately in a stereoscopic presentation. The utility of stereo-photography in the diagnosis of glaucoma stems from the need for representation of the three-dimensional structure of the optic nerve head.

Stereoscopic imaging is regarded as the 'gold standard' for optic nerve head observation and for glaucoma diagnosis. It has been used both as a qualitative and a quantitative measure against which diagnostic imaging instruments and new perimetric algorithms for the discrimination of glaucomatous damage are compared (Medeiros, Zangwill *et al*, 2005; Sung *et al*, 2002; Wollstein *et al*, 2000a). Stereo-photography of the optic nerve head has been used in large longitudinal studies of the diagnosis and progression of glaucoma (Feuer, Parrish *et al*, 2002; The European Glaucoma Prevention Study Group, 2003).

Other semi-automated imaging techniques like the SLO and the newer automated imaging instruments such as the OCT, the GDx and the RTA have enabled a less time-consuming examination and quantitative analysis of the retinal properties. As previously described in the introductory chapter (Chapter 1), some of the limitations associated with the performance of automated imaging instruments include the uncontrolled interferences of the anatomical features with the automated algorithms

(Jonas *et al*, 1998c); the use of surrogate measures such as the nerve fiber layer thickness in order to identify glaucomatous change and the substantial overlap of results for normal and pathological eyes as a result of the high physiological variability in combination with uncontrolled measurement errors. These factors hinder the use of automated imaging in early glaucoma detection. Stereoscopic photography is still ranked as the most sensitive method of all for the diagnosis of glaucoma at all stages (Bowd, Zangwill *et al*, 2004; Greaney *et al*, 2002).

Despite the widely recognized contribution of stereoscopic disc analysis for disease discrimination, the diagnosis of glaucoma has largely relied on non-stereoscopic techniques that are traditionally used for routine eye examination because of practical reasons (AGIS, 1994; Harper, Reeves *et al*, 2000b; Spry *et al*, 1999; Theodossjades & Murdoch, 2001; Watkins *et al*, 2003). Monoscopic imaging is also considered for telemedicine applications because of the low cost of monoscopic digital cameras and the fact that computer systems required to perform storage, processing and analysis of monoscopic images need to have rather ordinary specifications (Constable *et al*, 2000; Eikelboom, Barry *et al*, 2000).

Quantitative methods have been shown to be superior to qualitative subjective judgements for glaucoma (Caprioli, Prum *et al*, 1996; O'Connor *et al*, 1993). In addition, planimetry is less variable when performed under 3-dimentional rather than 2-dimentional conditions (Bartz-Schmidt, Sündtgen *et al*, 1995; Varma, Quigley *et al*, 1992a). Consequently, planimetry is usually performed on stereoscopic images for glaucoma diagnosis and detection of progression. Planimetric optic nerve head analysis from stereoscopic fundus photographs is

known to detect early glaucomatous damage with high sensitivity and specificity (Garway-Heath, Poinoosawmy *et al*, 1999; Jonas *et al*, 2000). Viewing systems that allow planimetry with personal computers have been successfully used for early diagnosis of glaucoma (Garway-Heath, Ruben *et al*, 1998a) and currently available stereoscopic disc analysis systems show promise for use in the clinical setting. These systems incorporate digital stereoscopic presentation units and computer-assisted planimetry software enabling automated quantification of the optic nerve head structures (Eikelboom *et al*, 2000; Morgan *et al*, 2005b; Sheen *et al*, 2004; Shuttleworth *et al*, 2000; Yogesan, Constable *et al*, 1999b).

5.1.1 Comparison of stereoscopic and monoscopic imaging evaluations

Imaging of the optic nerve head under stereoscopic or monoscopic viewing settings may result in measurement differences for the optic nerve head planimetric evaluation that further influence the sensitivity of the techniques for glaucoma diagnosis. Comparative studies employing the same technique and alternating viewing settings found that the mean group stereoscopic measurements for various aspects of the cup to disc ratio (CDR) was greater than the corresponding monoscopically derived estimates, across normal and glaucomatous eyes (Hanson, Krishnan *et al*, 2001; Morgan *et al*, 2005a; Varma, Steinmann *et al*, 1992b), with the exception of one study of normal eyes that reported the opposite results (Parkin *et al*, 2001). Measurement differences were also apparent between different techniques that required monocular or binocular viewing of the optic disc. In one example, subjectively estimated horizontal (HCDR) and vertical cup to disc ratios (VCDR) from simultaneous stereo-photographs were significantly higher relative to measurements derived by the HRT that incorporates monocular

observation of the ONH, among normal individuals and glaucoma patients (Zangwill, Shakiba *et al*, 1995). Similarly, estimates for both the VCDR and HCDR in normal individuals were found significantly smaller when derived by monoscopic assessment of digital images compared to the estimates obtained with fundus biomicroscopy (Hrynchak, Hutchings *et al*, 2003). Moreover, Watkins and colleagues (2003), using the HRT measurements as an objective reference, stated that the subjective evaluation of VCDR was more frequently underestimated by direct ophthalmoscopy (80%) than by fundus biomicroscopy (57%) (Watkins *et al*, 2003).

While it is common observation that the results between different methods of optic nerve head examination are not directly comparable (Correnti *et al*, 2003; Ikram *et al*, 2002), methodological differences that stem from the quality of the stereoscopic images, the method of stereoscopic presentation and the procedure of optic disc analysis are likely to account for the measurement discrepancies associated with stereoscopic imaging.

5.1.2 Cameras of sequential and simultaneous image capture

The quality of the component stereoscopic images, in terms of their separation as induced by cameras of sequential or simultaneous capture can be a source of variable stereo-view. A stereoscopic camera acquires two slightly disparate optic disc images that can fuse into a three-dimensional image when viewed appropriately. Alternatively, a monoscopic camera that is manually horizontally realigned to acquire two images of the same eye can effectively produce a stereo-pair of images (Tielsch, Katz *et al*, 1988). This is the manual-shift technique and is

widely applied given the clinical availability of monoscopic cameras. However, with this technique the stereo images are likely not to have a constant stereo separation and the quality of the resultant stereoscopic images relies heavily on the technical skills of the operator. The Zeiss fundus camera (Carl Zeiss, Thornwood, NY) incorporates a separator that enables sequential capture of a stereo pair with a constant stereo separation. The Allen separator is comprised by a rotating sheet of high refractive index glass material positioned with a 45 degrees angle to the axis of the light rays within the camera, thereby inducing a horizontal displacement of the light beam (Allen, 1964). Two consecutive exposures, each on either side of a dilated pupil, make up the stereo pair. Another type of sequential camera is the Discam camera, which has an inbuilt rapidly moving shutter and generates monochromatic digital sequential stereo images (Shuttleworth *et al*, 2000; Sung *et al*, 2002).

Conversely, the Donaldson camera was the first simultaneous camera able to produce good quality images (Donaldson, 1964). The Nidek 3DX (Nidek Corporation, Aisako, Japan) is a simultaneous camera that works on the same principles as the Donaldson camera with the additional feature of binocular eyepieces that can be adjusted for the refractive error of the examined eye focusing the images on the photographic film surface. The Nidek 3DX is using a single optical axis to obtain two photographs of the same eye with a fixed stereo-base of 3mm. While the Donaldson camera is no longer commercially available, the Nidek images are of superior quality and were more reproducible compared to images acquired by the Donaldson camera for planimetric evaluations (Greenfield, Zacharia *et al*, 1993). Minkler and colleagues (1992) compared the Nidek camera with

conventional sequential cameras and described it as faster and easier to use (Minkler, Nichols *et al*, 1992). The photographic resolving power of the camera was comparable to other sequential cameras in a study by Boes and colleagues (1996) (Boes, Spaeth *et al*, 1996). Nidek stereo images also had better stereo separation when compared to images acquired with the Zeiss fundus camera (Barry & Eikelboom, 1995) and this is probably the reason why they were most successful when ranking a series of ONH images based on the evaluation of the apparent cup depth (Boes *et al*, 1996). The Nidek 3-Dx simultaneous camera produced images with better stereopsis than the sequential Nikon NF-505 camera as subjectively evaluated by a panel of observers that viewed the two types of images in random order (Sheen, 2002). The Nidek-3Dx images have also been used successfully for the discrimination of glaucoma (Morgan *et al*, 2005a). Among other types of simultaneous fundus cameras is the Topcon (TRC-SS) usually used in conjunction with the IS 2000 Topcon image analyser for optic disc analysis (Varma, Spaeth *et al*, 1989b).

It is apparent that sequential capture may not provide true stereopsis, as the eye being imaged might move between the first and the second photograph. Moreover, with sequential cameras it is more difficult to maintain equal illumination and focus between the two exposures. Unlike sequential images, simultaneous stereo-pairs exhibit minimal differences in both horizontal and vertical alignment due to the minimal variation in the position of the examined eye. On cross evaluation the Zeiss camera with an Allen stereo separator was less reproducible than the Donaldson simultaneous camera on planimetry (Rosenthal, Kottler *et al*, 1977). A comparative study between sequential and simultaneous image stereo pairs, demonstrated that

variable stereo-angle separation could compromise depth perception and give variable results in subjective optic disc assessment (Boes *et al*, 1996). However, Feuer and colleagues (2002) comparing the effect of the camera type on planimetry described both sequential and simultaneous images as equally comparable and reproducible, although the study was limited by the use of the horizontal cup to disc ratio as the only reference for comparison (Feuer *et al*, 2002).

Unless in digital form, fundus photography is generally limited by the fact that image quality can only be evaluated once the film or image has been appropriately processed. Clear media and pupil dilation are prerequisites for good quality images by both monoscopic and stereoscopic cameras. With stereo photography, once good quality images are acquired, the quality of the resultant stereo image is also dependent upon the successful alignment of the stereo-pair. Variable centration of the images comprising the stereo pair creates visual discomfort for the observer of the stereoscopic image and might give an artifactual impression of alteration to the course of the vessels or change in the cup boundaries. However sequential images are still used for the longitudinal evaluation of glaucoma (Chauhan *et al*, 2001).

5.1.3 Stereo viewing systems

Slides or photographic transparencies can be viewed in stereo using mirror-based stereo-viewing systems in which each image of the stereo pair is separately projected onto a mirror angled at 45 degrees and becomes visible through a single eyepiece. The observer views the two images simultaneously through a binocular eyepiece and mentally fuses them, perceiving them as a single stereoscopic image (Harper & Reeves, 2000; Tielsch *et al*, 1988; Varma *et al*, 1992a). Stereoscopic

viewing is also enabled with handheld stereo viewers (Asahi Pentax Stereo Viewer II, Asahi Optical Co. Tokyo) (Parkin *et al*, 2001; Shuttleworth *et al*, 2000; Sung *et al*, 2002; Varma, Douglas *et al*, 1989a) through liquid crystal display (LCD) shutter goggles (Barry *et al*, 2000; Eikelboom *et al*, 2000; Yogesan *et al*, 1999a) or with the use of a liquid crystal panel such as the commercially available Z-screen (Morgan *et al*, 2005a). For the Discam system that is usually coupled with a handheld stereo viewer the images of the stereo pair are projected on the computer monitor side by side (Parkin *et al*, 2001; Shuttleworth *et al*, 2000; Sung *et al*, 2002) so vertical and/ or horizontal disparities between the monoscopic images are likely to make the resultant stereo image appear defocused, thereby compromising the definition of the disc and cup boundaries for planimetry. Conversely, the stereo pair can be automatically combined into a single interlaced image on the computer monitor and the LCD stereo viewer reveals to the observer only the properties of one component image at a time (Barry *et al*, 2000; Eikelboom *et al*, 2000; Morgan *et al*, 2005a; Yogesan *et al*, 1999a). The interlaced method enables stereoscopic presentation on computers with low or moderate processing power but is limited by the fact that it makes use of only half of the photographic information from each image of the stereo pair.

Comparison of subjective discrimination between normal and glaucomatous ONH images with the Z screen and the mirror-based stereo viewer respectively, revealed that the digital system was associated with improved sensitivity scores and faster sessions of optic disc assessment than the manual stereo viewer. The CrystalEyes stereoscopic viewing system (using the LCD shutter goggles) incorporates the same technology as the Z-screen stereo viewer (Stereographics Corporation, San

Rafael, CA) and the two systems have been equally reproducible for the planimetric evaluation of ONH images and for glaucoma detection, but the Z screen was subjectively evaluated as a more user-friendly technique (Sheen, 2002).

5.1.4 Interobserver variability in the assessment of stereo photography

Imaging of the ONH is limited by the low levels of interobserver agreement even between experienced observers (Tielsch *et al*, 1988; Varma *et al*, 1992b). Assessment variability is enhanced due to the physiologic natural variability of the optic disc topography, the multiple structural changes associated with glaucoma and the different criteria used for evaluation of glaucomatous damage. It has been suggested that CDR estimates by stereo-photographs are more valuable than clinical subjective assessment derived with routine eye examination methods in the evaluation of glaucomatous damage (Tielsch *et al*, 1988). However, inter-observer agreement was reported to be poorer for the subjective evaluation of the CDR from stereo-photographs than for subjective diagnosis (Varma *et al*, 1992a). It has been suggested that more accurate subjective estimate of the CDR can be achieved with the ophthalmoscope or fundus biomicroscopy, rather than with fundus photography because for these techniques the aperture of the light beam can be used as a comparison tool for the evaluation of the ONH features (Theodossjades & Murdoch, 2001). The results of the Bristol Glaucoma Shared Care Study (1999) reported low intra-observer agreement between clinical and photographic assessments of the cup to disc ratio (CDR) suggesting that caution is required when clinical decisions are facilitated by different techniques. Measurements of the CDR by planimetry on stereo photographs were up to 0.15 larger than the clinical stereoscopic examination, after correcting for systematic bias between the two methods (Spry *et*

al, 1999). Since the traditionally adopted criterion for clinically significant progression of glaucomatous cupping with respect to the CDR estimates is a change of 0.2 units it is apparent that even slight differences between methods may have profound effects on the sensitivity and specificity for glaucoma.

It is speculated that clinicians can be intuitive when delineating the cup boundaries and are prone to make use of additional photographic information such as the color variation of the optic disc in order to identify the cup, whereas automated instruments are completely masked to features other than the optic nerve head topography (Varma *et al*, 1989b). The mean VCDR was greater when calculated with the Topcon Imagenet semi-automated analysis system (mean = 0.50) than when subjectively assessed (mean = 0.39) (Ikram *et al*, 2002). Conversely, topographic measurements using the Discam system underestimated the VCDR compared to subjective estimation (Correnti *et al*, 2003). Alternatively, this difference in the measurements of the CDR may also stem from the fact that the above systems differ in the definition of the cup area and in the disc segmentation models they incorporate. With the Discam system the cup is delineated by the observer and the geometrical centre of the cup area is the reference point for all the measurements (Correnti *et al*, 2003; Shuttleworth *et al*, 2000). However, the Image-net system uses as a reference point the geometrical centre of the disc area, as the cup is defined by an automated algorithm (Ikram *et al*, 2002).

The results derived by stereo-photography are largely influenced by the ability of the clinicians who make the diagnosis and/or undertake planimetry. Various factors, including the expertise of the clinicians involved, influence the inter-observer

agreement for the diagnosis of glaucoma as well as the planimetry results. Among groups of clinicians with various levels of expertise the scores of intra-observer agreement are generally better than the corresponding inter-observer agreement levels (Abrams, Scott *et al*, 1994; Tielsch *et al*, 1988).

Abrams and colleagues (1994) reported that the intra-observer agreement amongst ophthalmologists was similar to that amongst optometrists in the assessment of the VCDR among glaucoma patients (Abrams *et al*, 1994). However, the inter-observer agreement was significantly higher for the ophthalmologists (k = 0.68) than for the optometrists (k = 0.56) with corresponding differences in the mean sensitivity and specificity scores, where ophthalmologists achieved a mean sensitivity of 78% and a mean specificity of 60% while for the optometrists the scores were 56% and 53% respectively. Similarly, inter-observer agreement was higher for experienced clinicians compared to optometry students for the assessment of the same set of stereo photographs (Hanson *et al*, 2001) and the study by Harper and colleagues (2000) showed that the average mean of differences on planimetry performed by optometrists and ophthalmologists was strongly associated with the experience of the observers within each group (Harper, Henson *et al*, 2000a). The inter-observer agreement among optometrists for glaucoma diagnosis and for the subjective estimation of CD ratios on glaucoma ONHs from stereoscopic photographs was also strongly associated with the specialised training and glaucoma patient experience of the observers (Spalding, Litwak *et al*, 2000).

Consequently, it is alleged that the use of a standardized protocol and training increases the reliability of subjective assessments of the optic nerve head and

planimetry (Feuer *et al*, 2002). First of all it is essential that all observers are experienced in the use of the imaging technique. Thus examinations with direct ophthalmoscopy and biomicroscopy are likely to be more successful because of the familiarization and practical skills that clinicians demonstrate with traditional clinical assessment methods (Theodossjades & Murdoch, 2001). However, even naïve observers are able to perform planimetry of the ONH and achieve accurate cup definition with a semi-automated imaging technique after receiving appropriate training (Sheen, 2002).

It is noted that the definition of the optic nerve head features can be variable even for expert clinical observers. Gloster's (1986) criteria for determination of the cup margins rely upon defining a point on a slope and are likely to lead to inherently variable estimations (Gloster, 1986). However, when the cup margins are defined at the scleral canal depth the results are probably more reproducible, since the scleral ring is usually easily identifiable (Jonas *et al*, 1993). A well-established consensus regarding the description of the optic disc features can minimize measurement differences due to variable criteria for the demarcation of the disc and cup area (Garway-Heath *et al*, 1999) and even equalize the performance of observers with different background and variable experience on optic disc analysis (Harper & Reeves, 2000).

Optic nerve head morphology is undoubtedly influencing the performance of the levels of interobserver variability. It is likely that inter-observer agreement would be more variable for highly myopic discs, tilted discs and discs with peripapillary atrophy; because with such discs the demarcation of parts of or all of the disc

margins can be extremely difficult. While most studies do not report the percentage of discs with special morphology in their cohorts there are indications of agreement between clinicians using computerized disc analysis were greatest for cups exhibiting gradually slopping walls (Varma *et al*, 1989b). Other studies that have used stereo photography report poor intra-observer agreement for the definition of small cups rather than large ones (Bartz-Schmidt *et al*, 1995; Harper & Reeves, 2000). From this result it can be hypothesised that for the discs with established cupping the cup boundaries are likely to be easily identifiable and as a consequence the estimation of the cup to disc ratio is less variable between observers. Never the less, when interobserver agreement was evaluated among images that didn't include very small discs and cups, the interobserver variability of measurements was found unrelated to the size of cup measurements (Parkin *et al*, 2001).

Interobserver agreement may also vary when the evaluation of different features is considered. For example, one of the studies examining the subjective assessment of the HCDR and the VCDR in glaucoma patients reported better interobserver agreement for the VCDR assessment (Hanson *et al*, 2001). However, on normal subjects Hrynchak and colleagues (2003) reported perfect agreement for the assessment of both vertical and horizontal CD ratios by biomicroscopy and digital monoscopic viewing respectively (Hrynchak *et al*, 2003). Several studies suggest that inter-observer agreement is also influenced by the viewing method utilized for the optic nerve head observation, regardless of the level of clinical experience of glaucoma (Hanson *et al*, 2001; Morgan *et al*, 2005a; Parkin *et al*, 2001). Generally, stereoscopic examinations are associated with better levels of agreement between

observers comparatively to monoscopic assessments. Parkin and colleagues (2001) reported greater inter-observer agreement (ICC = 0.84) for the area CDR as estimated by the Discam system with the stereoscopic rather than monoscopic observation (ICC = 0.63) (Hanson *et al*, 2001; Morgan *et al*, 2005a; Parkin *et al*, 2001). Similar discrepancies for the inter-observer agreement based on the estimates of the area CDR were also seen with the use of computer-assisted imaging based on custom software for planimetry; namely the mean ICC for three experienced observers in the study was 0.63 under monoscopic assessment and 0.74 for the stereoscopic observation (Morgan *et al*, 2005a).

5.2 Aims of study

The study aimed to perform a standardised comparison of the planimetric evaluation of normal and glaucomatous optic nerve heads, by a panel of experienced clinicians using a computer-assisted imaging technique that could provide both stereoscopic and monoscopic presentation. The investigation was concerned with systematic differences between the two different techniques of observation as demonstrated by the scored measurements and the agreement levels achieved between the observers. The study also explores the sensitivity on glaucoma diagnosis achieved with this technique and identifies the type of glaucomatous damage likely to be misdiagnosed by different viewing methods.

5.3 Methods

True colour simultaneous stereo images acquired with the Nidek fundus camera were digitized from single frame 35 mm film and presented on a computer monitor fitted with a Z Screen (Lipton Stereographics Corporation) which enabled

stereoscopic presentation utilizing LSC technology in combination with circular Polaroid glasses (Morgan et al, 2005b). New custom software developed in the School enabled mouse-controlled planimetry definition of the ONH images, as described in Chapter 4.

Optic nerve head images from normal and glaucomatous eyes were shuffled within a dataset that numbered 210 images in total including images acquired from OHT patients and images with suspicious configuration of the ONH. This observation dataset represented a selection of images likely to be acquired and examined in the clinical setting.

Stereoscopic and monoscopic presentation of the images was organised according to an A : B : B : A (or 1 : 2 : 2 : 1) design, where block A comprised stereoscopic images and block B monoscopic images. The four blocks consisted of 100, 110, 100 and 110 images respectively. Three experienced observers were appointed the task of the double observation of all images. All but one observer examined the images in exactly the same order. For Observer 3 the stereoscopic and monoscopic presentations were performed with same sequence but the images were assessed with the reversed order within each of the A and B blocks. However, all three observers were masked to the study design and to patient diagnosis.

There were no time restrictions placed on the task performed by the observers but the duration for each assessment was automatically recorded. The time frame applied by the software describes the period the image is presented on the monitor and terminates when the observer saves the assessment file for the given image.

The duration of each assessment is expressed in seconds and is automatically recorded in the corresponding measurement files generated by the custom software with the completion of each image assessment.

5.3.1 Training sessions

All three appointed clinicians had similar qualifications and had a special interest in glaucoma. Familiarization with the computer system was addressed in a single training session that was undertaken prior to the study seperately for each observer and was based on an independent set of 18 images. Within the training session each clinician had the opportunity to observe the software operations, cross-evaluate their assessments with the prototype assessments from an experienced glaucoma clinician and demonstrate their understanding of the study experiment performing a complete assessment on 5 images from the training set. This procedure was described in more detail within Chapter 4. The training session was performed under stereoscopic settings only, so that the observers could gain experience of the three-dimensional appearance on the monitor; modify the stereo presentation of the images on the monitor to acquire maximum visual comfort together with best stereo view and adjust the double cursors at the level of the retinal plane. The short dataset of images used in the training session was also assessed by all three observers prior to their first experimental assessment, in order to minimise the influence of learning on the assessments of the images included in the analysis.

The software operated by default on stereoscopic settings so that the monoscopic presentation had to be enabled in the beginning of all monoscopic sessions. The

computer display shifts from stereoscopic to monoscopic presentation with a single software command selecting one image from every stereo pair to be presented. However, in order to familiarise the observers with this change in operation, the training set of images was reassessed before the first monoscopic assessment and the second stereoscopic session.

5.3.2 Experimental procedure

Within each experimental session every observer retrieved the already aligned image stereo pair on the monitor using the designated order. The assessment was automatically computed and saved by each observer after the assessment of both intrapapillary and peripapillary features. The observers then proceeded to complete a questionnaire within which they provided a subjective description of the photographic and stereoscopic quality of the images and performed a clinical diagnosis based solely on the ONH topography. The photographic quality was evaluated on a 4-scale grade under both viewing modes and the image stereo presentation was graded on a 3-scale grade. The observers were encouraged to use their normal clinical practice for the classification of the entire dataset. At all times the observers were masked to the true identity of the images and their classification for the study. In order to replicate decisions in the clinical setting the three observers were required to provide a final classification for every ONH they assessed. The observers also graded every image on the degree of difficulty it would pose if their clinical evaluation was made only upon the imaging results. The completed questionnaire files were also used to record any reservations the observers had on the diagnosis of specific images, as well as additional comments

on the ONH topography. A template of the questionnaire is provided within the appendix.

5.4 Results

The characteristics for the normal individuals and the patients with glaucoma are summarised in table 1. The data were explored for normality using the Kolmogorov-Smirnov test, according to which, only the visual field indices were not normally distributed. Independent samples 2-tailed T tests or Mann-Whitney U tests were employed for the investigation of significant differences between the study cohorts.

	Normal (n = 51)		Glaucoma (n = 113)		T- test
	Mean	SD	Mean	SD	P
Age (years)	58.33	10.76	65.74	10.26	0.000
Sphere (DS)	0.52	1.99	0.87	1.80	0.273
Cylinder (DC)	-0.56	0.67	-0.75	0.73	0.112
Mean refractive error (DS)	0.24	1.98	0.49	1.83	0.433
K 1 (mm)	7.72	0.24	7.79	0.26	0.116
K 2 (mm)	7.64	0.26	7.77	0.28	0.004
MD (dB)	-0.06	1.40	-4.35	5.46	0.000
PSD	1.88	1.09	4.93	3.73	0.000

Table 5.1. *The group mean values and standard deviations for the age, refractive error, corneal curvatures and the visual field indices across the 51 normal individuals and the 113 patients with glaucoma included in the study.*

The group mean age of the patients with glaucoma was greater than that of the normal individuals ($p < 0.000$). The group means for the refractive status were similar between the two groups ($p = 0.433$). As expected, the group mean visual field indices, namely the group Mean Deviation and the group mean Pattern

Standard Deviation were both significantly worse for the patients with glaucoma ($p < 0.000$ and $p < 0.000$, respectively).

5.4.1 Questionnaire data

The summary of the evaluations made by the observers during their assessments, referring to the stereoscopic quality (table 5.2), the image quality (table 5.3) and the experienced difficulty of subjective diagnosis (table 5.4). These data, as derived during the stereoscopic and monoscopic sessions are presented graphically (figures 5.1-5.8), for the normal and glaucoma group, respectively.

	Stereo quality					
	Glaucoma group			Normal group		
%	ob 1	ob 2	ob 3	ob 1	ob 2	ob 3
Poor	20	20	1	35	18	0
Good	72	77	15	59	78	6
Very good	8	3	84	6	4	94

Table 5.2.*The quality of the stereoscopic presentation of the images as evaluated by each of the three observers and expressed as percentage of the total number of images.*

	image quality											
	glaucoma group						normal group					
	stereo			mono			stereo			mono		
%	ob1	ob2	ob3	ob1	ob2	ob3	ob1	ob2	ob3	ob1	ob2	ob3
inadequate	8.8	8.0	0.0	6.2	14.2	0.9	11.8	2.0	0.0	3.9	15.7	0.0
sufficient	20.4	54.9	8.0	30.1	68.1	8.8	29.4	54.9	2.0	19.6	68.6	2.0
quite good	69.0	37.2	15.9	63.7	17.7	15.0	58.8	43.1	2.0	76.5	15.7	9.8
excellent	1.8	0.0	76.1	0.0	0.0	75.2	0.0	0.0	96.0	0.0	0.0	88.2

Table 5.3. *The evaluation of the photographic quality as perceived by each observer under the stereoscopic and monoscopic examinations. The numbers of images appointed each of the four levels of quality are expressed in percentages.*

	assessment quality											
	glaucoma group						normal group					
	stereo			mono			stereo			mono		
%	ob1	ob2	ob3	ob1	ob2	ob3	ob1	ob2	ob3	ob1	ob2	ob3
very difficult	0.0	0.9	0.0	0.0	1.8	0.0	0.0	0.0	0.0	0.0	3.9	0.0
difficult	14.2	31.0	2.7	11.5	33.6	0.9	9.8	21.6	0.0	5.9	9.8	0.0
moderate	38.9	43.4	29.2	37.2	47.8	28.3	39.2	49.0	2.0	43.1	51.0	0.0
easy	46.9	24.8	68.1	51.3	16.8	70.8	51.0	29.4	98.0	51.0	35.3	100.0

Table 5.4 *The evaluation of the difficulty of assessment for each image, as perceived by each observer under the stereoscopic and monoscopic examinations. The numbers of images graded according to the four levels of difficulty are expressed in percentages.*

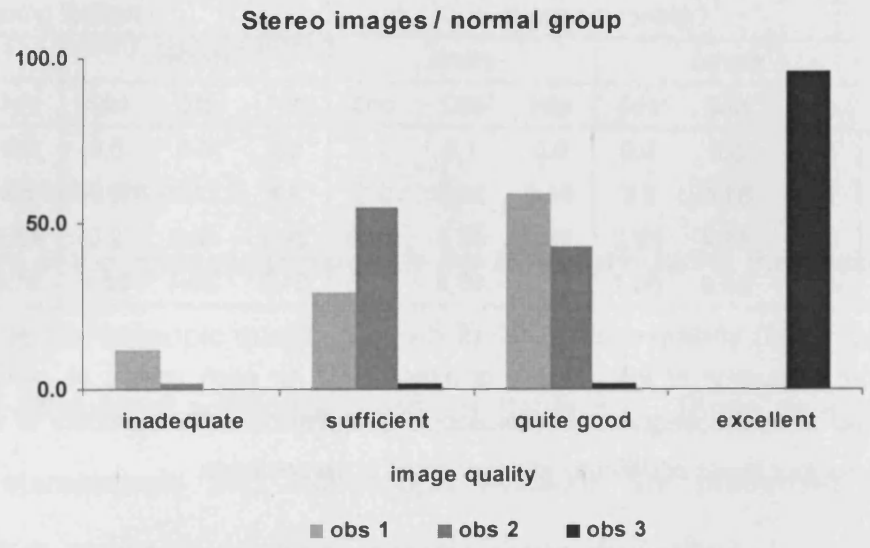

Figure 5.1 *The subjective grading of the photographic quality of the images for the normal group by all three observers under stereoscopic examination.*

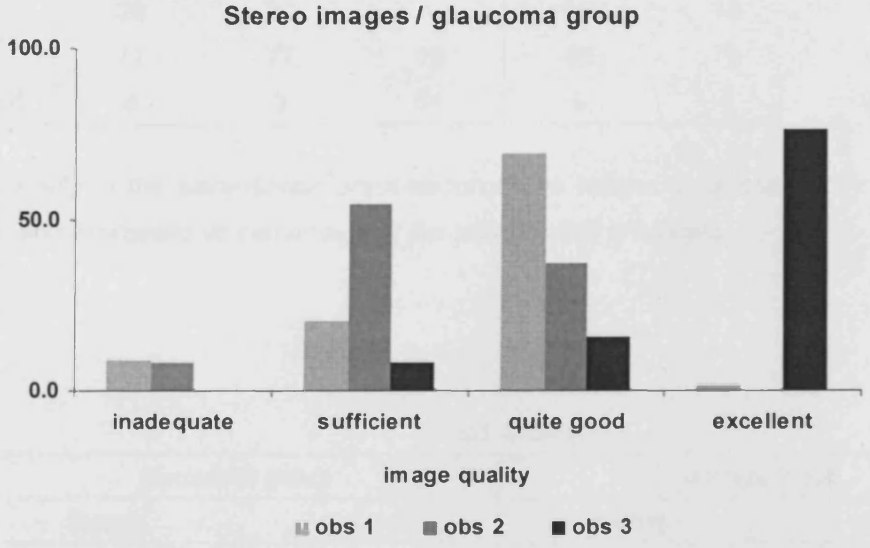

Figure 5.2 *The subjective grading of the photographic quality of the images for the glaucoma group by all three observers under stereoscopic examination.*

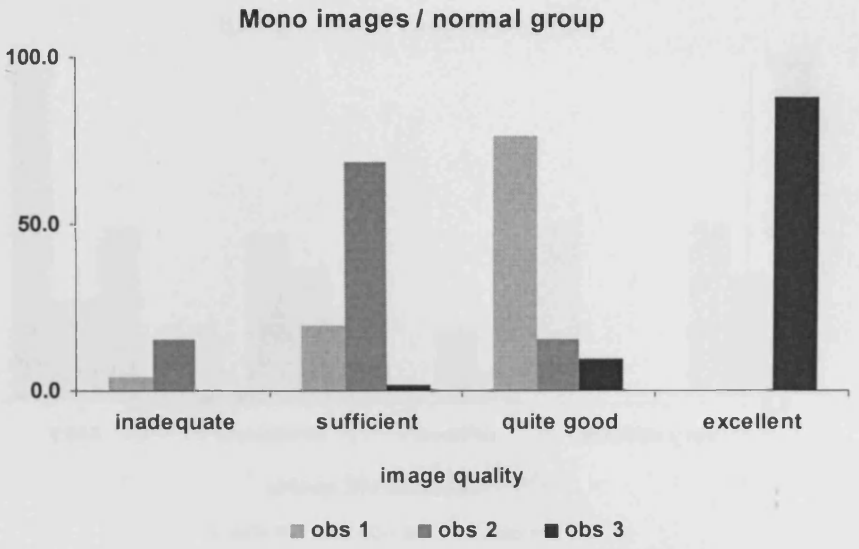

Figure 5.3 *The subjective grading of the photographic quality of the images for the normal group by all three observers under monoscopic examination.*

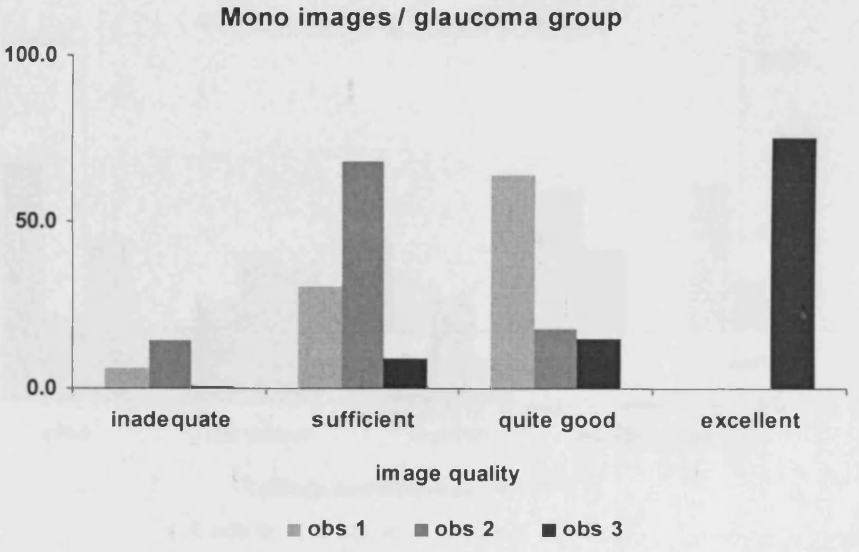

Figure 5.4 *The subjective grading of the photographic quality of the images for the glaucoma group by all three observers under monoscopic examination.*

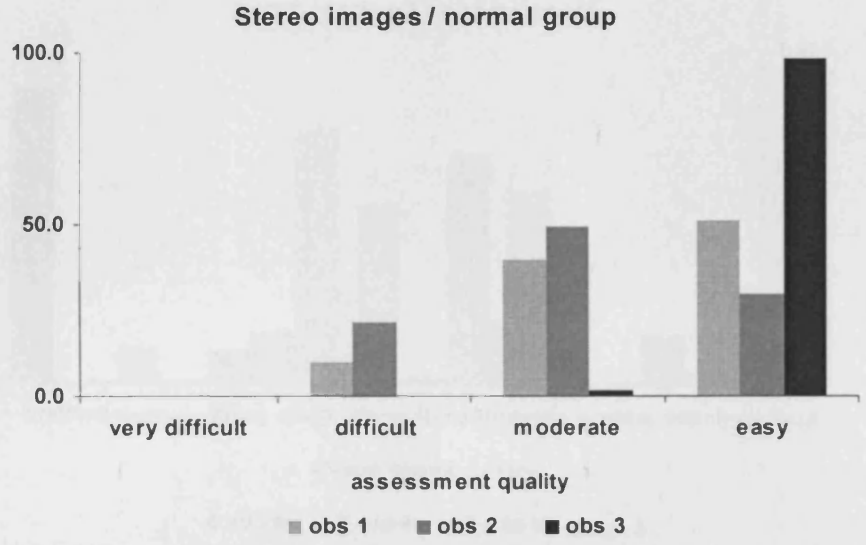

Figure 5.5 *The subjective grading of the assessment of the images for the normal group by all three observers under stereoscopic examination.*

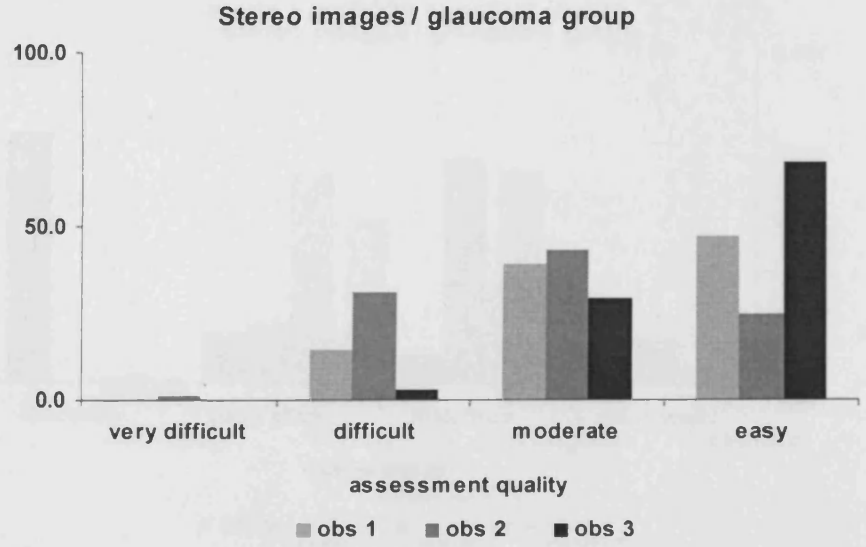

Figure 5.6 *The subjective grading of the assessment of the images for the glaucoma group by all three observers under stereoscopic examination.*

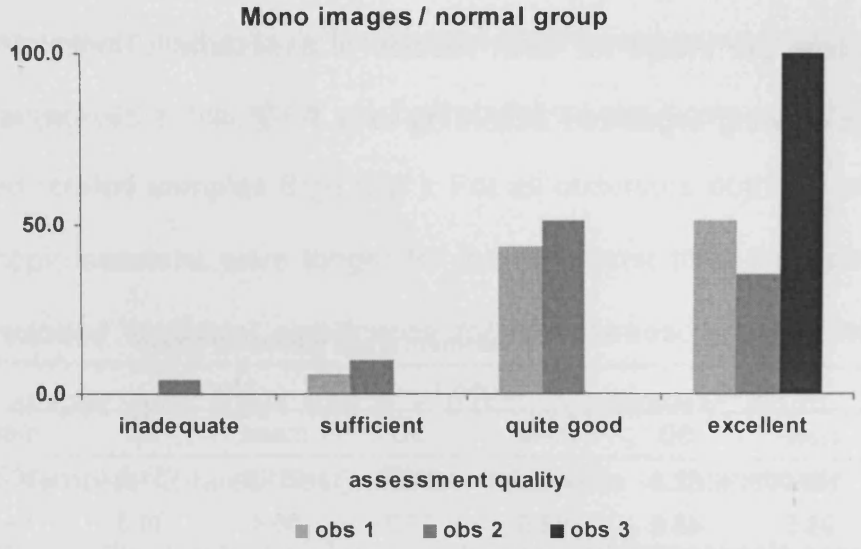

Figure 5.7 *The subjective grading of the assessment of the images for the normal group by all three observers under monoscopic examination*

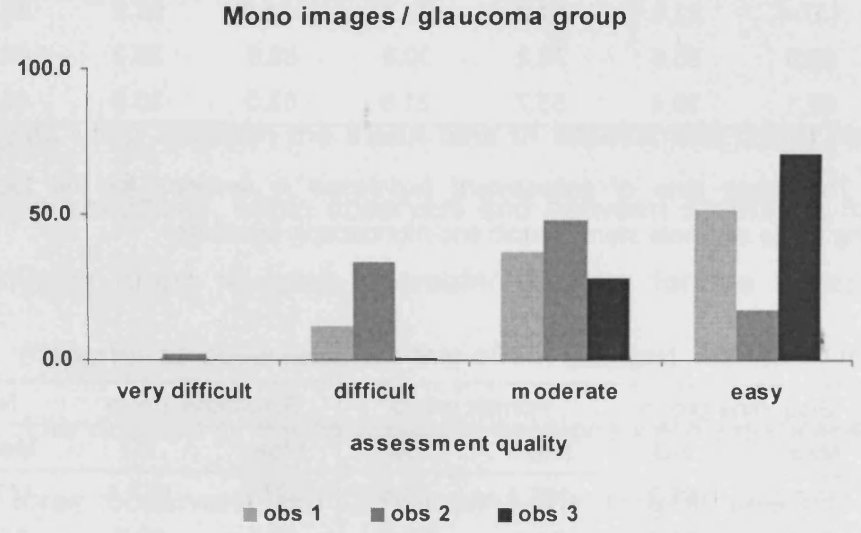

Figure 5.8 *The subjective grading of the assessment of the images for the glaucoma group by all three observers under monoscopic examination.*

5.4.2 Assessment times

The mean time per image for each session of assessment under stereoscopic or monoscopic viewing organized according to a 1 : 2 : 2 : 1 design, is tabulated in table 5.5.

	Assessment times glaucoma group							
	Stereo 1		Mono 1		Mono 2		Stereo 2	
Observer	mean	SD	mean	SD	mean	SD	mean	SD
1	136.0	62.1	144.8	212.9	131.8	51.6	102.8	33.8
2	98.5	45.0	83.5	23.2	85.4	34.3	64.9	23.0
3	103.2	41.3	83.8	63.4	85.1	31.1	79.2	28.9

	Assessment times normal group							
	Stereo 1		Mono 1		Mono 2		Stereo 2	
Observer	mean	SD	mean	SD	mean	SD	mean	SD
1	137.4	52.9	89.2	29.7	135.3	58.9	86.4	48.2
2	86.0	36.6	78.2	30.6	89.6	29.3	63.2	28.8
3	92.1	39.4	53.7	21.6	62.5	30.5	62.9	32.4

Table 5.5*. The mean time of assessment expressed in seconds for the four time periods corresponding to the alternate stereoscopic and monoscopic sessions.*

	Stereo				Mono			
	Glaucoma group		Normal group		Glaucoma group		Normal group	
Observer	Mean	SD	Mean	SD	Mean	SD	Mean	SD
1	117.8	51.2	106.4	55.6	137.6	147.4	117.2	54.2
2	81.3	38.4	72.1	33.7	84.6	29.7	85.1	30.0
3	88.8	36.9	74.3	37.8	86.1	48.2	59.0	27.4
Mean	96.0	7.9	84.3	11.7	102.8	63.3	87.1	14.7

Table 5.6. *The total mean time of assessment for the stereo and mono assessment for the normal and glaucoma groups, expressed in seconds.*

Comparison between the stereoscopic and monoscopic assessment and within each observer showed that overall, the stereoscopic sessions were longer than the monoscopic sessions but this effect reached statistical significance only for ob3 ($p < 0.000$; 2-tailed related samples Sign test). For all observers both the monoscopic and stereoscopic sessions were longer for the glaucoma than the normal group. This effect reached statistical significance for the stereoscopic and monoscopic assessment of Ob1 ($p = 0.004$ and $p < 0.000$, respectively; Mann- Whitney U independent samples 2-tailed test). There was also a statistically significant difference between the duration of the stereoscopic and monoscopic assessment of the normal group for Ob3 ($p = 0.005$; 2-tailed related samples Sign test) but all three observers performed equally long assessments with stereoscopic and monoscopic viewing for the glaucoma group.

Related samples t-test between the mean time of assessment under stereoscopic and monoscopic conditions, within observers and between observers, for the total number of images group revealed a greater duration for the stereo sessions compared to mono for all observers, but this effect reached statistical significance only for Ob3. The duration of the monoscopic sessions were significantly different between all three observers with Ob1 having the longest sessions and Ob3 performing the shortest assessment. For the stereoscopic sessions Ob1 performed longer assessments than Ob2 ($p < 0.000$) and Ob3 ($p = 0.035$), respectively. In turn, Ob2 performed statistically significant longer assessments than Ob3 ($p < 0.000$).

5.4.3 Planimetry

Planimetric measurements of disc area, neuroretinal rim area and cup area for normal and glaucomatous eyes as a function of observer are shown in tables 5.7 and 5.8.

	Stereoscopic assessment					
	Ob 1		Ob 2		Ob 3	
Normal group	Mean	SD	Mean	SD	Mean	SD
Disc Area (mm^2)	2.24	0.48	2.17	0.44	2.10	0.42
Rim Area (mm^2)	1.64	0.33	1.57	0.37	1.41	0.32
Cup Area (mm^2)	0.60	0.29	0.60	0.27	0.69	0.35
	Monoscopic assessment					
	Ob 1		Ob 2		Ob 3	
Normal group	Mean	SD	Mean	SD	Mean	SD
Disc Area (mm^2)	2.27	0.48	2.11	0.44	2.12	0.45
Rim Area (mm^2)	1.73	0.36	1.50	0.32	1.59	0.35
Cup Area (mm^2)	0.53	0.26	0.61	0.26	0.53	0.29

Table 5.7 *The mean and SD of the disc, the rim and the cup area measurements for the normal eyes, derived by stereoscopic and by monoscopic viewing as a function of observer.*

	Stereoscopic assessment					
	Ob 1		Ob 2		Ob 3	
Glaucoma group	Mean	SD	Mean	SD	Mean	SD
Disc Area (mm^2)	2.39	0.57	2.35	0.53	2.36	0.54
Rim Area (mm^2)	1.08	0.38	1.09	0.35	1.02	0.34
Cup Area (mm^2)	1.23	0.46	1.19	0.47	1.34	0.50
	Monoscopic assessment					
	Ob 1		Ob 2		Ob 3	
Glaucoma group	Mean	SD	Mean	SD	Mean	SD
Disc Area (mm^2)	2.40	0.58	2.34	0.54	2.36	0.55
Rim Area (mm^2)	1.17	0.42	1.15	0.37	1.15	0.39
Cup Area (mm^2)	1.32	0.46	1.26	0.46	1.20	0.50

Table 5.8 *The mean and SD of the disc, the rim and the cup area measurements for the normal eyes, derived by stereoscopic and by monoscopic viewing as a function of observer.*

The group mean stereoscopic and monoscopic disc area averaged for all three observers was significantly larger for the glaucoma group compared to the normal group. In the glaucoma group the mean stereoscopic optic disc area for all three observers was marginally greater than the measurements derived on the monoscopic assessments (p = 0.378; sig. 2-tailed paired samples t-test). By contrast, the group mean stereoscopic neuroretinal rim area and cup area as averaged among all three observers were significantly larger than the monoscopic (p = 0.00; sig. 2-tailed paired samples t-test), across the glaucoma group. Conversely, for the normal group the mean optic disc area for all three observers was greater for the monoscopic assessment but this did not reach statistical significance (p = 0.323; sig. 2-tailed paired samples t-test). Similarly the group mean monoscopic rim area for all three observers was marginally greater than the stereoscopic (p = 0.216; sig. 2-tailed paired samples t-test).

5.4.4 Interobserver agreement

Estimates for the agreement between observers for the assessment of the disc and rim area are shown in tables 5.9 and 5.10. The agreement was assessed by intraclass correlation coefficient (ICC), (two way mixed model, absolute agreement).

Interclass coefficient monoscopic viewing

	Disc				Rim		
	Ob 1	Ob 2	Ob 3		Ob 1	Ob 2	Ob 3
Ob 1	X	X	X	Ob 1	X	X	X
Ob 2	0.9399	X	X	Ob 2	0.8179	X	X
Ob 3	0.9137	0.9675	X	Ob 3	0.7885	0.8573	X

Table 5.9 *The interobserver agreement on the disc and rim measurements derived from the monoscopic assessment for the normal and glaucoma group, as estimated by ICC (two way mixed effects model, absolute agreement).*

Interclass coefficient stereoscopic viewing

	Disc				Rim		
	Ob 1	Ob 2	Ob 3		Ob 1	Ob 2	Ob 3
Ob 1	X	X	X	Ob 1	X	X	X
Ob 2	0.9511	X	X	Ob 2	0.8638	X	X
Ob 3	0.9179	0.9439	X	Ob 3	0.8094	0.7961	X

Table 5.10 *The interobserver agreement on the disc and rim measurements derived from the stereoscopic assessment for the normal and glaucoma group, as estimated by ICC (two way mixed effects model absolute agreement).*

Interobserver agreement was found to be very high for all planimetric measurements and not variable between stereoscopic and monoscopic assessments. With the stereoscopic assessment the agreement scores on both the disc and rim area measurements between Ob1 and Ob2 and between Ob1 and Ob3 showed a slight improvement.

5.4.5 Glaucoma diagnosis

Sensitivity and specificity were calculated for each observer according to their diagnosis which was based on the assessment of the optic disc only. The results are tabulated below (table 5.10). A comparison of the diagnostic precision of monoscopic and stereoscopic viewing is shown in table 5.11. Diagnostic precision was calculated as the percentage of true positive and true negative diagnosis relative to the total number of glaucoma patients and normal subjects included in the analysis.

	Ob 1		Ob 2		Ob 3	
	Sensitivity	Specificity	Sensitivity	Specificity	Sensitivity	Specificity
stereoscopic assessment	0.735	0.961	0.858	0.843	0.788	0.922
monoscopic assessment	0.628	1.000	0.743	0.922	0.611	0.961

Table 5.11 *The scores of sensitivity and specificity achieved by each of the three observers during stereoscopic and monoscopic examination, respectively.*

	Ob 1	Ob 2	Ob 3
stereoscopic assessment	80.488	85.366	82.927
monoscopic assessment	74.390	79.878	71.951

Table 5.12 *The diagnostic precision scored by each of the three observers during the stereoscopic and monoscopic examinations respectively.*

A consistent observation across all observers was that stereoscopic assessment yielded a higher sensitivity (0.74 - 0.86) for glaucoma compared to monoscopic assessment (0.61 - 0.74) (table 5.11). The specificity was higher for monoscopic assessment (0.91 - 1.0) compared to stereoscopic assessment (0.82 - 0.96). The diagnostic precision (table 5.12) was noticeably increased for stereoscopic observation; the mean score across the three Observers for stereoscopic viewing was 83 % compared to 75% for monoscopic viewing. The characteristics of the optic discs that were incorrectly identified by each of the three observers under the two viewing conditions are summarised in figure 5.9.

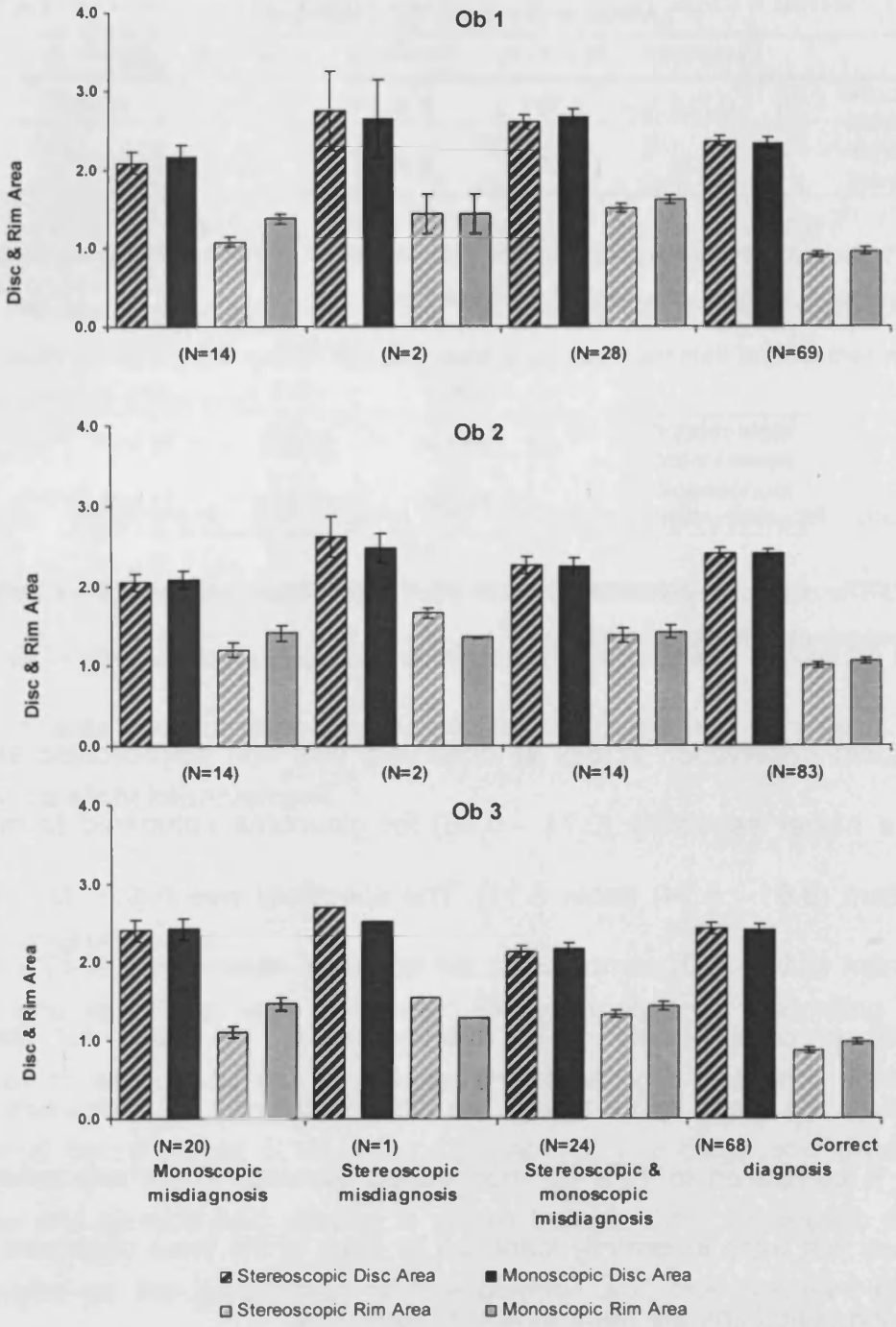

Figure 5.9 *The group mean disc and rim area measurements derived stereoscopically and monoscopically for 3 groups of glaucoma patients that were misdiagnosed with the monoscopic or the stereoscopic or by both methods, respectively, by each of the three observers.*

The disc and rim measurements as derived from the stereoscopic and monoscopic assessment respectively are graphically presented for the glaucomatous patients that were misdiagnosed according to the diagnosis under monoscopic presentation or according to the diagnosis for the stereoscopic diagnosis or by diagnosis regardless the viewing mode. There was no significant difference between correctly and incorrectly classified glaucomatous eyes when monoscopic viewing was used for assessment across the 3 observers. By contrast, when eyes were misclassified following stereoscopic viewing, the eyes tended to have larger rims and discs compared with those that were correctly classified. It can be speculated that larger discs demonstrating a diffuse pattern of rim loss can be difficult to diagnose.

The discs presented in figures 5.10 and 5.11 are those that all three observers consistently failed to identify when they examined them under monoscopic examination, but they successfully classified them under stereoscopic examination.

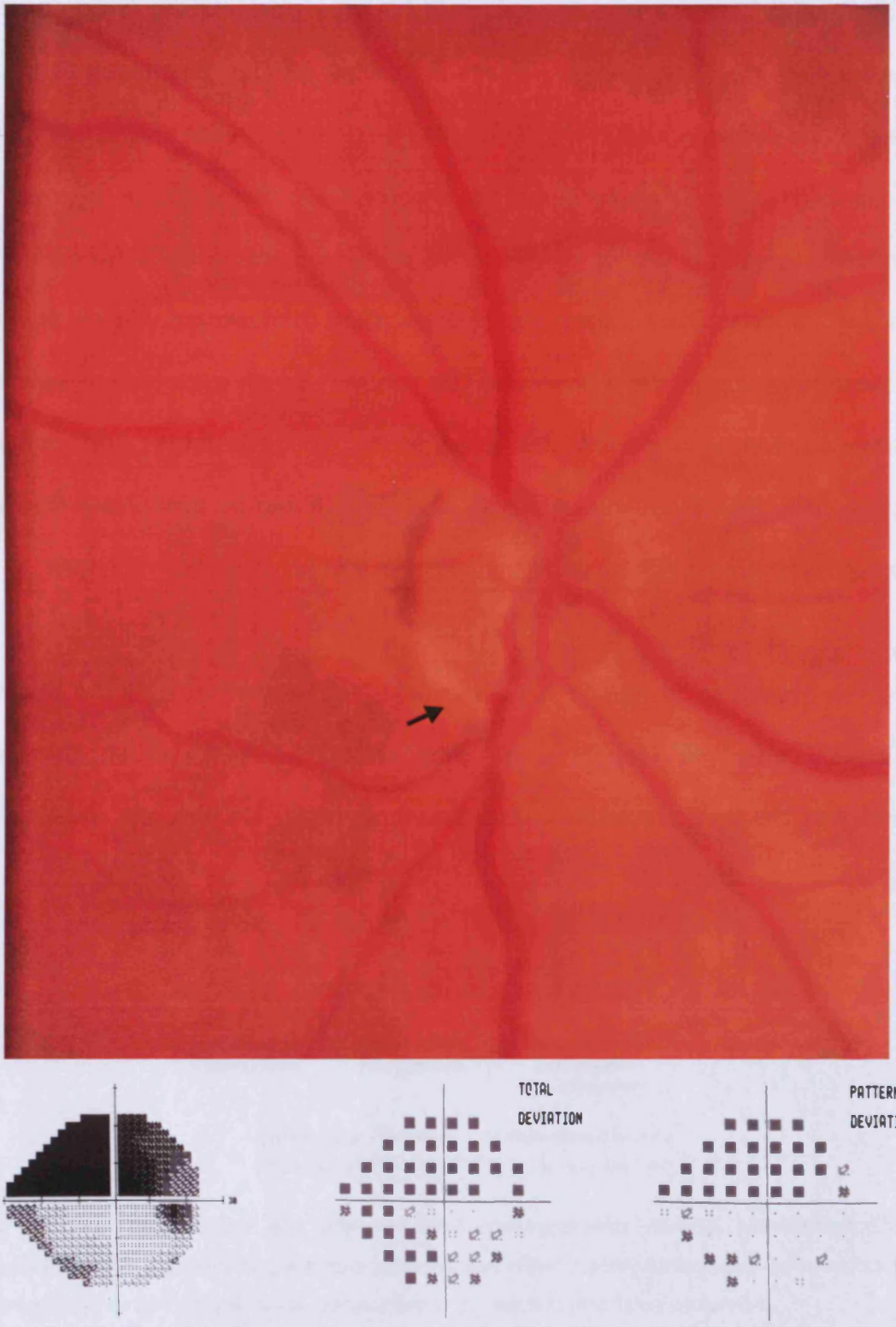

Figure 5.10 *The optic disc appearance and the visual field probability analysis plots for a glaucoma patient that was misdiagnosed by all three observers under monoscopic examination. The black arrowhead indicates an inferior- nasal rim notch.*

Figure 5.11 *The optic disc appearance and the visual field probability analysis plots for the L eye of a glaucoma patient that was misdiagnosed by all three observes under monoscopic examination. The black arrowhead indicates a superior-temporal rim notch.*

Both eyes shown in figures 5.2 and 5.3 demonstrate focal rim thinning changes associated with early to moderate visual field loss. The characteristics of these optic discs that were incorrectly identified as normal are tabulated below (Table 5.13).

	Case 1	Case 2
Gender	Female	Female
Age (years)	74	69
Sphere (Dpt)	1.75	3
Cylinder (Dpt)	-0.75	-1.5
Mean Refractive Error (Dpt)	1.38	2.25
K 1 (mm)	7.32	7.45
K 2 (mm)	7.29	7.57
MD (dB)	-16.7	-5.16
PSD	12.4	5.99

Table 5.13 *The biometrical information and visual field indices for the two cases of glaucoma patients that were misdiagnosed under monoscopic observation.*

Planimetry measurements demonstrate an overestimation of the rim area by all three observers at the monoscopic examination of the discs (Table 5.14).

		Figure 1			Figure 2		
		Ob 1	Ob 2	Ob 3	Ob 1	Ob 2	Ob 3
Monoscopic planimetry	Disc area (mm^2)	1.34	1.33	1.38	2.48	2.38	2.10
	Rim area (mm^2)	1.14	1.07	1.16	1.57	1.70	1.19
Stereoscopic planimetry	Disc area (mm^2)	1.36	1.35	1.42	2.45	2.17	2.11
	Rim area (mm^2)	0.86	0.84	0.82	1.35	1.24	1.16

Table 5.14 *The mean disc and mean rim area of the discs illustrated in figures 1:2 that correspond to the two cases of glaucoma patients that were misdiagnosed under monoscopic observation as measured by all three observer within the stereoscopic and monoscopic sessions.*

The patient classification was primarily based on the classification of stereoscopic optic discs by a single expert observer, allowing for discs with optic disc changes

and not detectable field defects to be included in the dataset. Therefore using a stricter definition of glaucoma only patients with the presence of optic disc changes and concurrent visual field loss were analysed. This criterion defined a subgroup of glaucoma discs with a group mean defect of -5.7 dB (SD 3.25) and group mean PSD of 5.98 (SD 1.91). The new classification of the glaucoma patients according to their visual field loss is described in table 5.15.

	Hoddapp Classification Modified by Litwak.					
	MILD (N=26)		MODERATE (N=22)		ADVANCE (N=30)	
	MEAN	SD	MEAN	SD	MEAN	SD
MD (dB)	-1.97	1.61	-4.25	1.77	-10.89	6.36
PSD	2.77	1.03	5.25	1.82	9.93	2.87

Table 5.15 *shows the classification of the glaucoma study group according to their visual field tests. The severity of visual field loss has been graded according with the Hodapp classification as modified by Litwak.*

The characteristics of optic discs in the subgroup of patients with definite glaucoma, which were incorrectly identified by each of the three observers under the two viewing conditions, are summarised in figure 5.12.

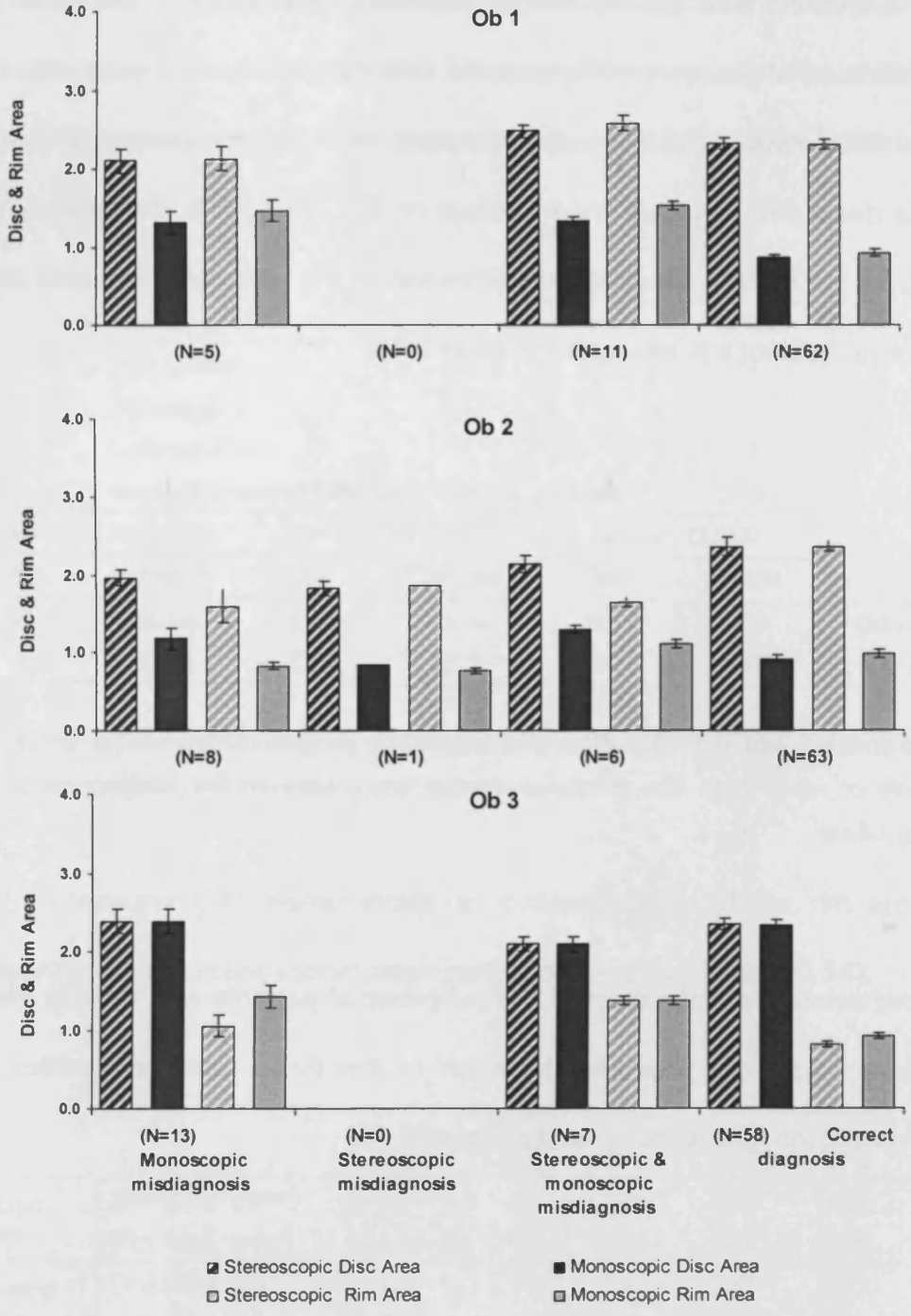

Figure 5.12 *The group mean disc and rim area measurements derived stereoscopically and monoscopically for 3 groups of glaucoma patients with both optic disc damage and visual field defects that were misdiagnosed with the monoscopic or the stereoscopic or by both methods, respectively, by each of the three observers.*

The diagnostic precision for the classification of these optic discs is shown in table 5.17.

	Ob 1		Ob 2		Ob 3	
	Sensitivity	Specificity	Sensitivity	Specificity	Sensitivity	Specificity
stereoscopic assessment	0.873	0.961	0.924	0.843	0.924	0.922
monoscopic assessment	0.797	1.000	0.835	0.922	0.747	0.961

Table 5.16 *The scores of sensitivity and specificity achieved by each of the three observers during stereoscopic and monoscopic examination.*

Diagnostic Precision	Ob 1	Ob 2	Ob 3
stereoscopic assessment	90.77	89.23	92.31
monoscopic assessment	87.69	86.92	83.08

Table 5.17 *The diagnostic precision achieved by each of the three observers during the stereoscopic and monoscopic examinations.*

It becomes apparent that the application of more strict classification criteria resulted in increased sensitivity for glaucoma detection for all observers, and increased the specificity for observer 3. Moderate increases in sensitivity for monoscopic assessment were also seen for the 3 observers but in each case this remained below the level achieved with stereoscopic viewing.

5.5 Discussion.

5.5.1 Planimetry measurements

The Group Mean values for the disc and rim areas were similar between stereoscopic and monoscopic viewing for the normal group. For the patients with glaucoma, the group mean values for the rim area were greater when derived by

the stereoscopic assessments than for the monoscopic. Other studies have reported a similar finding for the estimate of the CDR (Hanson *et al*, 2001; Morgan *et al*, 2005a; Varma *et al*, 1992b). The measurement discrepancies can be the misleading influence of the cup pallor for the demarcation of the cup boundaries when monoscopic examination is performed.

The uniform results obtained from the normal group on the disc and rim area measurements with both methods of image presentation must be associated with the lower ONH topography variability of the normal disc appearances in comparison to glaucomatous discs controlled by the selection criteria applied for this study, namely the exclusion of highly myopic eyes.

Several factors support the increased accuracy of the measurements obtained in this study. The criteria for demarcation of the disc and cup were the same as those employed by other planimetry studies. However, the use of floating cursors whose depth is adjusted to match that of the scleral rim, is likely to minimize the parallax effects especially for the measurement of the cup area and improve accuracy. Moreover, standardization of the optic cup delineation was favoured by the fact that the ophthalmologist that performed the classification assessed the discs first had first set the cursor depth at the level of the scleral canal and the 3 ophthalmologists that assessed the images later did not experience great stereo disparities. A similar type of standardization for the cup measurements is known to occur in measurements without 3d cursors (Eikelboom *et al*, 2000; Morgan *et al*, 2005b; Sheen *et al*, 2004; Shuttleworth *et al*, 2000; Yogesan *et al*, 1999b). Moreover, the technique for demarcation of the disc and cup used in the present study is similar to

that employed for the HRT and also used within the Discam system. This method requires a series of data points to be placed on the image, encircling the disc and cup circumference. This study compares with few others that undertook the task of the stereoscopic and monoscopic comparison of the optic nerve head under conditions in which the method of image presentation and the analysis tools have been standardized with use of the same cursors and scaling factors, exploring accuracy of assessment, agreement as well as diagnostic performance (Morgan *et al*, 2005a). However, comparisons are very difficult because none of these studies have calculated disc and rim area measurements making.

5.5.2 Interobserver agreement

The agreement between observers was expected to be relative to their extended experience in glaucoma diagnosis. This was demonstrated for all planimetry measurements under both the monoscopic and stereoscopic observations. Interobserver agreement is the highest ever reported and was very similar between the stereoscopic and monoscopic observations. These findings confirm the results of Varma *et al* (1992) and compare well with the studies that have employed computer-assisted optic disc analysis methods to perform an evaluation of stereoscopic imaging against monoscopic (Parkin *et al*, 2001). It can be speculated that the task of planimetric assessment of the disc for both intrapapillary and peripapillary features contributes towards more detailed observations and more accurate clinical decisions by all observers, thereby improving their agreement levels (Theodossjades & Murdoch, 2001).

All observers had experience on planimetry using the HRT and had the same years of experience on glaucoma diagnosis. One of the observers (Ob3) was from a different institution and another (Ob2) was the most familiar with the stereoscopic assessment and planimetry on computer assisted planimetry (Morgan et al, 2005a). The well defined consensus for optic disc assessment and the familiarization of the observers with the software operations, achieved by the training sessions, must have supported a good outcome of agreement (Harper & Reeves, 2000).

This imaging system has been developed in a research clinical environment so both the operations of the software have been improved under the specialized supervision of clinical staff. Therefore, the software operations are straight forward and quick to perform; the software display is simple and logical, so that the software can be learned on presentation without time consuming training procedures. Standardization of training and experience has been explored before in association with increased interobserver agreement of assessment (Feuer et al, 2002; Sheen et al, 2004). The demonstration of the pre-assessed images in the training set communicated a consensus on the description for the ONH features and the training with the double cursor has provided additional instructions for the demarcation of the cup area. Two of the three observers have worked in the same institution but all three observers had similar qualification and equivalent years of experience in clinical glaucoma detection.

5.5.3 Glaucoma diagnosis

The classification initially applied on the dataset was based on both the evaluation of ONH appearance and the evidence of visual field loss. Structural changes are

known to precede visual sensitivity losses up to 40 or 50% in glaucomatous damage, classification criteria of the disease status based on visual field loss only, undoubtedly limits the diagnostic measures obtained by studies that aimed to evaluate the diagnostic power of imaging techniques (Margo, Harman *et al*, 2002; Medeiros *et al*, 2005).

The examination of the cases that were misclassified on monoscopic examination but were successfully classified on stereoscopic examination across all observers suggested that the observers failed to observe areas of focal rim loss under monoscopic conditions. Such cases of glaucoma misdiagnosis have never been identified in the past and generally there is no previous report of focal or diffuse damage being less apparent in monoscopic or stereoscopic images.

At all cases great care was taken that the observers assessed half of the monoscopic images prior to assessment of the stereoscopic image and vice versa. This experimental design enhanced the objectivity of the comparisons made between monoscopic and stereoscopic assessments as most of the studies have reported consecutive sessions of stereo and mono evaluation, with different orders. The possibility of experience with one technique creating a learning effect and favouring the performance of the other can not be overlooked however this is the only study that controlled for examination bias by using alternate stereoscopic and monoscopic imaging sessions following the 1 : 2 : 2 : 1 design.

The digital formation is particularly suited to clinical use where images can be directly archived from the image capture station. The Z screen interface is well

suited to the clinical environment since it requires robust un-powered polarised glasses for the stereoscopic image to be perceptible. The alignment, processing, stereo display and calculation are also very quick procedures unlike other optic disc analysis systems that have reported image assessment time in the range of 10 min each (Yogesan *et al*, 1999b).

5.5.4 Possible limitations

It has been suggested that structural optic disc characteristics should not be used as a criterion for inclusion in studies evaluating the diagnostic accuracy of imaging techniques as this might lead to an overestimation of the sensitivity of the instrument (Garway-Heath *et al*, 1998b).

The dataset used in this study did not include borderline cases or glaucoma suspects as all cases of glaucoma suspects and other images that could result in controversial assessment were excluded. However it did include a group of early preperimetric glaucoma cases. Hence, the reported sensitivity and specificity scores might not be equally reproducible when different study groups are evaluated as all diagnostic tests become more sensitive with more severe damage. A smaller consequence of this is that our study group selection might hinder comparisons with a large number of similar studies that have utilized the visual field standards of glaucomatous damage.

The software could provide only disc, cup and rim area measurements, so it can only be compared with limited number of studies. As previously reviewed, most studies have measured cup to disc ratios. While, even the studies that give VCDRs

and HCDRs are not practically comparable because they can be derived by subjective evaluation or they are calculated with various imaging methods that segment the cup and disc areas in different ways. For example, both HRT and the Discam system uses the centre of the disc as a reference of all measurements but the custom software employed in this study uses the centre of the cup as a reference.

In the present study, a single expert observer was used to decide disease diagnosis. Patients with normal visual fields and glaucomatous optic nerve head appearances were classified as glaucomatous if evaluation of the optic nerve head revealed features of glaucomatous optic neuropathy at least twice. For the patients with abnormal visual fields, a second expert evaluation of the optic nerve was performed to decide the state of the optic disc.

For the current study, the quality of the images that were finally analysed was at least of adequate level and produced sufficient stereo perception as evaluated subjectively by the expert observer and over the experiment by all three observers independently. The dataset however did include photos that were not optimal but the selection was representative of images that are usually acquired in clinical settings. Implementation of image enhancement techniques was not applied for the purpose of more realistic standards of assessment. Harper & Reeves (2000) had pointed out that a selection of image quality might be causing a bias on the results, improving agreement between observers. Nevertheless, Parkin and colleagues (2001) deliberately investigated high quality images in order to highlight the

differences of assessment under stereoscopic and monoscopic situations (Parkin *et al*, 2001).

Some studies arranged that at least 3 months period of time would separate the assessments, in order to reduce the possibility of bias caused by memory. Several studies are reported not to have such arrangements (Parkin *et al*, 2001). Never the less, the 1:2:2:1 design must have limited bias although the assessments were performed consecutively. It was not possible to set time limitations.

No time limits were applied in the observation of the stereoscopic and monoscopic examinations, unlike Hanson *et al* (2001) that had restricted the assessment within a time limit of 2 seconds. The task performed in the current study was however more complicated, including diagnosis, evaluation of the images and assessment of both intra and peripapillary retina features.

5.6 Conclusion

The comparison of stereoscopic and monoscopic assessments reveal a diagnostic advantage of stereoscopic monoscopic imaging of the optic nerve head. Stereoscopic presentation was a consistently more sensitive method for glaucoma diagnosis and can be very useful for small very localized changes, like the identification of focal rim loss which apparently can be overlooked when assessing the ONH topography with monoscopic viewing.

This system is suitable for clinical use because it can be easily implemented on computers and monitors with low specification. Also, it is evident that a high volume of optic disc stereo photographs can be processed fast and efficiently, thereby this

system could be utilised for glaucoma screening. Our findings would support use of this modality in the clinical context and suggest that the use of digital stereoscopic imaging for a detailed and subjective evaluation of the optic nerve head is well suited to clinical use.

Chapter 6 Clinical evaluation of peripapillary atrophy in normal and glaucomatous eyes

6.1 Peripapillary atrophy

Peripapillary atrophy can be a normal anatomic variation in the formation of the optic nerve head over the embryonic stages of development, leading to a misalignment of the retinal tissues (Fantes & Anderson, 1989; Nevarez *et al*, 1988). Conversely, it is a degeneration of the RPE cells evident as irregular distribution of melanin and the appearance of hypo/hyper-pigmented retinal areas denoting alpha zone (α zone); or complete absence of the RPE layer, revealing the choroidal vessels and scleral tissue describing beta zone (β zone) (Jonas, Gusek *et al*, 1988b; Jonas & Naumann, 1988; Kubota, Jonas *et al*, 1993). Histopathology findings have shown that the Alpha type of PPA represents pigmentary and structural change of the RPE while the Beta type represents an advanced damage of the peripapillary tissue involving degeneration of the RPE accompanied by loss of the adjacent photoreceptors and the choriocapillaries (Kubota *et al*, 1993).

6.2 Occurrence of PPA in normal and glaucomatous eyes

Clinical studies of normal eyes have estimated a prevalence of any type of peripapillary atrophy ranging from 86% (Jonas *et al*, 1988b; Jonas & Naumann, 1988) to 59% (Ramrattan *et al*, 1999), with zone Beta being present at a percentage of 15% (Jonas *et al*, 1988b; Jonas & Naumann, 1988) to 13% (Ramrattan *et al*, 1999). However, there is prevalence of PPA in glaucomatous eyes. While zone Alpha is prevalent among the general population, zone Beta has been reported to be three times more frequent among primary open angle

glaucoma patients (Jonas *et al*, 1988b; Jonas & Naumann, 1988). Moreover, peripapillary atrophy differs among the glaucomatous eyes depending on the subtype of glaucomatous damage they demonstrate. Increased prevalence of PPA is observed among the NTG, myopic and senile sclerotic glaucomatous optic discs (Jonas *et al*, 1999b; Jonas & Budde, 2000), which could be an indication of PPA being more involved with the pathogenesis of certain types of glaucoma (Jonas *et al*, 1999a). Moreover, the prevalence of PPA increases with age (Jonas *et al*, 1988b; Jonas & Naumann, 1988) and with myopic refractive error among populations of healthy eyes (Ramrattan *et al*, 1999) and also in glaucomatous patients (Dichtl *et al*, 1996) .

6.3 Speculations on glaucomatous aetiology of PPA

As opposed to initial speculations, current knowledge suggests that PPA is not just a normal retinal feature that is exposed in glaucoma because of the loss of the overlying nerve fibre layer, (Jonas *et al*, 1988c). On the contrary, pathophysiology of PPA can be perplexed. The area around the disc, where peripapillary atrophy is developed, is considered to represent an anatomic vulnerability of the blood–retinal barrier, as it is the area where RPE terminates naturally. Anderson (1983), suggested that the chorioretinal crescents formed in the peripapillary region may allow substances from the choroid to reach superficial layers of the retina and alter the environment of the ganglion cells (Anderson, 1983). The elasticity of the lamina cribrosa and the mechanical stretching of the retina in myopic eyes can be contributing factors in the formation of such areas of leakage at the disc margins. Not surprisingly, fluorescein angiography evaluation of enlarging myopic crescents in healthy eyes and areas of glaucomatous beta peripapillary atrophy revealed a

dislocation of the ring of Zinn-Haller, clearly indicating retinal stretching (Yasuzumi, Ohno-Matsui *et al*, 2003).

Moreover, the posterior cilliary arteries responsible for the ONH blood supply and giving support to the peripapillary retina are shown to have poor perfusion in POAG. Blood flow insufficiency could result into visible peripapillary atrophy of the RPE and the choroid. It is speculated that PPA is related to choroidal rather than the retinal circulation. Hayreh (1989) first speculated that the choroidal circulation could effect the ONH deep within the cup (Hayreh, Klugman *et al*, 1989). Other studies have reported a decreased choroidal thickness within the peripapillary region for glaucoma patients (Kubota et al, 1993), and Cohen (1993) described the hypothesis of a retinal barrier defect at the level of the choroid of the ONH (Cohen, 1993). Rader et al (1994) noted vascular constriction in OAGS within PPA, but hypothesised that this was a secondary effect of the atrophy (Rader *et al*, 1994). However, O'Brart (1997) showed that the PPA region of glaucomatous eyes was associated with areas of impaired choroidal circulation and hypofluorescence (O'Brart, de Souza Lima *et al*, 1997). In support of the above, it is important to note that PPA was significantly greater for normal eyes and glaucomatous eyes with haemorrhages than without (Hayakawa *et al*, 1998) and haemorrhages are consistently occurring in spatial correlation with the PPA areas (Hayakawa *et al*, 1998; Lee *et al*, 1998; Sugiyama *et al*, 1997b).

The glaucomatous compression of the lamina cribrosa would compress the peripapillary choriocapillaries and damage both the RPE and the deep retinal layers (Jonas, Budde *et al*, 2001). Several studies add support to the association of PPA

development with other glaucomatous features of vascular insufficiency (Jonas & Budde, 2000). Jonas and colleagues (2001) reported structural abnormalities in vessels within the areas of atrophy and have suggested that development of PPA as well as rim thinning correlates with the ONH areas that lie most distant to the central vessel trunk (Jonas et al, 2001). In cases of most advanced glaucoma, visual field loss was also associated with reduced blood flow of the neuroretinal rim (Harju & Vesti, 2001). Conversely, high concentration of lipofuscin granules evident as fundus autofluorescence, has been reported in areas of peripapillary atrophy for ocular hypertensive and glaucoma patients (Lammer *et al*, 2005). This molecule of retinal metabolical by-product takes place in the mitochondria and has been strongly linked with degenerative areas of AMD (Boulton, Rozanowska *et al*, 2001) but only recently was researched in glaucoma eyes. Lipofuscin formation by aged neurons does result in cellular dysfunction in a number of lysosomal diseases (Neufeld, 1991). Furthermore, both cultured glial cells and RPE cells were shown to undergo accelerated lipofuscinogenesis when submitted to oxidative stress (Brunk & Terman, 2002).

Lipofuscin molecules could also trigger microglial activation and thereby, initiate secondary glaucomatous degeneration. It is speculated that when the accumulation of the lipofuscin molecules inside the microglia reaches toxic levels, the cells respond with activation so that they can proliferate and redistribute their waste. Lipofuscin is constantly accumulated over time in neurones, so microglia that rapidly dispose apoptotic neurones by phagocytosis are likely to reach high concentrations of lipofuscin and become upregulated (Terman & Brunk, 2004). Eventually, activation of the microglia would stimulate glaucomatous damage by

secondary degeneration. Not surprisingly, glial cells were found in higher concentrations around the peripapillary region in post-mortem examination of glaucomatous eyes (Neufeld *et al*, 1997). The presence of astrocytes and microglia is a definite sign of injury at the area, where the glial cells predominately perform phagocytosis of the dying cells and other unwanted substances. However, a secondary degeneration of the tissue may also be in effect, as activated astrocytes and microglia are able to induce excitotoxic effects through NO production and oversupply of trophic factors such as VNGF and BDNF. Such an excitotoxic environment would disrupt the RPE and give rise to PPA (Neufeld, 1999; Neufeld & Gachie, 2003).

6.4 Clinical observation of PPA in the course of glaucomatous damage

A number of studies highlight the association of PPA with the earliest stages of glaucoma. Kasner *et al* (1989) estimated a threefold increase in the likelihood of OHT patients to progress into glaucoma in the presence of peripapillary crescents (Kasner, Feuer *et al*, 1989). Similarly, Jonas *et al* (1994) reported that OHT patients had smaller rim area and larger PPA than the normal eyes (Jonas & Königsreuther, 1994). Quigley (1994) revealed an association of PPA with the development of VF loss in OHT patients (Quigley, 1994b). Stewart and colleagues (1995) using computerised digital planimetry hypothesised that the amount of PPA could signify the risk of glaucomatous damage for OHT patients (Stewart *et al*, 1995). The study identified that an extent of PPA that was half the size of the disc area was associated with progressing glaucomatous damage. Similarly, Tezel and colleagues (1997) on a longitudinal study of OHT patients reported that both the presence and extent of PPA were key factors for the progression to glaucoma (Tezel *et al*, 1997a;

Tezel *et al*, 1997b). Only 36 % of the progressing OHT eyes had Beta zone peripapillary atrophy at the baseline examination suggesting that PPA was an acquired feature accompanying glaucomatous damage. Moreover, the multivariate model described by the study suggested that there was a three times greater likelihood of eyes with zone Beta peripapillary atrophy to develop optic disc damage and/ or visual field loss. Most importantly the OHT eyes showing progression to glaucoma demonstrated increase of PPA areas before other ONH changes became evident. In such cases, the PPA Alpha zone either developed or enlarged from baseline with also the likelihood to converted to Beta zone (Stewart *et al*, 1995; Tezel *et al*, 1997a; Tezel *et al*, 1997b).

In cases of established glaucoma pathology, the areas of Beta zone are strongly correlated with the rim loss and the VFT loss (Jonas *et al*, 1988b; Park, Tomita *et al*, 1996a; Park *et al*, 1996b). Also, a spatial correlation of the PPA areas with the sectors of the optic nerve mostly affected by glaucomatous damage, as well as their spatial correspondence with the visual field defects is reported (Emdadi *et al*, 1998; Hall *et al*, 2001). Most importantly, expansion of the atrophic areas is always observed in the progressing stages of the disease (Tezel *et al*, 1997a; Tezel *et al*, 1997b; Uchida *et al*, 1998).

6.5 Distribution and quantification of PPA

In normal eyes the total PPA area was widest and had the highest frequency in the temporal region, followed by the inferior, the superior and finally the nasal part of the optic disc circumference (Jonas *et al*, 1992a). This pattern is similar to glaucomatous eyes, but both zone Alpha and zone Beta are enlarged. As

demonstrated with experimentally induced glaucomatous damage on animal models (Hayreh *et al*, 1999), glaucomatous zone Alpha is distributed around the optic disc in a manner similar to the normal eye, but this pattern appears more distinct (Jonas *et al*, 1999a; Jonas & Budde, 2000). Zone Beta in glaucomatous eyes usually has a uniform distribution around the ONH (Uhm *et al*, 1998) although it can be considerably different in size between the various glaucoma groups (Jonas *et al*, 1999a). The differences between the two zones in the glaucomatous eye are particularly apparent on the nasal side (Jonas *et al*, 1999a; Jonas & Budde, 2000).

Quantification of peripapillary atrophy among normal and different subgroups of glaucoma eyes by manual planimetry estimated that the mean area of Alpha zone among normal eyes was 0.57mm^2 (SD = 0.57); increasing in eyes with ordinary glaucoma (0.78 ±0.67mm^2) and focal normal pressure glaucoma (0.87 ±0.60mm^2), while eyes with age-related sclerotic glaucoma included the widest Alpha zone (1.04 ±0.92mm^2) (Jonas *et al*, 1999a). Correspondingly, Beta zone was significantly the smallest in normal eyes (0.18 ±0.57mm^2) and the largest in sclerotic POAG eyes (1.00 ±0.37mm^2), followed by eyes with ordinary POAG (mean area and SD: 0.66 ±1.06mm^2) and eyes with focal normal pressure glaucoma (0.34 ±0.36mm^2) (Jonas *et al*, 1999a). In highly myopic glaucoma eyes the myopic crescent was significantly larger than the beta zone in any other group (4.11 ±3.42mm^2) (Jonas *et al*, 1999a). The mean gradient of the total area of PPA over the disc area (PPA / disc area ratio) was estimated to be 0.41 ±0.32 mm^2 for OAG patients (Uchida *et al*, 1999). The measurements were derived with the HRT and the add-on Atrophy Zone Analysis software that gives an approximate evaluation of the PPA areas as an

extension of the disc area and includes the scleral ring in the measurements (Park *et al*, 1996a; Park *et al*, 2001).

6.6 Interobserver agreement for the evaluation of PPA

It becomes apparent that there is variability on the reported average PPA areas depending possibly on the sample selection and undoubtedly on the method of evaluation. However it is a consistent finding that PPA is enlarged in glaucoma. The high inter-individual variation in the normal appearance suggests that PPA zones can only be effectively assessed on an individual basis over a longer follow-up period. Moreover, in comparison to Zone Alpha, Zone Beta is more reproducible (Park *et al*, 2001; Uchida *et al*, 1998). For all the above reasons, discrimination between glaucomatous and healthy eyes cannot be achieved by the observation of PPA alone (Jonas *et al*, 2000; Jonas, 2005).

The interpretative difficulties in PPA evaluation are evident through the lower scores of inter- observer agreement reported for this feature. One of the first reports by Tuulonen and colleagues (1996) assessing PPA on stereo photos by planimetry presented high interobserver correlation and agreement for the values (Tuulonen, Jonas *et al*, 1996). However, other studies have performed more subjective evaluations of PPA areas. Assessment of PPA by opthalmoscopic examination of the optic disc, performed by a panel of optometrists that made a subjective description of the extent of PPA areas and their relative location, was associated with a fair level of interobserver agreement (Kappa statistics = 0.12 – 0.51) (Theodossjades & Murdoch, 2001). Similarly, two panels of observers consisting of ophthalmologists and optometrists, respectively described the extent of PPA on a 5-

point scale as a proportion of the total disc circumference. Harper and colleagues (2000) estimated that the inter-observer agreement was 0.45 and 0.53, while the mean intra-observer agreement was 0.66 and 0.68 for the group of optometrists and ophthalmologists, respectively (Harper & Reeves, 2000).

6.7 Correlation of PPA with other features of glaucomatous damage

Jonas *et al* (1988) and Park *et al* (1996a, 1996b) showed that Beta zone correlated with the rim area (Jonas *et al*, 1988b; Park *et al*, 1996a, 1996b). The extent of peripapillary atrophy increases with increase in the extent of ONH cupping as expressed in terms of the C/D ratio (Jonas *et al*, 1992a) and with a decrease in the neuroretinal rim width (Emdadi *et al*, 1998; Jonas & Grundler, 1997b; Park *et al*, 1996b). Zone Beta is associated with a mostly concentric loss of rim width and both zones showed a spatial correlation with the sectors exhibiting the most marked rim loss (Jonas *et al*, 1988b; Jonas *et al*, 1999b).

6.8 Peripapillary atrophy and visual field loss

Peripapillary atrophy has been associated with enlargement of the blind spot (Jonas *et al*, 1991), while Alpha and beta zone correspond psychophysically to relative scotoma and absolute scotomas, respectively. In glaucomatous eyes many studies have identified the association of beta zone with visual field damage (Jonas *et al*, 1988b; Park *et al*, 1996a, 1996b) which is also evident with a strong spatial correlation of the beta zone expansion to the location of the visual field defects (Emdadi *et al*, 1998; Hall *et al*, 2001). This aspect of topographical association of the PPA has been also identified in retrospective studies. Tezel and colleagues

(2000) revealed the the association of PPA location and expansion with subsequent development of visual field defects (Tezel *et al*, 2000).

6.9 Aims of study

Quantification of peripapillary atrophy in normal subjects and glaucoma patients using custom made software specialised for planimetry. Investigation of the correlation between PPA α and β areas with other diagnostically significant glaucomatous ONH features.

6.10 Methodology

The analysis of the disc and the peripapillary retina was performed with custom software (figure 6.1).

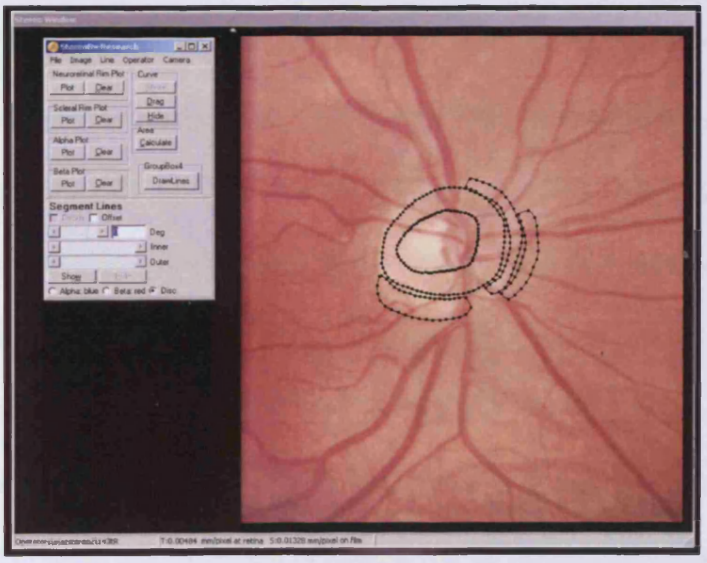

Figure 6.1 *The software interface and an example of an image that has been planimetrically assessed. The demarcated areas of the cup, the disc and the peripapillary region are apparent. The add-on software for the PPA measurements is described in chapter 4.*

The operations of the add-on software that enabled the quantification of PPA areas into 5 degree sectors and the classification of those areas into zones are described in detail within Appendix I. The observers demarcated the areas of PPA, being present in zones of alpha (PPA α) and beta (PPA β) type, for 51 normal eyes and 113 glaucoma eyes (table 6.1), that were planimetrically evaluated under stereoscopic viewing conditions, as described in chapter 5.

	Normal (N=51)		Glaucoma (N=113)	
Parameter	Mean	SD	Mean	SD
Age (years)	58.33	10.76	65.74	10.26
Sphere (Dpt)	0.52	1.99	0.86	1.8
Cylinder (Dpt)	-0.56	0.67	0.75	0.73

Table 6.1. *The group mean values and standard deviations for the age, refractive error and the visual field indices across the 51 normal individuals and the 113 patients with glaucoma comprising the two study groups.*

The methodology used for the evaluation of the presence and extent of PPA is described in chapter 4. The analysis was based on the planimetry results derived under stereoscopic viewing of the ONH only. PPA should not be affected by the stereoscopic or monoscopic conditions. However, in consideration of the results of the study presented in Chapter 5 that suggested monoscopic planimetry underestimated the rim and disc areas, stereoscopic planimetry was considered optimal for the investigation of the possible correlations between the PPA areas and the other intrapapillary features.

PPA areas were described as a global parameter and also distinguished between zones for each eye according to the measurements derived by all three observers

and as an average across the three observers. All PPA values were also presented as a ratio over the corresponding disc area in order to enable comparisons with other studies that have used similar estimates of PPA (Kono, Zangwill *et al*, 1999b; Kono, Sample *et al*, 2000; Tezel *et al*, 2001).

As an additional feature of the planimetry software, a polynomial (Nerb) function fitted to the points demarcating the disc margins determined the major and minor axes of the optic disc. These data provided a quantitative description of the degree of tilt of the major axis of the optic disc and the degree to which the optic disc was oval in shape, enabling the investigation of the extent and location of PPA areas with reference to the anatomical configuration of the optic disc in normal and glaucomatous discs. The shape factor for the disc area was expressed as the gradient of the minimum over the maximum disc diameter, constituting the index of tilt (Tay, Seah *et al*, 2005) and ranging from 1 (for a circle) to 0 (for an irregular shape). The authors suggested a cut-off value of ≤0.8 for the index of tilt to describe a tilted disc configuration. The above disc shape analysis was performed in the preliminary stages of this study for both the normal and glaucoma group by the expert observer (JEM). All correlations were investigated using the group mean parameters of disc shape as determined by the expert observer only.

The group mean total sum of PPA as a global value and also distinguished into alpha and beta zones was calculated for each eye by each of the three observers. Also, the mean sum of PPA within each of 72 sectors around the ONH (each sector subtending 5 degrees) across the normal and glaucoma group was plotted in radar

charts for the three observers and also for the average observer demonstrating the distribution patterns and the sectorial expansion of PPA.

The diagnostic significance of peripapillary atrophy in the glaucomatous eyes and the correlations of the demarcated areas for both the Alpha and the Beta zones with other glaucomatous features were explored with a multivariable regression analysis using the planimetry results of the disc and rim areas as independent variables.

The correlation of PPA with the visual field examination results was investigated through the correlation of the PPA values to the visual field global indices. The total demarcated PPA area for each of the normal subjects and the glaucoma patients by each of the three observers and also for the mean of all observers was plotted against the MD and PSD values that were derived by W-W perimetry and the full threshold algorithm test for both study groups at recruitment. The above analysis was repeated for the normalised values of the PPA areas divided by the corresponding total disc area of the same ONH, in order to correct for the influence of refractive errors and the disc size. and it improved the correlation coefficients for the analysis.

Finally, the agreement between observers for the assessment of PPA was described by Intraclass-Correlation-Coefficients (two way mixed effects model, absolute agreement).

6.11 Results

Comparison between the two study groups showed that the group mean age of the patients with glaucoma was greater than that of the normal individuals ($p < 0.000$; Mann-Whitney U test). Also, there were no significant differences for the group mean spherical and cylindrical refractive errors at a 0.001 level of significance ($p = 0.206$ and $p = 0.024$; Mann-Whitney U test) (table 6.1).

The disc shape parameters as defined by the expert observer across the two study groups, are summarized in table 6.2

		Orientation	Major Length	Minor Length	Min/max Length
Normal Group	MEAN	115.37	1.64	1.47	0.89
	SD	37.53	0.17	0.16	0.05
Glaucoma Group	MEAN	108.95	1.74	1.55	0.90
	SD	29.51	0.20	0.20	0.05
P-value; Mann - Whitney U		0.079	0.003	0.004	0.663

Table 6.2 *The group mean parameters describing the optic disc shape, as evaluated by the expert observer, across the normal and glaucoma group.*

Exploring the distribution of the disc shape parameters with the Shapiro-Wilk test for normality showed that all parameters were not normally distributed for the glaucoma group. The orientation of the ellipse and the shape factor (min/max length) were also not normally distributed for the normal group. The two groups show significant differences only for the parameters of the minimum (Min Length) and maximum (Max Length) disc diameter ($p = 0.003$ and $p = 0.004$, respectively; Mann-Whitney U Asymp. sig. 2-tailed). However, the discs in both groups appeared vertically oval. Using a cut-off value of an index of tilt of ≤ 0.8 (Tay *et al*, 2005), the

disc shape analysis revealed that 3 normal optic discs (5.9%) and 8 glaucomatous discs (7.08%) presented a significant disc tilt.

6.11.1 Frequency of PPA

The proportion of normal and glaucomatous eyes that featured PPA is shown in as a function of observer in the combined table 6.3.

	Normal (N=51)			
%	OB1	OB2	OB3	Mean OB
PPA α	56.9	80.4	21.6	53.0
PPA β	21.6	68.6	0.00	30.1
PPA α & β	17.6	58.8	0.00	25.5
PPA total	60.8	90.2	29.4	60.1

	Glaucoma (N=113)			
%	OB1	OB2	OB3	Mean OB
PPA α	69.9	84.1	20.4	58.1
PPA β	34.5	70.8	2.7	36.0
PPA α & β	21.2	66.4	0.9	29.5
PPA total	76.1	88.5	22.1	62.2

Table 6.3. *Proportion of normal and glaucomatous eyes across the two study groups featuring PPA areas.*

An example of PPA areas that were present in a normal and glaucomatous eye, as outlined by one of the observers is presented in figure 6.2.

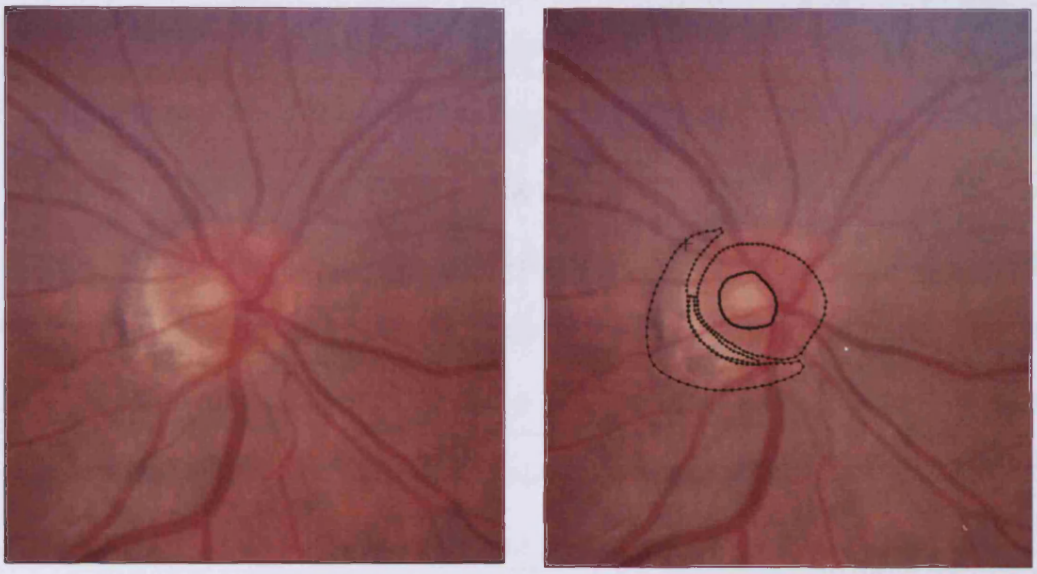

Disc area: 1.76mm^2 ; Rim area: 1.22 mm^2 ; PPA α: 0.89 mm^2 ; PPA β: 0.37 mm^2

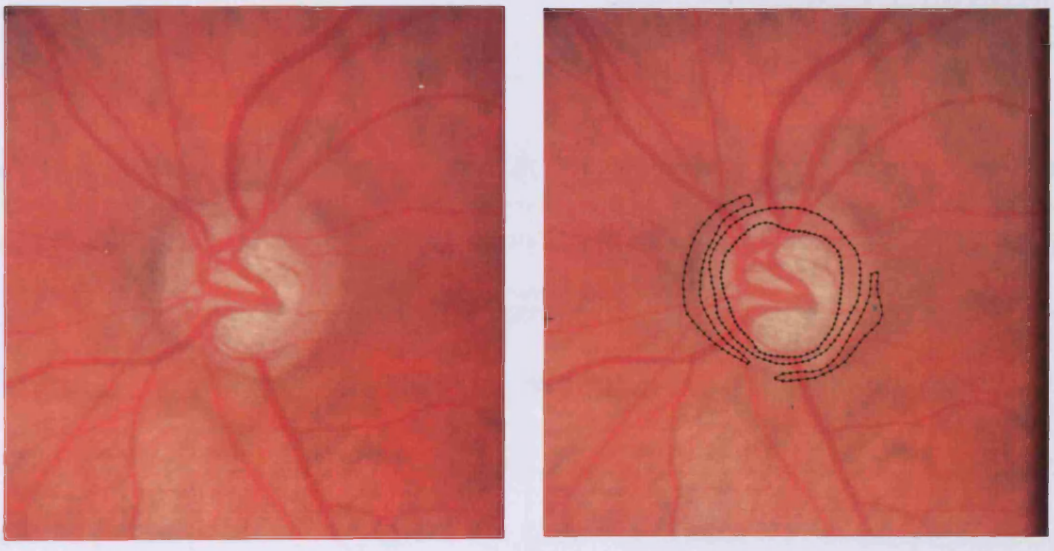

Disc area: 2.87 mm ^{2} ; Rim area: 0.84 mm ^{2} ; PPA α: 0.69 mm ^{2} ; PPA β: 0.19 mm^2

Figure 6.2. *Computer display of a normal (above) and a glaucomatous eye (below) featuring PPA areas before and after they were planimetrically analysed by one of the observers. The corresponding planimetry results are also provided.*

6.11.2 Quantification of PPA

The group mean PPA global area averaged for all three observers was consistently larger for the glaucoma group compared to the normal group. This effect was also seen when the Alpha and Beta areas were evaluated separately and was maintained when the gradients of those areas over the disc area were calculated. However, it is apparent that there is a wide difference between the three observers in their evaluation of the areas of atrophy.

		Normal (N=51)					
Area (mm^2)		PPA α	PPA α / Disc	PPA β	PPA β / Disc	Total PPA	PPA /Disc
OB1	MEAN	0.24	0.11	0.09	0.04	0.33	0.15
	SD	0.24	0.11	0.22	0.11	0.35	0.18
OB2	MEAN	0.58	0.27	0.28	0.14	0.86	0.41
	SD	0.46	0.23	0.27	0.14	0.52	0.26
OB3	MEAN	0.13	0.06	0.03	0.02	0.16	0.08
	SD	0.28	0.14	0.15	0.07	0.30	0.15

		Glaucoma (N=113)					
Area (mm^2)		PPA α	PPA α / Disc	PPA β	PPA β / Disc	Total PPA	PPA /Disc
OB1	MEAN	0.39	0.17	0.16	0.06	0.54	0.24
	SD	0.46	0.19	0.33	0.12	0.64	0.25
OB2	MEAN	0.70	0.30	0.40	0.17	1.10	0.48
	SD	0.67	0.29	0.50	0.19	0.92	0.39
OB3	MEAN	0.18	0.07	0.02	0.01	0.20	0.08
	SD	0.46	0.16	0.16	0.05	0.54	0.17

Table 6.4. *The sum of PPA described as alpha (α), beta (β), and total areas (mm^2) averaged across the two study groups for each of the three observers. The gradient of the mean sum areas of atrophy over the corresponding sum of disc area, as calculated by each of the three observers is also provided.*

	Area (mm^2)	Disc	rim	PPA α	PPA β
Normal (N = 51)	Mean	2.17	1.54	0.32	0.13
	SD	0.43	0.31	0.24	0.18
Glaucoma (N = 113)	Mean	2.37	1.06	0.42	0.19
	SD	0.53	0.33	0.39	0.28
Mann - Whitney U	P-value	0.012	0.000	0.175	0.144

Table 6.5. *Planimetry results for the two study groups averaged for the three observers.*

The group mean PPA area, distinguished in Alpha and Beta zones and averaged for all three observers, showed an increase for the glaucoma group compared to the normal group, but the results of the comparison did not reach statistical significance. Conversely, the group mean optic disc area and rim area averaged for the three observers were significantly greater for the glaucoma group (p = 0.012 and p = 0.000, respectively; Mann - Whitney U test, Sig. 2-tailed).

6.11.3 Interobserver agreement

The interobserver agreement was assessed by Intraclass Correlation Coefficients (ICC, two way mixed effects model, absolute agreement). The three observers reached on average, moderate levels of agreement when assessing the Alpha zone (mean ICC = 0. 60; range = 0.52 - 0.66; two way mixed effects model, absolute agreement) and the Beta zone (mean ICC = 0. 61; range = 0.50 - 0.70; two way mixed effects model, absolute agreement).

6.11.4 Distribution of PPA

The distribution of PPA areas was investigated over 72 sectors around the optic disc, subtending 5 Degrees each. The measurements by each of the three observers for the normal and glaucoma group are graphically presented on radar charts (Figures 6.3 - 6.6).

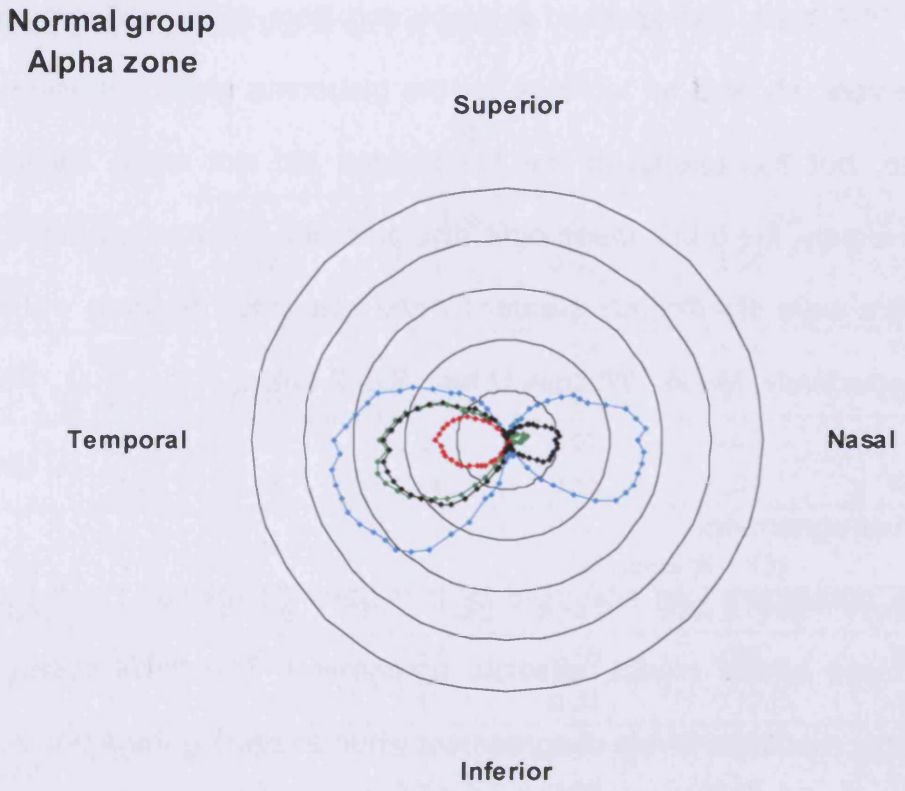

Figure 6.3. *Graphical illustration of the distribution of the normal mean group sum of PPA area (mm2), zone alpha, as defined by the three observers (OB1: green outline; OB2: blue outline; OB3: red outline) and also, averaged across the three observers (Mean OB: black outline). The radar chart is plotted in steps of 0.005mm^2.*

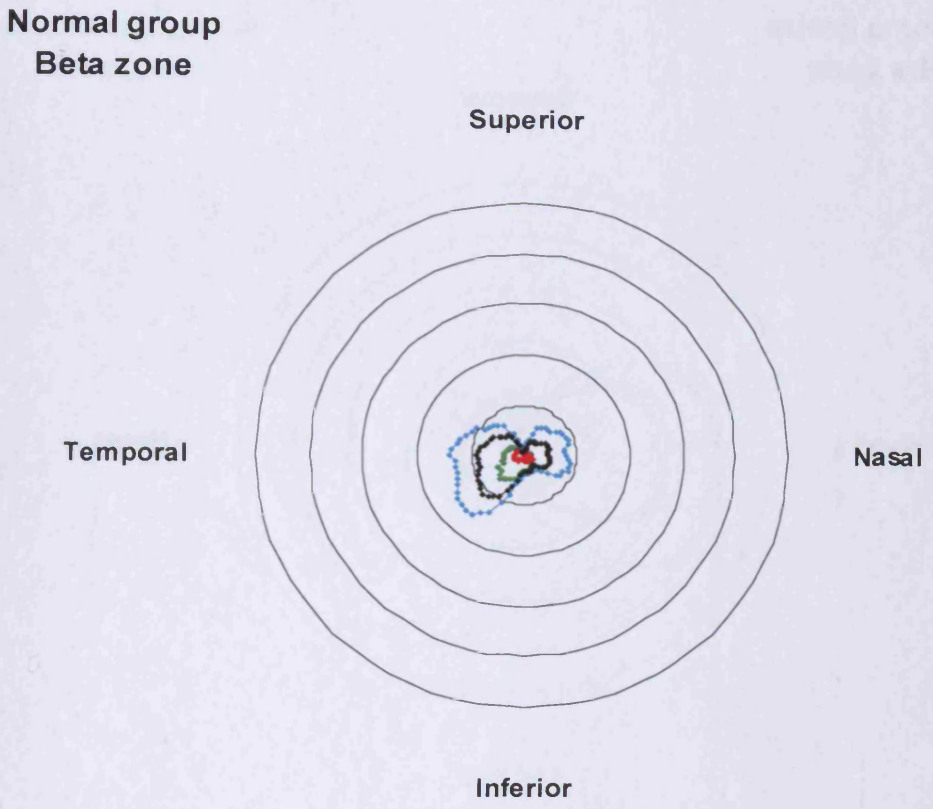

Figure 6.4 *Graphical illustration of the distribution of the normal mean group sum of PPA area (mm^2), zone alpha, as defined by the three observers (OB1: green outline; OB2: blue outline; OB3: red outline) and also, averaged across the three observers (Mean OB: black outline). The radar chart is plotted in steps of 0.005mm^2.*

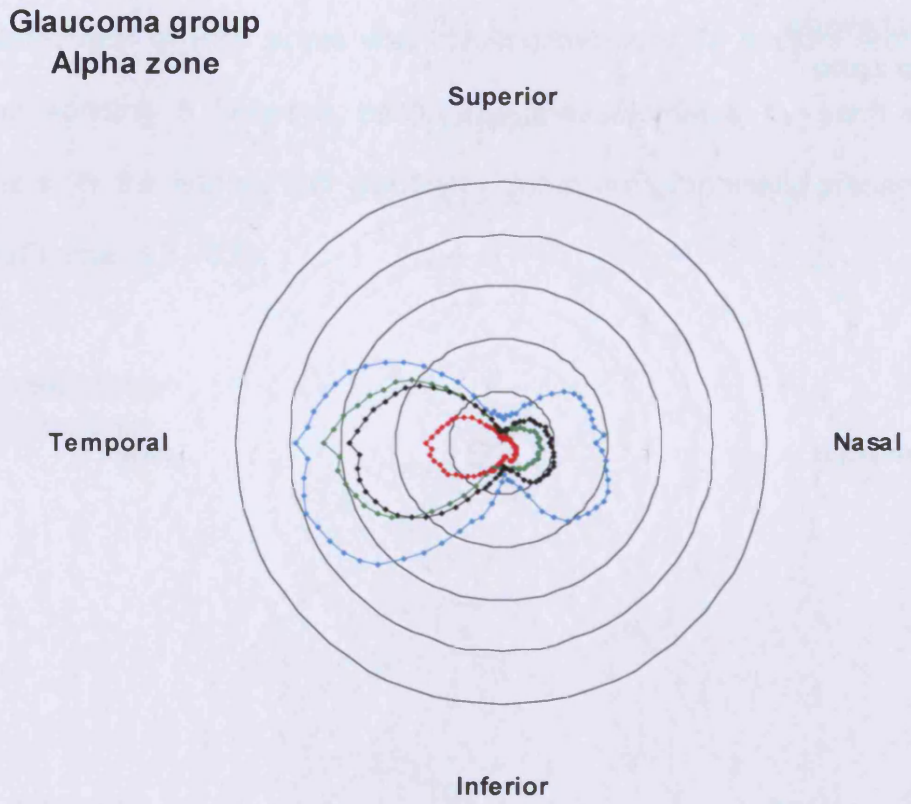

Figure 6.5 *Graphical illustration of the distribution of the glaucoma mean group sum of PPA area (mm^2), zone alpha, as defined by the three observers (OB1: green outline; OB2: blue outline; OB3: red outline) and also, averaged across the three observers (Mean OB: black outline). The radar chart is plotted in steps of 0.005mm^2.*

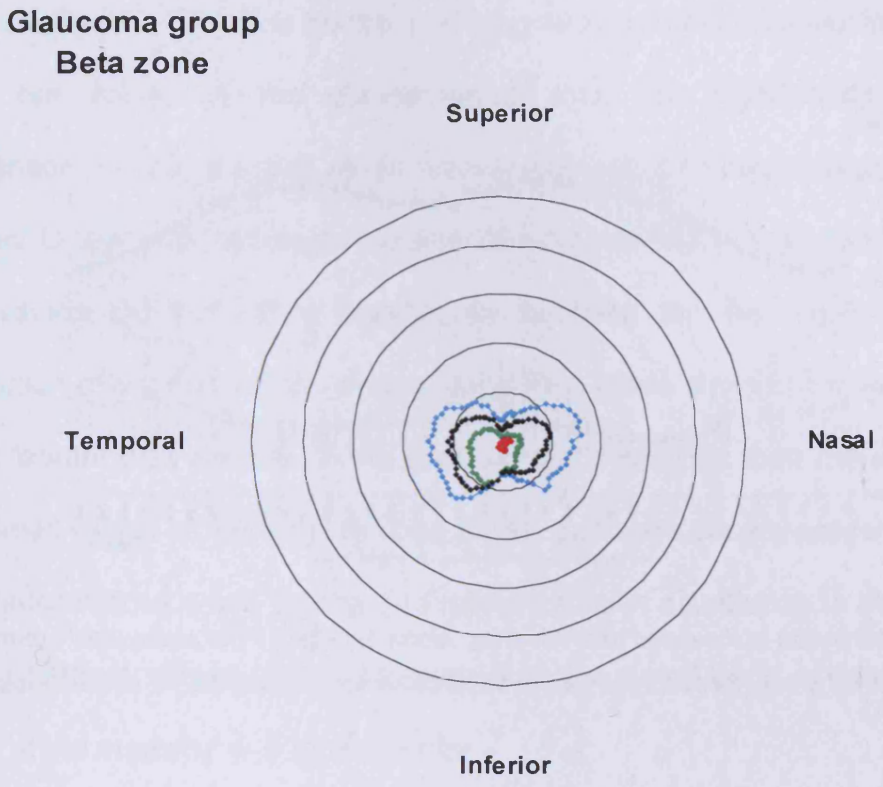

Figure 6.6 *Graphical illustration of the distribution of the glaucoma mean group sum of PPA area (mm^2), zone Beta, as defined by the three observers (OB1: green outline; OB 2: blue outline; OB3: red outline) and also, averaged across the three observers (Mean OB: black outline). The radar chart is plotted in steps of 0.005mm^2.*

6.11.5 Correlations of PPA with the rim areas

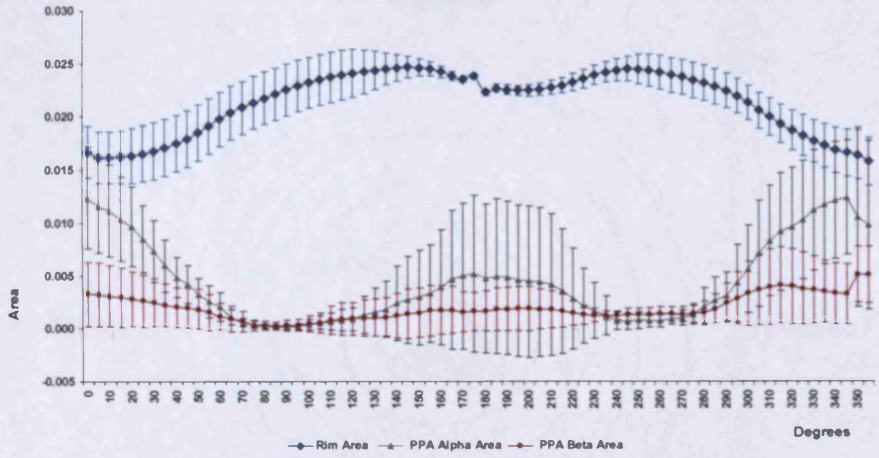

Figure 6.7 *The distribution of the mean total rim area; Alpha and Beta PPA areas (mm^2) (error bars: ± 1SD), for the normal group, as averaged for the three observers across the 72 sectors around the ONH.*

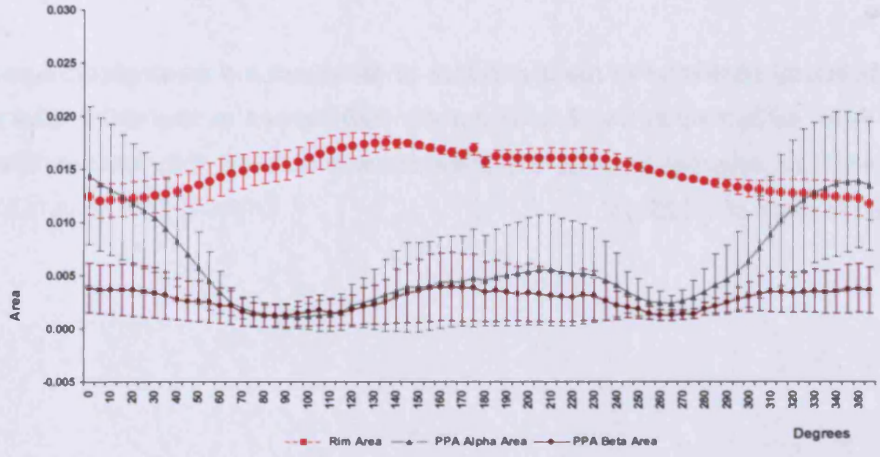

Figure 6.8 *The distribution of the mean total rim area; Alpha and Beta PPA areas (mm^2) (error bars: ± 1SD), for the glaucoma group, as averaged for the three observers across the 72 sectors around the ONH.*

From the sectorial distribution of the rim and PPA areas it appears that there is a correspondence of the alpha zone expansion within the sectors where the normal

rim band is most narrow (figure 6.7) and the glaucomatous damage has mostly occurred (figure 6.8) in the normal and glaucomatous eyes, respectively. The group mean rim values of the glaucomatous eyes are significantly decreased in comparison to the normal mean values, across all sectors ($p = 0.000$; Mann Whitney U test) and although the interobserver variability was high and the mean PPA values did not differ significantly between the two groups the sectorial distribution revealed that the mean Alpha PPA areas showed higher peaks across the horizontal disc sectors of the average glaucoma eye than the average normal eye. Small values of mean Beta zone areas, that were equally present in the normal and glaucomatous eyes, seemed to follow a similar distribution to the Alpha zones, namely highest values at the temporal and the nasal parts of the optic disc and lowest at the superior and inferior poles.

Simple linear regression using the rim area as independent variables and zonal PPA as the dependent variable across the normal eyes resulted in the equation *Alpha = 0.002; Rim area + 0.315*; with $R^2 = 0.000$ ($p = 0.989$). When the disc area was investigated as the only independent the regression equation was *Alpha= 0.013 Disc area + 0.288*; $R^2 = 0.001$ ($p = 0.870$). Beta zone showed a negative correlation with the disc area ($R^2 = 0.002$; $p = 0.765$; *Beta = -0.018 Disc area + 0.172*) and a stronger negative correlation with the rim area ($R^2 = 0.035$; $p = 0.189$; *Beta = -0.112 Rim area + 0.304)* across the normal group. It is noted that none of the correlations reached a significant level.

For the glaucoma group, simple linear regression showed that Alpha was positively correlated with the Disc area ($R^2 = 0.000$; $p = 0.088$; *Alpha = 0.015 Disc area+*

0.394) and the rim area (R^2 = 0.032; p = 0.207; *Alpha = 0.209 Rim area + 0.194*) but Beta zone showed negative correlation for both the rim area (R^2 = 0.066; p = 0.070; *Beta = -0.190 Rim area + 0.370)* and the disc area (R^2 = 0.000; p = 0.933; *Beta = - 0.005 Disc area + 0.169*). As for the normal group, none of the correlations between PPA and the intrapapillary areas reached a significant level across the glaucoma group.

The combination of the Rim area and Disc area as independent variables improved the predictive power of the regression analysis. Simultaneous multiple regression of the normal group mean Alpha zone area upon the group mean disc area and the group mean rim resulted in the equation: *MeanAlpha Area = 0.028 x MeanDiscArea - 0.029 x MeanRimArea + 0.299*, that had a low predictive power with a value of R^2 = 0.001. For the same group, the simultaneous multiple regression of the group mean Beta zone area upon the group mean disc area and the group mean rim resulted in the equation: *MeanBetaArea = 0.094 x MeanDiscAre a- 0.211 x MeanRimArea + 0.25,* that also had a low predictive power with a value of R^2=0.056. For the glaucoma group the simultaneous multiple regression the group mean Alpha zone area and Beta zone area upon the group mean disc area and the group mean rim showed a predictive power, R^2 = 0.041 (*MeanAlphaArea = -0.078 x MeanDiscArea- 0.284 x MeanRimArea + 0.297) and* R^2=0.09 (*MeanBetaArea = 0.082 x MeanDiscArea- 0.269 x MeanRimArea + 0.281*), respectively.

When the disc shape parameters were investigated as independent variables in the simultaneous multivariate analysis with PPA areas no improvement of the predictive power of the regression equation was achieved.

6.11.6 Association of PPA with the visual field indices

The sum of zonal PPA areas averaged for the three observers and normalised by the corresponding total disc area within each eye was plotted against the MD and PSD visual field indices across the normal group as presented in figures 6.9- 6.12. The mean normal group MD and PSD values were 0.06 (±1.40) and 1.88 (±1.09), respectively.

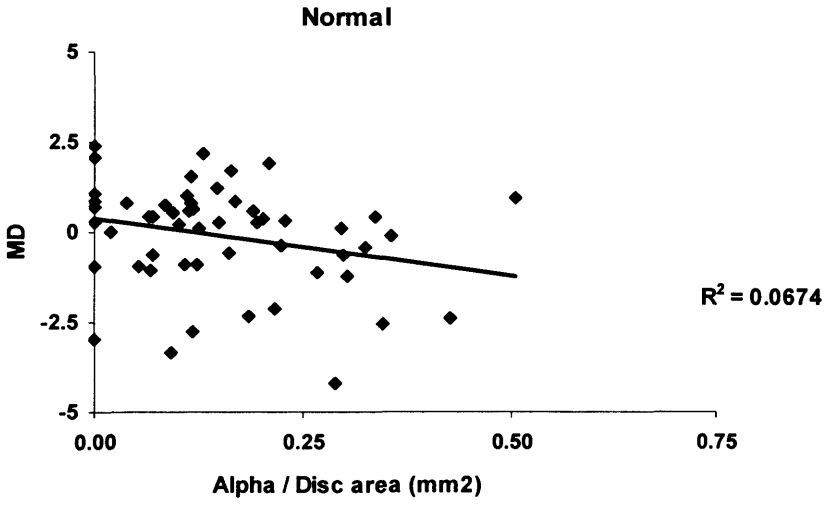

Figure 6.9. *Scatterplot of the total Alpha zone PPA area (mm^2) normalised for the global disc area (mm^2) within each eye and averaged across the three observers, against the MD indices across the normal group (p = 0.196); Predicted MD = -2.039 Alpha / Disc Area +0.260.*

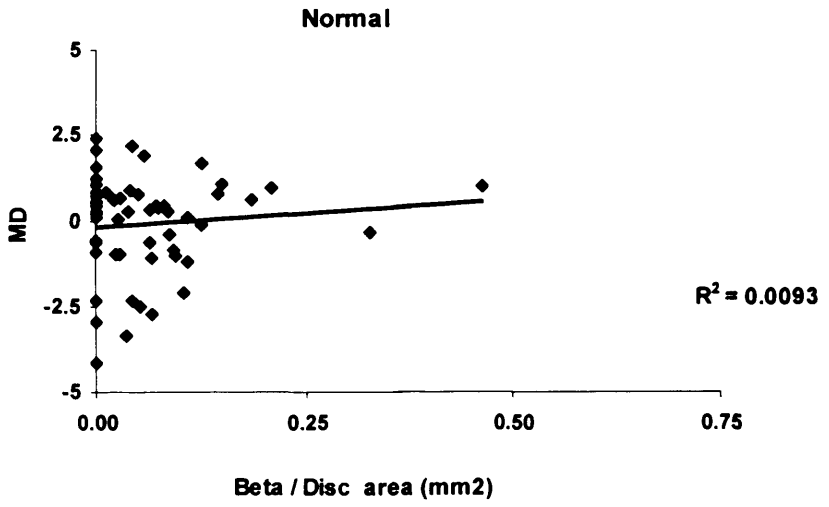

Figure 6.10. *Scatterplot of total Beta zone PPA area (mm^2) normalised for the global disc area (mm^2) within each eye and averaged across the three observers , plotted against the MD indices across the normal group (p = 0.382); Predicted PSD =2.009 Beta / Disc Area= -0.187.*

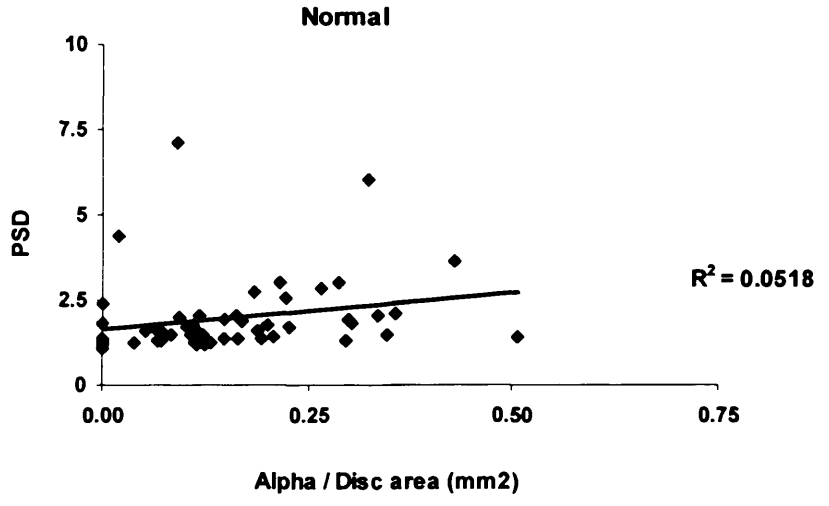

Figure 6.11. *Scatterplot of total Alpha zone PPA area (mm^2) normalised for the global disc area (mm^2) within each eye and averaged across the three observers, against the PSD indices across the normal group. (p=0.097); Predicted PSD =2.042 Alpha /Disc Area = +1.560.*

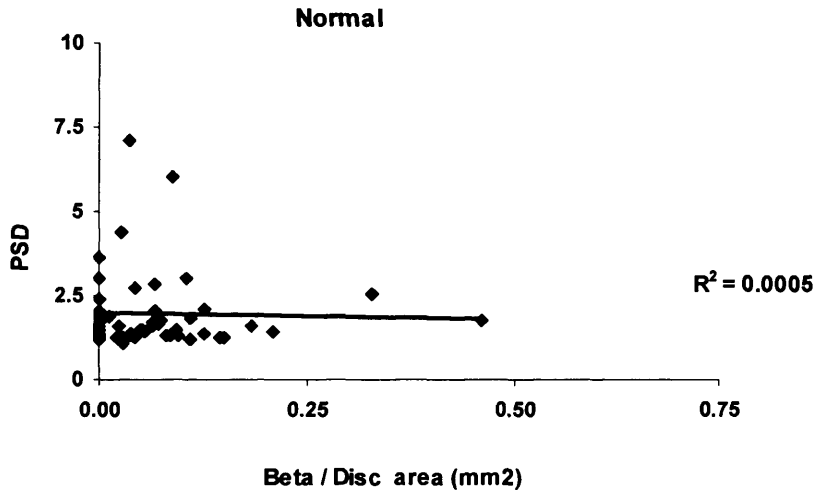

Figure 6.12. *Scatterplot of the total Beta zone PPA area (mm^2) normalised for the global disc area (mm^2) within each eye and averaged across the three observers, against the PSD indices across the normal group (p=0.989) Predicted PSD = 0.024 Beta / Disc Area = +1.879.*

Both types of PPA didn't show strong correlations with the MD indices across the normal group. The correlation coefficients were $R^2 = 0.034$ for the normalised Alpha zone and $R^2 = 0.016$ for the normalised Beta zone, but both correlations did not reach significance. The normalised Alpha zone was also not a good predictor for the PSD values across the normal group ($R^2 = 0.055$; $p = 0.097$) and this was similar for Beta zone ($R^2 = 0.000$; $p = 0.989$).

Scatterplots of the sum of zonal PPA areas normalised by the total disc area within each glaucomatous eye against the corresponding MD and PSD visual field indices are presented in figures 6.13 - 6.16. The mean glaucoma group MD (4.35 ±5.46) and PSD (4.93 ±3.73) values were significantly different from the mean group normal values ($p = 0.000$; Mann-Whitney U test).

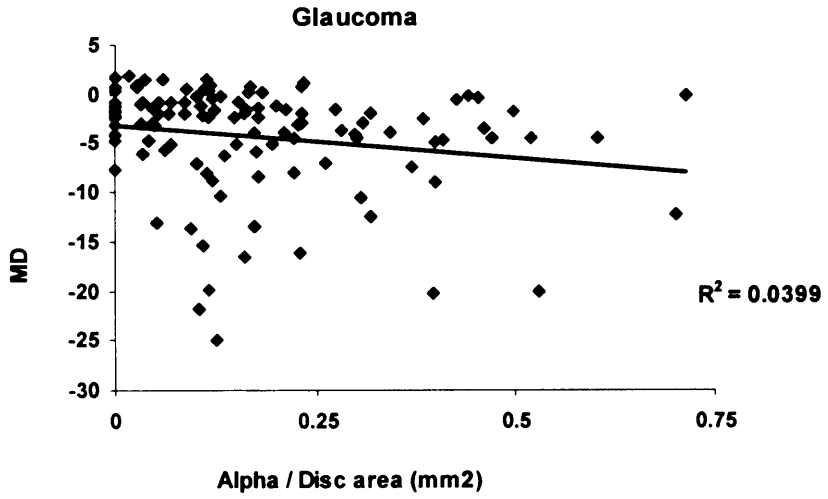

Figure 6.13. *Scatterplot of the total Alpha zone PPA area (mm^2) normalised for the global disc area (mm^2) within each eye and averaged across the three observers, against the MD indices across the glaucoma group. Predicted (MD) = -3.168 x (Alpha/ Disc area) -6.513; p-value = 0.044.*

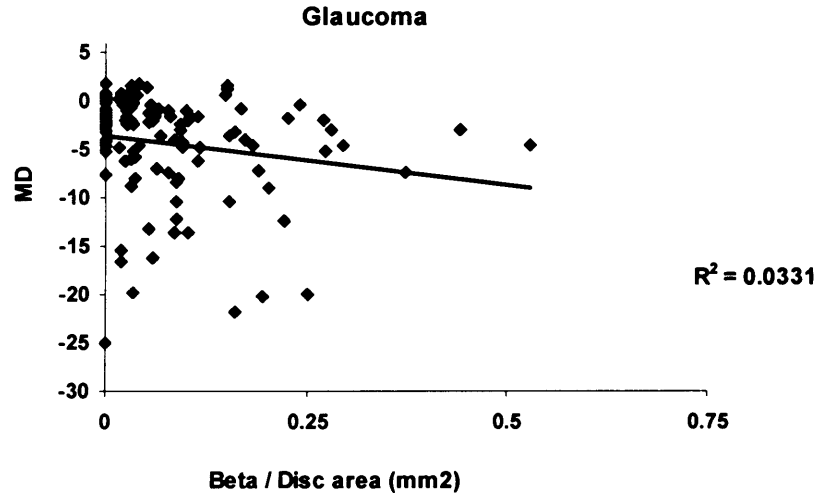

Figure 6.14. *Scatterplot of the total Beta zone PPA area (mm^2) normalised for the global disc area (mm^2) within each eye and averaged across the three observers, against the MD indices across the glaucoma group. Predicted (MD) = -10.059 x (Beta / Disc area) -3.539; p-value =0.059.*

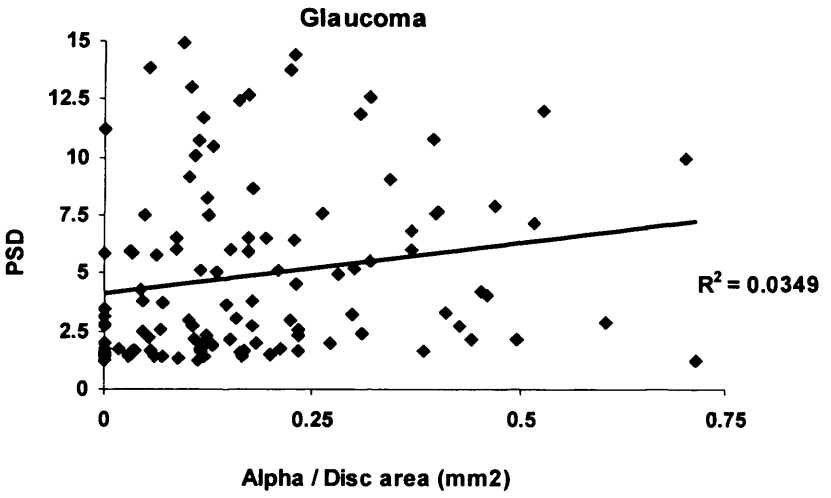

Figure 6.15. *Scatterplot of the total Alpha zone PPA area (mm^2) normalised for the global disc area (mm^2) within each eye and averaged across the three observers, against the PSD indices across the glaucoma group. Predicted (PSD) = 4.183 x (Alpha / Disc area) +4.188; p-value =0.061.*

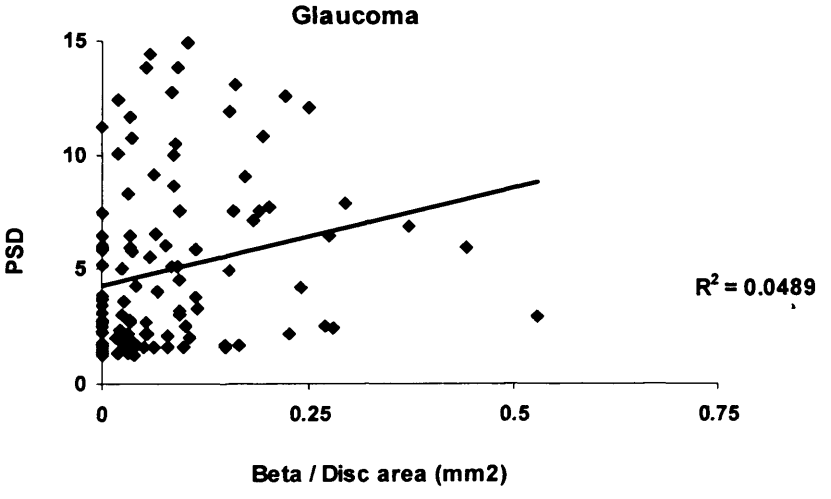

Figure 6.16. *Scatterplot of the total Beta zone PPA area (mm^2) normalised for the global disc area (mm^2) within each eye and averaged across the three observers, against the PSD indices across the glaucoma group. Predicted (PSD) = 8.385 x (Beta / Disc area) +4.261; p-value =0.021.*

Normalised PPA areas were negatively correlated to the MD indices across the glaucoma group. The correlation coefficients were R^2 = 0.036 (p-value = 0.044) for the Alpha / Disc area and R^2 = 0.032 (p-value = 0.059) for the Beta / Disc area

reaching a significance level at 0.05 level only for the Alpha zone. PSD did not prove to be a strong predictor for the normalised Alpha zone (R^2 = 0.031; p-value = 0.061) but the correlation did reach a significant level for the normalised Beta zone with a correlation coefficient R^2 = 0.047 (p-value = 0.021).

6.12 Discussion

6.12.1 PPA quantification and distribution

The computerized imaging technique presented in this study produced a detailed account of the presence of PPA across the investigated glaucoma and normal eyes. The frequency of both zones of atrophy was greater for the glaucoma group, in agreement with most previous observations (Jonas *et al*, 1992a; Jonas *et al*, 1999a; Jonas & Budde, 2000; Uhm *et al*, 1998). Also, the results obtained in this study reveal an increase of PPA in glaucoma, although the difference in the PPA zones between the normal and glaucoma eyes did not reach statistical significance. It is noted that the study utilised the same definition for the alpha and beta zones of PPA as previous studies (Jonas *et al*, 1989a; Tezel *et al*, 1997a; Tezel *et al*, 1997b; Uchida *et al*, 1999). However the sample selection included patients with different subgroups of glaucoma pathology, mainly high tension glaucoma. That could probably explain the smaller amounts of PPA. It has been speculated that PPA might be associated with a more chronic course of damage, whereas, glaucoma associated with high pressures has a more rapid development (Jonas *et al*, 1992a).

Also, the sample selection might account for the small values of PPA. The present study included myopic eyes <5Dpt and the two study groups did not differ significantly in their refractive error. PPA areas are associated with the refractive

error and previous studies on the quantification of PPA had evaluated glaucomatous and normal eyes with myopia up to 8 Dpt (Jonas *et al*, 1988b).

The observed distribution patterns for the two zones of PPA across the two groups did comply with the ones previously reported (Jonas *et al*, 1988b; Jonas & Hayreh, 2000; Park *et al*, 1996b) This was also evident for Beta zone that although very small, differentiated between the two groups as it expanded at the nasal side of the optic disc for the glaucoma group and had a tendency to expand rather concentrically around the glaucomatous disc (Jonas *et al*, 1999a; Uhm *et al*, 1998).

6.12.2 Association of PPA with the disc area

Both zones showed an association with the disc size as revealed by the multivariate analysis. The correlation of disc size and PPA is commonly observed and has encouraged the use of the normalised values for PPA (Tezel et al, 1997b; Uchida et al, 1999). Surprisingly, the values of PPA did not show significant differences between the groups, although the stereoscopically derived mean disc area, averaged across the three observers, did have a significant difference between normal and glaucomatous eyes.

The inclusion of tilted discs in the study group would cause a variation in the optic disc size, increasing the difficulty to evaluate even the rim boundaries especially at the temporal ONH sector. Chihara (1994) suggested that index of ovalness correlated with small disc size (Chihara & Chihara, 1994). However the authors defined this parameter as the gradient of the largest over the smallest disc diameter. Conversely Tay (2005) correlated optic disc tilt with myopic eyes and

larger axial length (Tay *et al*, 2005). Regardless of the definition of the index of tilt, the results of the present study did not reveal an association with disc size. This is likely to be associated with the sample selection that did not include myopic or larger than average discs for both groups. This finding also suggests that an association of PPA with disc tilt would also become apparent for larger optic discs.

6.12.3 Association of PPA with the rim area

The spatial association of PPA with rim thinning within the glaucoma group has been a consistent finding across the three observers and is in agreement with other reports (Jonas *et al*, 1988b; Jonas *et al*, 1993; Jonas & Grundler, 1997b; Jonas *et al*, 1999a). However, the two zones showed weak correlations with the rim values, an effect that is definitely influenced by the small values of PPA. The present analysis also identified that the spatial expansion of PPA was generally associated with the thinnest rim areas across the glaucomatous group, however it is important to consider that the study group included moderate and advanced cases of glaucomatous damage so the rim area was overall decreased for the glaucoma eyes compared to the normal.

6.12.4 Association of PPA with the visual field loss

The MD value is the mean of the arithmetic differences between the measured sensitivity and the age-matched expected normal value at each location. Thus, it summarises the deviations of height for the examined eye (Heijl, Lindgren *et al*, 1987a) and consequently, with increased visual field loss the corresponding MD values become increasingly negative. Not surprisingly, when the correlation of PPA with functional damage was investigated across the glaucoma group the MD values

were found to be negatively associated with the alpha areas at a significant level. The correlation with the beta zone did not reach a significant level but this is likely to be attributed to a preferential classification of the areas of atrophy as Alpha rather than Beta zone, thus the average quantity of Beta areas remained very low.

Unlike the MD values the PSD values were significantly positively correlated with the extent of Beta zone across the glaucoma group. The PSD indices are the summary of the shape of the visual field and increase with increase in disparity of shape between the measured field and that of the normal reference field (Heijl *et al*, 1987a). It is noted that the formula calculating the PSD values includes the corresponding MD values so, when the PSD values tend to be zero the shape of the measured field matches that of the reference field regardless of the reduction of the visual field height. This finding is in agreement with the description of beta zone as a more severe type of atrophy, associated with more advanced glaucomatous damage (Jonas *et al*, 1988b; Jonas & Grundler, 1997b; Jonas *et al*, 1999a).

6.12.5 Interobserver agreement in the assessment of PPA

Moderate agreement was achieved in assessing PPA by glaucoma clinicians. This complies with other reports demonstrating the difficulty in the assessment of PPA. However, the agreement between observers was at similar levels with reference to the zonal classification of the PPA. The comparison between studies using Kappa statistics is meaningless as this parameter is highly dependent on the investigated samples. However, previous reports for multiple assessments of PPA revealed more reproducible Beta zone compared to Alpha zone areas (Harper *et al*, 2000b; Tezel *et al*, 1997a; Tuulonen *et al*, 1996). Also, clinical experience was shown to

influence the agreement between observers (Harper *et al*, 2000b). It is speculated that the observers in the present study became more familiar with the characteristic features of PPA through the initial training session. Also it is noted that all three observers had similar levels of experience with glaucomatous eyes.

6.12.6 Possible limitations

The results of the study could only compare with other studies that have used computer based analysis because of the magnification factors influencing the measurements. Comparisons of the present study with other studies that have used the Atrophy Analysis Software (Park *et al*, 1996b; Park *et al*, 2001) would also not provide meaningful conclusions. Unlike HRT, the present system for planimetry incorporates a segmentation of the disc with reference to the cup centre and the peripapillary measurements do not include the structure of the scleral ring.

The two study groups were not age-matched and the mean age of glaucoma patients was significantly higher than the mean age of normal subject. Since PPA is known to increase with age in normal subjects (Curcio *et al*, 2000) this could be important for the identification of glaucomatous PPA from the normal age-related increase of PPA. However the results of this study showed no significant differences between the zones for the two groups.

The PPA area could not be associated with the IOP levels because these data were not available. However all glaucoma patients were receiving IOP lowering treatment and all normal subjects had repeated readings of IOP within normal limits. Moreover, it is speculated from the literature that at a given time the association of

PPA area with IOP would be equally weak as it has been observed for the progressive stages of the disease (Tezel *et al*, 1997b).

The PPA area could not be associated with the axial length of the eyes (Kubota *et al*, 1993). Unfortunately, biometric information was not available for the study so this association was not confirmed. However, the groups did not include highly myopic eyes (the exclusion criteria were eyes >5Dpt). Therefore, it can be assumed that the range of the axial length values within the study groups must have been small for both groups.

Whilst investigating the association of PPA with the functional loss it is important to consider that using the MD or PSD indices does not give us information about the spatial correlation of PPA areas with the defected areas of the visual field. Such analysis has been previously performed based on subjective evaluation of the perimetry results in correlation with retinal nerve fibre layer defects (Hall *et al*, 2001; Uchida *et al*, 1999).

The use of only three observers could be a limiting factor for the reliability of our conclusions. It is noted that the planimetric evaluation performed in previous studies were performed by one or two observers only (Jonas & Naumann, 1988; Park *et al*, 1996b). However, increasing the number of observers would have increased the power of the statistical analysis and possibly minimize the differences between observers in their quantification of the PPA areas.

The training of the observers was not focused on PPA, aiming to avoid bias within the observers for the planimetry assessment of PPA and also for the subjective diagnosis of glaucoma. However, a more intensive training of the observers on the appearances of PPA could have improved the levels of interobserver agreement.

Furthermore, it is inferred that PPA is associated with glaucomatous damage so masking the ONH features while assessing the peripapillary retina could have limited the diagnostic bias. However one of the aims of the study was to maintain similarities with the clinical setting. Thus, the observation of the PPA areas was concurrent with the examination of the ONH.

6.13 Conclusions

The assessment of the ONH stereophotographs with computer assisted planimetry provided an accurate description of the presence, the extent and severity of PPA across samples of normal and glaucomatous population. The sample selection might have accounted for the small values of PPA (myopic eyes >5 were excluded) but the observed distribution patterns did comply with the ones previously reported.

Moderate agreement was achieved in assessing PPA by glaucoma clinicians, in both normal and glaucomatous eyes. The considerable examination differences between expert observers suggest that the clinical definition of the zonal PPA is too broad, limiting the value of PPA for the clinical diagnosis of early glaucomatous damage. Our results suggest that the degree of PPA (both α and β) are related to optic disc size and that rim area may influence the link between the extent of PPA β and the development of glaucomatous optic neuropathy.

Chapter 7 Quantitative analysis of the neuroretinal rim for the discrimination of normal and glaucomatous discs

7.1 Introduction

7.1.1 The neuroretinal rim area

The rim is the cross sectional part of the disc area occupied by the nerve fibres. The boundaries of the rim coincide with the outer margins of the disc area and the outer margins of the cup when the cup borders are defined as the point where the nerve fibres first deviate towards the lamina. One would logically describe the structure of the rim as the equivalent of the nerve fibres volume from the retina. However, there are many controversies as to the extent that smaller discs and rims include less nerve fibres (Funaki *et al*, 1998; Jonas *et al*, 1992b; Mikelberg *et al*, 1989; Quigley *et al*, 1991b).

It is a consistent finding that the neuro-retinal rim correlates with the size of the disc area and as a general observation, larger discs include bigger rims, while small discs are presented with thinner rims (Jonas *et al*, 1988d; Jonas *et al*, 1992b). The inter-individual variability in the disc area would be also influencing the size of the neuro-retinal rim. Such differences in the disc area are largely associated with other anatomical features like the size of the scleral canal (Jonas *et al*, 1988a) and the axial length of the eye (Rudnicka *et al*, 2001). Also variability in the disc size is known to exist with reference to gender (Ramrattan *et al*, 1999) and race (Varma *et al*, 1994; Zangwill *et al*, 2004a).

Variations of the rim size among normal eyes can be primarily attributed to random differences in the number of the fibres included in each eye. It is known that the mature retina includes only the ganglion cells that are successfully connected with target cells in the brain while those ganglion cells that fail to do so, are known to degenerate by apoptosis during development (Provis *et al*, 1985). It can be speculated that the different diameters of the remaining active retinal ganglion cell axons, after this process of clearance of the excess and not functional ganglion cells, in combination with the distinct variation in fibres size depending on their origin from the periphery or the most central retinal locations, (represented at the rim with the so-called retinotopical arrangement), may further determine both the size, as well as, the composition of the rim.

The density and configuration of the rim are also likely to be influenced by the architecture of the lamina cribrosa and the size of the pores within which the fibres are arranged. The anatomical features of the optic nerve head structure may determine the route of the fibres within the disc area before they dive into the cup, thereby influencing the rim. It is proposed that the laminar pores are formed before the cup; thus the cup is actually formed resulting from the fibres that never reach the optic nerve head and the regression of the hyaloid artery.

Similarly, it can be inferred that factors able to modulate the proportion of the non-neural part of the rim may also alter its size. Glial cells are normally attached to the fibres and the rich capillary network at the ONH area and are an important component of the rim. Histological and planimetric analysis of non-glaucomatous eyes with total loss of axons beyond the optic nerve head suggested that less than

half of the rim area is occupied by nerve fibres (Drance & King, 1992).Thus variability in the glial cells included in the rim may pose a considerable variability in the volume and most likely, the overall size of the rim. Moreover, the glia have the unique ability to relocate and even aggregate once stimulated, so they could even account for the plasticity of the rim as commonly observed under transient conditions of IOP elevation (Azuara-Blanco *et al*, 1998). However, the influence of other, not yet investigated factors could not be excluded when considering the normal size variability of the rim area.

7.1.2 The ISNT rule

The physiologic shape of the rim is strongly associated with the distribution of all other features of the retina, besides the disc area. Firstly, the retinal location of the foveola, which lies temporally and slightly inferiorly to the ONH, is thought to play a major determinant role in the distribution of the retinal nerve fibres. As the next important factor, the retinotopical arrangement of the fibres needs to be considered, resulting in fibres with the smallest calliper reaching predominantly the temporal part of the disc. Not surprisingly, the configuration of the rim is in coordination with the diameter of the retinal arterioles that are observed to be wider in the inferior temporal than in the superior temporal region of the ONH and the overall visibility of the RNF bundles is better at the inferior than the superior sectors of the rim (Jonas & Schiro, 1993). Furthermore, within the disc, the wider pores of the lamina cribrosa are observed in the inferior and the superior poles (Jonas *et al*, 1988d).

The shape of the rim is predominantly formed by the vertically oval disc and the horizontal oval shape of the cup. As explained by Jonas and colleagues (1988;

1998), in horizontally oval discs the retinal nerve fibre bundles have a longer part of the disc circumference to enter, than in vertically oval discs (Jonas *et al*, 1988c; Jonas *et al*, 1998a). Consequently, the retinal nerve fibres are more crowded in vertically oval discs and this leads to relatively wider rim areas inferiorly and superiorly (Jonas *et al*, 1998a).

The neuroretinal rim configuration in normal eyes is usually clinically described with the "ISNT rule". This rule summarises the observations by morphometric analysis of optic discs across a healthy Caucasian population and is named after the four main sectors of the disc, forming an acronym that denotes the sequence of the broadest parts of the rim width in normal eyes (Jonas *et al*, 1988c). Thus, according to the ISNT rule the width of the rim band is broadest inferiorly, followed by the superior part, the nasal and finally the temporal part. The above characteristic rim configuration as well as the associations of this configuration with the other features of the disc was also identified in healthy monkey eyes that were morphometrically analysed (Jonas & Hayreh, 2000).

7.1.3 Glaucomatous rim loss

The accelerated glaucomatous ganglion cell loss manifests at the ONH with representative changes of the rim volume and configuration. Airaksinen and colleagues (1992) estimated that the annual loss of rim area in deteriorating glaucomatous eyes was 3.47%, as opposed to normal eyes that demonstrated a rate of age related decrease that involved approximately 0.23% of their initial rim area and reported that the slope of the decreasing rim area was significant in 57% of the OHT patients and 79% of the glaucoma patients in their cohorts (Airaksinen,

Tuulomen *et al*, 1992). In early stages of the disease VFT recording is insensitive so, although changes of the ONH and the rim are present, they might not be distinguishable before almost a 30% of axons are effected (Quigley *et al*, 1982). Early glaucomatous damage has been associated with either diffuse or focal rim loss (Jonas *et al*, 1993). The patterns of rim loss, diffuse or localised are highly variable depending on the stage of the disease (Jonas *et al*, 1999b). In eyes with established damage the rim changes correlate strongly with the visual field defects (Emdadi *et al*, 1998). At all times, the rim changes show strong spatial correlation with all the other structural changes that can be observed at the ONH region, including the peripapillary retina (Jonas & Naumann, 1988; Jonas *et al*, 1999b). Moreover, the rim area can be different between subgroups of glaucomatous pathophysiology (Broadway *et al*, 1999). Also, contrary to glaucomatous damage, non-glaucomatous neuropathy is mostly not associated with rim loss (Jonas & Budde, 2000).

7.1.4 The neuroretinal rim measurement in glaucoma diagnosis.

Quantification of the rim area is a useful indicator of the presence of glaucoma (Garway-Heath & Hitchings, 1998). Discriminant functions incorporated in automated imaging techniques evaluate topographic rim measurements derived from healthy eyes and produce promising results for glaucoma detection (Mardin *et al*, 1999; Wollstein *et al*, 2000a; Wollstein *et al*, 2000b). The total rim area as evaluated by HRT was shown to assist the discrimination of NTG and OAG eyes and identify OHT eyes (Kiriyama, Ando *et al*, 2003)

Moreover, the prediction intervals of the regression line describing the relation between the rim and optic disc areas can determine the normal range of rim size in a given healthy population (Caprioli *et al*, 1987), although the correlation between the rim and disc size allows an overlap of rim size between normal and glaucomatous groups, especially in early glaucomatous stages (Caprioli, 1992; O'Connor *et al*, 1993). The HRT incorporates a quantitative analysis (Moorfields Regression analysis) based on the global and regional rim values. The diagnostic value of the rim measurements has been reported to be high for global and even more, for regional estimates of the rim size. The segmental analysis of the rim seems superior to the summary measurements, as it allows the focal type of rim damage to be investigated. Such damage is usually observed close to the poles of the optic disc and is likely to be identified by the visual field testing (Garway-Heath & Hitchings, 1998). The Moorfields analysis incorporated in the HRT, allows an automated image analysis and diagnostic evaluation by correlation of the obtained rim values with the disc area measurements across eight sectors of the optic disc and performing regression analysis based on a set database of healthy ONHs (Mikelberg, 1993). The automated diagnosis that becomes available with this analysis is based on the classification of the sectorial rim areas in comparison to the normative values of the database.

The HRT automated disc analysis and statistical evaluation of the results highlight the deviation of the neuroretinal rim areas from the normative database and may assist clinical judgments. The HRT has a reported diagnostic precision that was found to compare favourably with the subjective glaucoma diagnosis by expert observers. However, several factors limit the accurate definition of the rim area with

this method. It is a known problem that the HRT is using an arbitrary set reference plane for the determination of the rim, with the boundaries of the cup subjected to the fluctuating IOP levels and other active forces of disc compliance (Tan *et al*, 2004). Also the interference of the vessels' volume increases the difficulty in measuring the rim, especially in the nasal aspect of the disc (Jonas *et al*, 1998c). Moreover, the disc margins can be difficult to discern on the HRT reflectance images for optic discs with Beta peripapillary atrophy adjacent to the scleral canal (Kono *et al*, 1999b).

While quantitative analysis of the ONH topography may increase the diagnostic precision of imaging techniques, subjective evaluation of stereophotographs remains a highly sensitive method for the diagnosis of early glaucoma (Greaney *et al*, 2002). In clinical practice, subjective glaucoma diagnosis may rely on the subjective evaluation of the rim configuration. The ISNT rule has been used by clinicians as a determinant of normality.

Based on a study of a Caucasian population by Jonas and colleagues (1988) suggested that the neuroretinal rim was usually broadest in the inferior disc region, followed by the superior; the nasal and finally the temporal disc area, thus complying with the ISNT rule (Jonas *et al*, 1988b). It is noted that the rule was established with morphometric analysis of stereophotographic transparencies that involved the photos being projected with magnification up to 20x and the disc and cup being outlined manually and measured on paper. The obtained measurements were subsequently corrected for the various factors of magnification using Littman's formula. Also, in order to compare various optic disc regions with each other, the

disc was divided into four sectors, the temporal superior sector; the temporal inferior; the temporal horizontal and the nasal sector. These sectors subtended 90, 90, 60 and 120 degrees, respectively, while the temporal superior sector and the temporal inferior were tilted by 15 degrees towards the temporal side of the vertical optic disc axis (Jonas *et al*, 1988b).

A study with a similar design and methods also identified the ISNT rule in a smaller cohort of healthy eyes while using 10 degree sectors segmentation of the disc (Budde *et al*, 2000). However, the Vellore Eye Study (2003), having the experimental design and methodology of the 1988 population study by the same research group, showed that the neuroretinal rim across a random Indian population sample had a characteristic configuration but granted a broader definition of the ISNT rule. In this population, no significant differences were identified for the rim width between the inferior, superior and nasal disc sectors, apart from the smallest rim band that was clearly observed at the temporal horizontal optic disc sector within each eye (Jonas, Thomas *et al*, 2003). The physiological rim configuration denoted by ISNT is based on the vertically oval shape of the optic disc and the horizontally oval shape of the optic cup. However, the rule was only partly fulfilled in the Indian population, although the morphometric analysis confirmed that in those eyes the mean vertical disc diameter was 6% longer than the horizontal one (Jonas *et al*, 2003).

Several studies have explored the application of the ISNT rule or similar parameters describing the normal rim shape for the clinical glaucoma diagnosis. The neuroretinal rim configuration was identified as an important feature assisting the

diagnosis of early glaucomatous optic nerve damage in progressed ocular hypertensive eyes, before they exhibit development of visual field defects with W-W perimetry (Jonas & Konigsreuther, 1994). Moreover, as a result of the ISNT normal rim configuration in combination with the patterns of preferential rim loss at the poles of the optic disc occurring in early glaucomatous damage the ratio of the I/T and S/T rim width was found statistically significantly greater in normal eyes than ocular hypertensive. However, the diagnostic power of the rim width comparisons only reached 58.5% (Jonas *et al*, 1998c). Quantitative evaluation of the ISNT rule by imaging techniques like the HRT and OCT suggested that the rule was applicable in 17% of a small cohort of healthy multiethnic eyes, although subjective assessment based on stereophotographs concluded that the rim configuration of 79% of normal eyes and 28% of glaucomatous complied with the condition I≥S≥N≥T (Harizman, Chiang *et al*, 2005). This study highlighted the extended empirical application of the ISNT rule while quantitative analysis of the rim shape and size with modern imaging techniques does not always verify this condition (Dichtl *et al*, 1996). Moreover, it is not clear if the discrepancies between the studies that described the normal rim configuration in different population samples are a reflection of their methodological differences or a result of the great anatomical variability seen in the normal eye. It is noted that there are some considerations regarding the accuracy of magnification correction applied on the measurements of the disc and rim areas derived with this method of topographical analysis (Jonas *et al*, 1988d; Jonas *et al*, 1999b; Ramrattan *et al*, 1999).

7.2 Aims of study

The study aimed to evaluate the utility of neuroretinal rim area measurements in discriminating normal and glaucomatous optic discs. Also, to quantify the shape of the rim and investigate the diagnostic value of the ISNT rule, using measurements of the rim area derived with stereoscopic optic disc assessments of normal and glaucomatous discs and a modern technique of computer assisted planimetry.

7.3 Methods

Stereoscopic optic disc photographs from 51 normal and 113 glaucomatous eyes obtained with a simultaneous Nidek 3Dx stereoscopic fundus camera were analysed using a digital, stereoscopic viewing (Z–screen). Three expert observers, obtained planimetric measurements on all optic discs to provide neuroretinal and optic disc size measurements at 5 degrees intervals. The reference diagnosis of glaucoma was made independently on the basis of optic disc and the corresponding visual field examination. The operations of the software enabling planimetry, as well as the experimental procedures are described in detail within chapter 4.

In short description, the custom display software employed in this study enabled the demarcation of the margin of the optic disc as the inner border of Elschnig's rim using a stereoscopically viewed cursor whose depth could be adjusted to match that of the retinal plane. With the cursor set at this level, the observers then demarcated the inner border of the neuroretinal rim as the intersection of the retinal nerve fibre layer surface with the plane of the scleral canal. Algorithms for the

correct scaling of the measurements were implemented in the software code (Sheen, 2002).

7.3.1 Quantitative analysis of the neuroretinal rim

Multiple linear regression analysis performed with neuroretinal rim area as the dependent value and the optic disc, age and refraction as the independent values across a cohort of 51 normal subjects (table 7.1) revealed that of all variables, the disc area had the largest correlation with the dependent variable. Therefore, simple linear regression analysis was performed on normal optic disc global areas and their neuroretinal rim global areas with prediction intervals of 95%, for each of the three observers. The normal status of the optic disc topography was determined via cross-evaluation of the optic disc appearance and the visual field scores, with procedures that were described in chapter 4. The data points, representing normal subjects, that fell bellow the prediction intervals were considered for the estimation of specificity scores for the quantitative analysis. Pilot studies showed that Log transformation of the data only improved marginally the spread around the regression lines, without influencing the confidence intervals for normality. Thereby, this method was not incorporated in the quantitative analysis described in this chapter.

Planimetry data derived from the cohort of 113 glaucoma patients (table 7.1) that were also classified by a combination of imaging and perimetry criteria, were added to the above scatterplots and were compared to the normal regression line, Data points, representing glaucoma patients that fell outside the normal prediction

intervals (95% cut-off) were classed as abnormal. These data were expressed as the sensitivity scores of the quantitative analysis.

Parameters	Normal (n=51)	Glaucoma (n=113)
Age (years)	58.33 (10.76)	65.74
Mean Equivalent Sphere	0.24(1.98)	0.49
MD	-0.06 (1.40)	-4.35 (5.46)
PSD	1.88 (1.09)	4.93 (3.73)
Disc Area (mm^2)	2.17(0.43)	2.37(0.53)
Rim Area (mm^2)	1.54 (0.31)	1.06(0.33)

Table 7.1. *Summary of the mean age; refractive error; visual field indices and the group mean stereoscopic planimetry results, averaged for the three observers across the normal and glaucoma group.*

Subsequently, the rim and disc area data were arranged into 12 sectors subtending 30 degrees each (table 7.1) and the above regression analysis was repeated for the sectorial planimetry data.

Sectors	A	B	C	D	E	F
Degrees	0-30	30-60	60-90	90-120	120-150	150-180
Sectors	G	H	I	J	K	L
Degrees	180-210	210-240	240-270	270-300	300-330	330-360

Table 7.2 *Description of the disc segmentation for the sectorial quantitative analysis of the rim area into 12 sectors subtending 30 degrees each, named after a letter of the alphabet.*

Regression analysis of the sectorial rim against the sectorial disc was performed with 95% prediction intervals used as a cut off, for each of the three observers across the normal and glaucoma groups. The scores for all 12 sectors had to be within the normal confidence limits for a disc to be classed as normal by the sectorial quantitative analysis. Similarly, if at least one segment of the

glaucomatous discs fell below the normal prediction intervals as determined by the normal disc and rim data for the given segment, then the disc was classified as abnormal.

For observation of the diagnostic power of the global and sectorial quantitative analysis on glaucoma patients at different stages of glaucomatous damage, the glaucoma group (N=113) was divided into two subgroups, the group of patients with field loss (N=79) and the group of the earliest glaucoma cases (N=34) that is referred to as preperimetric glaucoma group (table 7.3).

Parameters	Glaucoma (n=79)	Glaucoma (n=34)
Age (years)	67.03 (10.04)	62.65 (10.30)
Mean Equivalent Sphere	+ 0.61 (1.72)	+0.19 (2.05)
MD	-5.98 (5.70)	-0.60(1.79)
PSD	6.17 (3.75)	2.09 (1.38)
Disc Area (mm^2)	2.32 (0.51)	2.48 (0.57)
Rim Area (mm^2)	0.94 (0.29)	1.32 (0.24)

Table 7.3. *Summary of the mean age; refractive error; visual field indices and the group mean stereoscopic planimetry results, averaged for the three observers across the two subgroups of glaucoma patients, with (N = 79) and without visual field loss (N = 34).*

The frequency of abnormal segments across the glaucomatous discs was calculated according to the measurements derived by each observer and each sector was associated with a diagnostic score.

The analysis of planimetry results in sectors allowed the observation of regional patterns of rim loss. The presence of 1 abnormal segment or 2 adjacent abnormal segments within the same disc denoted focal rim loss. Conversely, diffuse

glaucomatous damage was described as more than two abnormal segments. Using these criteria, glaucomatous discs were reclassified according to the type of neuroretinal rim loss they presented.

7.3.2 Investigation of the diagnostic value of ISNT rule

The investigation of useful predictors of glaucomatous rim loss was extended to a simple quantitative evaluation of the rim configuration as described by the ISNT rule. The measurements of the rim area were computed in segments of 5° around the optic disc but for the present analysis, the rim area was summed in four new sectors. Each sector corresponded to the inferior (I), superior (S), nasal (N) and temporal (T) regions of the disc, respectively and was equal to 10° for the first part of the analysis and to 30° for the second part of the analysis. The statistical analysis aimed to compare the rim area of the four sectors and evaluate if the condition I>S>N>T was fulfilled in each of the normal subjects of the cohort (N = 51), also employed for the procedures of the quantitative analysis that were described in this section (table 7.1). According to a previous report the condition I>S>N>T may indicate normality (Jonas *et al*, 1988c). Therefore, for the ISNT rule to be obeyed the three Boolean comparisons, I>S, S>N and N>T had to be true. In cases where any of these comparisons returned false, the rule was considered not to be fulfilled. This procedure was repeated for the estimates of the rim as defined by each of the three expert observers. Subsequently, the condition I>S>N>T was investigated among a cohort of glaucomatous patients (N=79) with established glaucomatous damage (table 7.3) and the percentage of subjects from the two study groups obeying the rule of I>S>N>T was defined for each observer. The number of normal and glaucomatous optic discs obeying the rule was then expressed as sensitivity

and specificity estimates of the ISNT rule predicting normality and subserving glaucoma diagnosis.

Given the greater variability in the configuration of the nasal and temporal segments and the possibility that measurements in these areas could have confounded the detection of glaucomatous damage using the ISNT rule, we next restricted the above investigation of the rim sectors to the comparison of the inferior and superior segments only. In this case optic discs were classified as normal if the inferior segment exceeded the superior segment (condition I>S).

The possibility that the shape or size of the optic disc would be a confounding factor in the evaluation of the ISNT rule, was explored with a multiple linear regression analysis where the ISNT rule score (0 or 1) was the outcome and age, disc size, orientation and degree of ellipse (maximum over minimum axis) were the explanatory variables.

Analysis was performed using Excel 2000 (Microsoft) and SPSS for Windows (11 & 12.5). Data distributions were tested for normality using the Shapiro-Willks test and were then subjected to the relevant parametric or non-parametric tests.

7.4 Results

There were significant differences between the samples of normal subjects and glaucoma patients overall with reference to their age characteristics (p=0.000, Mann-Whitney U Asymp. Sig. 2-tailed) and consequently, the glaucoma groups

included more hyperopic eyes ($p < 0.000$, Mann-Whitney U Asymp. Sig. 2-tailed). In addition, the mean rim area was significantly different between the two study groups.

The diagnostic scores associated with the subjective diagnosis of the dataset under stereoscopic conditions by the three observers are described in table 7.4.

		Observers		
		1	2	3
Specificity	Normal Group (N=51)	0.83	0.84	0.92
Sensitivity	Glaucoma Group (N=113)	0.73	0.87	0.80
	Perimetric Group (N= 79)	0.97	0.92	0.92
	Preperimetric (N= 34)	0.38	0.74	0.50
Diagnostic precision	Glaucoma Group (N=113)	0.76	0.86	0.84
	Perimetric Group (N= 79)	0.92	0.89	0.92
	Preperimetric (N= 34)	0.52	0.77	0.63

Table 7.4. *The diagnostic scores for the three expert observers based on their subjective assessments for the group of 51 normal subjects; the group of 78 glaucoma patients with concurrent optic disc damage and visual field loss and for the subgroup of the 34 preperimetric glaucoma patients, under stereoscopic conditions.*

The specificity values scored by the three observers ranged between 83%, by observer 1 and 92%, by observer 3. Observer 2 scored sensitivity markedly higher than the other observers for the preperimetric glaucoma subgroup (74%). This group was associated with the greatest variability between the diagnostic scores by the three observers, with the diagnostic precision ranging between 52% and 77%.

7.4.1 Quantitative analysis of the neuroretinal rim

The correlation of the neuroretinal rim area measurements with the optic disc area measurements across the normal group is shown with a series of scatterplots, based on the stereoscopic planimetry results derived by each of the three observers (Figures 7.1 to 7.3).

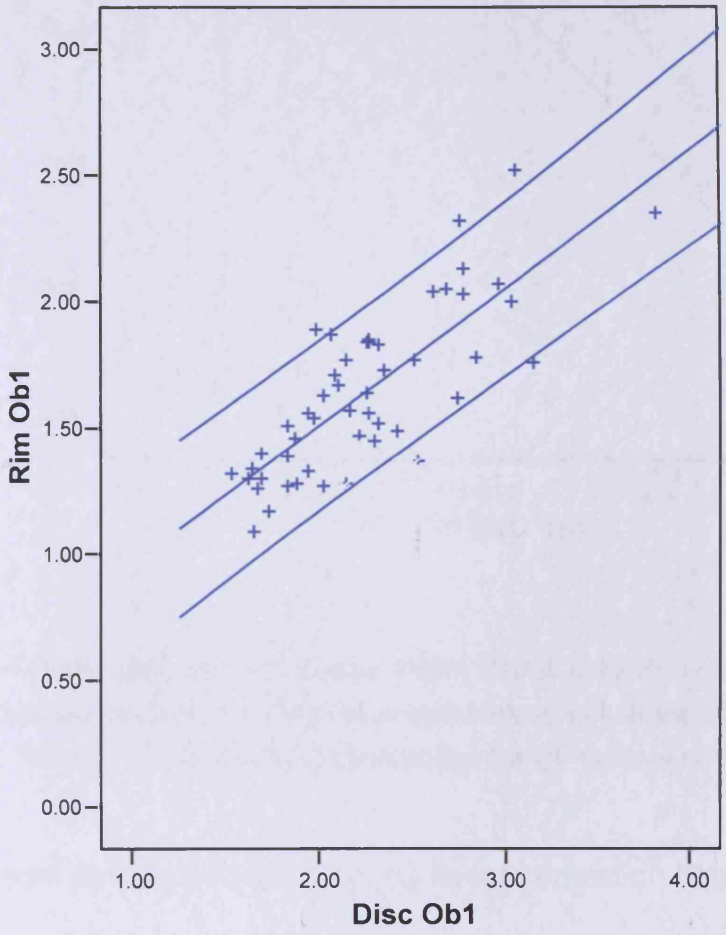

Figure 7.1 *Scatterplot of the rim area values (mm^2) against the disc area (mm^2) values, as measured by observer 1 across the normal group. Linear best fit line with 95% intervals for normality Predicted (Rim area) = 0.547 x (Disc area) + 0.412; p-value =0.000; R^2 = 0.636.*

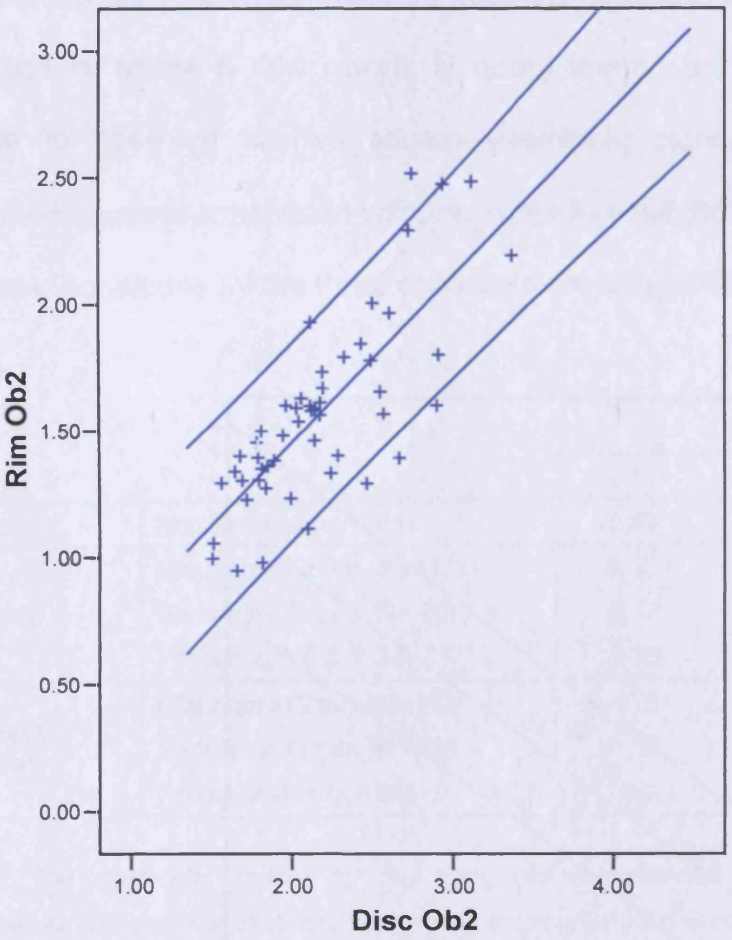

Figure 7.2 *Scatterplot of the rim area values (mm^2) against the disc area (mm^2) values, as measured by observer2 across the normal group. Linear best fit line with 95% intervals for normality. Predicted Rim area = 0.657 x (Disc area) + 0.142; p-value =0.00; R^2 = 0.610.*

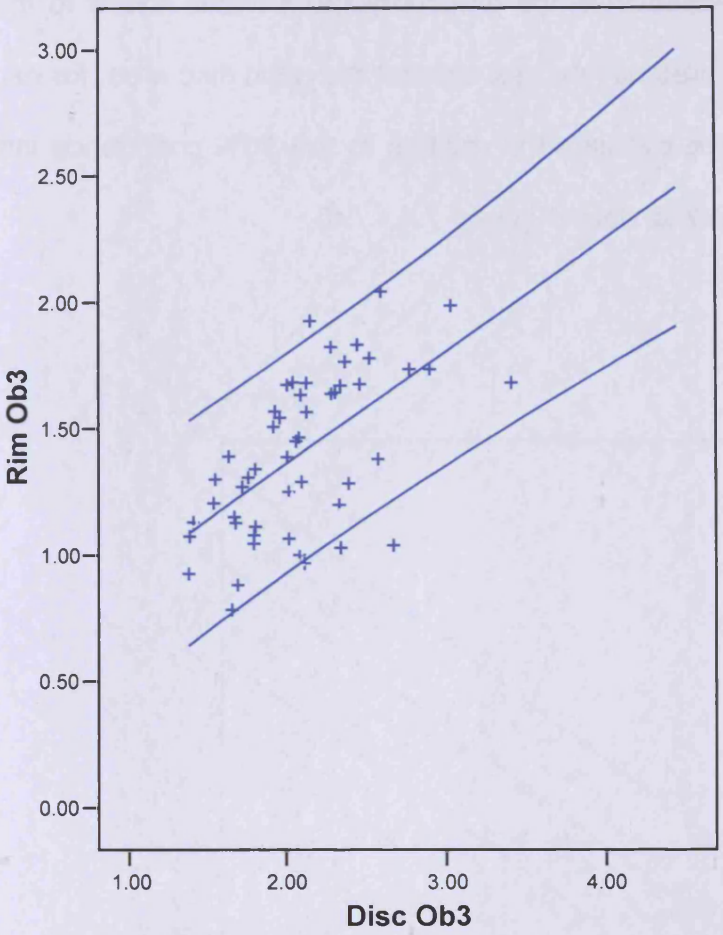

Figure 7.3 *Scatterplot of the rim area values (mm^2) against the disc area (mm^2) values, as measured by observer3 across the normal group. Linear best fit line with 95% intervals for normality. Predicted Rim area = 0.469+ 0.447 x (Disc area); p-value =0.13; R^2 = 0.346.*

The present study described a strong linear correlation between computer assisted planimetry of the disc and rim areas across the normal group. The mean reported slope was 0.55 (range: 0.45 - 0.66) and the mean correlation coefficient was r^2 = 0.54 (range: 0.37 - 0.64), that reached significance for only two of the observers.

7.4.2 Global rim area quantitative analysis

The planimetry data derived from the glaucoma group were added to the scatter plots of the normal neuroretinal rim area against the optic disc area, for each of the three observers and were evaluated in relation to the 95% confidence intervals of the best-fit line for the normal data (Figures 7.4 - 7.6)

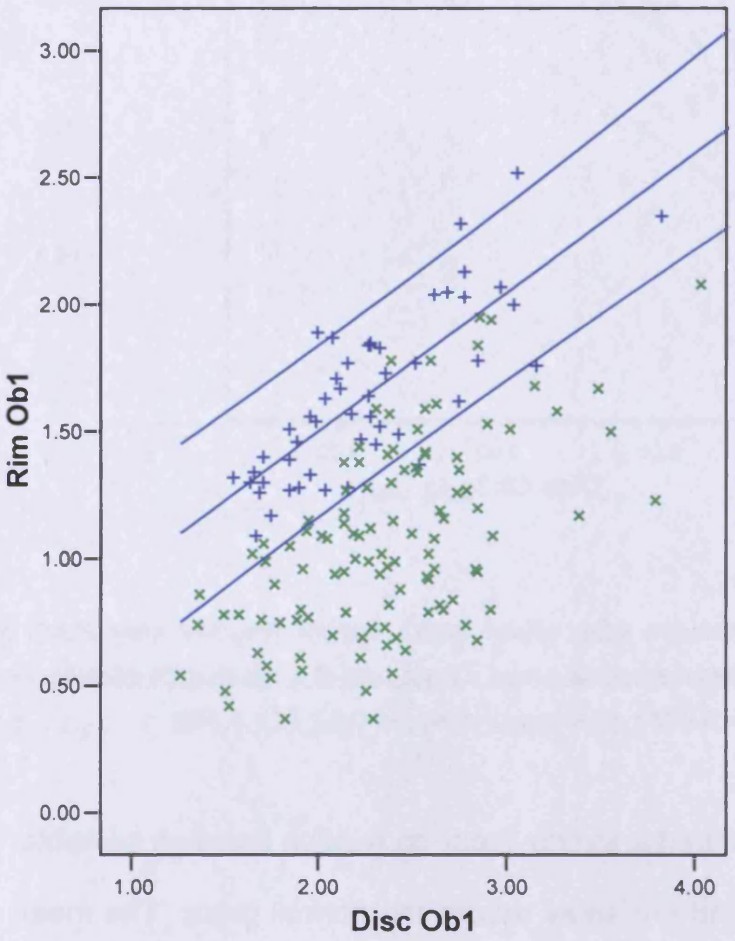

Figure 7.4 *Regression analysis of the rim area values (mm^2) against the disc area (mm^2) values, as measured by observer 1, across the normal group and glaucoma group. Linear best fit line with 95% intervals for normality.*

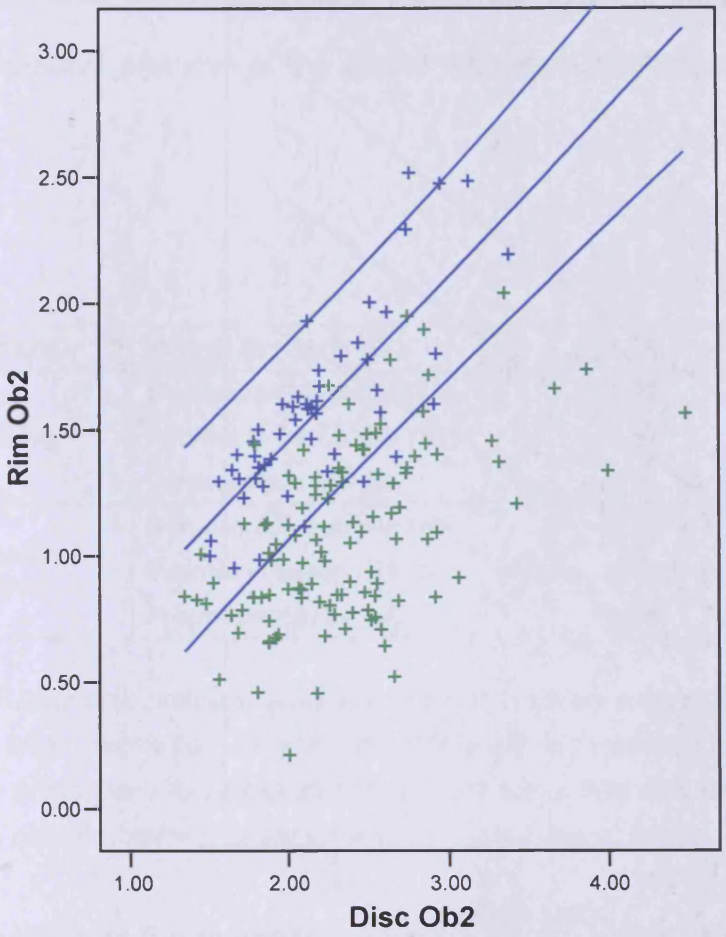

Figure 7.5 *Regression analysis of the rim area values (mm^2) against the disc area (mm^2) values, as measured by observer 2 across the normal group and the glaucoma group. Linear best fit line with 95% intervals for normality.*

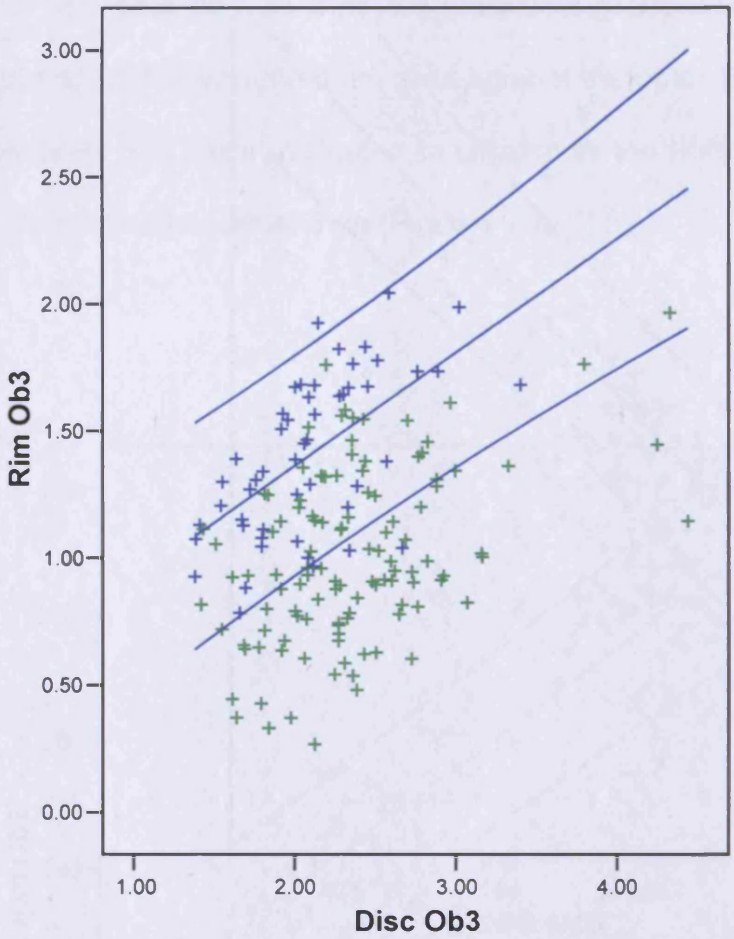

Figure 7.6 *Regression analysis of the rim area values (mm^2) against the disc area (mm^2) values, as measured by observer 3, across the normal group and the glaucoma group. Linear best fit line with 95% intervals for normality.*

Observation of the rim and disc area data points across the normal and glaucomatous groups that are presented in figures 7.4 - 7.6 reveals that there is an overlap of normal and glaucomatous values of the total rim area. Thus, a number of glaucomatous rim values fall within the prediction intervals set at the level of 95%. This is a consistent observation across the regression plots by all three observers. The data points derived from the glaucoma group that fell bellow the prediction

intervals were used for the calculation of the sensitivity scores and the normal discs that fell outside the 95% prediction intervals determined the specificity scores for the quantitative analysis of the global rim measurements, by each observer (table 7.5).

		Observers		
		1	**2**	**3**
Specificity	Normal Group (N=51)	1.00	0.94	0.96
Sensitivity	Glaucoma Group (N=113)	0.82	0.70	0.65
	Perimetric Group (N= 79)	0.87	0.84	0.82
	Preperimetric (N= 34)	0.71	0.38	0.26
Diagnostic Precision	Glaucoma Group (N=113)	0.88	0.77	0.75
	Perimetric Group (N= 79)	0.92	0.88	0.87
	Preperimetric (N= 34)	0.88	0.72	0.68

Table 7.5 *Diagnostic precision according to the quantitative analysis of the global neuroretinal rim and disc areas (regression analysis with 95% prediction intervals) for the total normal and total glaucoma group (top); the group of patients with visual field loss (middle) and the preperimetric glaucoma patients (bottom), by each of the three observers (1, 2& 3).*

The specificity of the regression analysis for the global rim measurements against the corresponding global disc area measurements ranged between 0.94 - 1.00 across the three observers. Sensitivity values showed a greater variation between the observers, with the scores by observer 1 being markedly higher across the total glaucoma group and also separately for the perimetric (N = 79) and preperimetric patients (N = 34). The perimetric and preperimetric groups were associated with a mean sensitivity value of 0.84 (±0.03) and 0.45 (±0.23) respectively. Correspondently, the diagnostic precision was highest for observer 1 (88%) although all three observers were successful when evaluating the definitive cases of glaucoma (perimetric group).

The quantitative analysis of the global rim and disc areas improved specificity compared to the subjective diagnosis for all three observers, but on average across the observers, the mean sensitivity values decreased for both glaucoma subgroups. The average diagnostic precision appeared improved for the preperimetric glaucoma eyes but there were marked differences in the performance between observers.

7.4.3 Sectorial rim area quantitative analysis

The procedure for the global quantitative analysis was performed for each of the 12 sectors around the disc. The correlation coefficient r^2 for each of the regression analysis is given in table 7.6.

	Correlation coefficient r^2					
Sectors	Ob1		Ob2		Ob3	
A	0.710	<0.000	0.743	<0.000	0.548	<0.000
B	0.139	0.007	0.762	<0.000	0.501	<0.000
C	0.083	0.041	0.754	<0.000	0.480	<0.000
D	0.004	0.001	0.717	<0.000	0.298	<0.000
E	0.042	0.151	0.784	<0.000	0.192	0.001
F	0.182	0.002	0.882	<0.000	0.514	<0.000
G	0.259	<0.000	0.889	<0.000	0.608	<0.000
H	0.202	0.001	0.865	<0.000	0.686	<0.000
I	0.309	<0.000	0.799	<0.000	0.730	<0.000
J	0.393	<0.000	0.790	<0.000	0.697	<0.000
K	0.318	<0.000	0.728	<0.000	0.661	<0.000
L	0.130	0.009	0.709	<0.000	0.600	<0.000

Table 7.6 *The correlation coefficient (r^2) and level of significance (p-value) of the regression analysis of the segmental neuroretinal rim and disc areas (regression analysis with 95% prediction intervals) across the 12 sectors, for the total normal and total glaucoma group by each of the three observers (1, 2& 3).*

On average across the 12 sectors the disc and rim measurements obtained by Observer 2 showed the best correlation with $r^2 = 0.79$ (±0.06), followed by observer 3 with $r^2 = 0.54$ (±0.16), and observer 1 with $r^2 = 0.23$ (±0.19). The three different sets of data also differed in the sectors that demonstrated the greatest correlation between the disc and rim data. Sector A, located at the temporal region (0 - 30 Deg; $R^2 = 0.71$; $p < 0.000$) was the best for observer 1, sector G at the nasal part of the disc (180 - 210 Deg; $R^2 = 0.889$; $p < 0.000$) showed the highest correlation based on planimetry by observer 2 and the data from observer 3 reached the best correlation at the inferior-nasal region, within sector I (240 - 270 Deg; $R^2 = 0.889$; $p < 0.000$)

The number of glaucoma patients identified as abnormal by the rim values within each sector are graphically presented in figure 7.7 for the total glaucoma group and separately for the subgroup of preperimetric glaucoma patients (N = 34) in figure 7.8.

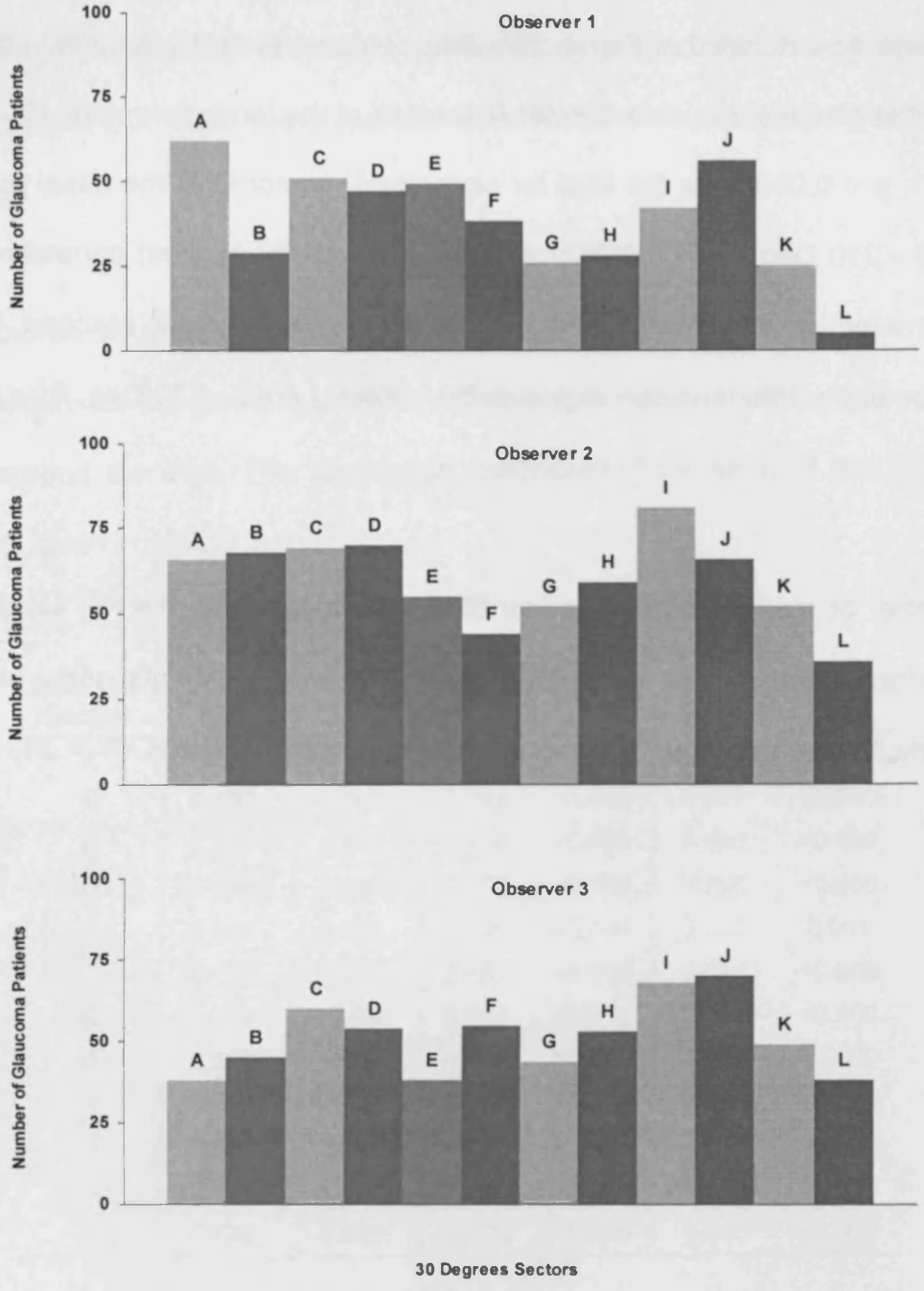

Figure 7.7 *Frequency of the optic nerve sectors (subtending 30 degrees) that were classed as abnormal with the quantitative analyses (linear regression with 95% prediction intervals) of the measurements of the rim and disc areas at the corresponding regions, across the total glaucoma group (N = 113) by observer 1 (top); observer 2 (middle) and observer 3 (bottom), respectively.*

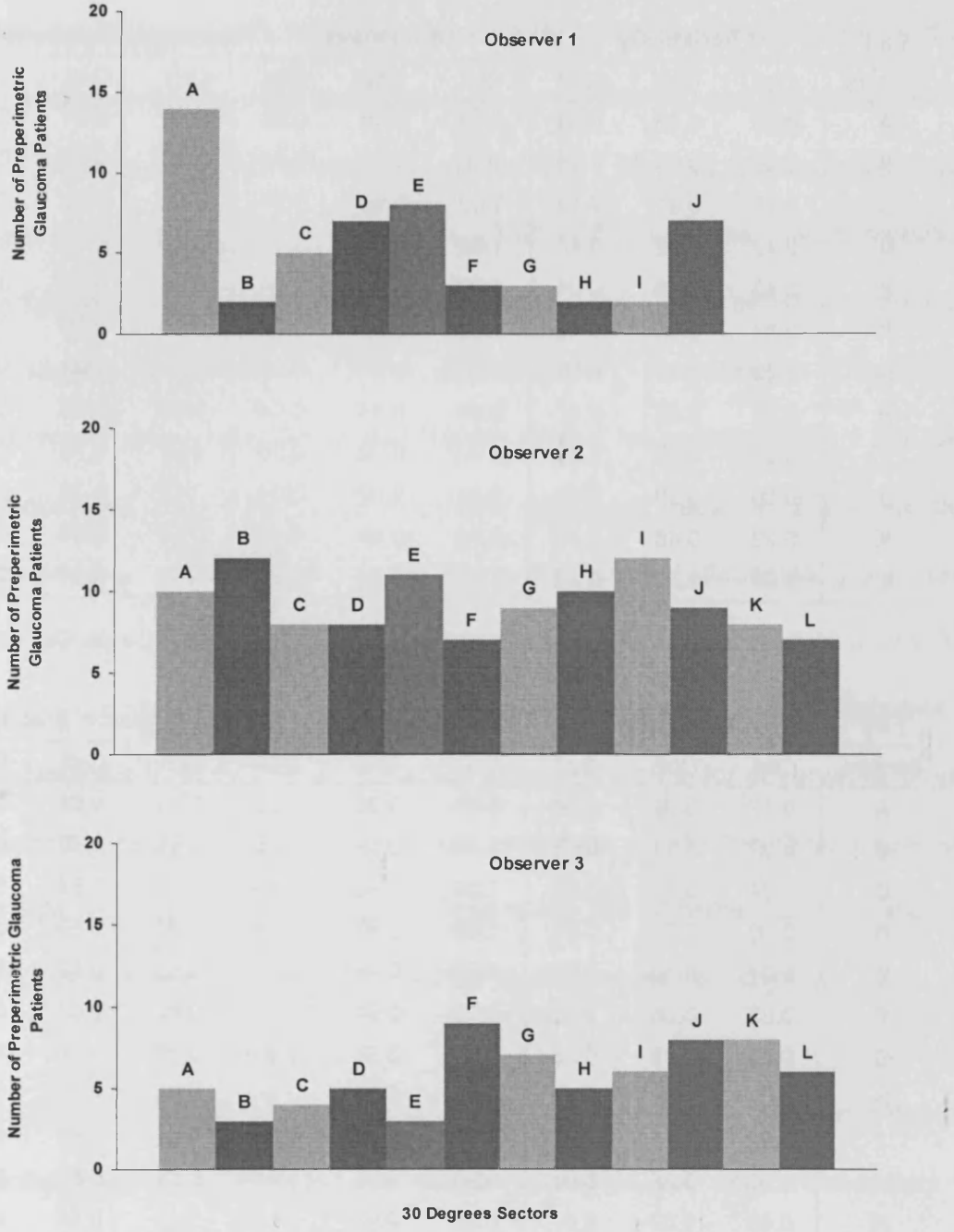

Figure 7.8 *Frequency of the optic nerve sectors (subtending 30 degrees) classed as abnormal with the quantitative analyses (linear regression with 95% prediction intervals) of the measurements of the rim and disc areas at the corresponding regions, across the preperimetric glaucoma group (N = 34) by observer 1 (top); observer 2 (middle) and observer 3 (bottom), respectively.*

The diagnostic scores for each sector are summarised in table 7.7a and b.

(a)	Sensitivity			Specificity			Diagnostic precision		
Sectors	Ob1	Ob2	Ob3	Ob1	Ob2	Ob3	Ob1	Ob2	Ob3
A	0.55	0.58	0.34	0.98	0.98	0.96	0.68	0.71	0.53
B	0.26	0.60	0.40	1.00	0.92	0.96	0.49	0.70	0.57
C	0.45	0.61	0.53	1.00	0.90	0.94	0.62	0.70	0.66
D	0.42	0.62	0.48	1.00	0.92	0.94	0.60	0.71	0.62
E	0.43	0.49	0.34	1.00	0.96	0.94	0.61	0.63	0.52
F	0.34	0.39	0.49	1.00	0.94	0.92	0.54	0.56	0.62
G	0.23	0.47	0.39	0.96	0.94	0.96	0.46	0.62	0.57
H	0.25	0.52	0.47	0.98	0.94	0.94	0.48	0.65	0.62
I	0.37	0.73	0.60	1.00	0.92	0.96	0.57	0.79	0.71
J	0.50	0.59	0.62	0.98	0.92	0.94	0.65	0.70	0.72
K	0.22	0.46	0.43	0.96	0.94	0.96	0.45	0.61	0.60
L	0.04	0.32	0.34	1.00	0.92	0.96	0.34	0.51	0.53

(b)	Sensitivity			Specificity			Diagnostic precision		
Sectors	Ob1	Ob2	Ob3	Ob1	Ob2	Ob3	Ob1	Ob2	Ob3
A	0.12	0.09	0.04	0.98	0.98	0.96	0.64	0.62	0.59
B	0.02	0.11	0.03	1.00	0.92	0.96	0.61	0.60	0.59
C	0.04	0.07	0.04	1.00	0.90	0.94	0.62	0.57	0.58
D	0.06	0.07	0.04	1.00	0.92	0.94	0.62	0.58	0.58
E	0.07	0.10	0.03	1.00	0.96	0.94	0.63	0.62	0.58
F	0.03	0.06	0.08	1.00	0.94	0.92	0.61	0.59	0.58
G	0.03	0.08	0.06	0.96	0.94	0.96	0.59	0.60	0.60
H	0.02	0.09	0.04	0.98	0.94	0.94	0.60	0.60	0.58
I	0.02	0.11	0.05	1.00	0.92	0.96	0.61	0.60	0.60
J	0.06	0.08	0.07	0.98	0.92	0.94	0.61	0.58	0.59
K	0.00	0.07	0.07	0.96	0.94	0.96	0.58	0.59	0.60
L	0.00	0.06	0.05	1.00	0.92	0.96	0.60	0.58	0.60

Table 7.7 *Diagnostic precision calculated according to the quantitative analysis of the segmental neuroretinal rim and disc areas (regression analysis with 95% prediction intervals) for the normal (N = 51) and (a) the total glaucoma group (N = 113); and (b) the group of preperimetric glaucoma patients (N = 34), across the 12 sectors (subtending 30Degrees) of the optic nerve, by each observer.*

The mean sensitivity scores across the 12 sectors were highest for observer2 (53%); followed by observer3 (45%) and observer1 (34%) for the total glaucoma group. The sectorial analysis was less sensitive for the preperimetric group and the mean sensitivity scores across the 12 sectors were 4%, 8% and 5% for observers 1, 2 and 3, respectively. For observer 1, sector A (0 - 30 deg) was associated with the highest sensitivity (55%) and sector L (330 - 360) with the lowest sensitivity scores (4%). Observer 2 and observer 3 also scored the lowest sensitivity within the temporal region, at sectors L (32%) and A (34%), respectively. The highest sensitivity score was within the nasal-inferior region, at sector I (240 - 270 deg; 73%) for observer 2 and the temporal-inferior region, at sector J (270 - 300 deg; 62%) for observer 3. The diagnostic precision for the total glaucoma group (table 7.6.a) ranged between 34 - 68% for observer1; 51 - 79% for observer 2 and 52 - 72% for observer3 across the 12 sectors. The same parameter ranged between 58 - 64% for observer 1; 57 - 62% for observer 2 and 58 - 60% for observer 3, among the preperimetric glaucoma patients. When averaged across the three observers, the diagnostic precision assumed the highest value (69%) within sector J and I for the total glaucoma group and sector A (62%) for the preperimetric group.

When diagnosis was made according to the sectorial evaluation of the rim defining all glaucoma patients by at least one abnormal sector, the diagnostic scores for each observer were estimated to be as follows (table 7.8).

		Observers		
		1	2	3
Specificity	Normal Group (N=51)	0.90	0.80	0.84
Sensitivity	Glaucoma Group (N=113)	0.73	0.67	0.68
	Perimetric Group (N= 79)	0.90	0.80	0.78
	Preperimetric (N= 34)	0.32	0.38	0.47
Diagnostic Precision	Glaucoma Group (N=113)	0.78	0.71	0.74
	Perimetric Group (N= 79)	0.90	0.80	0.81
	Preperimetric (N= 34)	0.67	0.64	0.69

Table 7.8 *Diagnostic precision calculated according to the quantitative analysis of the segmental neuroretinal rim and disc areas (regression analysis with 95% prediction intervals) for the normal (N=51); (a) the total and (b) preperimetric glaucoma group respectively.*

The specificity of the regression analysis for the sectorial rim measurements against the corresponding disc area measurements ranged between 0.80 – 0.90 across the three observers, which were slightly lower that the values achieved from the global analysis (0.96 ± 0.03). Sensitivity values that by observer 1 that achieved the highest scores with the global analysis remained high across the total glaucoma group and the perimetric group (90%) but were the lowest of all observers for the the preperimetric patients (32%). The perimetric and preperimetric groups were associated with a mean sensitivity value of 0.83 (±0.06) and 0.39 (±0.07) respectively. The diagnostic precision with the sectorial analysis was more variable between observers across the perimetric group (range 80- 90%) than the preperimetric group (range 64- 69%). Observer 1 achieved the highest diagnostic score between the three observers across the total glaucoma group (78%) which was lower than the highest score evaluated by the global analysis (88%) and the subjective diagnosis (86%).

7.4.4 Rim configuration

The rim loss pattern evident in each of the glaucoma patients was characterised according to the results of the sectorial rim abnormality, as it was defined by the regression analysis of the sectorial rim and disc values for the three observers. The frequency of diffuse or focal damage across the total glaucoma group and also with reference to the preperimetric patients is shown in table 7.9.

		Observers		
		1	2	3
Glaucoma Group (N=113)	Diffuse	63	69	73
	Focal	19	7	4
Preperimetric Group (N= 34)	Diffuse	10	10	13
	Focal	7	3	2

Table 7.9 *Classification of glaucomatous discs according to the type of neuroretinal rim loss (diffuse / focal) as defined by the segmental rim analysis for each observer.*

Observer1 had the smallest number of misdiagnosed preperimetric patients (17) followed by observer2 (21) and observer3 (19). Thus, among the patients correctly identified by each observer the percentage of preperimetric patients with diffuse loss ranged from 59% (observer1) to 87% (observer3). The patients with visual field loss also showed predominantly diffuse rim loss. The mean proportion of perimetric glaucoma patients with focal loss across the three observers was 60% of the sample.

The distribution of the rim values across the 12 sectors around the disc by each of the observers was graphically presented for the normal, the total glaucoma group (figure 7.9.) and the subgroups of preperimetric and perimetric glaucoma patients (figure 7.10).

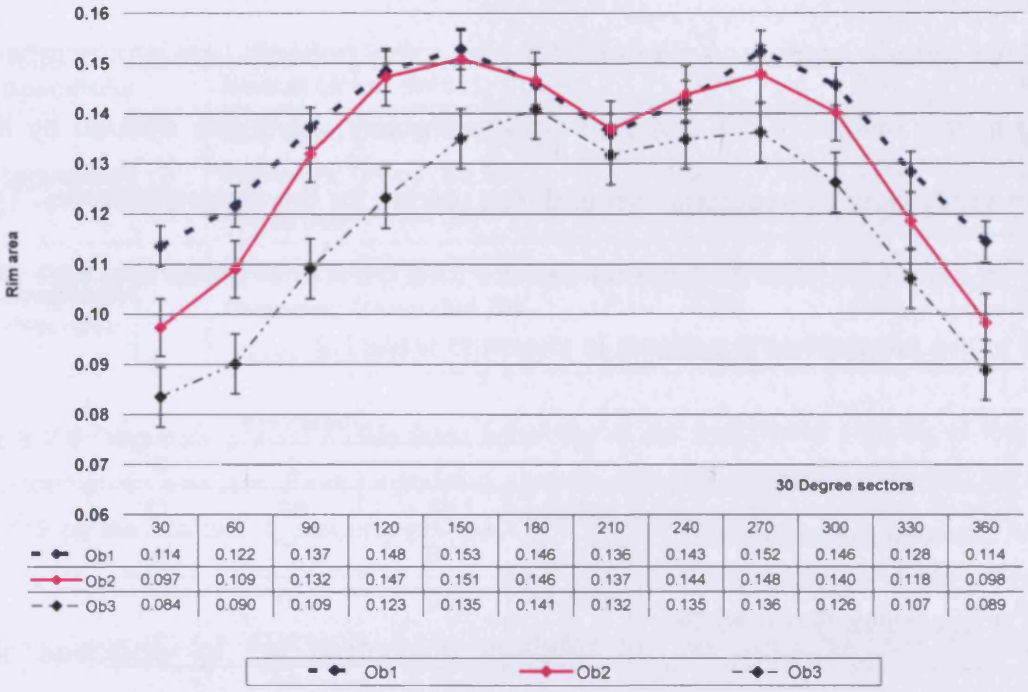

	30	60	90	120	150	180	210	240	270	300	330	360
Ob1	0.114	0.122	0.137	0.148	0.153	0.146	0.136	0.143	0.152	0.146	0.128	0.114
Ob2	0.097	0.109	0.132	0.147	0.151	0.146	0.137	0.144	0.148	0.140	0.118	0.098
Ob3	0.084	0.090	0.109	0.123	0.135	0.141	0.132	0.135	0.136	0.126	0.107	0.089

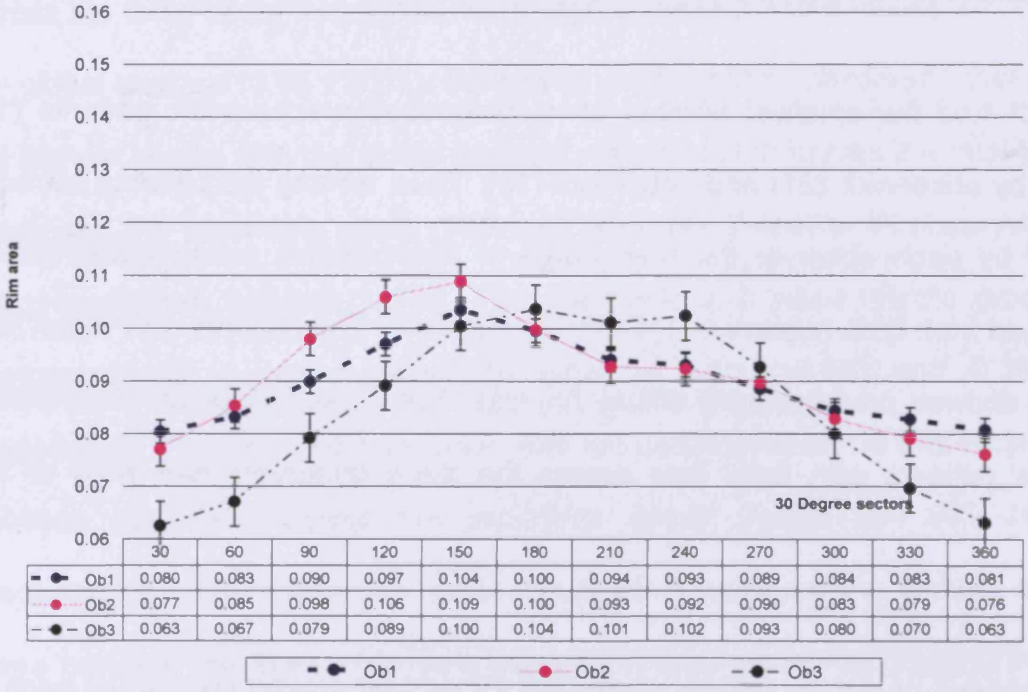

	30	60	90	120	150	180	210	240	270	300	330	360
Ob1	0.080	0.083	0.090	0.097	0.104	0.100	0.094	0.093	0.089	0.084	0.083	0.081
Ob2	0.077	0.085	0.098	0.106	0.109	0.100	0.093	0.092	0.090	0.083	0.079	0.076
Ob3	0.063	0.067	0.079	0.089	0.100	0.104	0.101	0.102	0.093	0.080	0.070	0.063

Figure 7.9 *The distribution of the group mean rim area (mm^2) across 12 sectors, subtending 30 Degrees around the disc, for the normal group (top) and the total glaucoma group (below), as assessed by the three observers (1,2,3)*

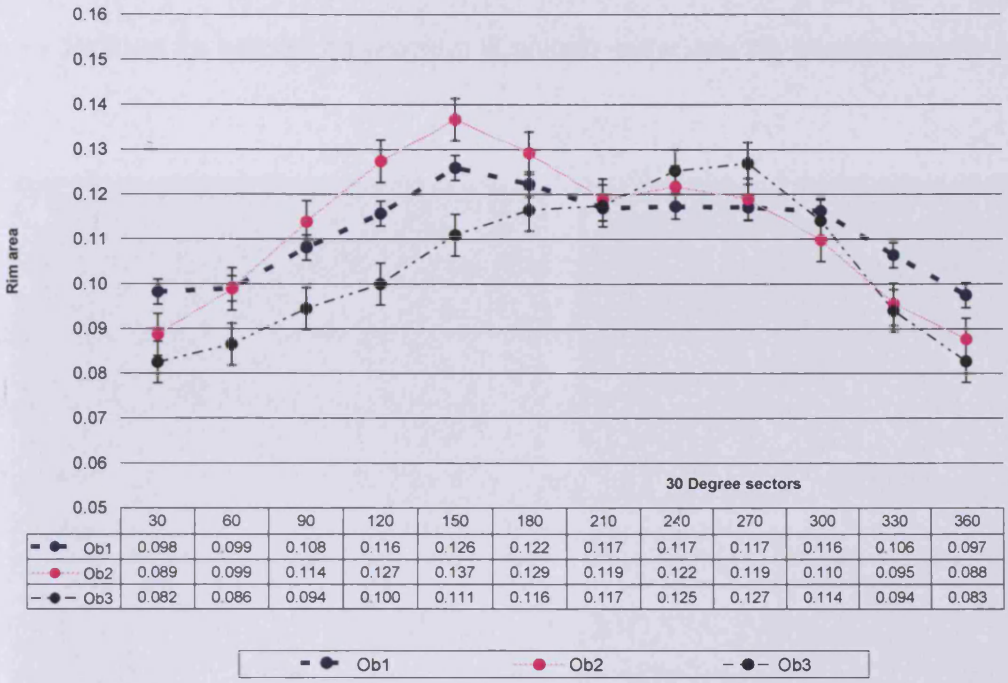

	30	60	90	120	150	180	210	240	270	300	330	360
Ob1	0.098	0.099	0.108	0.116	0.126	0.122	0.117	0.117	0.117	0.116	0.106	0.097
Ob2	0.089	0.099	0.114	0.127	0.137	0.129	0.119	0.122	0.119	0.110	0.095	0.088
Ob3	0.082	0.086	0.094	0.100	0.111	0.116	0.117	0.125	0.127	0.114	0.094	0.083

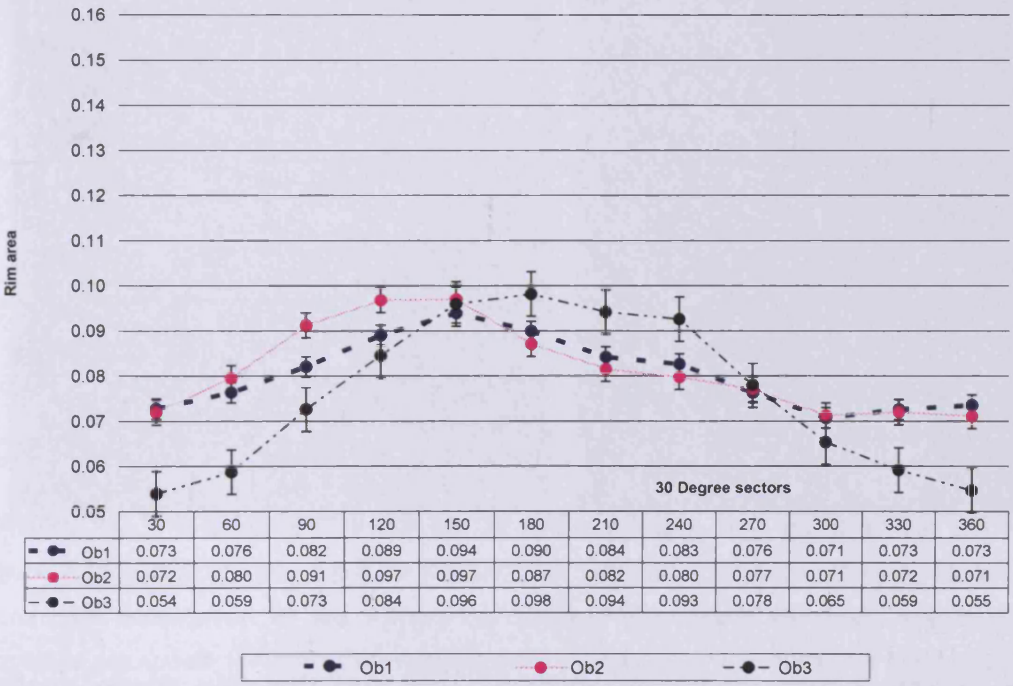

	30	60	90	120	150	180	210	240	270	300	330	360
Ob1	0.073	0.076	0.082	0.089	0.094	0.090	0.084	0.083	0.076	0.071	0.073	0.073
Ob2	0.072	0.080	0.091	0.097	0.097	0.087	0.082	0.080	0.077	0.071	0.072	0.071
Ob3	0.054	0.059	0.073	0.084	0.096	0.098	0.094	0.093	0.078	0.065	0.059	0.055

Figure 7.10 *The distribution of the group mean rim area (mm^2) across 12 sectors, subtending 30 Degrees around the disc, for the group of early (preperimetric) glaucoma patients (top) and the group of glaucoma patients with detectable visual field loss (below), as assessed by the three observers (1,2,3).*

The mean normal rim presented a characteristic curve that was also detected among the preperimetric group of patients. Furthermore, the mean group rim areas across the glaucomatous groups were distinctly depressed across all sectors.

7.4.5 Evaluation of disc shape

The disc shape parameters namely, the size of the maximum and minimum disc diameter; the orientation of the maximum disc diameter (Elliptic orientation) adjusted for a scale between 0 - 180 degrees and the ratio of the minimum over the maximum disc diameter (Form Factor) are calculated for the normal group and the glaucoma patient subgroups (table 7.10).

Normal Group	Ob1		Ob2		Ob3	
Parameters	Mean	SD	Mean	SD	Mean	SD
Max Disc Diameter	1.77	0.20	1.74	0.18	1.70	0.18
Min Disc Diameter	1.58	0.17	1.55	0.17	1.53	0.16
Elliptic Orientation	103.80	29.54	106.52	30.43	106.55	27.57
Form Factor	0.89	0.06	0.89	0.06	0.90	0.05

Perimetric Group	Ob1		Ob2		Ob3	
Parameters	Mean	SD	Mean	SD	Mean	SD
Max Disc Diameter	1.82	0.21	1.80	0.20	1.80	0.20
Min Disc Diameter	1.60	0.20	1.59	0.18	1.61	0.19
Elliptic Orientation	101.67	26.37	101.04	30.37	101.32	27.76
Form Factor	0.88	0.06	0.89	0.05	0.90	0.05

Table 7.10 *The results of the disc shape analysis across the normal group and the glaucoma subgroups.*

The discs in both groups appeared vertically oval and the disc shape analysis identified 3 (ob1), 6 (ob2) & 1(ob3) normal optic discs with a significant disc tilt, namely a Form Factor ≤ 8. For the glaucomatous groups the scores were 7 (ob1), 3 (ob2) & 2 (ob3) for the three observers respectively.

7.4.6 Quantification of the ISNT rule

The segmentation of the rim values for the ISNT rule comparisons is shown in figure 7.11.

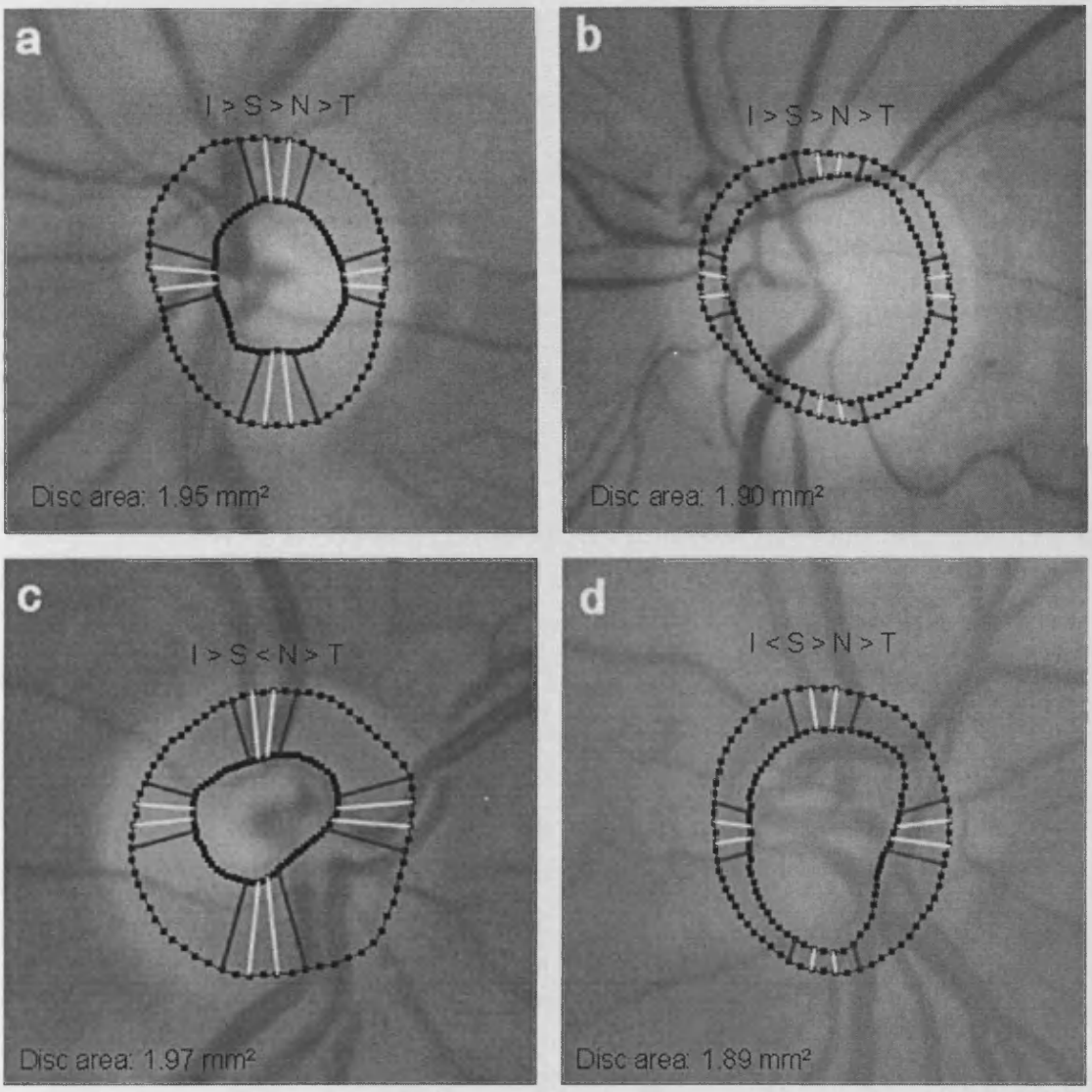

Figure 7.11 *Optic disc photographs showing the segments used to define the 10 and 30 degree sectors for comparison of the Inferior (I), Superior (S), Nasal (N) and Temporal (T) sectors. Examples are shown for normal and glaucomatous optic discs that follow the ISNT rule (a,b) and for normal and glaucomatous optic discs that do not follow the ISNT rule (c,d).*

The results of the comparison between sectorial rim areas for the investigation of the ISNT rule, based on measurements made by the 3 observers, reclassified the two study groups. The diagnostic outcome of ISNT, expressed with sensitivity and specificity scores, the number of discs fulfilling the rule and with diagnostic precision estimates, is described in tables 7.11 and 7.12.

For the evaluation of the ISNT rule a stricter definition of glaucoma was thought appropriate. Thereby, the rim configuration was evaluated among the glaucoma patients with concurrent optic disc changes and visual field loss with W-W perimetry (table 7.11). This subgroup comprised of 79 optic discs, including 26 cases with mild field loss; 22 cases with moderate field loss and 30 cases of advanced field loss (Hodapp Classification Modified by Litwak.).

	Perimetric Group						
	I>S>N>T for 10 degree segments						
Observer	Normal	%	Perimetric Glaucoma	%	Sensitivity	Specificity	Diagnostic precision
1	7	14	5	6	0.94	0.14	0.63
2	7	14	6	8	0.92	0.14	0.61
3	5	10	3	4	0.96	0.10	0.62
	I>S>N>T for 30 degree segments						
1	5	10	5	6	0.94	0.10	0.61
2	7	14	5	6	0.94	0.14	0.63
3	7	14	4	5	0.95	0.14	0.63

Table 7.11 *Diagnostic outcome for the detection of glaucoma based on the rule I>S>N>T for the Inferior (I), Superior (S), Nasal (N), Temporal (T) for 10 and 30 degrese segments.*

The ISNT rule yielded a mean sensitivity of 94% (range: 92% - 96%) and a mean specificity of 13% (range: 10% - 14%) for glaucoma discrimination based on the 10 degree sectors. When the 30 degree sectors where considered for the

comparisons, the ISNT rule yielded the same mean diagnostic scores across the three observers.

The diagnostic outcome of the condition I>S is shown in table 7.12.

	I>S for 10 degree segments						
Observer	Normal	%	Perimetric Glaucoma	%	Sensitivity	Specificity	Diagnostic precision
1	27	53	29	37	0.63	0.53	0.59
2	29	57	24	31	0.69	0.57	0.64
3	30	59	36	46	0.54	0.59	0.56
	I>S for 30 degree segments						
1	27	53	28	36	0.64	0.53	0.60
2	28	55	22	28	0.72	0.55	0.65
3	33	65	37	47	0.53	0.65	0.58

Table 7.12 *Diagnostic outcome for the detection of glaucoma based on the rule I>S for the Inferior (I), Superior (S) for 10 and 30 degrees segments. The relationship to the Nasal and Temporal sectors was not included in this analysis.*

The condition I>S as a single indication of normality yielded a mean sensitivity of 62%, (range = 54% - 69%) and a mean specificity of 56%, (range = 53% - 59%) for glaucoma discrimination based on the measurements of the 10 degree sectors. Based on the 30 degrees sectors, the new mean diagnostic scores were almost unchanged, at 63% for the mean sensitivity (range = 53% - 72%) and 58% (range = 53% - 65%) for the mean specificity. However, compared to the analysis for the ISNT rule, the evaluation only of the superior and inferior sectors decreased the sensitivity of the method but succeeded a higher specificity, consistently for all three observers.

7.5 Discussion

7.5.1 Quantification of the rim area

The linear correlation between the disc and rim measurements has been previously shown for planimetry performed with manual and automated imaging techniques (Caprioli *et al*, 1987; Garway-Heath & Hitchings, 1998; Jonas & Naumann, 1988). The results of this study confirmed the dependency of the rim size on the disc size, but the evaluated relationships were different between observers and somewhat weaker than those previously reported. This is the effect of the variability associated with the subjective demarcation of the disc and cup areas. The mean correlation coefficient for the three observers of this study was $R^2 = 0.54$ (range: 0.37 - 0.64). Other studies have reported similar rates of increase for the rim area in association with the disc size. Jonas and co-workers (1988) reported a range of regression slopes (0.30 - 0.62) for a Caucasian population using manual planimetry (Jonas *et al*, 1988c) and Varma and colleagues (1994) estimated a slope of 0.58 for a white population using the Topcon Imagenet and computer planimetry of stereophotographs (Varma *et al*, 1994). It is important to consider that these results would vary with the definition of the cup and the method of assessment employed in every study.

The sectorial slopes of the rim showed a wide variability across sectors and also between the analyses for the three observers. However, no specific pattern of change could be identified although there are previous reports suggesting that the rim slopes were more pronounced in the inferior than the temporal regions of the disc (Budde *et al*, 2000). These results highlight the variability between observers

upon the rim definition that also appears exacerbated when the sectorial rim areas are analysed.

7.5.2 Diagnostic value of the global and sectorial rim analysis

Glaucoma discrimination according to the average of the available scores was achieved with 45% sensitivity and 97% specificity. These values compare well with the study by Garway Heath & Hitchings (1998) that performed similar quantitative analysis using computerised planimetry and reported specificity of 98.9% and sensitivity of 41.5% for early glaucoma diagnosis using linear regression of the global rim values with a cut-off derived from the 95% prediction intervals (Garway-Heath & Hitchings, 1998).

Glaucoma detection based on the quantitative analysis using the global neuroretinal rim was expected to be less sensitive than the same analysis based on segmental values as global analysis is likely to misdiagnose glaucomatous discs with focal loss only. The study by Garway-Heath and Hitchings (1998) showed that the sensitivity of the quantitative evaluation in early glaucoma increased dramatically when the neuroretinal rim area was incorporated in the regression analysis in the form of 30 degrees sectors (specificity = 95.5% and sensitivity = 73.6%; 95% prediction intervals) (Garway-Heath & Hitchings, 1998). In the present study the global analysis compared to the segmental analysis was associated with higher specificity scores but on average across the observers the sensitivity scores for the perimetric and preperimetric glaucoma groups tended to be lower with the sectorial analysis. However, for the perimetric group a wider variability between the observers was also seen for their diagnostic scores derived with the segmental

analysis. Overall, the quantitative analysis of the rim values obtained with stereoscopic planimetry by the three expert observers of the study did not markedly improve the diagnostic precision achieved by the same expert observers with subjective evaluation of the optic disc topography under stereoscopic conditions.

7.5.3 Patterns of focal and diffuse glaucomatous rim loss

The classification of glaucomatous rim loss was based on the results of the sectorial regression analysis for all discs. It was a consistent finding for all three observers that the dataset of discs analysed in the present study included predominantly cases of diffuse glaucomatous rim loss. This was also true for the preperimetric glaucoma group. A possible explanation for these results is the fact that the pattern of glaucomatous rim loss depends strongly on the type of glaucomatous pathology. The group of patients included in this study mainly demonstrated high-pressure glaucoma and most of them were also treated with iop-lowering medication. Moreover, the preperimetric group included mainly former ocular-hypertensive patients. Particularly in high pressure glaucoma the rim is often concentrically diminished without the development of rim notches while in normal pressure glaucoma the rim usually has localised defects in the temporal inferior and superior sectors. Also diffuse rim loss has been demonstrated in OAGs in strong association with advanced age and later stages of the disease (Broadway *et al*, 1999; Jonas & Xu, 1993), although early glaucomatous loss has also been presented with both focal and diffuse patterns of damage (Emdadi *et al*, 1998).

7.5.4 Possible limitations for the quantification of the rim area

Other studies have used regression analysis of the segmental rim without correcting for the disc size (O'Connor *et al*, 1993) or regressing the sectorial rim areas against the total disc area for each eye (Garway-Heath & Hitchings, 1998), or even the mean disc sector for each eye (Budde *et al*, 2000). In the present study, the sectorial rim area was regressed against the corresponding sectorial disc area. It is unknown how this method might have contributed to the between- sector variability of the rim area. However, if the rim is indeed variable regionally and remains highly correlated with the disc area, as previously suggested (Budde *et al*, 2000), then this approach is the most appropriate to express the true correlation between rim and disc areas and must have improved the results of the sectorial regression analysis.

The high sensitivity specificity scores reported in the present study could be attributed to the expertise of the three observers in assessing the disc and cup areas. Moreover, the disease discrimination scores might be overestimated because of the inclusion of patients with moderate and advanced glaucomatous visual field loss in the sample of glaucoma patients. As expected, a lower diagnostic precision was estimated for the preperimetric patients. However, the diagnostic outcome based on the early glaucoma cases might have been influenced by the small sample size of the preperimetric group and the fact that this group was defined by subjective diagnosis of a single expert ophthalmologist.

It is also important to consider that these results would vary with the definition of the cup and the method of assessment employed in every study. The present study

employed computerised planimetry and the definition of the rim was performed by subjective evaluation. The results of the present study can compare only with other studies that have used similar definition of the rim areas. Also the cup boundaries were determined with stereoscopic viewing of the fundus photographs at the level of the scleral canal which can differ from monoscopically derived measurements. In addition, the planimetry software employed in this study performed a segmentation of the disc using the cup rather than the disc centre, which could have influenced the results of the segmental analysis. The segmentation model can be a source of small discrepancies between the measurements of different techniques however; this factor is yet to be determined.

The scatter of the values and therefore the width of the prediction interval for normality could be further reduced by increasing the number of normal subjects and possibly by controlling for parameters of normal variability such as the age, the gender and racial characteristics of the participants (Caprioli *et al*, 1987). It is noted that both groups investigated in this study featured average disc sizes and were mostly Caucasian although the patients were not specifically selected according to their ethnic classification. Moreover, the sample of glaucomatous discs analysis in this study did not include discs with special configuration such as highly myopic and severely tilted discs, which might even suggest another limitation referring to the degree the analysed discs were representative of the discs evaluated in clinical setting.

7.5.5 The diagnostic value of the rim configuration

The ISNT rule was verified on average across the three observers in a proportion of 13% of the normal study group and 6% of all glaucoma patients with moderate to advanced glaucoma by evaluation of 10 and 30 degrees sectors respectively. Consequently, the diagnostic power of the ISNT comparison in the diagnosis of patients with moderate glaucoma was rather poor with a mean scored diagnostic precision of 62% (range 61 - 63%) and very low specificity (11%). This finding could be attributed to the normal variability in the rim configuration among healthy eyes that is pronounced between populations of different ethnic background (Jonas *et al*, 2003) but could also be prominent between different samples of the same population.

The diagnostic precision was not markedly improved when evaluating the Inferior and Superior segments only (inferior greater than superior indicating normality) with the highest score being 65% for observer 2 for the analysis of the 30 degrees sectors. The I>S condition was verified on average across the three observers in a proportion of 56% (10 degrees sectors)and 59% (30 degrees sectors) of the normal study group, thus was associated with a maximum specificity of 65% by evaluation of 30 degree sectors. However, this condition was also found on average, in 38% of the glaucoma patients suggesting a maximum sensitivity score of 72%. A previous study that evaluated the rim width ratio I/S across a group of glaucoma patients reported comparatively lower sensitivity scores, namely a sensitivity of 25% and 11% at fixed specificity of 80% and 95% respectively (Jonas, Budde *et al*, 2004). Although the present study did not evaluate the rim width but the rim area across the two sectors, in both cases the glaucoma group included

eyes with high pressure and diffuse pattern of rim loss so this is not a source of the discrepancies noted between the studies.

7.5.6 Possible limitations for the quantification of the sectorial rim width

For the investigation of the diagnostic value of the rim configuration, the possibility that the optic discs might have been recruited on the basis of the ISNT rule can not be excluded. In that case, our sample would include greater number of glaucomatous discs that fail the ISNT rule and our evaluations could be biased. Moreover, in making the comparison of the relative width of the inferior, superior, nasal and temporal neuroretinal rim segments for the discrimination of normal from glaucomatous eyes in early to moderate glaucoma, we used a robust definition of glaucomatous damage based on the presence of characteristic optic disc cupping and the presence of a corresponding visual field defect. Since the presence of visual field defect would indicate the presence of moderate to advance disease, our dataset would contain patients with moderate rather than minimal damage. Therefore, the sensitivity scores would be expected to be overestimated.

The present analysis was based on a dataset of discs with definite features of glaucomatous damage by optic disc analysis and all cases with suspicious disc appearances had been were excluded in the preliminary stages of the study. The selection criteria for the study could have biased the results if the ISNT rule is likely to be more helpful in cases where glaucoma abnormality is not easy to determine.

Similarly, the recruitment of glaucomatous discs on the basis of visual field loss would tend to identify discs with focal loss. In such cases, the evaluation of ISNT

rule could be misleading for the diagnosis of glaucomatous damage because the rim configuration would be very similar to normal. However, the regression analysis results suggested that the sample of glaucomatous discs investigated in the present study included a high percent of cases with diffuse loss.

The precision with which the measurements are made also appeared to have little significant effect on the outcome of the ISNT evaluation. Disc diagnosis did not include an intermediate category, thus in cases where the rim estimates in any given sector were equal the comparison returned false and the ISNT rule was not satisfied. However, in a subsequent analysis in which equivalence of sectors was considered to verify the ISNT rule, the estimated diagnostic precision did not show a significant improvement.

The usual way in which the ISNT comparison is used in clinical practise is based on subjective evaluation as opposed to quantitative results. It is therefore likely, that subjective comparison is based on broader defined sectors or possibly the evaluation of the temporal rim configuration only. However, comparative evaluation of the rim width based not on the observers' subjective judgments and not on planimetric measurements would be expected to result in further reductions of the diagnostic precision due to the variability inherent with the subjective assessment of the rim configuration.

Finally, an important limiting factor in the study could be the limited sample size. While this is similar to many studies comparing the efficacy of diagnostic approaches in the detection of glaucoma cases, it is possible that selection bias

might have influenced the results to such extent that it would be difficult to extrapolate them to the general population.

7.6 Conclusion

The difficulty associated with the definition of the cup borders is evident in the small variability showed for the regression slopes of the normal rim against the normal disc areas, as defined by the three expert observers.

The data presented in this chapter suggest that the use of the ISNT comparison rule has limited diagnostic power in the detection of glaucomatous optic neuropathy. Since the ISNT rule may have been applied in the initial referral of the patients in this study to the hospital eye service, it is likely that this would have enriched the glaucoma group with cases that failed the ISNT rule and had a positive diagnosis of glaucoma. For this reason, selection bias would strengthen the conclusions of this study, which is that the ISNT rule should be applied with caution when excluding the presence of glaucoma.

On the basis of the present study, it could be argued that an abbreviated form of the ISNT rule, may yield a better diagnostic value in the detection of glaucomatous discs. The condition I>S was associated with the highest sensitivity scores of all the conditions investigated in the study. However, characterisation of the rim configuration and/or quantification of specific sectors in glaucomatous eyes don't yield adequate diagnostic power.

It is concluded that the detection of subjective indicators of damage, deviation of vessels, loss of tissue under vessels, exposure of the lamina cribrosa and focal thinning of the neuroretinal rim may be more valuable signs for the detection of disease. Alternatively, quantitative analysis based on the size of the optic disc (for example the linear regression analysis) can facilitate a more reliable comparison of the neuroretinal rim area and could be optimally incorporated in the computer stereoscopic system supporting subjective glaucoma diagnosis.

Chapter 8 General conclusions and proposals for future work

8.1 General conclusions

8.1.1 Clinical evaluation of threshold response in Short-Wavelength Automated Perimetry

The normal variability incorporated in SWAPPAC leads to underestimation of the magnitude of the statistical significance both of the TD and of the PD values compared to W-W perimetry, thereby compromising the current technique in the investigation of OHT and POAG. While the technique shows promise, there are inherent limitations of the algorithm confounding the widespread clinical application of the method in the identification of early glaucomatous damage.

8.1.2 Comparison of monoscopic and stereoscopic computer assisted planimetry in the evaluation of the normal and glaucomatous optic nerve head

At the onset, it was hoped that this method of computer-assisted planimetry would compliment the subjective diagnosis of glaucoma in the clinical setting enabling quantitative analysis with easy and cost effective stereo view. The availability of stereoscopic and monoscopic observation with the same technique permitted the evaluation of a known source of discrepancies between studies of planimetry. As expected, the change in viewing settings certainly affected the planimetry results for the definition of the cup area. A set of glaucoma damage discs that showed an increased difficulty of diagnosis under monoscopic assessment was for discs with glaucomatous rim notch.

Stereoscopic view can improve the accuracy of the quantitative evaluation of the ONH in glaucoma by better definition of the cup. Although intrarobserver variability in determining the cup borders remains greater than the variability on disc border demarcation with stereoscopic planimetry systems, the element of stereoscopic viewing allows the assessment of the cup on the basis of contour and not colour and facilitates the observer in the use of additional retinal features, like the change of course of the vessels, to interpret retinal topography.

The computer planimetry system presented in this study provides planimetry measurements that are magnification corrected and most importantly, it has been proved to be a highly user friendly technique through evaluation by clinical staff. The interactive feature of the software allows interobserver variation of the measurements but this can be limited with training.

8.1.3 Clinical evaluation of peripapillary atrophy in normal and glaucomatous eyes

The better understanding of glaucomatous pathology has highlighted the factors that large interobserver variability of assessments and overlapping results between normal and pathological eyes yield the main limitations for the quantification and zonal description of PPA.

Familiarising the clinicians with the PPA features and masking the ONH features while assessing the peripapillary retina could improve interobserver variability and limit the diagnostic bias.

8.1.4 Quantitative analysis of the neuroretinal rim for the discrimination of normal and glaucomatous discs

Quantitative analysis of the rim area with linear regression analysis based on the size of the optic disc facilitates the reliable evaluation of the neuroretinal rim width. Comparisons of sectorial rim measurements obtained with custom planimetry software improved the discrimination of glaucomatous damage, but the increased confidence limits for normality suggest that even with quantitative analysis the earliest signs of diffuse rim loss may be overlooked.

The normal variability in the configuration of the rim also confounds the within-subject subjective and / or quantitative evaluation of the rim configuration between different regions of the same optic disc. Subjective diagnosis based on established knowledge of the normal anatomical distribution of the nerve fibres within the ONH, as incorporated in the empirical ISNT rule and accounting for the rim sectors that are most likely to be effected at the earliest stages of glaucoma, was proven not a good indicator of glaucomatous damage.

8.2 Proposals for future work

8.2.1 Normative database of optic disc stereophotographs

Quantitative analysis of the rim area as a discriminating factor for glaucomatous damage relays on the values of a normative database (Caprioli, 1992; Garway-Heath & Hitchings, 1998; Wollstein *et al*, 1998; Wollstein *et al*, 2000a). However, the measurement discrepancies need to exceed the normal between subject variability in order to be indicative of glaucomatous axonal loss and rim thinning. In addition, planimetry is subjected to measurement errors due to observer variability

in the definition of the optic disc and cup borders. An extended database of ONH planimetry measurements derived from normal eyes as assessed by multiple expert observers could narrow the confidence limits for normality, enable more accurate quantitative analysis and thereby, facilitate clinical decisions. The planimetry software presented in this thesis enables the storage of multiple assessments for the same ONH and could be further programmed so that it can register all planimetry measurements and subsequently perform a statistical analysis on them.

8.2.2 Planimetry of retinal vessels for investigation of glaucomatous changes

The measurement of vessel calliper for the assessment of the retinal vasculature has been used for the identification of the earliest changes associated with diseases of vascular aetiology (Flammer, Pache *et al*, 2001; Haefliger, Meyer *et al*, 1994; Hubbard, Brothers *et al*, 1999; Sherry, Wang *et al*, 2002; Stefansson *et al*, 2005; Wang, Mitchell *et al*, 2004; Wong, Klein *et al*, 2004). Computer assisted techniques are currently available to perform automated tracing of the vessel width and multiple measurements along the course of the vessels over a wider area of observation (Gang, Chutatape *et al*, 2002; Knudtson, Lee *et al*, 2003; Owen, Ellis *et al*, 2002; Pedersen *et al*, 2000; Sherry *et al*, 2002; Suzuki, 1995). Glaucoma has been associated with vascular changes, (Flammer, Orgul *et al*, 2002; Garhofer, Zawinka *et al*, 2004) although there are controversies regarding the findings of previous planimetry studies on vascular constriction (Hall *et al*, 2001; Jonas, Nguyen *et al*, 1989b; Papastathopoulos & Jonas, 1999; Rankin & Drance, 1996). A software function for semi-automated assessment of the vessels' diameter incorporated in a stereoscopic planimetry system would enable clinical research

studies to elucidate regional changes of the retinal vasculature across the glaucomatous retina in association with topographic measurements of the ONH.

8.2.3 Detection of glaucomatous progression with stereo chronoscopy and chronometry

Glaucomatous progression can be optimally identified with assessment of a serial of optic disc images obtained longitudinally (Heijl, 1989; Quigley, 1985; Takamoto & Schwartz, 1985). Computerised stereo chronoscopy and chronometry utilise stereoscopic viewing to obtain an enhanced perception of the optic disc topography and perform quantitative analysis in order to identify the smallest structural changes due to glaucomatous pathology (Barry *et al*, 2000; Berger, Patel *et al*, 2000). Modern imaging techniques are concerned with the detection and also with the efficient follow up examination of glaucoma patients. The clinical application of the stereoscopic planimetry system presented in this thesis would be more complete with the addition of such progression analysis features. The current technical features of the custom planimetry system in reference enable real time stereoscopic presentation of ONH image pairs and provide an automated record of magnification corrected measurements of the optic disc features within segments of 5 degrees. Additional programming could enable the statistical comparison of serial planimetry measurements and facilitate the subjective diagnosis of glaucomatous progression.

Appendix

StereoDx

Research Version 2.1b

©Cardiff University

UK

2004

Contents

Introduction	1
Entering the program	4
Adjusting the image presentation	8
Adjusting the stereoscopic viewing	8
Creating Contour lines	11
Calculation procedure	13
Automated analysis	14
Adjusting the contour lines	16
Assessment of the retinal properties	18
Recording the assessment	19
Continuing the program operation	19
Closing the program	20
Appendix: file output format	i-vi

List of figures

Figure 1 The stereo viewer control panel 5

Figure 2 Observer registration 5

Figure 3 Image retrieval 6

Figure 4 The Scale Window 7

Figure 5 The alignment command 8

Figure 6 The line control panel 9

Figure 7 The "save alignment" command 10

Figure 7 The password entry window 10

Figure 8 Data point application. 11

Figure 9 Assessment of the ONH parameters 12

Figure 10 Calculation output 13

Figure 11 Automated analysis windows 14

Figures 12 A, B and C Segment lines control panel 15

Figure 13 Rim line definition 16

Figure 14 Line cursor 18

Figure 15 The save assessment command 19

Figure 16 The exit programme command 20

List of tables

Table 1 The scaling parameters i

Table 2 Global areas i

Table 3 5 Degrees segmental measurements ii

Table 4 30 Degrees segmental measurements iii

Table 5 Disc data points coordinates v

Table 6 Rim data points coordinates vi

Introduction

StereoDx is a stereo-enabled interactive program for the viewing and analysis of stereoscopic images. It can display pairs of true colour bitmap images with the same size (in pixels) including up to 1280 pixels. Images of larger size can also be displayed but are limited by graphics card limitations. The system operates under Windows 2000 and is disabled under Windows 95, XP or NT because of the requirement to link with the OpenGL graphics library which has been used to render in stereo. The system is also capable to operate under Windows 98 but stereo support may be variable.

This manual contains only brief instructions on how to use the program. Not all the features of the program are covered but can be described on an ad hoc basis depending on the aims of any given project.

In order to install the software, the stereo.exe file has to be transferred to the destination folder, preferably under the C:/ drive. No other files need to be installed. StereoDx should enable stereo quad buffering automatically, provided the graphics card already installed in the PC is stereo enabled. For the purpose, please consult the documentation for the graphics card. The program is enabled for stereo-viewing both with Crystal Eyes Shutter glasses and with the Z screen (2000 and 2000i) from Stereographics (www.stereographics.com). Images are rendered in quad buffered format without compression and therefore the monitor refresh should exceed 100 Hz for flicker free stereo.

Image file names

Images should be stored as JPEG files. The program uncompresses these files and converts them to a stereo-format files (the extension for these files is *.tcg). Note that the *.tcg files are uncompressed and therefore will take up a lot of disc space (c. 5MB per eye). These files can be deleted if required but they will be generated again next time the same *.jpg files are opened. As the JPEG file is unpacked and the *.tcg file is created there is a slight time delay. The *.tcg file is a custom format and cannot be opened with commercially available graphics packages.

The program identifies only files with the naming convention ***filenumbernp.jpg***, where the *file number* is a string specific for the file e.g. *a00001*; *n*: determines the eye side specified as L or R and *p*: determines the stereo-pair image specified as l or r lowercase characters.

Example

a00001Lr.jpg is the right hand stereo-image for the left eye from patient *a00001*. Note that in Windows the file extensions can be obscured in explorer and files can be given double extensions if named manually e.g. a00001Lr.jpg.jpg. These files will not load.

When loading two images for a stereo-pair of a patient's left eye the following files need to be selected:

a00001Lr.jpg and a00001Ll.jpg

Conversely, for the images derived from the right eye of the same patient, the following images need to be selected:

a00001Rr.jpg and a00001Rl.jpg

When selecting a single image, the program assumes that it is a simultaneous stereo-pair (e.g. from the Nidek 3DX or Discam). This would result into a single image to split into the respective stereo-pairs and displayed in stereo.

Scaling factors

The program provides retinal measurements in true dimensions (mm) only if the images have been retrieved with the Nidek 3Dx. Using this camera and as long as the images of the slide film are digitised in full frame, the images are scaled correctly based on keratometry and refraction settings for the eye. While for dimensionless variables such as CD ratios the measurements will be accurate regardless of scaling for all other images the measurements although displayed in mm will not be accurate. For the magnification formula registered in the program, the camera settings for the Nidek 3DX were taken from the work by Rudnicka *et al* (1998) and the algorithms for correcting the scaled images were taken from the work by Garway-Heath *et al* (1998).

The coefficients for any camera can be inserted into the software so that the images can be appropriately scalled. In particular, the 'a' and 'b' coefficients need to be known variables and in most cases, these values can be retrieved from the Rudnicka paper (1998) taking into account if the camera is telecentric or not. For

images that are film based, the size of the digitised area should also be calculated and the images should not be cropped prior to loading in StereoDx.

Latest revision: 10.2.04 2.1b.

Starting the program
Double click on the desktop shortcut: **StereoDx** .This introduces you to the program opening a control panel window named **Stereo viewer** (Figure 1).

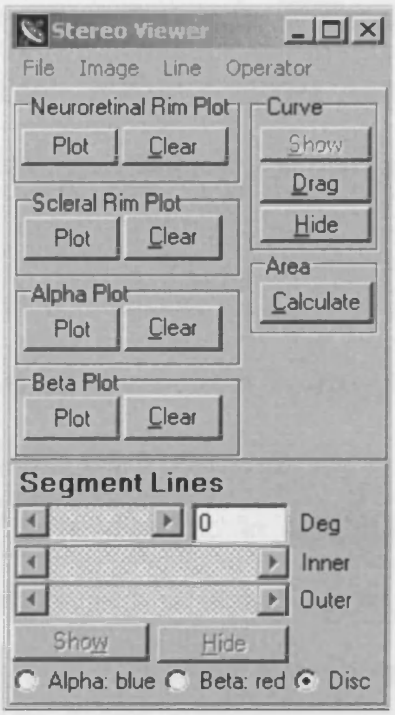

***Figure 1** shows the main control panel.*

Stereo viewer

Click on **Operator,** select **Sign in** and type in the code name of the operator i.e. name initials.

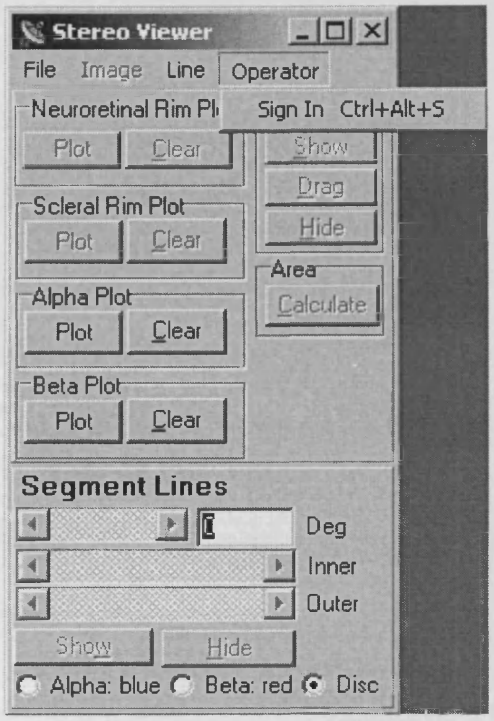

***Figure 2** shows the stereo viewer expanded for the operator's registration.*

A folder is automatically created in the C drive, named after the operator's code name hosting the saved observations.

Click **File** and select **Open** to go to the appropriate computer location that is the source of the images.

ex. **C: / Stereoimages/Joanna/**

Select and **open** a set of images that share the same ID number (**Figure 3**).

ex. IDNO **LL** & IDNO **LR** or IDNO **RL** & IDNO **RR**

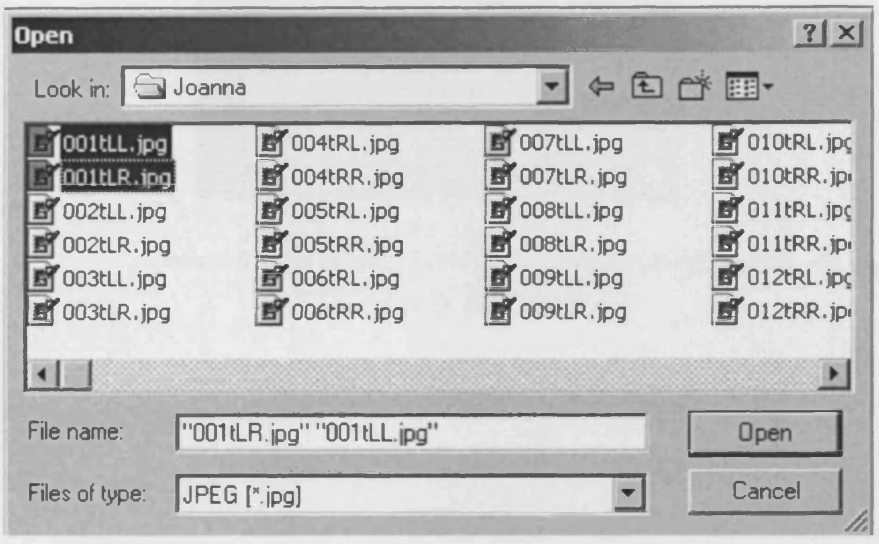

***Figure 3** shows the stereo-pair of an image selected to be viewed through the system.*

The program reads the image files and generates two new windows on the screen: **Scale Window** and **Stereo Window.**

The **Scale Window** lists the refractive parameters of the patient and sets the appropriate scaling of the measurements derived for real retinal size.

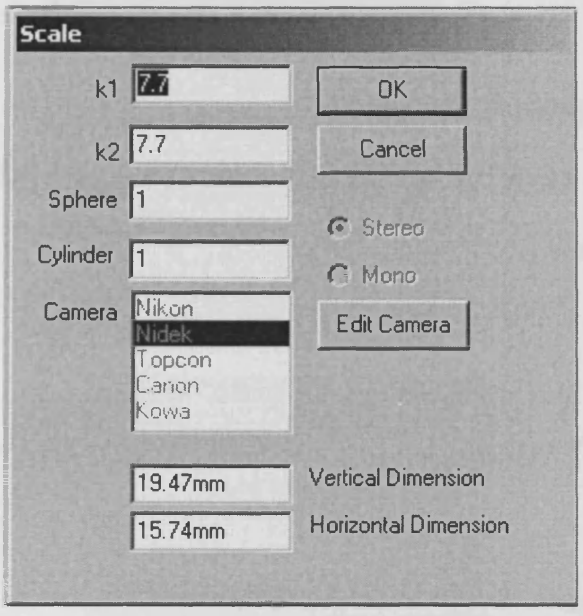

Figure 4 *shows the scale window that lists the ocular refractive parameters used in the magnification correction formula i.e. the principal corneal curvatures and spherical correction.*

Click **OK** at the **Scale Window** to close it down after applying any necessary alterations. The scaling parameters are saved together with the stereo images for a given eye. The *edit camera option* is temporarily unavailable as the system is locked for use with Nidek images only.

The **Stereo Window** presents the selected images.

The ID number of the displayed images and the name of the active operator's account are shown at the bottom margin of this window, throughout the assessment.

Adjusting the presentation

At the stereo viewer, **click** on **Image** and select **Stereo/Mono** to shift from stereoscopic to monoscopic view and vice versa.

Adjusting the stereoscopic presentation

At the stereo viewer, **click** on **Image** and select **Align,** to adjust the image set for comfortable stereo view.

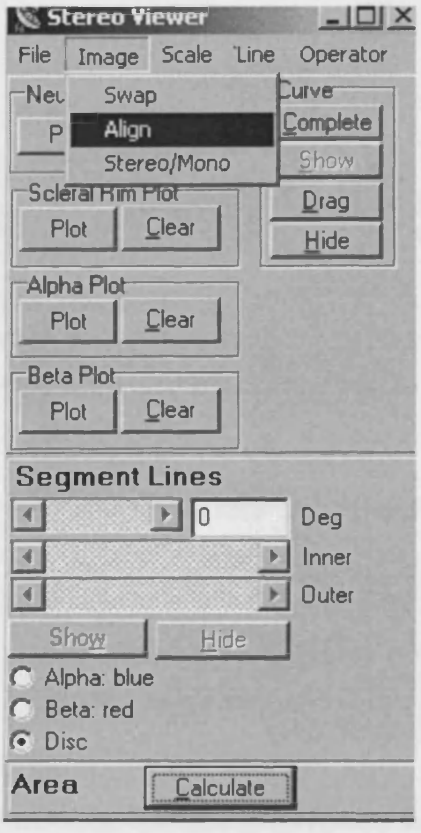

***Figure 5** shows the expanded control panel while adjusting the image presentation.*

The Stereo viewer panel expands automatically into the **Line control** section.

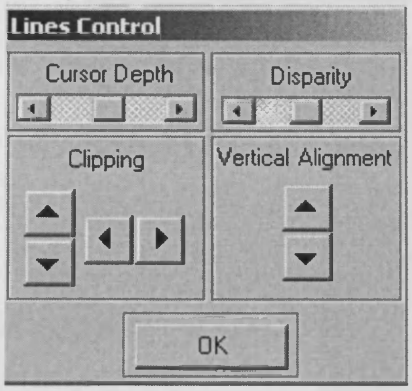

Figure 6 *shows the control panel options added for the adjustment of the images and the cursor depth.*

The revealed double cursors for **Disparity** and **Vertical alignment** reposition the images accordingly. The set of images can be aligned using the **Line control** buttons alternatively. For comfortable stereo view, the stereo pair is set at minimum disparity i.e. appearing almost as a single image when viewed without the special filters. Excess stereo effects are easily induced causing a lot of fatigue for the operators.

The new panel also facilitates the adjustment of the apparent **Cursor Depth** in correlation with the retinal plane. At various depth positions the cursor can outline the ONH structures without parallax effects. The cup is optimally defined as the intersection of a plane at the level of the scleral rim with the surface of the retinal nerve fibre layer.

Click on **File** and select **Save Alignment**. In order to save all the adjustments you have applied, you need to gain access to the alignment files using a password. At the new **password window,** type the word "*password*".

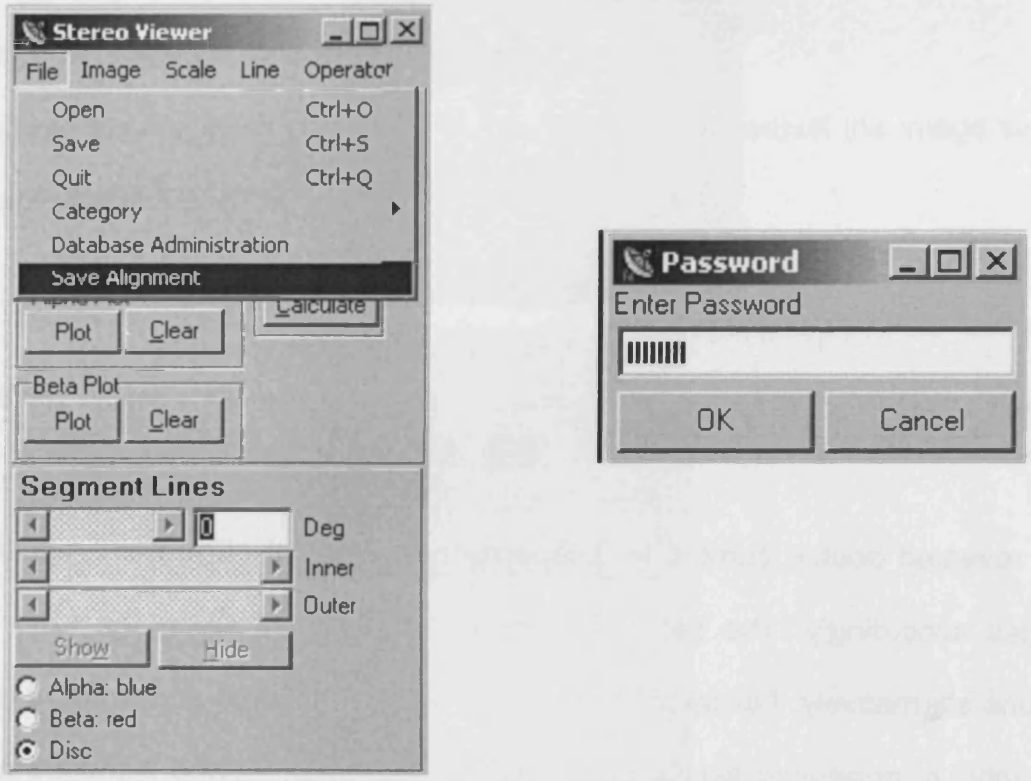

Figure 7 *shows the expanded control panel after applying the adjustments for the image presentation and the new window in which the password is recorded.*

Contour lines

Movements of the mouse direct the cross cursor on the areas of interest. Left clicks at the mouse control add reference points for the contour lines (figure 8). Right clicks will move the entire image. Scrolling the mouse wheel will zoom in and zoom out. Measurements can be made at any zoom level; these measurements will be correctly scaled.

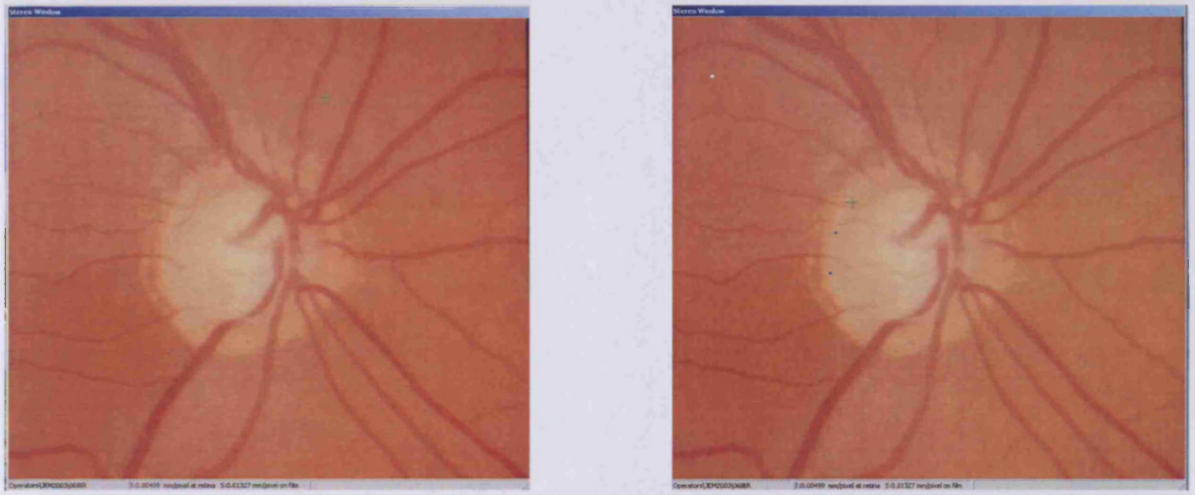

Figure 8 *shows an image displayed at the stereo-window before the assessment (left) and after the application of the first data points in the process of demarcating the disc margin (right).*

A random order may be followed for the demarcation of all the ONH parameters.

At the Stereo viewer,

- select **Plot,** under **Scleral rim,** to draw the disc margins.
- select **Plot**, under **Neuro-retinal Rim,** to draw the cup margins
- select **Plot** under **Alpha** & **Beta** to draw the areas of atrophy.

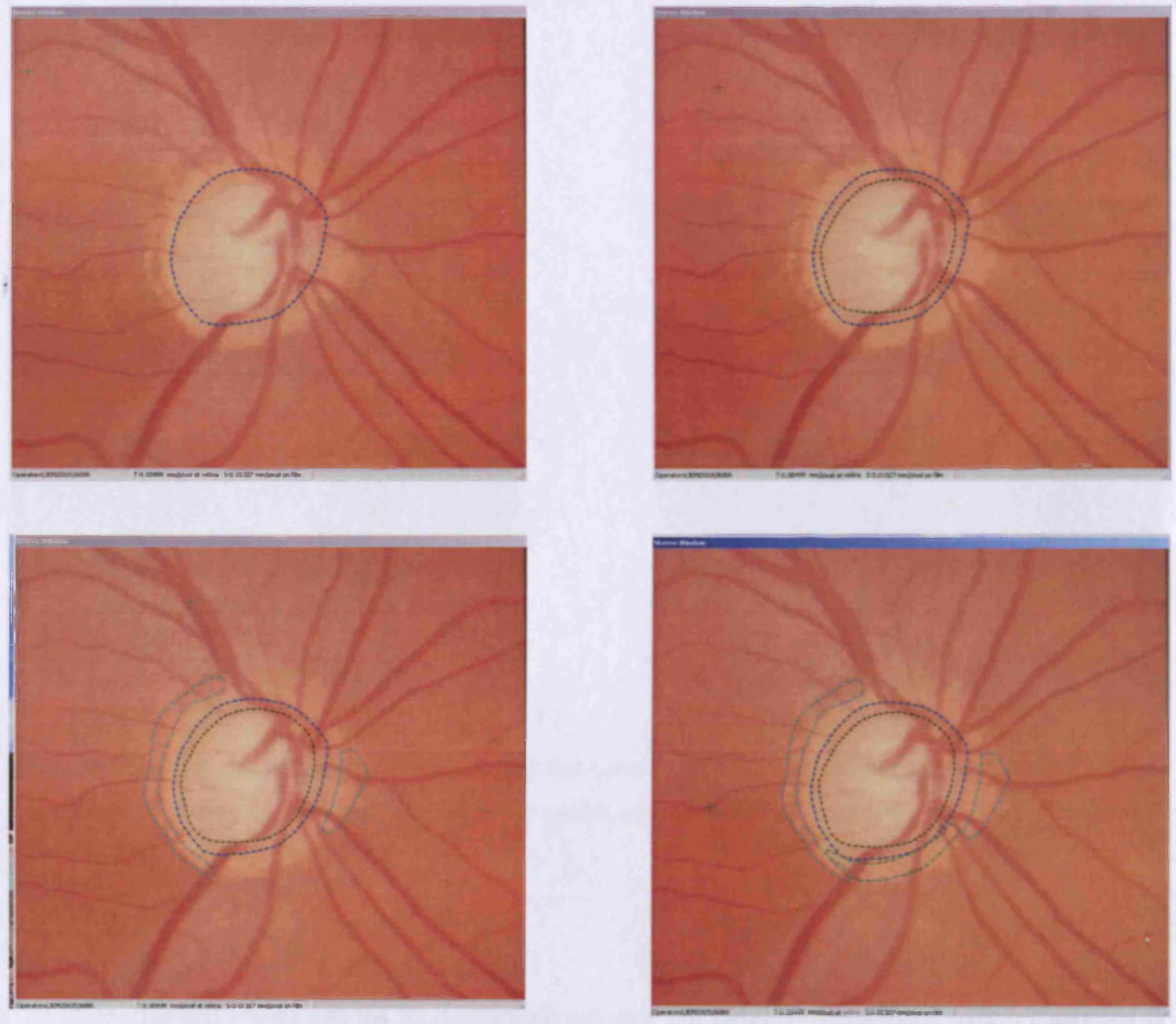

Figure 9. Drawing steps in the *assessment of an image: The disc contour line (top left), both the disc and cup contour lines (top right), the added contour lines for the areas of alpha (bottom, left) and beta zone (bottom, right) peripapillary atrophy as demarcated by a single operator. The contour lines for all presented areas of interest are colour coded.*

The areas of atrophy need to be plotted with care as this part of the software is added for research purposes only and has rudimentary functionality.

Using the **CLEAR** and **PLOT** buttons alternatively for each parameter, the operator may discard and/ or correct the drawn contour lines.

Calculated ONH parameters

At the Stereo viewer, select **Calculate** for the evaluation of the plotted areas.

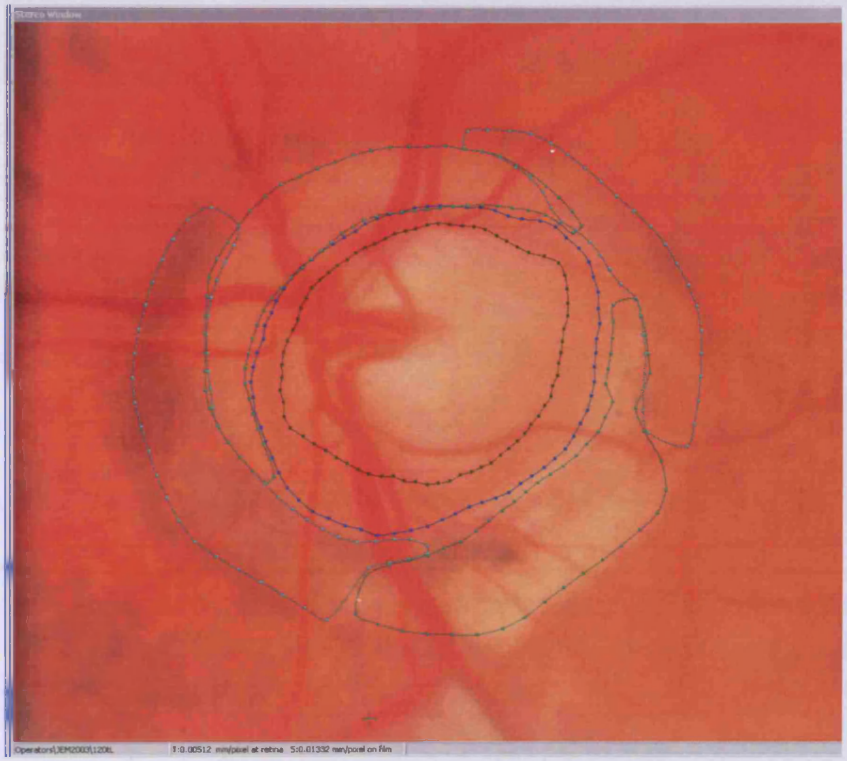

Figure 10 *shows the contour lines of the ONH structures as displayed after the calculating process.*

Calculations are simultaneously performed and the summaries of the derived planimetric measurements are recorded in the form of a file saved under your private operator account (see appendix).

Analysis

Two new windows are automatically generated after the calculation process, appearing next to the Stereo window. Note that the database function needs to be fully installed before becoming automatically available. Otherwise, the plot window can be closed without problems at this part of the analysis.

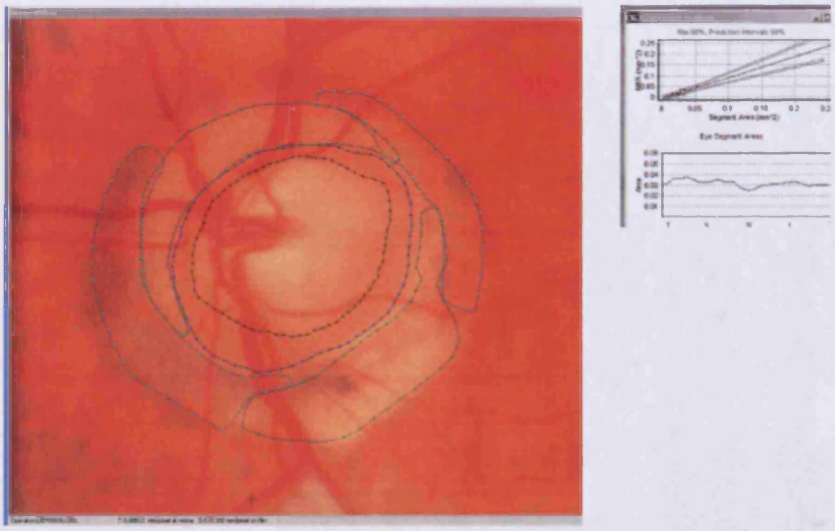

Figure 11 *shows a stereoscopically assessed image after the calculation of the disc and cup and peripapillary atrophy areas together with the windows of the simultaneous regression analysis of the measurements.*

The outlines of the cup and disc areas are shown on a cross axis chart in the **Mini GL window** (figure 12).

Figure 12 *shows the 'Mini GL window'.*

At the segment line panel

A line cursor rotating with 5degree intervals determines a direction around the ONH circumference. Direction of Zero degrees corresponds by default to the temporal side of each eye.

At the regression analysis window

The selected segment is statistically analysed in real time. It is noted that some versions of the software do not incorporate all the database functionality to use regression discrimination (version 2.1b).

At the Segment lines control panel

Use the double cursor, to set the direction of the line measurement.

These setting position automatically, the line cursor displayed at the **Mini GL window** and arrange the **regression analysis window** to present the graphical relationship of the rim for the given location.

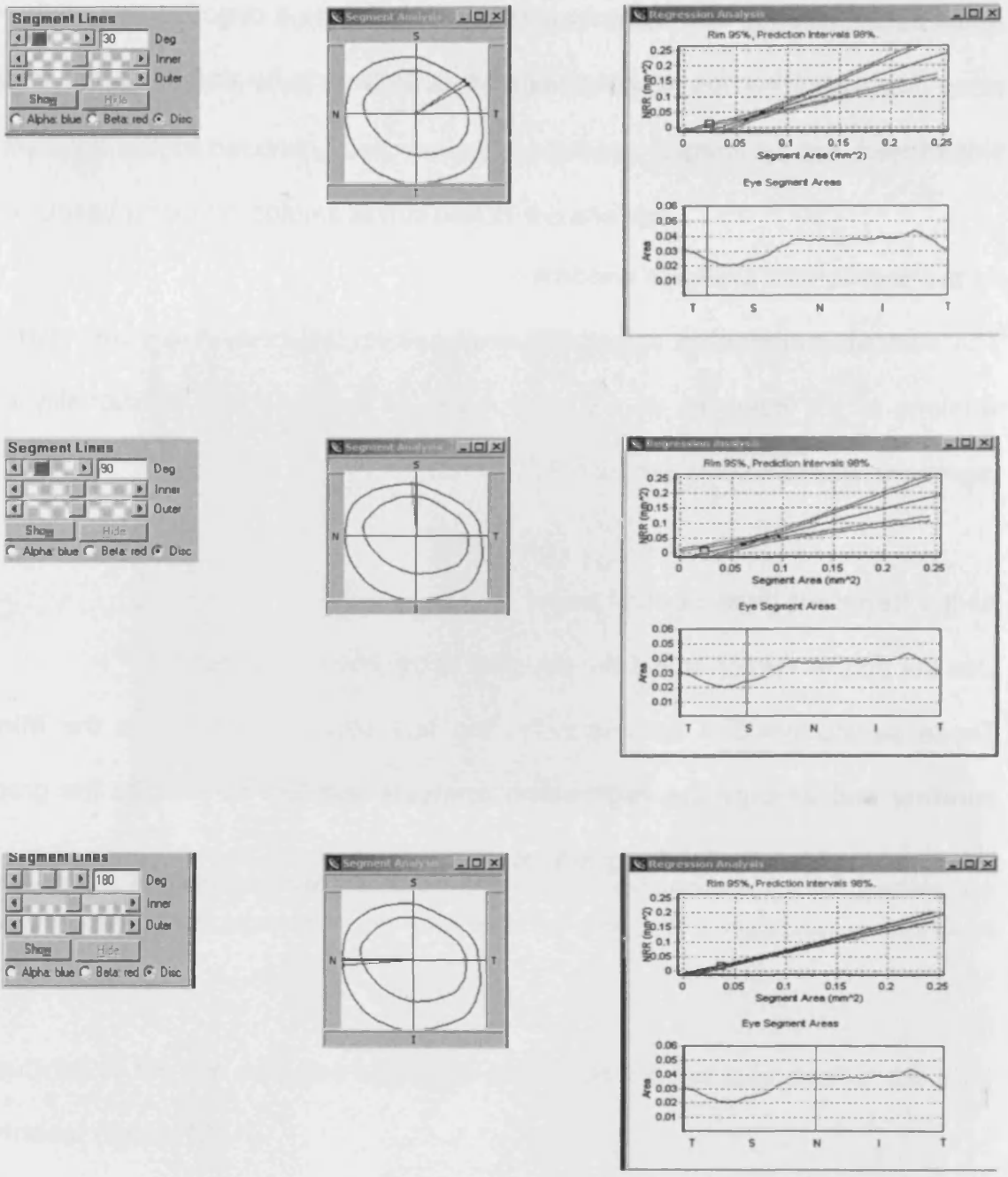

Figure 13 *shows the segment lines panel set to 30, 90 and180 degrees of rotation, the Mini GL window displays the 5-degrees interval at 30, 90 and 180 degrees of rotation, respectively and the Regression analysis function as performed at the Regression analysis window for the same degrees segment of measurement, for a left eye image.*

Adjusting the contour lines

The contour lines may be altered with a dragging function enabled by a right click on the mouse control; this allows for precise delineation of the neuroretinal rim.

For the final definition of the contour lines use the **Segment lines** control panel in the stereo viewer.

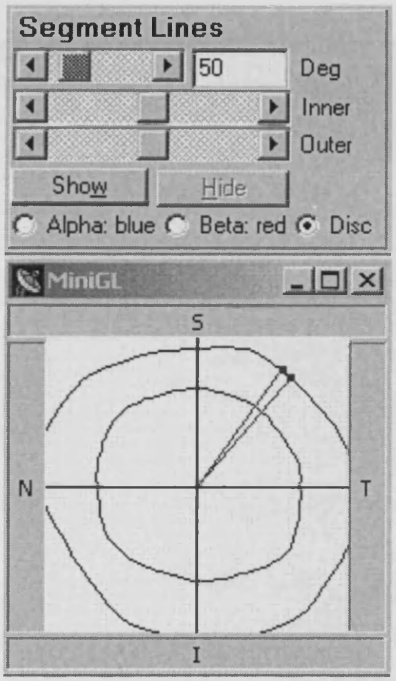

Figure14 *Adjusting the top cursor to" 50", the Mini GL Window displays the 50 degrees segments of measurement.*

At the stereo viewer

under Curve, click on **Hide** to make the contour lines at the stereo window disappear.

At the Segment lines control panel

Click on **Show** and

- Select **Alpha**, for the display of the margins of the Alpha zone.
- Select **Beta**, for the display of the margins of the Beta zone.
- Select **Disc**, for the display of the margins of the disc.

At the **Stereo window**, the contour lines are replaced by a line cursor that connects the outer most to the inner most margin of the selected area, corresponding to a given direction around the 360 degrees of the optic disc with 5 degrees intervals of rotation.

At the Segment lines control panel

Use the double cursor to set the direction of the line cursor. These settings will automatically position the line cursor displayed at the Mini **GL window** and arrange the **regression analysis window** to present the graphical relationship of the rim for the given location.

At the **Segment lines control panel** the next set of double cursors facilitate a modification of the contour lines by adjustments of the line size.

Select **Show** or **Hide** to make the line cursor appear and disappear on the Stereo widow respectively and switch to the display of the different areas.

Assessment of the retinal properties

At the Stereo viewer,

Click on **Line** and select **Draw Line.**

This command activates an independent cursor that enables to draw a size-controlled line at any location of the retina.

Figure 15 *shows a line drawn perpendicular to the temporal CRV.*

The size of the line is calculated in real time and the value is recorded at the bottom margin of the Stereo window, next to the scaling ratio (mm/pixels) applied for the film and retinal image.

Magnification is provided with the scrolling function of the mouse cursor, enabling a closer view of the areas of interest.

Recording the Assessment

At the stereo viewer

Click on **File** and select **Save** to record your assessment (Figure 17). The assessment is automatically saved in the operator's account.

***Figure 17** shows the stereo viewer as it is expanded to display the saving file command.*

Continuing the program operation

Close down all three windows: **Stereo window, Regression analysis window** and the **Mini GL window**

At the stereo viewer

Click on **File** and select **Open** to obtain a new set of images, restarting the above procedure.

This time, there is no need to sigh in your personal account again as the programme reserves that information from the previous session.

Closing the program

At the stereo viewer

Click on **File** and select **Quit** (Figure 15), exiting both the program and your operator account.

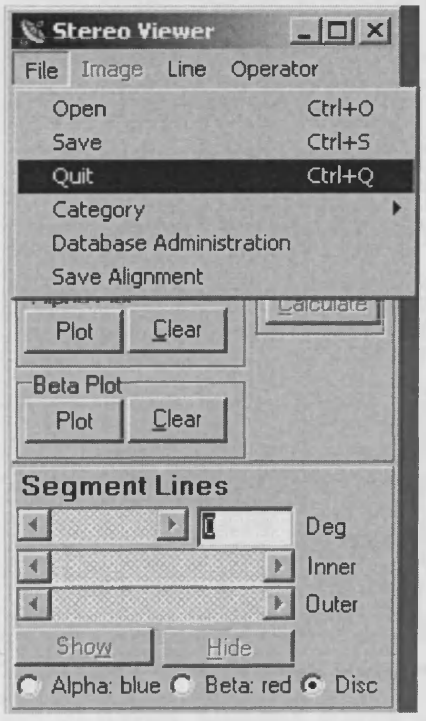

Figure 16 shows the stereo viewer as expanded to display the quitting the program command.

Appendix

Abbreviations

The planimetric parameters in the file are described with abbreviations.

Degree	degree at which measurement is made. 0 - 5 degrees is plotted under 0 degree, 5 - 10 under 5 degrees etc.
CupSeg	segmental area for the cup at the indicated degree
NRRSeg	the neuroretinal rim segment area
DiscSeg	the sum of the CupSeg and NRRSeg areas
ASeg & ***BSeg***	the peripapillary atrophy areas for alpha zone and beta zone, respectively

The '**D**' prefix refers to digital units for the various measurements prior to scaling. And all areas are given in mm^2.

File output format

C/D ratios (adjusted for eye side):
18/06/2003 10:46:56
Operator: Operators\JEM2003\
Root: C:\StereoImages\
Right: C:\StereoImages\Joanna\001tLR
Left: C:\StereoImages\Joanna\001tLL

Camera: NIDEK
Cylinder: = 0.00
Sphere: = 0.00
Rad1: = 7.89
Rad2: = 7.74
t: = 0.0049 *-these are size conversion factors*
t^2: = 0.0000 - *these are size conversion factors*

Table 1 *shows the scaling parameters*

----------Data summary----------
Cup Area: 1.4201 dig 59445 *-dig refers to pixel count in the image. multiplying a pixel count by a conversion factor will give true dimensions or areas*
Rim Area: 1.3197 dig 55241
Disc Area: 2.7398 dig 114686
Alpha Area: 0.0000 dig 0
Beta Area: 0.0000 dig 0

Table 2 *shows the global areas*

The following represents a summary of the disc segmental measurements (table 3).

Degree	DcupSeg	DNRRSeg	DdiscSeg	CupSeg	NRRSeg	DiscSeg	DASeg	DBSeg	Aseg	Bseg
0	867	602	1469	0.02071	0.01438	0.03509	0	0	0	
5	840	547	1387	0.02007	0.01307	0.03314	0	0	0	
10	826	545	1371	0.01973	0.01302	0.03275	0	0	0	
15	818	532	1350	0.01954	0.01271	0.03225	0	0	0	
20	801	523	1324	0.01914	0.01249	0.03163	0	0	0	
25	775	530	1305	0.01851	0.01266	0.03118	0	0	0	
30	752	543	1295	0.01797	0.01297	0.03094	0	0	0	
35	743	545	1288	0.01775	0.01302	0.03077	0	0	0	
40	744	514	1258	0.01777	0.01228	0.03005	0	0	0	
45	727	496	1223	0.01737	0.01185	0.02922	0	0	0	
50	721	491	1212	0.01722	0.01173	0.02895	0	0	0	
55	702	505	1207	0.01677	0.01206	0.02884	0	0	0	
60	696	525	1221	0.01663	0.01254	0.02917	0	0	0	
65	700	533	1233	0.01672	0.01273	0.02946	0	0	0	
70	710	548	1258	0.01696	0.01309	0.03005	0	0	0	
75	725	566	1291	0.01732	0.01352	0.03084	0	0	0	
80	751	568	1319	0.01794	0.01357	0.03151	0	0	0	
85	772	564	1336	0.01844	0.01347	0.03192	0	0	0	
90	778	541	1319	0.01859	0.01292	0.03151	0	0	0	
95	817	540	1357	0.01952	0.01290	0.03242	0	0	0	
100	844	537	1381	0.02016	0.01283	0.03299	0	0	0	
105	885	522	1407	0.02114	0.01247	0.03361	0	0	0	
110	913	522	1435	0.02181	0.01247	0.03428	0	0	0	
115	903	557	1460	0.02157	0.01331	0.03488	0	0	0	
120	894	608	1502	0.02136	0.01453	0.03588	0	0	0	
125	898	670	1568	0.02145	0.01601	0.03746	0	0	0	
130	912	742	1654	0.02179	0.01773	0.03951	0	0	0	
135	917	789	1706	0.02191	0.01885	0.04076	0	0	0	
140	945	826	1771	0.02258	0.01973	0.04231	0	0	0	
145	959	875	1834	0.02291	0.02090	0.04381	0	0	0	
150	956	955	1911	0.02284	0.02281	0.04565	0	0	0	
155	931	1047	1978	0.02224	0.02501	0.04725	0	0	0	
160	892	1099	1991	0.02131	0.02625	0.04756	0	0	0	
165	858	1112	1970	0.02050	0.02657	0.04706	0	0	0	
170	831	1124	1955	0.01985	0.02685	0.04670	0	0	0	
175	816	1124	1940	0.01949	0.02685	0.04635	0	0	0	
180	783	1083	1866	0.01871	0.02587	0.04458	0	0	0	
185	784	1011	1795	0.01873	0.02415	0.04288	0	0	0	
190	783	945	1728	0.01871	0.02258	0.04128	0	0	0	
195	782	900	1682	0.01868	0.02150	0.04018	0	0	0	
200	781	873	1654	0.01866	0.02086	0.03951	0	0	0	
205	785	845	1630	0.01875	0.02019	0.03894	0	0	0	
210	788	817	1605	0.01883	0.01952	0.03834	0	0	0	
215	797	794	1591	0.01904	0.01897	0.03801	0	0	0	
220	799	796	1595	0.01909	0.01902	0.03810	0	0	0	
225	767	813	1580	0.01832	0.01942	0.03775	0	0	0	
230	747	844	1591	0.01785	0.02016	0.03801	0	0	0	
235	717	882	1599	0.01713	0.02107	0.03820	0	0	0	
240	698	923	1621	0.01668	0.02205	0.03873	0	0	0	
245	684	973	1657	0.01634	0.02324	0.03959	0	0	0	
250	680	1008	1688	0.01625	0.02408	0.04033	0	0	0	
255	677	1020	1697	0.01617	0.02437	0.04054	0	0	0	
260	705	987	1692	0.01684	0.02358	0.04042	0	0	0	
265	728	968	1696	0.01739	0.02313	0.04052	0	0	0	
270	744	923	1667	0.01777	0.02205	0.03982	0	0	0	
275	787	904	1691	0.01880	0.02160	0.04040	0	0	0	
280	833	880	1713	0.01990	0.02102	0.04092	0	0	0	
285	885	859	1744	0.02114	0.02052	0.04166	0	0	0	
290	947	801	1748	0.02262	0.01914	0.04176	0	0	0	
295	992	747	1739	0.02370	0.01785	0.04154	0	0	0	
300	997	739	1736	0.02382	0.01765	0.04147	0	0	0	
305	1000	762	1762	0.02389	0.01820	0.04209	0	0	0	
310	998	822	1820	0.02384	0.01964	0.04348	0	0	0	
315	976	886	1862	0.02332	0.02117	0.04448	0	0	0	
320	958	953	1911	0.02289	0.02277	0.04565	0	0	0	
325	926	971	1897	0.02212	0.02320	0.04532	0	0	0	
330	910	964	1874	0.02174	0.02303	0.04477	0	0	0	
335	902	918	1820	0.02155	0.02193	0.04348	0	0	0	
340	901	811	1712	0.02152	0.01937	0.04090	0	0	0	
345	882	722	1604	0.02107	0.01725	0.03832	0	0	0	
350	868	658	1526	0.02074	0.01572	0.03646	0	0	0	
355	835	572	1407	0.01995	0.01366	0.03361	0	0	0	

Table 3 *shows the calculated areas of the ONH planimetric parameters in 5 degrees intervals.*

Degree	Cup Digits	NRR Digits	Disc Digits	Cup	NRR	Disc
0	4927	3279	8206	0.11771	0.07833	0.19604
30	4389	3094	7483	0.10485	0.07392	0.17877
60	4354	3304	7658	0.10402	0.07893	0.18295
90	5140	3219	8359	0.12279	0.07690	0.19970
120	5525	4510	10035	0.13199	0.10774	0.23973
150	5284	6461	11745	0.12623	0.15435	0.28059
180	4698	5657	10355	0.11223	0.13514	0.24738
210	4615	4946	9561	0.11025	0.11816	0.22841
240	4172	5879	10051	0.09967	0.14045	0.24012
270	5188	5114	10302	0.12394	0.12217	0.24611
300	5855	5133	10988	0.13987	0.12263	0.26250
330	5298	4645	9943	0.12657	0.11097	0.23754

Table 4 *shows the calculated areas of the ONH planimetric parameters in 30 degrees intervals.*

Tables 5 and 6 give the co-ordinates for the rim and the disc respectively. This has been added as a research function and the measurements are presented in an unrefined format.

Contour line of the Disc margins

Points72 x/y curve coord

157.0 12.0
154.0 27.0
151.0 42.0
147.0 57.0
141.0 71.0
134.0 85.0
126.0 98.0
117.0 110.0
108.0 122.0
96.0 131.0
84.0 140.0
72.0 148.0
60.0 156.0
47.0 163.0
34.0 170.0
20.0 175.0
6.0 181.0
-8.0 184.0
-23.0 185.0
-38.0 185.0
-53.0 185.0
-69.0 184.0
-84.0 180.0
-99.0 176.0
-114.0 170.0
-130.0 164.0
-145.0 157.0
-161.0 150.0
-175.0 139.0
-188.0 128.0
-201.0 115.0
-213.0 100.0
-222.0 84.0
-228.0 67.0
-232.0 48.0
-232.0 30.0
-231.0 12.0
-226.0 -5.0
-221.0 -23.0
-213.0 -39.0
-205.0 -54.0
-198.0 -69.0
-188.0 -83.0
-179.0 -97.0
-168.0 -110.0
-157.0 -122.0
-145.0 -133.0
-132.0 -144.0
-118.0 -153.0
-104.0 -163.0
-89.0 -170.0
-73.0 -177.0
-57.0 -182.0
-40.0 -182.0
-23.0 -183.0
-6.0 -182.0
11.0 -182.0
28.0 -179.0
45.0 -176.0
61.0 -168.0
76.0 -160.0
91.0 -151.0
106.0 -142.0
121.0 -132.0
136.0 -121.0
147.0 -107.0
157.0 -92.0
164.0 -75.0
166.0 -56.0
164.0 -38.0
162.0 -20.0
160.0 -4.0

Table 5 *shows the coordinates of the plotting points demarcating the disc area.*

Contour line of the Cup margins

Points 72 x/y curve coord

115.0 12.0
115.0 24.0
113.0 36.0
108.0 47.0
105.0 58.0
98.0 68.0
90.0 77.0
83.0 86.0
76.0 95.0
68.0 103.0
60.0 111.0
50.0 116.0
40.0 121.0
30.0 125.0
20.0 130.0
10.0 135.0
-1.0 139.0
-12.0 142.0
-23.0 143.0
-34.0 146.0
-46.0 147.0
-59.0 146.0
-72.0 146.0
-83.0 142.0
-94.0 136.0
-105.0 129.0
-115.0 121.0
-125.0 114.0
-134.0 105.0
-143.0 96.0
-150.0 85.0
-155.0 73.0
-158.0 61.0
-159.0 48.0
-160.0 36.0
-159.0 23.0
-157.0 12.0
-156.0 1.0
-154.0 -11.0
-152.0 -22.0
-148.0 -33.0
-144.0 -44.0
-139.0 -55.0
-133.0 -65.0
-126.0 -74.0
-117.0 -82.0
-108.0 -89.0
-97.0 -94.0
-86.0 -98.0
-76.0 -101.0
-65.0 -105.0
-55.0 -108.0
-44.0 -110.0
-34.0 -114.0
-23.0 -116.0
-12.0 -119.0
0.0 -121.0
13.0 -122.0
26.0 -122.0
40.0 -123.0
52.0 -119.0
63.0 -111.0
74.0 -104.0
83.0 -94.0
91.0 -84.0
97.0 -72.0
102.0 -60.0
107.0 -48.0
111.0 -37.0
114.0 -24.0
116.0 -12.0
116.0 0.0

***Table 6** shows the coordinates of the plotting points demarcating the cup area.*

Digital planimetric evaluation of peripapillary atrophy in normal and glaucomatous eyes

Invest Ophthalmol Vis Sci 2004;45: E-Abstract 5561. © 2004 ARVO

I. Bourtsoukli[1], I.A. Cunliffe[2], R.J. Kumar[3], E.A. Ansari[3], R.V. North[1], J.M. Wild[1] and J.E. Morgan[3]

[1] Optometry & Vision Sciences, Cardiff University, Cardiff, United Kingdom
[2] Opthalmology, Birmingham Heartlands Hospital, Birmingham, United Kingdom
[3] Ophthalmology, University of Wales College of Medicine, Cardiff, United Kingdom

Abstract

Purpose: To investigate the relationship between glaucomatous optic nerve head damage and the extent of peripapillary atrophy (PPA), as assessed by multiple, experienced observers.

Methods: Optic disc images from 43 control subjects (mean age 59.2 years, SD 10.5 years) and 117 patients with early–moderate open angle glaucoma (mean age 65.5 years, SD 10.3) were digitised and analysed by digital stereoscopic planimetry. Patient diagnosis was based on analysis of the optic disc and visual field. Optic disc analysis was performed by 3 ophthalmlologists trained to fellowship standard in glaucoma who were masked to patient diagnosis. Stereoscopic images were viewed using a Z screen (Stereographics Corp.) with quad buffered display (24 bits per pixel true color). Custom cursors enabled neuroretinal rim measurements at the level of the scleral rim. Peripapillary α and ß zone atrophy was measured at 10 degree intervals around the disc. Images were scaled to compensate for camera–eye magnification effects.

Results: The group mean planimetry results and mean global visual field indices are shown. There was considerable interobserver variation in the assessment of PPA. Although there was a trend for α and ß zone atrophy to increase in glaucoma this did not reach statistical significance. Multivariate analysis with disc and rim

area, age, MD ,PSD and diagnosis indicated PSD as an explanatory variable for PPA α(P=0.005) and rim area for PPA ß (P=0.001).

		MD	PSD	DISC	RIM	ALPHA	BETA
Control group	MEAN	0.32	1.67	2.16	1.54	0.29	0.13
	SD	0.91	0.56	0.38	0.29	0.23	0.19
Gluacoma group	MEAN	–4.19	4.84	2.32	1.06	0.4	0.17
	SD	5.44	3.71	0.42	0.33	0.34	0.2
Sign.(2–tailed)		p<0.05	p<0.05	p<0.05	p<0.05	p=0.07	p=0.2

Conclusions: Considerable interobserver variation was noted in the assessment of PPA in both normal and glaucomatous eyes. Further work is required before PPA estimates can be used as reliable indicators of glaucomatous optic nerve head damage in the clinical setting.

Patterns of Normal Neuroretinal Rim Configuration: The Reliability of the ISNT Rule in Clinical Decisions for Glaucoma

Invest Ophthalmol Vis Sci 2005;46: E-Abstract 2494. © 2005 ARVO

J.M. Wild[1], I. Bourtsoukli[1], I.A. Cunliffe[2], E.A. Ansari[3], K. Rajkumar[3], R.V. North[1] and J.E. Morgan[1]

[1] Optometry and Vision Sciences, Cardiff University, Cardiff, United Kingdom
[2] Ophthalmology, Birmingham Heartlands Hospital, Birmingham, United Kingdom
[3] Ophthalmology, University Hospital of Wales, Cardiff, United Kingdom

Abstract

Background: The width of the neuroretinal rim in normal eyes is considered to follow a distinct pattern – the ISNT rule: the rim is widest in the inferior sector of the disc, followed by the superior, the nasal, and the temporal sectors[1].

Purpose: To determine the efficacy of the ISNT rule for the detection of open angle glaucoma (OAG) based on digital stereoscopic optic disc analysis.

Methods: Optic disc images from 51 normal subjects (mean age 58.9 years, SD 10.6) and from 80 patients with early to severe OAG (mean age 66.7 years, SD 10.4) were digitised and then analysed by planimetry, masked to patient diagnosis, by three ophthalmologists trained to fellowship standard in glaucoma. Diagnosis, by two experts, was based on concurrent disc damage and visual field loss. Stereoscopic images were viewed using a Z screen (Stereographics Corp.) with quad buffered display (24 bits per pixel true colour) and were corrected for magnification factors. The rim was measured with custom cursors at the level of the scleral rim and in 5–degree intervals. The rim area was summed in four equal sectors (I,S,N,T) subtending 10° and 30° respectively. Analysis was based on the rule that I>S>N>T indicated normality.

Results:

Group mean parameters

	Disc (mm2) Mean Observer	Rim (mm2) Mean Observer	MD Mean /SD	PSD Mean /SD	Refrac.Error Mean/ SD
Glaucoma	2.32	0.95	-5.9 / 5.7	6.1 / 3.8	1.9 / 1.1
Normal	2.17	1.53	-0.1 / 1.4	1.9 / 1.1	0.2 / 2.0

Reliability of ISNT rule

	10° segments			30° segments		
	OB1	OB2	OB3	OB1	OB2	OB3
Sensitivity	0.94	0.91	0.96	0.94	0.93	0.95
Specificity	0.14	0.12	0.10	0.10	0.12	0.14
Diagnostic Precision	62.60	60.31	62.12	61.07	61.07	63.36

Conclusions: The ISNT rule can be used to detect glaucomatous optic neuropathy with high sensitivity but low specificity: the data suggest that it should be used with caution in clinical practice.

References: 1.Jonas, Gusek & Naumann, 1988. IOVS 29: 1151–1158.

References

Abrams, L. S., Scott, I. U., Spaeth, G. L., Quigley, H. A. & Varma, R. (1994). Agreement among optometrists, ophthalmologists, and residents in evaluating the optic disc for glaucoma. *Ophthalmology* 101, 1662-1667

Adams, A., Johnson, C. & Lewis, R. (1991). S-cone pathway sensitivity loss in ocular hypertension and early glaucoma has nerve fibre bundle pattern In: *Colour vision deficiencies*, 535-542

Agar, A., Yip, S. S., Hill, M. A. & Coroneo, M. T. (2000). Pressure related apoptosis in neuronal cell lines. *Journal of Neuroscience Research* 60, 495-503

AGIS (1994). The advanced glaucoma intervention study (AGIS) 1: Study design and methods and baseline characteristics of study patients. *Controlled Clinical Trials* 15, 299-325

Airaksinen, P. J., Tuulomen, A. & Alanko, H. I. (1992). Rate and pattern of neuroretinal rim area decrease in ocular hypertension and glaucoma. *Archives of Ophthalmology* 110, 206-210

Ali, M. R. & Amir, T. (1991). Critical flicker frequency under monocular and binocular conditions. *Perceptual and Motor Skills* 72, 383-386

Allen, L. (1964). Ocular fundus photography. *American Journal of Ophthalmology* 57, 17-28

Alm, A. (1993). Ocular circulation In: *Adler's physiology of the eye*, (Ed. Hart, W. M.) Mosby, St Louis 198-227

Anderson, C. M. & Swanson, R. A. (2000). Astrocyte glutamate transport: Review of properties, regulation, and physiological functions. *Glia* 32, 1-14

Anderson, D. R. (1970). Vascular supply to the optic nerve of primates. *American Journal of Ophthalmology* 70, 341-351

Anderson, D. R. (1983). The mechanisms of damage of the optic nerve In: *Glaucoma Update II*, (Eds. Krieglstein, G. K. & Leydhecker, W.) Springer Verlag, Hamburg, 89-93

Anderson, D. R. (1996). Glaucoma, capillaries and pericytes. 1. Blood flow regulation. *Ophthalmologica* 210, 257-262

Anderson, D. R. & Patella, V. M. (1999). In: *Automated static perimetry,* Mosby, Inc., St. Louis.

Andersson, S., Åsman, P., Cunliffe, I. A. & Wild, J. M. (2001). In *European Association for Vision and Eye Reseach*, Alicante, Spain

Apple, D. J., Rabb, M. F. & Walsh, P. M. (1982). Congenital anomalies of the optic disc. *Survey of Ophthalmology* 27, 3-41

Arend, O., Remky, A., Plange, N., Martin, B. J. & Harris, A. (2002). Capillary density and retinal diameter measurements and their impact on altered retinal circulation in glaucoma: A digital fluorescein angiographic study. *British Journal of Ophthalmology* 86, 429-433

Azuara-Blanco, A., Harris, A., Cantor, L. B., Abreu, M. M. & Weinland, M. (1998). Effects of short term increase of intraocular pressure on optic disc cupping. *British Journal of Ophthalmology* 82, 880-883

Balazsi, A. G., Rootman, J., Drance, S. M. & Schulzer, M. (1984). The effect of age on the nerve fibre population of the optic nerve. *American Journal of Ophthalmology* 97, 760-766

Barry, C. J. & Eikelboom, R. H. (1995). Comparison of stereo optic disc photographs from the Nidek 3Dx and Zeiss retinal cameras. *Australian and New Zealand Journal of Ophthalmology* 23, 203-205

Barry, C. J., Eikelboom, R., Kanagasingam, Y., Jitskaia, L., Morgan, W., *et al.* (2000). Comparison of optic disc image assessment methods when examining serial photographs for glaucomatous progression. *British Journal of Ophthalmology* 84, 28-30

Bartz-Schmidt, K. U., Sündtgen, M., Widder, R. A., Weber, J. & Krieglstein, G. K. (1995). Limits of two-dimensional planimetry in the follow-up of glaucomatous optic discs. *Graefe's Archive for Clinical and Experimental Ophthalmology* 233, 284-290

Bartz-Schmidt, K. U., Thumann, G., Jonescu-Cuypers, C. P. & Krieglstein, G. K. (1999). Quantitative morphologic and functional evaluation of the optic nerve head in chronic open-angle glaucoma. *Survey of Ophthalmology* 44 S41-53

Beaumont, P. E. & Kang, H. K. (2002). Clinical characteristics of retinal venous occlusions occurring at different sites. *British Journal of Ophthalmology* 86, 572-580

Bebie, H., Fankhauser, F. & Spahr, J. (1976). Static perimetry: Strategies. *Acta Ophthalmologica (Copenhagen)* 54, 325-338

Bengtsson, B., Lindgren, A., Heijl, A., Lindgren, G., Åsman, P., *et al.* (1997). Perimetric probability maps to separate change caused by glaucoma from that caused by cataract. *Acta Ophthalmologica Scandinavica* 75, 184-188

Bengtsson, B. & Heijl, A. (2000). False-negative responses in glaucoma perimetry: Indicators of patient performance or test reliability? *Investigative Ophthalmology & Visual Science* 41, 2201-2204

Bengtsson, B. (2003). A new rapid threshold algorithm for short-wavelength automated perimetry. *Investigative Ophthalmology & Visual Science* 44, 1388-1394

Bengtsson, B. & Heijl, A. (2003). Normal intersubject threshold variability and normal limits of the SITA SWAP and full threshold SWAP perimetric programs. *Investigative Ophthalmology & Visual Science* 44, 5029-5034

Benjamin, L. E., Hemo, I. & Keshet, E. (1998). A plasticity window for blood vessel remodelling is defined by pericyte coverage of the preformed endothelial network and is regulated by PDGF-B and VEGF. *Development* 125, 1591-1598

Berger, J. W., Patel, T. R., Shin, D. S., Piltz, J. R. & Stone, R. A. (2000). Computerized stereochronoscopy and alternation flicker to detect optic nerve head contour change. *Ophthalmology* 107, 1316-1320

Berthold, K., Riemer, T. & Vilser, W. (2002). Retina model, a knowledge-based model of the retinal microcirculation. *Investigative Ophthalmology & Visual Science* 43, E-abstract 514

Bettelheim, F. A. & Ali, S. (1985). Light scattering of normal human lens III. Relationship between forward and back scatter of whole excised lenses. *Experimental Eye Research* 41, 1-9

Bettleheim, F. A. & Chylack, L. T. (1985). Light scattering of whole excised human cataractous lenses. Relationships between different light scattering properties. *Experimental Eye Research* 41, 19-30

Bhutto, I. A. & Amemiya, T. (2002). Choroidal vasculature changes in spontaneously hypertensive rats - transmission electron microscopy and scanning electron microscopy with casts. *Ophthalmic Research* 34, 54-62

Bigun, J., Choy, K.-W. & Olsson, H. (2001). Evidence on skill differences of women and men concerning face recognition. *Lecture Notes in Computer Science* 2091, 44 - 50

Blum, M., Bachmann, K., Wintzer, D., Riemer, T., Vilser, W., *et al.* (1999). Noninvasive measurement of the Bayliss effect in retinal autoregulation. *Graefe's Archive for Clinical and Experimental Ophthalmology* 237, 296-300

Blum, M., Scherf, C., Bachmann, K. & Strobel, J. (2001). Age-related contractility of human retinal arterioles during pure oxygen breathing. *Ophthalmologe* 98, 265-268

Blumenthal, E. Z., Sample, P. A., Berry, C. C., Lee, A. C., Girkin, C. A., *et al.* (2000a). Evaluating sources of variability for standard and SWAP visual fields in glaucoma patients, suspects and normals. *Investigative Ophthalmology & Visual Science* 41, B442

Blumenthal, E. Z., Sample, P. A., Zangwill, L., Lee, A. C., Kono, Y., *et al.* (2000b). Comparison of long-term variability for standard and short-wavelength automated perimetry in stable glaucoma patients. *American Journal of Ophthalmology* 129, 309-313

Blumenthal, E. Z. & Weinreb, R. N. (2001). Assessment of the retinal nerve fiber layer in clinical trials of glaucoma neuroprotection. *Survey of Ophthalmology* 45, S305-S312

Boeglin, R. J., Caprioli, J. & Zulauf, M. (1992). Long-term fluctuation of the visual field in glaucoma. *American Journal of Ophthalmology* 113, 396-400

Boehm, A. G., Koeller, A. U. & Pillunat, L. E. (2005). The effect of age on optic nerve head blood flow. *Investigative Ophthalmology & Visual Science* 46, 1291-1295

Boes, D. A., Spaeth, G. L., Mills, R. P., Smith, M., Nicholl, J. E., *et al.* (1996). Relative optic cup depth assessments using three stereo photograph viewing methods. *Journal of Glaucoma* 5, 9-14

Bonomi, L., Marchini, G., Marraffa, M., Bernardi, P., De Franco, I., *et al.* (1998). Prevalence of glaucoma and intraocular pressure distribution in a defined population - the Egna-Neumarkt study. *Ophthalmology* 105, 209-215

Borras, T. (2003). Gene expression in the trabecular meshwork and the influence of intraocular pressure. *Progress in Retinal and Eye Research* 22, 435-463

Boulton, M. & Dayhaw-Barker, P. (2001). The role of the retinal pigment epithelium: Topographical variation and ageing changes. *Eye* 15, 384-389

Boulton, M., Rozanowska, M. & Rozanowski, B. (2001). Retinal photodamage. *Journal of Photochemistry and Photobiology B: Biology* 64, 144-161

Bowd, C., Zangwill, L. M., Medeiros, F. A., Hao, J. C., Chan, K., *et al.* (2004). Confocal scanning laser ophthalmoscopy classifiers and stereophotograph evaluation for prediction of visual field abnormalities in glaucoma-suspect eyes. *Investigative Ophthalmology & Visual Science* 45, 2255-2262

Brazitikos, P. D., Safran, A. B., Simona, F. & Zulauf, M. (1990). Threshold perimetry in tilted disc syndrome. *Archives of Ophthalmology* 108, 1698-1700

Broadway, D. C., Drance, S. M., Parfitt, C. M. & Mikelberg, F. S. (1998). The ability of scanning laser ophthalmoscopy to identify various glaucomatous optic disc appearances. *American Journal of Ophthalmology* 125, 593-604

Broadway, D. C., Nicolela, M. T. & Drance, S. M. (1999). Optic disc appearances in primary open-angle glaucoma. *Survey of Ophthalmology* 43, S223-S243

Brodsky, M. C. (1994). Congenital optic disc anomalies. *Survey of Ophthalmology* 39, 89-112

Brunk, U. T. & Terman, A. (2002). Lipofuscin: Mechanisms of age-related accumulation and influence on cell function. *Free Radical Biology and Medicine* 33, 611-619

Buckley, C., Hadoke, P. W. F., Henry, E. & O'Brien, C. (2002). Systemic vascular endothelial cell dysfunction in normal pressure glaucoma. *British Journal of Ophthalmology* 86, 227-232

Buckley, C. H., Hadoke, P. W. F. & Obrien, C. J. (1997). Use of isolated ocular arteries in vitro to define the pathology of vascular changes in glaucoma. *British Journal of Ophthalmology* 81, 599-607

Budde, W. M. & Jonas, J. B. (1999). Family history of glaucoma in the primary and secondary open-angle glaucomas. *Graefe's Archive for Clinical and Experimental Ophthalmology* 237, 554-557

Budde, W. M., Jonas, J. B. & Schonherr, U. (1999). Age-related macular degeneration and optic disc morphology. *American Journal of Ophthalmology* 127, 220-221

Budde, W. M., Jonas, J. B., Martus, P. & Grundler, A. E. (2000). Influence of optic disc size on neuroretinal rim shape in healthy eyes. *Journal of Glaucoma* 9, 357-362

Budde, W. M. & Jonas, J. B. (2003a). Influence of cilioretinal arteries on neuroretinal rim and parapapillary atrophy in glaucoma. *Investigative Ophthalmology & Visual Science* 44, 170-174

Budde, W. M. & Jonas, J. B. (2003b). Influence of cilioretinal arteries on functional damage in open-angle glaucoma. *Ophthalmologe* 100, 1067-1070

Budenz, D. L., Feuer, W. J. & Anderson, D. R. (1993). The effect of simulated cataract on the glaucomatous visual field. *Ophthalmology* 100, 511-517

Buono, L. M., Foroozan, R., Sergott, R. C. & Savino, P. J. (2002). Is normal tension glaucoma actually an unrecognized hereditary optic neuropathy? New evidence from genetic analysis. *Current Opinion in Ophthalmology* 13, 362-370

Burgoyne, C. F. (2004). Image analysis of optic nerve disease. *Eye* 18, 1207-1213

Burgoyne, C. F., Crawford Downs, J., Bellezza, A. J., Francis Suh, J.-K. & Hart, R. T. (2005). The optic nerve head as a biomechanical structure: A new paradigm for understanding the role of IOP-related stress and strain in the pathophysiology of glaucomatous optic nerve head damage. *Progress in Retinal and Eye Research* 24, 39-73

Burk, R. O. W., Rohrschneider, K., Noack, H. & Volcker, H. E. (1992). Is optic disc size a topographic risc factor in normal-tension glaucoma. *Investigative Ophthalmology & Visual Science* 33, 1279-1279

Calkins, D. J. (2001). Seeing with S-cones. *Progress in Retinal and Eye Research* 20, 255 - 287

Callaway, E. M. (1998). Local circuits in primary visual cortex of the macaque monkey. *Annual Review of Neuroscience* 21, 47-74

Caprioli, J., Sears, M. & Miller, J. M. (1987). Patterns of early visual field loss in open-angle glaucoma. *American Journal of Ophthalmology* 103, 512 - 517

Caprioli, J. (1992). Discrimination between normal and glaucomatous eyes. *Investigative Ophthalmology & Visual Science* 33, 153-159

Caprioli, J., Prum, B. & Zeyen, T. (1996). Comparison of methods to evaluate the optic nerve head and nerve fiber layer for glaucomatous change. *American Journal of Ophthalmology* 121, 659-667

Casagrande, V. A. (1994). A third parallel visual pathway to primate area V1. *Trends in Neuro Science* 17, 305 - 311

Casson, E., Johnson, C. & Shapiro, L. (1993). Longitudinal comparison of temporal-modulation perimetry with white-on-white and blue-on-yellow perimetry in ocular hypertension and early glaucoma. *Journal of the Optical Society of America A - Optics Image Science and Vision* 10, 1792-1806

Chakravarthy, U. & Gardiner, T. A. (1999). Endothelium-derived agents in pericyte function/dysfunction. *Progress in Retinal and Eye Research* 18, 511-527

Chauhan, B. C., Mohandas, R. N., Whelan, J. H. & McCormick, T. A. (1993). Comparison of reliability indices in conventional and high-pass resolution perimetry. *Ophthalmology* 100, 1089 - 1094

Chauhan, B. C., Blanchard, J. W., Hamilton, D. C. & LeBlanc, R. P. (2000). Technique for detecting serial topographic changes in the optic disc and peripapillary retina using scanning laser tomography. *Investigative Ophthalmology & Visual Science* 41, 775-782

Chauhan, B. C., McCormick, T. A., Nicolela, M. T. & LeBlanc, R. P. (2001). Optic disc and visual field changes in a prospective longitudinal study of patients with glaucoma: Comparison of scanning laser tomography with conventional perimetry and optic disc photography. *Archives of Ophthalmology* 119, 1492-1499

Chauhan, B. C., Pan, J. Y., Archibald, M. L., LeVatte, T. L., Kelly, M. E. M., *et al.* (2002). Effect of intraocular pressure on optic disc topography, electroretinography, and axonal loss in a chronic pressure- induced rat model of optic nerve damage. *Investigative Ophthalmology & Visual Science* 43, 2969-2976

Chen, Y. M., Vartiainen, N. E., Ying, W. H., Chan, P. H., Koistinaho, J., *et al.* (2001). Astrocytes protect neurons from nitric oxide toxicity by a glutathione-dependent mechanism. *Journal of Neurochemistry* 77, 1601-1610

Chihara, E. & Honda, Y. (1992). Multiple defects in the retinal nerve fiber layer in glaucoma. *Graefe's Archive for Clinical and Experimental Ophthalmology* 230, 201-205

Chihara, E. & Chihara, K. (1994). Covariation of optic disc measurements and ocular parameters in the healthy eye. *Graefe's Archive for Clinical and Experimental Ophthalmology* 232, 265-271

Chihara, E., Liu, X., Dong, J., Takashima, Y., Akimoto, M., *et al.* (1997). Severe myopia as a risk factor for progressive visual field loss in primary open-angle glaucoma. *Ophthalmologica* 211, 66-71

Cho, N., Poulsen, G. L., Ver Hoeve, J. N. & Nork, M. (2000). Selective loss of s-cones in diabetic retinopathy. *Archives of Ophthalmology* 118, 1393 - 1400

Choi, H. (1988). Glutamate neurotoxicity and diseases of the nervous system. *Neuron* 1, 623-634

Chylack, L. T., Wolfe, J. K., Singer, D. M., Leske, M. C., Bullimore, M. A., *et al.* (1993). The lens opacities classification system III. *Archives of Ophthalmology* 111, 831-837

Cioffi, G. A. (2001). Three common assumptions about ocular blood flow and glaucoma. *Survey of Ophthalmology* 45, S325-S331

Clark, A. F., Steely, H. T., Dickerson, J. E., Jr., English-Wright, S., Stropki, K., *et al.* (2001). Glucocorticoid induction of the glaucoma gene myoc in human and monkey

trabecular meshwork cells and tissues. *Investigative Ophthalmology & Visual Science* 42, 1769-1780

Cohen, J. M. (1993). An overview of enhancement techniques for peripheral field loss. *Journal of the American Optometric Association* 63, 60-70

Coleman, A. L. (1999). Glaucoma. *The Lancet* 354, 1803-1810

Constable, I. J., Yogesan, K., Eikelboom, R., Barry, C. & Cuypers, M. (2000). Fred Hollows lecture: Digital screening for eye disease. *Clinical and Experimental Ophthalmology* 28, 129-132

Correnti, A. J., Wollstein, G., Price, L. L. & Schuman, J. S. (2003). Comparison of optic nerve head assessment with a digital stereoscopic camera (Discam), scanning laser ophthalmoscopy, and stereophotography. *Ophthalmology* 110, 1499-1505

Cubbidge, R. P., (1997). Examination variability in short-wavelength automated perimetry. Aston University, Ph.D.

Cunha-Vaz, J. G. & Maurice, D. M. (1967). The active transport of fluorescein by the retinal vessels and the retina. *Journal of Physiology* 191, 467-486

Cunha-Vaz, J. G. (2004). The blood-retinal barriers system. Basic concepts and clinical evaluation. *Experimental Eye Research* 78, 715-721

Curcio, C. A. & Allen, K. A. (1990). Topography of ganglion-cells in human retina. *Journal of Comparative Neurology* 300, 5-25

Curcio, C. A., Sloan, K. R., Kalina, R. E. & Hendrickson, A. E. (1990). Human photoreceptor topography. *Journal of Comparative Neurology* 292, 497-523

Curcio, C. A., Allen, K. A., Sloan, K. R., Lerea, C. L., Hurley, J. B., *et al.* (1991). Distribution and morphology of human cone photoreceptors stained with anti-blue opsin. *Journal of Comparative Neurology* 312, 610 - 624

Curcio, C. A., Saunders, P. L., Younger, P. W. & Malek, G. (2000). Peripapillary chorioretinal atrophy: Bruch's membrane changes and photoreceptor loss. *Ophthalmology* 107, 334-343.

Curcio, C. A., Millican, C. L., Bailey, T. & Kruth, H. S. (2001). Accumulation of cholesterol with age in human Bruch's membrane. *Investigative Ophthalmology & Visual Science* 42, 265-274

Dacey, D. M. & Petersen, M. R. (1992). Dendritic field size and morphology of midget and parasol ganglion cells in the human retina. *Proceedings of the National Academy of Sciences of the United States of America* 89, 9666 - 9670

Dacey, D. M. & Lee, B. B. (1994). The blue-on opponent pathway in primate retina originates from a distinct bistratified ganglion-cell type. *Nature* 367, 1278 - 1281.

Dacey, D. M. (2000). Parallel pathways for spectral coding in primate retina. *Annual Review Neuroscience* 23, 743-775

Danbolt, N. C. (2001). Glutamate uptake. *Progress in Neurobiology* 65, 1-105

Dandona, L., Quigley, H. A., Brown, A. E. & Enger, C. (1990). Quantitative regional structure of the normal human lamina cribrosa. A racial comparison. *Archives of Ophthalmology* 108, 393-398

De Lima Silveira, L. C. (2004). Comparative study of the primate retina In: *The primate visual system*, (Eds. Kaas, J. H. & Collins, C. E.) CRC Press, Boca Raton, 29-52

De Monasterio, F. M., Schein, S. J. & McCrane, E. P. (1981). Staining of blue-sensitive cones of the macaque retina by a fluorescent dye. *Science* 213, 1278-1281

De Valois, R. L., Webster, M. A., De Valois, K. K. & Lingelbach, B. (1986). Temporal properties of brightness and color induction. *Vision Research* 26, 887-897

Delaey, C. & Van de Voorde, J. (2000). Regulatory mechanisms in the retinal and choroidal circulation. *Ophthalmic Research* 32, 249-256

Delgado, M. F., Nguyen, N. T., Cox, T. A., Singh, K., Lee, D. A., *et al.* (2002). Automated perimetry: A report by the American Academy of Ophthalmology. *Ophthalmology* 109, 2362-2374

Demirel, S. & Johnson, C. A. (2000). Isolation of short-wavelength sensitive mechanisms in normal and glaucomatous visual field regions. *Journal Of Glaucoma* 9, 63-73

Dengler-Harles, M., Wild, J. M., Cole, M. D., O'Neill, E. C. & Crews, S. J. (1990). The influence of forward light scatter on visual field indices in glaucoma. *Graefe's Archive for Clinincal and Experimental Ophthalmology* 228, 326-331

Diaz-Araya, C. M., Provis, J. M., Penfold, P. L. & Billson, F. A. (1995). Development of microglial topography in human retina. *Journal of Comparative Neurology* 363, 53-68

Dichtl, A., Jonas, J. B. & Mardin, C. Y. (1996). Comparison between tomographic scanning evaluation and photographic measurement of the neuroretinal rim. *American Journal of Ophthalmology* 121, 494-501

Distelhorst, J. S. & Hughes, G. M. (2003). Open-angle glaucoma. *American Family Physician* 67, 1937-1944

Dolman, C. L., McCormick, A. Q. & Drance, S. M. (1980). Aging of the optic nerve. *Archives of Ophthalmology* 98, 2053-2058

Donaldson, D. (1964). A new camera for stereoscopic fundus photography. *Transactions of the American Ophthalmological Society* 62, 429-458

Dowling, J. E. (1987). In: *The retina. An approachable part of the brain,* The Belknap Press of Harvard University Press, Cambridge.

Drance, S. M. & King, D. (1992). The neuroretinal rim in descending optic atrophy. *Graefe's Archive for Clinical and Experimental Ophthalmology* 230, 154-157

Drasdo, N., Aldebasi, Y. H., Chiti, Z., Mortlock, K. E., Morgan, J. E., *et al.* (2001). The S-cone PhNR and pattern ERG in primary open angle glaucoma. *Investigative Ophthalmology & Visual Science* 42, 1266-1272

Dreyer, E. B. (1998). A proposed role for excitotoxicity in glaucoma. *Journal of Glaucoma* 7, 62-67

Duijm, H. F., van den Berg, T. J. & Greve, E. L. (1997). Choroidal haemodynamics in glaucoma. *British Journal of Ophthalmology* 81, 735-742

Eikelboom, R. H., Barry, C. J., Jitskaia, L., Voon, A. S. P. & Kanagasingam, Y. (2000). Neuroretinal rim measurement error using PC-based stereo software. *Clinical and Experimental Ophthalmology* 28, 178-180

Eisner, A. & MacLeod, D. I. A. (1980). Blue-sensitive cones do not contribute to luminance. *Journal of the Optical Society of America* 70, 121-123

Emara, B. Y., Tingey, D. P., Probst, L. E. & Motolko, M. A. (1999). Central corneal thickness in low-tension glaucoma. *Canadian Journal of Ophthalmology* 34, 319-324

Embleton, S. J., Hosking, S. L., Hilton, E. J. R. & Cunliffe, I. A. (2002). Effect of senescence on ocular blood flow in the retina, neuroretinal rim and lamina cribrosa, using scanning laser doppler flowmetry. *Eye* 16, 156-162

Emdadi, A., Zangwill, L., Sample, P. A., Kono, Y., Anton, A., *et al.* (1998). Patterns of optic disc damage in patients with early focal visual field loss. *American Journal of Ophthalmology* 126, 763-771

Emdadi, A., Kono, Y., Sample, P. A., Maskaleris, G. & Weinreb, R. N. (1999). Parapapillary atrophy in patients with focal visual field loss. *American Journal of Ophthalmology* 128, 595-600

Fantes, F. E. & Anderson, D. R. (1989). Clinical histologic correlation of human peripapillary anatomy. *Ophthalmology* 96, 20-25

Farber, D. B., Flannery, J. G., Lolley, R. N. & Bok, D. (1985). Distribution patterns of photoreceptors, protein and cyclic nucleotides in the human retina. *Investigative Ophthalmology & Visual Science* 36, 558-570

Faubert, J. (2002). Visual perception and aging. *Canadian Journal of Experimental Psychology* 56, 164-176

Felius, J., de Jong, L. A., van den Berg, T. J. & Greve, E. L. (1995). Functional characteristics of blue-on-yellow perimetric thresholds in glaucoma. *Investigative Ophthalmology & Visual Science* 36, 1665-1674

Ferraridileo, G., Davis, E. B. & Anderson, D. R. (1991). Angiotensin-II binding-receptors in retinal and optic-nerve head blood-vessels - an autoradiographic approach. *Investigative Ophthalmology & Visual Science* 32, 21-26

Ferro, C. J. & Webb, D. J. (1997). Endothelial dysfunction and hypertension. *Drugs* 53, 30-41

Feuer, W. J., Parrish, R. K., Schiffman, J. C., Anderson, D. R., Budenz, D. L., *et al.* (2002). The ocular hypertension treatment study: Reproducibility of cup/disc ratio measurements over time at an optic disc reading center. *American Journal of Ophthalmology* 133, 19-28

Flammer, J., Drance, S. M., Fankhauser, F. & Augustiny, L. (1984). Differential light threshold in automated static perimetry. Factors influencing short-term fluctuation. *Archives of Ophthalmology* 102, 876-879

Flammer, J., Drance, S. M., Augustiny, L. & Funkhouser, A. (1985). Quantification of glaucomatous visual field defects with automated perimetry. *Investigative Ophthalmology & Visual Science* 26, 176-181

Flammer, J., Pache, M. & Resink, T. (2001). Vasospasm, its role in the pathogenesis of diseases with particular reference to the Eye. *Progress in Retinal and Eye Research* 20, 319-349

Flammer, J., Orgul, S., Costa, V. P., Orzalesi, N., Krieglstein, G. K., *et al.* (2002). The impact of ocular blood flow in glaucoma. *Progress in Retinal and Eye Research* 21, 359-393

Flanagan, J., Hrynchak, P., Hurst, M., Prokopich, C. L. & Winn, B. (1999). In: *Clinical procedures in Primary Eye Care,* Butterworth-Heinemann, Oxford.

Flugel, C., Tamm, E. R., Mayer, B. & Lutjen-Drecoll, E. (1994). Species differences in choroidal vasodilative innervation: Evidence for specific intrinsic nitrergic and vip-positive neurons in the human eye. *Investigative Ophthalmology & Visual Science* 35, 592-599

Formaz, F., Riva, C. E. & Geiser, M. (1997). Diffuse luminance flicker increases retinal vessel diameter in humans. *Current Eye Research* 16, 1252-1257

Forrester, J. V., Dick, A. D., McMenamin, P. & Lee, W. R. (1999). In: *The Eye. Basic sciences in practice,* WB Saunders, London.

Fournier, A. V., Damji, K. F., Epstein, D. L. & Pollock, S. C. (2001). Disc excavation in dominant optic atrophy: Differentiation from normal tension glaucoma. *Ophthalmology* 108, 1595-1602

Funaki, S., Shirakashi, M. & Abe, H. (1998). Relation between size of optic disc and thickness of retinal nerve fibre layer in normal subjects. *British Journal of Ophthalmology* 82, 1242-1245

Funaki, S., Shirakashi, M., Yaoeda, K., Abe, H., Kunimatsu, S., *et al.* (2002). Specificity and sensitivity of glaucoma detection in the Japanese population using scanning laser polarimetry. *British Journal of Ophthalmology* 86, 70-74

Gang, L., Chutatape, O. & Krishnan, S. M. (2002). Detection and measurement of retinal vessels, in fundus images using amplitude modified second-order gaussian filter. *IEEE Transactions on Biomedical Engineering* 49, 168-172

Garhofer, G., Zawinka, C., Resch, H., Huemer, K. H., Schmetterer, L., *et al.* (2004). Response of retinal vessel diameters to flicker stimulation in patients with early open angle glaucoma. *Journal of Glaucoma* 13, 340-344

Gartner, S. & Henkind, P. (1981). Aging and degeneration of the human macula: 1. Outer nuclear layer and photoreceptors. *British Journal of Ophthalmology* 65, 23-28

Garway-Heath, D. F., Wollstein, G. & Hitchings, R. A. (1997). Aging changes of the optic nerve head in relation to open angle glaucoma. *British Journal of Ophthalmology* 81, 840-845

Garway-Heath, D. F. & Hitchings, R. A. (1998). Quantitative evaluation of the optic nerve head in early glaucoma. *British Journal of Ophthalmology* 82, 352-361

Garway-Heath, D. F., Ruben, S. T., Viswanathan, A. & Hitchings, R. A. (1998a). Vertical cup/disc ratio in relation to optic disc size: Its value in the assessment of the glaucoma suspect. *British Journal of Ophthalmology* 82, 1118-1124

Garway-Heath, D. F., Rudnicka, A. R., Lowe, T., Foster, P. J., Fitzke, F. W., *et al.* (1998b). Measurement of optic disc size: Equivalence of methods to correct for ocular magnification. *British Journal of Ophthalmology* 82, 643-649

Garway-Heath, D. F., Poinoosawmy, D., Wollstein, G., Viswanathan, A., Kamal, D., *et al.* (1999). Inter- and intraobserver variation in the analysis of optic disc images: Comparison of the Heidelberg Retina Tomograph and computer assisted planimetry. *British Journal of Ophthalmology* 83, 664-669

Gasser, P. & Flammer, J. (1987). Influence of vasospasm on visual function. *Documenta Ophthalmologica* 66, 3-18

Gauthier, I., Tarr, M. J., Anderson, A. W., Skudlarski, P. & Gore, J. C. (1999). Activation of the middle fusiform 'face area' increases with expertise in recognizing novel objects. *Nature Neuroscience* 2, 568 - 573

Gherghel, D., Orgul, S., Prunte, C., Gugleta, K., Lubeck, P., *et al.* (2000). Interocular differences in optic disc topographic parameters in normal subjects. *Current Eye Research* 20, 276-282.

Gherghel, D., Orgul, S., Gugleta, K. & Flammer, J. (2001). Retrobulbar blood flow in glaucoma patients with nocturnal over-dipping in systemic blood pressure. *American Journal of Ophthalmology* 132, 641-647

Gilpin, L. B., Stewart, W. C., Hunt, H. H. & Broom, C. D. (1990). Threshold variability using different goldmann stimulus sizes. *Acta Ophthalmologica* 68, 674-676

Girkin, C. A., McGwin, G., Jr., McNeal, S. F. & DeLeon-Ortega, J. (2003). Racial differences in the association between optic disc topography and early glaucoma. *Investigative Ophthalmology & Visual Science* 44, 3382-3387

Girkin, C. A., McGwin, G., Jr., Xie, A. & Deleon-Ortega, J. (2005). Differences in optic disc topography between black and white normal subjects. *Ophthalmology* 112, 33-39

Glovinsky, Y., Quigley, H. A., Dandona, L., Brown, A. E. & Dunkelberger, G. R. (1991a). Large ganglion-cells are selectively damaged in experimental glaucoma. *Investigative Ophthalmology & Visual Science* 32, 1103-1103

Glovinsky, Y., Quigley, H. A. & Dunkelberger, G. R. (1991b). Retinal ganglion-cell loss is size dependent in experimental glaucoma. *Investigative Ophthalmology & Visual Science* 32, 484-491

Goldblum, D. & Mittag, T. (2002). Prospects for relevant glaucoma models with retinal ganglion cell damage in the rodent eye. *Vision Research* 42, 471-478

Graham, S. L., Drance, S. M., Chauhan, B. C., Swindale, N. V., Hnik, P., *et al.* (1996). Comparison of psychophysical and electrophysiological testing in early glaucoma. *Investigative Ophthalmology & Visual Science* 37, 2651-2662

Graham, S. L. & Drance, S. M. (1999). Nocturnal hypotension: Role in glaucoma progression. *Survey of Ophthalmology* 43, S10-S16

Greaney, M. J., Hoffman, D. C., Garway-Heath, D. F., Nakla, M., Coleman, A. L., *et al.* (2002). Comparison of optic nerve imaging methods to distinguish normal eyes from those with glaucoma. *Investigative Ophthalmology & Visual Science* 43, 140-145

Greenfield, D. S., Zacharia, P. & Schuman, J. S. (1993). Comparison of Nidek 3Dx and Donaldson simultaneous stereoscopic disc photography. *American Journal of Ophthalmology* 116, 741-747

Greenstein, V. C., Halevy, D., Zaldi, Q. & Koenig, K. L. (1996). Chromatic and luminance system deficits in glaucoma. *Vision Research* 36, 621-629

Greve, E. L. (1980). Peritest. Glaucoma symposium. Diagnosis and therapy. In: *Documenta ophthalmologica proceedings series 22*, (Ed. L., G. E.) Dr. W Junk Publishers, The Hague, 71-74

Grodum, K., Heijl, A. & Bengtsson, B. (2002). Optic disc hemorrhages and generalized vascular disease. *Journal of Glaucoma* 11, 226-230

Guthauser, U. & Flammer, J. (1988). Quantifying visual field damage caused by cataract. *Am Jour of Ophthalmol* 106, 480-484

Haas, A., Flammer, J. & Schneider, U. (1986). Influence of age on the visual fields of normal subjects. *American Journal of Ophthalmology* 101, 199-203

Haefliger, I. O. & Flammer, J. (1989). Increase of the short-term fluctuation of the differential light threshold around a physiologic scotoma. *American Journal of Ophthalmology* 107, 417-420

Haefliger, I. O., Flammer, J. & Luscher, T. F. (1992). Nitric-oxide and endothelin-1 are important regulators of human ophthalmic artery. *Investigative Ophthalmology & Visual Science* 33, 2340-2343

Haefliger, I. O., Flammer, J. & Luscher, T. F. (1993). Heterogeneity of endothelium-dependent regulation in ophthalmic and ciliary arteries. *Investigative Ophthalmology & Visual Science* 34, 1722-1730

Haefliger, I. O., Meyer, P., Flammer, J. & Luscher, T. F. (1994). The vascular endothelium as a regulator of the ocular circulation - a new concept in ophthalmology. *Survey of Ophthalmology* 39, 123-132

Hafez, A. S., Bizzarro, R. L. G. & Lesk, M. R. (2003). Evaluation of optic nerve head and peripapillary retinal blood flow in glaucoma patients, ocular hypertensives, and normal subjects,. *American Journal of Ophthalmology* 136, 1022-1031

Hall, J. K., Andrews, A. P., Walker, R. & Piltz-Seymour, J. R. (2001). Association of retinal vessel caliber and visual field defects in glaucoma. *American Journal of Ophthalmology* 132, 855-859

Hancock, S. A., (2000). Structure and function in primary open angle glaucome. Aston University, Ph.D.

Hanson, S., Krishnan, S. K. & Phillips, J. (2001). Observer experience and cup: Disc ratio assessment. *Optometry and Vision Science* 78, 701-705

Harizman, N., Chiang, A., Oliveira, C., Liebmann, C. A., Liebmann, J. M., *et al.* (2005). Can the isnt rule be applied to patients of african ancestry. *Investigative Ophthalmology & Vision Science* 46, 4805-

Harju, M. & Vesti, E. (2001). Blood flow of the optic nerve head and peripapillary retina in exfoliation syndrome with unilateral glaucoma or ocular hypertension. *Graefe's Archive for Clinical and Experimental Ophthalmology* 239, 271-277.

Harper, R., Henson, D. & Reeves, B. C. (2000a). Appraising evaluations of screening/diagnostic tests: The importance of the study populations. *British Journal of Ophthalmology* 84, 1198-1202

Harper, R. & Reeves, B. (2000). The sensitivity and specificity of direct ophthalmoscopic optic disc assessment in screening for glaucoma: A multivariate analysis. *Graefe's Archive for Clinical and Experimental Ophthalmology* 238, 949-955

Harper, R., Reeves, B. & Smith, G. (2000b). Observer variability in optic disc assessment: Implications for glaucoma shared care. *Ophthalmic and Physiological Optics* 20, 265-273

Harris, A., Harris, M., Biller, J., Garzozi, H., Zarfty, D., *et al.* (2000). Aging affects the retrobulbar circulation differently in women and men. *Archives of Ophthalmology* 118, 1076-1080

Hart, W. M., Silverman, S. E., Trick, G. L., Nesher, R. & Gordon, M. O. (1990). Glaucomatous visual field damage luminance and color contrast sensitivities. *Investigative Ophthalmology and Visual Science* 31, 359-367

Hartwick, A. T. E. (2001). Beyond intraocular pressure: Neuroprotective strategies for future glaucoma therapy. *Optometry and Vision Science* 78, 85-94

Harwerth, R. S., Smith III, E. L. & Chandler, M. (1999). Progressive visual field defects from experimental glaucoma: Measurements with white and coloured stimuli. *Optometry and Vision Science* 76, 558-570

Harwerth, R. S., Crawford, M. L., Frishman, L. J., Viswanathan, S., Smith, E. L., *et al.* (2002). Visual field defects and neural losses from experimental glaucoma. *Progress in Retinal and Eye Research* 21, 91-125

Harwerth, R. S., Carter-Dawson, L., Smith, E. L., III, Barnes, G., Holt, W. F., *et al.* (2004). Neural losses correlated with visual losses in clinical perimetry. *Investigative Ophthalmology & Visual Science* 45, 3152-3160

Harweth, R. S., Carter-Dawson, L., Shen, F., Smith III, E. L. & Crawford, M. L. J. (1999). Ganglion cell losses underlying visual field defects from experimental glaucoma. *Investigative Ophthalmology & Visual Science* 40, 2242-2250

Hatch, W. V., Flanagan, J. G., Williams-Lyn, D. E., Buys, Y. M., Farra, T., *et al.* (1999). Interobserver agreement of Heidelberg Retina Tomograph parameters. *Journal of Glaucoma* 8, 232-237

Hayakawa, T., Sugiyama, K., Tomita, G., Kawase, K., Onda, E., *et al.* (1998). Correlation of the peripapillary atrophy area with optic disc cupping and disc hemorrhage. *Journal of Glaucoma* 7, 306-311

Hayreh, S. S. (1963). The cilio-retinal arteries. *British Journal of Ophthalmology* 47, 71-89

Hayreh, S. S. (1974). Anatomy and physiology of the optic nerve head. *Transactions - American Academy of Ophthalmology and Otolaryngology* 78, 240 - 254

Hayreh, S. S., March, W. & Anderson, D. R. (1979). Pathogenesis of block of rapid orthograde axonal transport by elevated intraocular pressure. *Experimental Eye Research* 28, 515-523

Hayreh, S. S., Klugman, M. R., Podhajsky, P. & Kolder, H. E. (1989). Electroretinography in central retinal vein occlusion. Correlation of electroretinographic changes with pupillary abnormalities. *Graefe's Archive for Clinical and Experimental Ophthalmology* 227, 549-561

Hayreh, S. S. (1990). In vivo choroidal circulation and its watershed zones. *Eye* 4, 273-289

Hayreh, S. S. (1996). Blood supply of the optic nerve head. *Ophthalmologica* 210, 285-295

Hayreh, S. S. (1999). Retinal and optic nerve head ischaemic disorders and atherosclerosis: Role of serotonin. *Progress in Retinal and Eye Research* 18, 191-221

Hayreh, S. S., Pe'er, J. & Zimmerman, M. B. (1999). Morphologic changes in chronic high-pressure experimental glaucoma in rhesus monkeys. *Journal of Glaucoma* 8, 56-71.

Hayreh, S. S. & Jonas, J. B. (2001). Optic disc morphology after arteritic anterior ischaemic optic neuropathy. *Ophthalmology* 108, 1586-1594

Healey, P. R., Mitchell, P., Smith, W. & Wang, J. J. (1998). Optic disc hemorrhages in a population with and without signs of glaucoma. *Ophthalmology* 105, 216-223

Heijl, A. & Drance, S. M. (1983). Changes in differential threshold in patients with glaucoma during prolonged perimetry. *British Journal of Opthalmology* 67, 512-516

Heijl, A. (1985). Computerised perimetry. *Transactions of the Ophthalmological Societies of the United Kingdom* 104, 76-87

Heijl, A., Lindgren, G. & Olsson, J. (1987a). A package for the statistical analysis analysis of visual fields. *Documenta Opthalmologica Proceedings Series* 3, 153-168

Heijl, A., Lindgren, G. & Olsson, J. (1987b). Normal variability of static perimetric threshold values across the central visual field. *Archives of Ophthalmology* 105, 1544-1549

Heijl, A. & Lund, J. S. (1987). The implications of the results of computerized perimetry in normals for the statistical evaluation of glaucomatous visual fields In: *Glaucoma Update III*, (Ed. Krieglstein, G. K.) Springer-Verlag, Berlin,,

Heijl, A. (1989). Effect of IOP on the visual field in ocular hypertension and glaucoma. *International Ophthalmology* 13, 119-124

Heijl, A., Lindgren, G., Olsson, J. & Asman, P. (1992). On weighted visual field indices. *Graefe's Archive for Clinical and Experimental Ophthalmology* 230, 397-398

Heijl, A. & Bengtsson (1996). The effect of perimetric experience in patients with glaucoma. *Archives of Ophthalmology* 114, 19-22

Heijl, A., Leske, M. C., Bengtsson, B., Hyman, L. & Hussein, M. (2002). Reduction of intraocular pressure and glaucoma progression - results from the early manifest glaucoma trial. *Archives of Ophthalmology* 120, 1268-1279

Hendry, S. H. C. & Reid, R. C. (2000). The koniocellular pathway in primate vision. *Annual Review of Neuroscience* 23, 127-153

Henkind, P. (1967). New observations on the radial peripapillary capillaries. *Investigative Ophthalmology & Visual Science* 6, 103-108

Henry, E., Newby, D. E., Webb, D. J. & O'Brien, C. (1999). Peripheral endothelial dysfunction in normal pressure glaucoma. *Investigative Ophthalmology & Visual Science* 40, 1710-1714

Henson, D. B., Artes, P. H. & Chauhan, B. C. (1999). Diffuse loss of sensitivity in early glaucoma. *Investigative Ophthalmology & Visual Science* 40, 3147-3151

Hernandez, M. R. (2000). The optic nerve head in glaucoma: Role of astrocytes in tissue remodeling. *Progress in Retinal and Eye Research* 19, 297-321

Herndon, L. W., Challa, P. & Allingham, R. R. (2003). Glaucoma in Ghana, West Africa: Clinical features and the role of mutations in myocilin. *Ophthalmology Clinics of North America* 16, 631-637

Heron, G., Adams, A. J. & Husted, R. (1988). Central visual fields for short wavelength sensitive pathways in glaucoma and ocular hypertension. *Investigative Ophthalmology & Visual Science* 29, 64-72

Hitchings, R. (1991). The ocular pulse. *British Journal of Ophthalmolgy* 75, 65

Hodapp, E., Parrish II, R. K. & Anderson, D. (1993). In: *Clinical decisions in glaucoma,* St. Louis, Mosby.

Hoh, S. T., Aung, T. & Chew, P. T. (2002). Medical management of angle closure glaucoma. *Seminars in Ophthalmology* 17, 79-83

Holopigian, K., Seiple, W., Greenstein, V., Kim, D. & Carr, R. E. (1997). Relative effects of aging and age-related macular degeneration on peripheral visual function. *Optometry and Vision Science* 74, 152-159

Holtkamp, G. M., Kijlstra, A., Peek, R. & de Vos, A. F. (2001). Retinal pigment epithelium-immune system interactions: Cytokine production and cytokine-induced changes. *Progress in Retinal and Eye Research* 20, 29-48

Hrynchak, P., Hutchings, N., Jones, D. & Simpson, T. (2003). A comparison of cup-to-disc ratio evaluation in normal subjects using stereo biomicroscopy and digital imaging of the optic nerve head. *Ophthalmic and Physiological Optics* 23, 51-59

Huang, D., Swanson, E. A., Lin, C. P., Schuman, J. S., Stinson, W. G., *et al.* (1991). Optical coherence tomography. *Science* 254, 1178-1181

Hubbard, L. D., Brothers, R. J., King, W. N., Clegg, L. X., Klein, R., *et al.* (1999). Methods for evaluation of retinal microvascular abnormalities associated with hypertension/sclerosis in the atherosclerosis risk in communities study. *Ophthalmology* 106, 2269-2280

Hubel, D. H. (1988). In: *Eye, brain and vision,* Scientific American Library, New York.

Hudson, C., Wild, J. M. & Archer-Hall, J. (1993). Maximizing the dynamic-range of the humphrey field analyzer for blue-on-yellow perimetry. *Ophthalmic and Physiological Optics* 13, 405-408.

Hudson, C., Wild, J. M. & O'Neill, E. C. (1994). Fatigue effects during a single session of automated static threshold perimetry. *Investigative Opthalmology & Visual Science* 35, 268-270

Hurcomb, P. G., Wolffsohn, J. S. & Napper, G. A. (2001). Ocular signs of systemic hypertension: A review. *Ophthalmic and Physiological Optics* 21, 430-440

Hutchings, N., Wild, J. M., Hussey, M. K., Flanagan, J. G. & Trope, G. E. (2000). The long-term fluctuation of the visual field in stable glaucoma. *Investigative Ophthalmology & Visual Science* 41, 3429-3436

Hutchings, N., Hoskins, S., Wild, J. & Flannigan, J. (2001). Long-term fluctuation in short-wavelength automated perimetry in glaucoma suspects and glaucoma patients. *Investigative Ophthalmology & Visual Science* 42, 2332-2337

Hyung, S. M., Kim, D. M., Hong, C. & Youn, D. H. (1992). Optic disc of the myopic eye: Relationship between refractive errors and morphometric characteristics. *Korean Journal of Ophthalmology* 6, 32-35.

Iester, M., Mochi, B., Lai, S., Rathschuler, F., Rolando, M., *et al.* (1997). Intraimage reproducibility of measurements in the macular area using a computerized system. *International Ophthalmology* 21, 153-159

Iester, M., Mikelberg, F. S., Courtright, P., Burk, R. O. W., Caprioli, J., *et al.* (2001). Interobserver variability of optic disc variables measured by confocal scanning laser tomography. *American Journal of Ophthalmology* 132, 57-62

Iester, M., Tizte, P. & Mermoud, A. (2002). Retinal nerve fiber layer thickness changes after an acute increase in intraocular pressure. *Journal of Cataract and Refractive Surgery* 28, 2117-2122

Ikram, M. K., Borger, P. H., Assink, J. J. M., Jonas, J. B., Hofman, A., *et al.* (2002). Comparing ophthalmoscopy, slide viewing, and semiautomated systems in optic disc morphometry. *Ophthalmology* 109, 486-493

Jacobson, N., Andrews, M., Shepard, A. R., Nishimura, D., Searby, C., *et al.* (2001). Non-secretion of mutant proteins of the glaucoma gene myocilin in cultured trabecular meshwork cells and in aqueous humor. *Human Molecular Genetics* 10, 117-125

Janknecht, P. & Funk, J. (1994). Optic nerve head analyser and Heidelberg Retina Tomograph: Accuracy and reproducibility of topographic measurements in a model eye and in volunteers. *British Journal of Ophthalmology* 78, 760-768

Jean-Louis, S., Lovasik, J. V. & Kergoat, H. (2005). Systemic hyperoxia and retinal vasomotor responses. *Investigative Ophthalmology & Visual Science* 46, 1714-1720

Johnson, C. A. & Keltner, J. L. (1987). Optimal rates of movement for kinetic perimetry. *Archives of Ophthalmology* 105, 73-75

Johnson, C. A., Adams, A. J., Twelker, J. D. & Quigg, J. M. (1988). Age-related-changes in the central visual-field for short- wavelength-sensitive pathways. *Journal of the Optical Society of America A - Optics Image Science and Vision* 5, 2131-2139

Johnson, C. A., Adams, A. J., Casson, E. J. & Brandt, J. D. (1993). Progression of early glaucomatous visual-field loss as detected by blue-on-yellow and standard white-on-white automated perimetry. *Archives of Ophthalmology* 111, 651-656

Johnson, C. A. & Nelson-Quigg, J. (1993). A prospective three-year study of response properties of normal subjects and patients during automated perimetry. *Ophthalmology* 100, 269-274

Johnson, C. A. (1994). Selective versus nonselective losses in glaucoma. *Journal of Glaucoma* 3, 532-544

Johnson, C. A., Brandt, J. D., Khong, A. M. & Adams, A. J. (1995). Short-wavelength automated perimetry in low-risk, medium-risk and high-risk ocular hypertensive eyes - initial base-line results. *Archives of Ophthahlmology* 113, 70-76

Johnson, C. A. & Casson, E. J. (1995). Effects of luminance, contrast, and blur on visual acuity. *Optometry and Vision Science* 72, 864-869

Johnson, P. C. (1986). Autoregulation of blood flow. *Circulation Research* 59, 483-495

Jonas, J. B., Gusek, G. C., Guggenmoos-Holzmann, I. & Naumann, G. O. (1988a). Size of the optic nerve scleral canal and comparison with intravital determination of optic disc dimensions. *Graefe's Archive for Clinical and Experimental Ophthalmology* 226, 213-215

Jonas, J. B., Gusek, G. C. & Naumann, G. O. (1988b). The parapapillary region of normal and glaucoma eyes. I. Planimetric values of 312 glaucoma and 125 normal eyes. *Klinische Monatsblätter für Augenheilkunde* 193, 52-61.

Jonas, J. B., Gusek, G. C. & Naumann, G. O. H. (1988c). Morphometric optic disc evaluation in normals and glaucoma. *Ophthalmic Research* 20, 76-76

Jonas, J. B., Gusek, G. C. & Naumann, G. O. H. (1988d). Optic disc, cup and neororetinal rim size, configuration and correlations in normal eyes. *Investigative Opthalmology & Visual Science* 29, 1151-1158

Jonas, J. B. & Naumann, G. O. (1988). Parapapillary region in normal and glaucoma eyes. II. Correlation of planimetric findings to intrapapillary, perimetry and general data. *Klinische Monatsblätter für Augenheilkunde* 193, 182-188.

Jonas, J. B. & Naumann, G. O. (1989). Parapapillary retinal vessel diameter in normal and glaucoma eyes. II. Correlations. *Investigative Ophthalmology & Visual Science* 30, 1604-1611.

Jonas, J. B., Nguyen, N. X. & Naumann, G. O. (1989a). Optic disc morphometry in simple optic nerve atrophy. *Acta Ophthalmologica (Copenhagen)* 67, 199-203.

Jonas, J. B., Nguyen, X. N. & Naumann, G. O. H. (1989b). Parapapillary retinal vessel diameter in normal and glaucoma eyes. I. Morphometric data. *Investigative Ophthalmology & Visual Science* 30, 1599-1603

Jonas, J. B., Zach, F. M., Gusek, G. C. & Naumann, G. O. H. (1989c). Pseudoglaucomatous physiologic large cups. *American Journal of Ophthalmology* 107, 137-144

Jonas, J. B., Gusek, G. C. & Fernandez, M. C. (1991). Correlation of the blind spot size to the area of the optic disc and parapapillary atrophy. *American Journal of Ophthalmology* 111, 559-565.

Jonas, J. B., Fernandez, M. C. & Naumann, G. O. H. (1992a). Glaucomatous parapapillary atrophy - occurrence and correlations. *Archives of Ophthalmology* 110, 214-222

Jonas, J. B., Schmidt, A. M., Mullerbergh, J. A., Schlotzerschrehardt, U. M. & Naumann, G. O. H. (1992b). Human optic-nerve fiber count and optic disc size. *Investigative Ophthalmology & Visual Science* 33, 2012-2018

Jonas, J. B., Fernandez, M. C. & Sturmer, J. (1993). Pattern of glaucomatous neuroretinal rim loss. *Ophthalmology* 100, 63-68

Jonas, J. B. & Schiro, D. (1993). Visibility of the normal retinal nerve-fiber layer correlated with rim width and vessel caliber. *Graefes Archive for Clinical and Experimental Ophthalmology* 231, 207-211

Jonas, J. B. & Xu, L. (1993). Parapapillary chorioretinal atrophy in normal-pressure glaucoma. *American Journal of Ophthalmology* 115, 501-505

Jonas, J. B. & Fernandez, M. C. (1994). Shape of the neuroretinal rim and position of the central retinal-vessels in glaucoma. *British Journal of Ophthalmology* 78, 99-102

Jonas, J. B. & Konigsreuther, K. A. (1994). Optic disc appearance in ocular hypertensive eyes. *American Journal of Ophthalmology* 117, 732-740

Jonas, J. B. & Königsreuther, K. A. (1994). Optic disc appearance in ocular hypertensive eyes. *American Journal of Ophthalmology* 117, 732-740

Jonas, J. B. & Xu, L. (1994). Optic disc hemorrhages in glaucoma. *American Journal of Ophthalmology* 118, 1-8

Jonas, J. B. & Papastathopoulos, K. I. (1995). Pressure-dependent changes of the optic disc in primary open-angle glaucoma. *American Journal of Ophthalmology* 119, 313-317.

Jonas, J. B. & Dichtl, A. (1996). Evaluation of the retinal nerve fiber layer. *Survey of Ophthalmology* 40, 369-378

Jonas, J. B. & Grundler, A. E. (1997a). Correlation between mean visual field loss and morphometric optic disc variables in the open-angle glaucomas. *American Journal of Ophthalmology* 124, 488-497

Jonas, J. B. & Grundler, A. E. (1997b). Parapapillary atrophy in the focal type of normal-pressure glaucoma. *Investigative Ophthalmology & Visual Science* 38, 5365-5365

Jonas, J. B., Budde, W. M. & Lang, P. (1998a). Neuroretinal rim width ratios in morphological glaucoma diagnosis. *British Journal of Ophthalmology* 82, 1366-1371

Jonas, J. B., Grundler, A. E. & Gonzales-Cortes, J. (1998b). Pressure-dependent neuroretinal rim loss in normal-pressure glaucoma. *American Journal of Ophthalmology* 125, 137-144

Jonas, J. B., Mardin, C. Y. & Grundler, A. E. (1998c). Comparison of measurements of neuroretinal rim area between confocal laser scanning tomography and planimetry of photographs. *British Journal of Ophthalmology* 82, 362-366

Jonas, J. B., Budde, W. M. & Lang, P. J. (1999a). Parapapillary atrophy in the chronic open-angle glaucomas. *Graefe's Archive for Clinical and Experimental Ophthalmology* 237, 793-799

Jonas, J. B., Budde, W. M. & Panda-Jonas, S. (1999b). Ophthalmoscopic evaluation of the optic nerve head. *Survey of Ophthalmology* 43, 293-320

Jonas, J. B. & Hayreh, S. S. (1999). Optic disc morphology in experimental central retinal artery occlusion in rhesus monkeys. *American Journal of Ophthalmology* 127, 523-530

Jonas, J. B., Bergua, A., Schmitz-Valckenberg, P., Papastathopoulos, K. I. & Budde, W. M. (2000). Ranking of optic disc variables for detection of glaucomatous optic nerve damage. *Investigative Ophthalmology & Visual Science* 41, 1764-1773

Jonas, J. B. & Budde, W. M. (2000). Diagnosis and pathogenesis of glaucomatous optic neuropathy: Morphological aspects. *Progress in Retinal and Eye Research* 19, 1-40

Jonas, J. B. & Hayreh, S. S. (2000). Ophthalmoscopic appearance of the normal optic nerve head in rhesus monkeys. *Investigative Ophthalmology & Visual Science* 41, 2978-2983

Jonas, J. B., Budde, W. M., Nemeth, J., Grundler, A. E., Mistlberger, A., *et al.* (2001). Central retinal vessel trunk exit and location of glaucomatous parapapillary atrophy in glaucoma. *Ophthalmology* 108, 1059-1064

Jonas, J. B., Thomas, R., George, R., Berenshtein, E. & Muliyil, J. (2003). Optic disc morphology in south india: The Vellore Eye study. *British Journal of Ophthalmology* 87, 189-196

Jonas, J. B., Budde, W. M. & Martus, P. (2004). The optic disc hemifield test. *J Glaucoma* 13, 108-113

Jonas, J. B. (2005). Clinical implications of peripapillary atrophy in glaucoma. *Current Opinion in Ophthalmology* 16, 84-88

Kanazawa, I. (2001). How do neurons die in neurodegenerative diseases? *Trends in Molecular Medicine* 7, 339-344

Kasner, O., Feuer, W. J. & Anderson, D. R. (1989). Possibly reduced prevalence of peripapillary crescents in ocular hypertension. *Canadian Journal of Ophthalmology* 24, 211-215

Kassoff, A., Kassoff, J., Buehler, J., Eglow, M., Kaufman, F., *et al.* (2001). A randomized, placebo-controlled, clinical trial of high-dose supplementation with vitamins c and e, beta carotene, and zinc for age-related macular degeneration and vision loss - AREDS Report No. 8. *Archives of Ophthalmology* 119, 1417-1436

Katz, J. & Sommer, A. (1987). A longitudinal study of the age-adjusted variability of automated visual fields. *Archives of Ophthalmology* 105, 1083-1086

Katz, M. L., Rice, L. M. & Gao, C. (1999). Reversible accumulation of lipofuscin-like inclusions in the retinal pigment epithelium. *Investigative Ophthalmology & Visual Science* 40, 171-181

Kesen, M. R., Spaeth, G. L., Henderer, J. D., Pereira, M. L., Smith, A. F., *et al.* (2002). The Heidelberg Retina Tomograph vs clinical impression in the diagnosis of glaucoma. *American Journal of Ophthalmology* 133, 613-616

Kilbride, P. E., Hutman, L. P., Fishman, M. & Read, J. S. (1986). Foveal cone pigment density difference in the aging human-Eye. *Vision Research* 26, 321-325

Kim, L. S., (2003). Aspects of the threshold response in automated perimetry. Cardiff University, PhD

Kim, Y. Y., Kim, J. S., Shin, D. H., Kim, C. & Jung, H. R. (2001). Effect of cataract extraction on blue-on-yellow visual field. *American Journal of Ophthalmology* 132, 217-220

King-Smith, P. E., Grigsby, S. S., Vingrys, A. J. & Benes, S. C. (1994). Efficient and unbiased modifications of the QUEST threshold method: Theory, stimulations, experimental evaluation and practical implementation. *Vision Research* 34, 885-912

King, A. J. W., Bolton, N., Aspinall, P. & O'Brien, C. J. (2000). Measurement of peripapillary retinal nerve fiber layer volume in glaucoma. *American Journal of Ophthalmology* 129, 599-607

Kiriyama, N., Ando, A., Fukui, C., Nambu, H., Nishikawa, M., *et al.* (2003). A comparison of optic disc topographic parameters in patients with primary open angle glaucoma, normal tension glaucoma, and other hypertension. *Graefe's Archive for Clinical and Experimental Ophthalmology* 241, 541-545

Kiss, B., Polska, E., Dorner, G., Polak, K., Findl, O., *et al.* (2002). Retinal blood flow during hyperoxia in humans revisited: Concerted results using different measurement techniques. *Microvascular Research* 64, 75-85

Klein, B. E. K., Klein, R., Meuer, S. M. & Goetz, L. A. (1993). Migraine headache and its association with open-angle glaucoma - the Beaver Dam Eye Study. *Investigative Ophthalmology & Visual Science* 34, 3024-3027

Klein, B. E. K., Klein, R. & Lee, K. E. (2004). Heritability of risk factors for primary open-angle glaucoma: The Beaver Dam Eye Study. *Investigative Ophthalmology & Visual Science* 45, 59-62

Knudtson, M. D., Lee, K. E., Hubbard, L. D., Wong, T. Y., Klein, R., *et al.* (2003). Revised formulas for summarizing retinal vessel diameters. *Current Eye Research* 27, 143-149

Knudtson, M. D., Klein, B. E. K., Klein, R., Wong, T. Y., Hubbard, L. D., *et al.* (2004). Variation associated with measurement of retinal vessel diameters at different points in the pulse cycle. *British Journal of Ophthalmology* 88, 57-61

Koeberle, P. D. & Ball, A. K. (1999). Nitric oxide synthase inhibition delays axonal degeneration and promotes the survival of axotomized retinal ganglion cells. *Experimental Neurology* 158, 366-381

Koike, M., Shibata, M., Ohsawa, Y., Nakanishi, H., Koga, T., *et al.* (2003). Involvement of two different cell death pathways in retinal atrophy of cathepsin d-deficient mice. *Molecular and Cellular Neurosciences* 22, 146-161

Kolb, H., Linberg, K. A. & Fisher, S. K. (1992). Neurons of the human retina: A Golgi study. *Journal of Comparative Neurology* 318, 147-187

Kono, Y., Chi, Q., Tomita, G., Yamamoto, T. & Kitazawa, Y. (1996). High-pass resolution perimetry and a humphrey field analyzer as indicators of glaucomatous optic disc abnormalities. *Ophthalmology* 104, 1496-1502

Kono, Y., Jonas, J. B., Zangwill, L., Berry, C. C. & Weinreb, R. N. (1999a). Agreement of measurement of parapapillary atrophy with confocal scanning laser ophthalmoscopy and planimetry of photographs. *Journal of Glaucoma* 8, 105-110

Kono, Y., Zangwill, L., Sample, P. A., Jonas, J. B., Emdadi, A., *et al.* (1999b). Relationship between parapapillary atrophy and visual field abnormality in primary open-angle glaucoma. *American Journal of Ophthalmology* 127, 674-680

Kono, Y., Sample, P. A., Emdadi, A. & Weinreb, R. N. (2000). Comparative study between pointwise and ranked threshold distribution analyses of change in serial fields for short- wavelength automated perimetry. *Journal of Glaucoma* 9, 419-427

Kubota, T., Jonas, J. B. & Naumann, G. O. H. (1993). Decreased choroidal thickness in eyes with secondary angle- closure glaucoma - an etiologic factor for deep retinal changes in glaucoma. *British Journal of Ophthalmology* 77, 430-432

Kwon, Y. H., Park, H. J., Jap, A., Ugurlu, S. & Caprioli, J. (1998). Test-retest variability of blue-on-yellow perimetry is greater than white-on-white perimetry in normal subjects. *American Journal of Ophthalmology* 126, 29-36

Laabich, A., Li, Guangyu & Cooper, N. G. F. (2001). Characterization of apoptosis-genes associated with NMDA mediated cell death in the adult rat retina. *Molecular Brain Research* 91, 34-42

Lachenmayr, B., Drance, S., Chauhan, B. C., House, P. H. & Lalani, S. (1991). Diffuse and localized glaucomatous field loss in light sense, flicker and resolution perimetry. *Graefe's Arch Clin. Exp. Ophthalmol* 229, 267-273

Lammer, R., Link, B., Viestenz, A., Horn, F. K. & Mardin, C. Y. (2005). Measurement of autofluorescence in the parapapillary atrophic zone in patients with ocular hypertension. *Investigative Ophthalmology & Visual Science* 46, E-abstract 2513

Law, S. K., Choe, R. & Caprioli, J. (2001). Optic disc characteristics before the occurrence of disc hemorrhage in glaucoma patients. *American Journal of Ophthalmology* 132, 411-413

Ledoux, S. P., Shen, C. C., Grishko, V. I., Fields, P. A., Gard, A. L., *et al.* (1998). Glial cell-specific differences in response to alkylation damage. *Glia* 24, 304-312

Lee, A., Mukesh, B. N., McCarty, C. A. & Taylor, H. R. (2003). Risk factors associated with the incidence of open-angle glaucoma: The visual impairment project. *Investigative Ophthalmology & Visual Science* 44, 3783-3789

Lee, M. S., Shin, D. S. & Berger, J. W. (2000). Grading, image analysis, and stereopsis of digitally compressed fundus images. *Retina - the Journal of Retinal and Vitreous Diseases* 20, 275-281

Lee, S. B., Uhm, K. B. & Hong, C. (1998). Retinal vessel diameter in normal and primary open-angle glaucoma. *Korean Journal of Ophthalmology* 12, 51-59.

Lee, S. S. & Schwartz, B. (1992). Role of the temporal cilioretinal artery in retaining central visual-field in open-angle glaucoma. *Ophthalmology* 99, 696-699

Lennie, P. (1980). Parallel visual pathways: A review. *Vision Research* 20, 561-594

Leske, M. C., Nemesure, B., He, Q., Wu, S.-Y., Fielding Hejtmancik, J., *et al.* (2001). Patterns of open-angle glaucoma in the Barbados Family Study. *Ophthalmology* 108, 1015-1022

Levin, L. A. & Gordon, L. K. (2002). Retinal ganglion cell disorders: Types and treatments. *Progress in Retinal and Eye Research* 21, 465-484

Levy, N. S., Crapps, E. E. & Bonney, R. C. (1981). Displacement of the optic nerve head. Response to acute intraocular pressure elevation in primate eyes. *Archives of Ophthalmology* 99, 2166-2174

Lipton, L. (2002). In: *Stereographic handbook for development of stereoscopic imaging applications,* Stereographics Corporation,

Liu, C. J., Chiou, H. J., Chiang, S. C., Chou, J. C., Chou, Y. H., *et al.* (1999). Variations in ocular hemodynamics in patients with early and late glaucoma. *Acta Ophthalmologica Scandinavica* 77, 658-662

Luna, J. D., Chan, C. C., Derevjanik, N. L., Mahlow, J., Chiu, C., *et al.* (1997). Blood-retinal barrier (BRB) breakdown in experimental autoimmune uveoretinitis: Comparison with vascular endothelial growth factor, tumor necrosis factor alpha, and interleukin-1beta-mediated breakdown. *Journal of Neuroscience Research* 49, 268-280

Luo, X. M., Heidinger, V., Picaud, S., Lambrou, G., Dreyfus, H., *et al.* (2001). Selective excitotoxic degeneration of adult pig retinal ganglion cells in vitro. *Investigative Ophthalmology & Visual Science* 42, 1096-1106

Lynch, S., Johnson, C. A. & Demirel, S. (1997). Is early damage in glaucoma selective for a particular cell type or pathway In: *Perimetry Update*, (Eds. Ed, W. M. & Heijl, A.) Kugler Publishers, Amsterdam, 253-261.

Mabuchi, F., Aihara, M., Mackey, M. R., Lindsey, J. D. & Weinreb, R. N. (2004). Regional optic nerve damage in experimental mouse glaucoma. *Investigative Ophthalmology & Visual Science* 45, 4352-4358

Marc, R. E. & Jones, B. W. (2003). Retinal remodeling in inherited photoreceptor degenerations. *Molecular Neurobiology* 28, 139-147

Marc, R. E., Jones, B. W., Watt, C. B. & Strettoi, E. (2003). Neural remodeling in retinal degeneration. *Progress in Retinal and Eye Research* 22, 607-655

Mardin, C. Y., Horn, F. K., Jonas, J. B. & Budde, W. M. (1999). Preperimetric glaucoma diagnosis by confocal scanning laser tomography of the optic disc. *British Journal of Ophthalmology* 83, 299-304

Margo, C. E., Harman, L. E. & Mulla, Z. D. (2002). The reliability of clinical methods in ophthalmology. *Survey of Ophthalmology* 47, 375-386

Mariani, A. P. (1982). Biplexiform cells: Ganglion cells of the primate retina that contact photoreceptors. *Science* 216, 1134-1136

Marra, G. & Flammer, J. (1991). The learning and fatigue effect in automated perimetry. *Graefe's Archive for Clinical and Experimental Ophthalmology* 229, 501-504

Matsumoto, C., Shirato, S., Haneda, M., Yamashiro, H. & Saito, M. (2003). Study of retinal nerve fiber layer thickness within normal hemivisual field in primary open-angle glaucoma and normal-tension glaucoma. *Japanese Journal of Ophthalmology* 47, 22-27

Matsuno, K., Kurimoto, Y., Umihira, J., Hoya, T. & Yoshimura, N. (2001). Comparative study of retinal nerve fiber layer loss in normal-tension glaucoma and chronic open-angle glaucoma. *Ophthalmologica* 215, 108-112

Medeiros, F. A., Zangwill, L. M., Bowd, C., Sample, P. A. & Weinreb, R. N. (2005). Use of progressive glaucomatous optic disc change as the reference standard for evaluation of diagnostic tests in glaucoma. *American Journal of Ophthalmology* 139, 1010-1018

Merigan, W. H. & Maunsell, J. H. R. (1993). How parallel are the primate visual pathways. *Annual Reviews of Neuroscience* 16, 369 - 402

Meyer, P., Flammer, J. & Luscher, T. F. (1993). Endothelium-dependent regulation of the ophthalmic microcirculation in the perfused porcine eye: Role of nitric oxide and endothelins. *Investigative Ophthalmology & Visual Science* 34, 3614-3621

Mikelberg, F. S., Drance, S. M., Schulzer, M., Yidegiligne, H. M. & Weis, M. M. (1989). The normal human optic-nerve - axon count and axon diameter distribution. *Ophthalmology* 96, 1325-1328

Mikelberg, F. S. (1993). Intraocular pressure and glaucoma. *Canadian Journal of Ophthalmology* 28, 251-253

Mikelberg, F. S. (1995). The interpretation of automated visual fields. *Canadian Journal of Ophthalmology* 30, 281-283

Miller, K. M. & Quigley, H. A. (1988). The clinical appearance of the lamina cribrosa as a function of the extent of glaucomatous optic nerve damage. *Ophthalmology* 95, 135-138

Minckler, D. S. (1980). The organization of nerve fiber bundles in the primate optic nerve head. *Archives of Ophthalmology* 98, 1630-1636

Minkler, D., Nichols, T. & Morales, R. (1992). Preliminary clinical experience with the Nidek 3Dx camera and lenticular stereodisc images. *Journal of Glaucoma* 1, 184 - 186

Mitchell, P., Smith, W., Chey, T. & Henley, P. R. (1997). Open-angle glaucoma and diabetes - the Blue Mountains Eye Study, Australia. *Ophthalmology* 104, 712-718

Moreno, M. C., Campanelli, J., Sande, P., Saenz, D. A., Sarmiento, M., *et al.* (2004). Retinal oxidative stress induced by high intraocular pressure. *Free Radical Biology and Medicine* 37, 803-812

Morgan, J., Caprioli, J. & Koscki, Y. (1999). Nitric oxide mediates excitotoxic and anoxic damage in rat retinal ganglion cells cocultured with astroglia. *Archives of Ophthalmology* 117, 1524-1529

Morgan, J. E., Jeffery, G. & Foss, A. J. (1998). Axon deviation in the human lamina cribrosa. *British Journal of Ophthalmology* 82, 680-683

Morgan, J. E. (2000). Optic nerve head structure in glaucoma: Astrocytes as mediators of axonal damage. *Eye* 14, 437-444

Morgan, J. E., Sheen, N. J. L., North, R. V., Choong, Y. & Ansari, E. (2005a). Digital imaging of the optic nerve head: Monoscopic and stereoscopic analysis. *British Journal of Ophthalmology* 89, 879-884

Morgan, J. E., Sheen, N. J. L., North, R. V., Goyal, R., Morgan, S., *et al.* (2005b). Discrimination of glaucomatous optic neuropathy by digital stereoscopic analysis. *Ophthalmology* 112, 855-862

Moss, I. D. & Wild, J. M. (1994). The influence of induced forward light scatter on the normal blue-on-yellow perimetric profile. *Graefe's Archive for Clinical and Experimental Ophthalmology* 232, 409-414

Moss, I. D., Wild, J. M. & Whitaker, D. J. (1995). The influence of age-related cataract on blue-on-yellow perimetry. *Investigative Ophthalmology & Visual Science* 36, 764-773

Moya, F. J., Brigatti, L. & Caprioli, J. (1999). Effect of aging on optic nerve appearance: A longitudinal study. *British Journal of Ophthalmology* 83, 567-572

Nagel, E., Wilser, W. & Lanzl, I. (2002). Functional analysis of retinal vessel diameter reaction to artificially raised intraocular pressure in glaucoma patients with and without dorzolamide therapy. *Vasa-Journal of Vascular Diseases* 31, 230-234

Nagel, E. & Vilser, W. (2004). Autoregulative behavior of retinal arteries and veins during changes of perfusion pressure: A clinical study. *Graefe's Archive for Clinical and Experimental Ophthalmology* 242, 13-17

Naskar, R., Vorwerk, C. K. & Dreyer, E. B. (2000). Concurrent downregulation of a glutamate transporter and receptor in glaucoma. *Investigative Ophthalmology & Visual Science* 41, 1940-1944

Navascues, J., Moujahid, A., Quesada, A. & Cuadros, M. A. (1994). Microglia in the Avian retina: Immunocytochemical demonstration in the adult Quail. *Journal of Comparative Neurology* 350, 171-186

Nemeth, J., Michelson, G. & Harazny, J. (2001). Retinal microcirculation correlates with ocular wall thickness, axial eye length, and refraction in glaucoma patients. *Journal of Glaucoma* 10, 390-395

Neufeld, A. H., Hernandez, M. R. & Gonzalez, M. (1997). Nitric oxide synthase in the human glaucomatous optic nerve head. *Archives of Ophthalmology* 115, 497-503

Neufeld, A. H. (1999). Microglia in the optic nerve head and the region of parapapillary chorioretinal atrophy in glaucoma. *Archives of Ophthalmology* 117, 1050-1056

Neufeld, A. H. & Gachie, E. N. (2003). The inherent, age-dependent loss of retinal ganglion cells is related to the lifespan of the species. *Neurobiology of Aging* 24, 167-172

Neufeld, E. F. (1991). Lysosomal storage diseases. *Annual Review of Biochemestry* 60, 257-280

Nevarez, J., Rockwood, E. J. & Anderson, D. R. (1988). The configuration of peripapillary tissue in unilateral glaucoma. *Archives of Ophthalmology* 106, 901-903

Nickells, R. W. (1999). Apoptosis of retinal ganglion cells in glaucoma: An update of the molecular pathways involved in cell death. *Survey of Ophthalmology* 43, S151-S161

Nicolela, M. T. & Drance, S. M. (1996). Various glaucomatous optic nerve appearances - clinical correlations. *Ophthalmology* 103, 640-649

Nicolela, M. T., Walman, B. E., Buckley, A. R. & Drance, S. M. (1996). Ocular hypertension and primary open-angle glaucoma: A comparative study of their retrobulbar blood flow velocity. *Journal of Glaucoma* 5, 308-310

Nicolela, M. T., Drance, S. M., Broadway, D. C., Chauhan, B. C., McCormick, T. A., *et al.* (2001). Agreement among clinicians in the recognition of patterns of optic disc damage in glaucoma. *American Journal of Ophthalmology* 132, 836-844

O'Brart, D. P., de Souza Lima, M., Bartsch, D. U., Freeman, W. & Weinreb, R. N. (1997). Indocyanine green angiography of the peripapillary region in glaucomatous eyes by confocal scanning laser ophthalmoscopy. *American Journal of Ophthalmology* 123, 657-666

O'Connor, D. J., Zeyen, T. & Caprioli, J. (1993). Comparisons of methods to detect glaucomatous optic-nerve damage. *Ophthalmology* 100, 1498-1503

Ogden, T. E. (1983). Nerve fiber layer of the macaque retina: Retinotopic organization. *Investigative Ophthalmology & Visual Science* 24, 85-98

Ogden, T. E. (1984). Nerve fiber layer of the primate retina: Morphometric analysis. *Investigative Ophthalmology & Visual Science* 25, 19-29

Ogden, T. E. (1994). Basic science and inherited retinal disease In: *Retina*, (Ed. Ryan, S. J.) Mosby, St. Louis,

Oku, H., Sugiyama, T., Kojima, S., Watanabe, T. & Azuma, I. (1999). Experimental optic cup enlargement caused by endothelin-1- induced chronic optic nerve head ischaemia. *Survey of Ophthalmology* 44, S74-S84

Onda, E., Cioffi, G. A., Bacon, D. R. & Van Buskirk, E. M. (1995). Microvasculature of the human optic nerve. *American Journal of Ophthalmology* 120, 92-102

Orgul, S., Croffi, G. A. & Van Buskirk, E. M. (1997). Variability of contour line alignment on sequential images with the Heidelberg Retina Tomograph. *Graefe's Archive for Clinical and Experimental Ophthalmology* 235, 82-86

Osborne, N. N., Ugarte, M., Chao, M., Childlow, G., Bae, J. H., *et al.* (1999). Neuroprotection in relation to retinal ischaemia and relevance to glaucoma. *Survey of Ophthalmology* 43, S102-S128

Osborne, N. N., Melena, J., Chidlow, G. & Wood, J. P. M. (2001). A hypothesis to explain ganglion cell death caused by vascular insults at the optic nerve head: Possible implication for the treatment of glaucoma. *British Journal of Ophthalmology* 85, 1252-1259

Osborne, N. N., Casson, R. J., Wood, J. P. M., Chidlow, G., Graham, M., *et al.* (2004). Retinal ischaemia: Mechanisms of damage and potential therapeutic strategies. *Progress in Retinal and Eye Research* 23, 91-147

Owen, C. G., Ellis, T. J., Rudnicka, A. R. & Woodward, E. G. (2002). Optimal green (red-free) digital imaging of conjunctival vasculature. *Ophthalmic and Physiological Optics* 22, 234-243

Palmberg, P. (2002). Answers from the ocular hypertension treatment study. *Archives of Ophthalmology* 120, 829-830

Panda, S. & Jonas, J. B. (1992). Decreased photoreceptor count in human eyes with secondary angle-closure glaucoma. *Investigative Ophthalmology & Visual Science* 33, 2532-2536

Papastathopoulos, K. I. & Jonas, J. B. (1995). Focal narrowing of retinal arterioles in optic nerve atrophy. *Ophthalmology* 102, 1706-1711.

Papastathopoulos, K. I. & Jonas, J. B. (1999). Follow up of focal narrowing of retinal arterioles in glaucoma. *British Journal of Ophthalmology* 83, 285-289

Park, K. H., Tomita, G., Liou, S. Y. & Kitazawa, Y. (1996a). Correlation between peripapillary atrophy and visual field loss in normal-tension glaucoma. *Investigative Ophthalmology & Visual Science* 37, 130-130

Park, K. H., Tomita, G., Liou, S. Y. & Kitazawa, Y. (1996b). Correlation between peripapillary atrophy and optic nerve damage in normal-tension glaucoma. *Ophthalmology* 103, 1899-1906

Park, K. H., Park, S. J., Lee, Y. J., Kim, J. Y. & Caprioli, J. (2001). Ability of peripapillary atrophy parameters to differentiate normal- tension glaucoma from glaucomalike disc. *Journal of Glaucoma* 10, 95-101.

Parkin, B., Shuttleworth, G., Costen, M. & Davison, C. (2001). A comparison of stereoscopic and monoscopic evaluation of optic disc topography using a digital optic disc stereo camera. *British Journal of Ophthalmology* 85, 1347-1351

Pedersen, L., Grunkin, M., Ersboll, B., Madsen, K., Larsen, M., *et al.* (2000). Quantitative measurement of changes in retinal vessel diameter in ocular fundus images. *Pattern Recognition Letters* 21, 1215-1223

Pederson, J. & Anderson, D. (1980). The mode of progressive disc cupping in ocular hypertension and glaucoma. *Archives of Ophthalmology* 98, 490-495

Pena, J. D. O., Netland, P. A., Vidal, I., Dorr, D. A., Rasky, A., *et al.* (1998). Elastosis of the lamina cribrosa in glaucomatous optic neuropathy. *Experimental Eye Research* 67, 517-524

Pennebaker, G. E., Stewart, W. C., Stewart, J. A. & Hunt, H. H. (1992). The effect of stimulus duration upon the components of fluctuation in static automated perimetry. *Eye* 6, 353-355

Philipson, B. (1969). Light scattering in lenses with experimental cataract. *Acta Ophthalmologica* 47, 1089-1101

Plange, N., Remky, A. & Arend, O. (2003). Colour doppler imaging and fluorescein filling defects of the optic disc in normal tension glaucoma. *British Journal of Ophthalmology* 87, 731-736

Polak, K., Schmetterer, L. & Riva, C. E. (2002). Influence of flicker frequency on flicker-induced changes of retinal vessel diameter. *Investigative Ophthalmology & Visual Science* 43, 2721-2726

Polo, V., Abecia, E., Pablo, L. E., Pinilla, I., Larrosa, J. M., *et al.* (2001). Functional and structural measurements in a multifactorial glaucoma risk model. *Acta Ophthalmologica Scandinavica* 79, 10-14

Provis, J. M., van Driel, D., Billson, F. A. & Russell, P. (1985). Human fetal optic nerve: Overproduction and elimination of retinal axons during development. *Journal of Comparative Neurology* 238, 92-100

Provis, J. M., Diaz, C. M. & Penfold, P. L. (1996). Microglia in human retina: A heterogeneous population with distinct ontogenies. *Perspectives on Developmental Neurobiology* 3, 213-222

Provis, J. M. (2001). Development of the primate retinal vasculature. *Progress in Retinal and Eye Research* 20, 799-821

Purcell, D. G. & Stewart, A. L. (1988). The face-detection effect - configuration enhances detection. *Perception and Psychophysics* 43, 355-366

Quigley, H. A., Adicks, E. M., Green, W. R. & Maumenee, A. E. (1981). Optic nerve damage in human glaucoma - the site of injury and suspectibility to damage. *Archives of Ophthalmology* 99, 635-649

Quigley, H. A., Addicks, E. M. & Green, W. R. (1982). Optic nerve damage in human glaucoma. III. Quantitative correlation of nerve fiber loss and visual field defect in glaucoma, ischaemic neuropathy, papilledema, and toxic neuropathy. *Archives of Ophthalmology* 100, 135-146

Quigley, H. A., Hohman, R. M., Addicks, E. M., Massof, R. W. & Green, W. R. (1983). Morphologic changes in the lamina cribosa correlated with neural loss in open-angle glaucoma. *American Journal of Ophthalmology* 95, 673-691

Quigley, H. A. (1985). Better methods in glaucoma diagnosis - editorial. *Archives of Ophthalmology* 103,

Quigley, H. A., Sanchez, R. M., Dunkelberger, G. R., L'Hernault, N. L. & Baginski, T., A. (1987). Chronic glaucoma selectively damages large optic nerve fibers. *Investigative Ophthalmology & Visual Science* 28, 913-920

Quigley, H. A., Brown, A. E., Morrison, J. D. & Drance, S. M. (1990). The size and shape of the optic disc in normal human eyes. *Archives of Ophthalmology* 108, 51-57

Quigley, H. A., Brown, A. & Dormanpease, M. E. (1991a). Alterations in elastin of the optic-nerve head in human and experimental glaucoma. *British Journal of Ophthalmology* 75, 552-557

Quigley, H. A., Coleman, A. L. & Dormanpease, M. E. (1991b). Larger optic-nerve heads have more nerve-fibers in normal monkey eyes. *Archives of Ophthalmology* 109, 1441-1443

Quigley, H. A. (1994a). Comment. *British Journal of Ophthalmology* 78, 879 - 880

Quigley, H. A. (1994b). Selective cell-death in glaucoma - does it really occur? *British Journal of Ophthalmology* 78, 879-880

Quigley, H. A., Enger, C., Katz, J., Sommer, A., Scott, R., *et al.* (1994). Risk-factors for the development of glaucomatous visual-field loss in ocular hypertension. *Archives of Ophthalmology* 112, 644-649

Quigley, H. A. (1995). Ganglion-cell death in glaucoma - pathology recapitulates ontogeny. *Australian and New Zealand Journal of Ophthalmology* 23, 85-91

Quigley, H. A., Nickells, R. W., Kerrigan, L. A., Pease, M. E., Thibault, D. J., *et al.* (1995). Retinal ganglion-cell death in experimental glaucoma and after axotomy occurs by apoptosis. *Investigative Ophthalmology & Visual Science* 36, 774-786

Quigley, H. A. (1998). Identification of glaucoma-related visual field abnormality with the screening protocol of frequency doubling technology. *American Journal of Ophthalmology* 125, 819-829

Rader, J., Feuer, W. J. & Anderson, D. R. (1994). Peripapillary vasoconstriction in the glaucomas and the anterior ischaemic optic neuropathies. *American Journal of Ophthalmology* 117, 72-80

Radius, R. L. (1980). Thickness of the retinal nerve fiber layer in primate eyes. *Archives of Ophthalmology* 98, 1625-1629

Radius, R. L. & Bade, B. (1981). Pressure-induced optic-nerve axonal-transport interruption in cat eyes. *Archives of Ophthalmology* 99, 2163-2165

Raff, M. C., Barres, B. A., Burne, J. F., Coles, H. S., Ishizaki, Y., *et al.* (1993). Programmed cell death and the control of cell survival: Lessons from the nervous system. *Science* 262, 695-700

Ramrattan, R. S., Wolfs, R. C. W., Jonas, J. B., Hofman, A. & de Jong, P. T. V. M. (1999). Determinants of optic disc characteristics in a general population: The Rotterdam study: Historical image. *Ophthalmology* 106, 1588-1596

Rankin, S. J. A. & Drance, S. M. (1996). Peripapillary focal retinal arteriolar narrowing in open angle glaucoma. *Journal of Glaucoma* 5, 22-28

Rankin, S. J. A., Drance, S. M., Buckley, A. R. & Walman, B. E. (1996). Visual field correlations with color doppler studies in open angle glaucoma. *Journal of Glaucoma* 5, 15-21

Rasker, M. T., vandenEnden, A., Bakker, D. & Hoyng, P. F. J. (1997). Deterioration of visual fields in patients with glaucoma with and without optic disc hemorrhages. *Archives of Ophthalmology* 115, 1257-1262

Rassam, S. M. B., Patel, V., Brinchmannhansen, O., Engvold, O. & Kohner, E. M. (1994). Accurate vessel width measurement from fundus photographs - a new concept. *British Journal of Ophthalmology* 78, 24-29

Riva, C. E., Grunwald, J. E. & Petrig, B. L. (1986). Autoregulation of human retinal blood flow : An investigation with laser doppler velocimetry. *Investigative Ophthalmology & Visual Science* 27, 1706 -1712

Robinson, F., Riva, C. E., Grunwald, J. E., Petrig, B. L. & Sinclair, S. H. (1986). Retinal blood flow autoregulation in response to acute increase of blood pressure. *Investigative Ophthalmology & Visual Science* 27, 1706-1712

Rodieck, R. W. (1998). In: *The first step in seeing,* Sinauer Associates, Sunderland, MA.

Roff, E. J., Hosking, S. L. & Barnes, D. A. (2001). The influence of contour line size and location on the reproducibility of topographic measurement with the Heidelberg Retina Tomograph. *Ophthalmic and Physiological Optics* 21, 173-181

Rosenthal, A., Kottler, M., Donaldson, D. & Falconer, D. (1977). Comparative reproducebility of the digital photogrammetric procedure utilising 3 methods of stereophotography. *Investigative Ophthalmology & Visual Science* 16, 54-60

Rudnicka, A. R., Frost, C., Owen, C. G. & Edgar, D. F. (2001). Nonlinear behavior of certain optic nerve head parameters and their determinants in normal subjects. *Ophthalmology* 108, 2358-2368

Rutishauser, C. & Flammer, J. (1988). Retests in static perimetry. *Graefe's Archive for Clinical and Experimental Ophthalmology* 226, 75-77

Saccà, S. C., Rolando, M., Marletta, A., Macrì, A., Cerqueti, P., *et al.* (1998). Fluctuations of intraocular pressure during the day in open-angle glaucoma, normal-tension glaucoma and normal subjects. *Ophthalmologica* 212, 115 - 119

Salvador-Silva, M., Aoi, S., Parker, A., Yang, P., Pecen, P., *et al.* (2004). Responses and signaling pathways in human optic nerve head astrocytes exposed to hydrostatic pressure in vitro. *Glia* 45, 364-377

Samdani, A. F., Dawson, T. M. & Dawson, V. L. (1997). Nitric oxide synthase in models of focal ischaemia. *Stroke* 28, 1283-1288

Samdani, A. F., Newcamp, C., Resink, A., Facchinetti, F., Hoffman, B. E., *et al.* (1997). Differential susceptibility to neurotoxicity mediated by neurotrophins and neuronal nitric oxide synthase. *Journal of Neuroscience* 17, 4633-4641

Sample, P., Esterson, F., Weinreb, R. & Boynton, R. (1988). The aging lens: In vivo assessment of light absorption in 84 human eyes. *Investigative Ophthalmology & Visual Science* 29, 1306-1311

Sample, P., Esterson, F. & Weinreb, R. (1989). A practical method for obtaining an index of lens density with an automated perimeter. *Investigative Ophthalmology & Visual Science* 30, 786-787

Sample, P. A., Boynton, R. M. & Weinreb, R. N. (1988). Isolating the color-vision loss in primary open-angle glaucoma. *American Journal of Ophthalmology* 106, 686-691

Sample, P. A. & Weinreb, R. N. (1990). Color perimetry for assessment of primary open-angle glaucoma. *Investigative Ophthalmology & Visual Science* 31, 1869-1875

Sample, P. A. & Weinreb, R. N. (1992). Progressive color visual field loss in glaucoma. *Investigative Ophthalmology & Visual Science* 33, 2068-2071

Sample, P. A., Taylor, J. D. N., Martinez, G. A., Lusky, M. & Weinreb, R. N. (1993). Short-wavelength color visual fields in glaucoma suspects at risk. *American Journal of Ophthalmology* 115, 225-233

Sample, P. A., Johnson, C. A., Haegerstrom-Portnoy, G. & Adams, A. J. (1996). Optimum parameters for short-wavelength automated perimetry. *Journal of Glaucoma* 5, 375-383

Sample, P. A., Irak, I., Martinez, G. A. & Yamagishi, N. (1997). Asymmetries in the normal short-wavelength visual field, implications for short-wavelength automated perimetry. *American Journal of Ophthalmology* 124, 46-52

Sanchez, R., Dunkelberger, G. & Quigley, H. A. (1986). The number and diameter distribution of axons in the monkey optic nerve. *Investigative Ophthalmology & Visual Science* 27, 1342-1350

Sandercoe, T. M., Madigan, M. C., Billson, F. A., Penfold, P. L. & Provis, J. M. (1999). Astrocyte proliferation during development of the human retinal vasculature. *Experimental Eye Research* 69, 511-523

Satilmis, M., Orgul, S., Doubler, B. & Flammer, J. (2003). Rate of progression of glaucoma correlates with retrobulbar circulation and intraocular pressure. *American Journal of Ophthalmology* 135, 664-669

Savage, G. L., Haegerstrom-Portnoy, G., Adams, A. J. & Hewlett, S. E. (1993). Age changes in the optical density of human ocular media. *Clinical Vision Science* 8, 97-108

Sawada, A. & Neufeld, A. H. (1999). Confirmation of the rat model of chronic, moderately elevated intraocular pressure. *Experimental Eye Research* 69, 525-531

Scheibel, M. E., Lindsay, R. D., Tomiyasu, U. & Scheibel, A. B. (1975). Progressive dendritic changes in aging human cortex. *Experimental Neurology* 47, 392-403

Schmetterer, L. & Polak, K. (2001). Role of nitric oxide in the control of ocular blood flow. *Progress in Retinal and Eye Research* 20, 823-847

Schuman, J. S., Hee, M. R., Puliafito, C. A., Wong, C., Pedut-Kloizman, T., *et al.* (1995). Quantification of nerve fiber layer thickness in normal and glaucomatous eyes using optical coherence tomography. *Archives of Ophthalmology* 113, 586-596

Searle, A., Shaw, D., Wild, J. & O'Neill, E. (1991a). Within and between test learning and fatigue effects in normal perimetric sensitivity In: *Perimetry Update 1990/91*, (Eds. Mills, R. P. & Heijl, A.) Kugler and Ghedini Publishers, Amsterdam, 533-537

Searle, A. E. T., Wild, J. M., Shaw, D. E. & O'Neill, E. C. (1991b). Time-related variation in normal automated static perimetry. *Ophthalmology* 98, 701-707

Shapley, R. & Perry, V. H. (1986). Cat and monkey retinal ganglion cells and their visual functional roles. *Trends in Neuroscience* 9, 229-235

Sheen, N., (2002). Evaluation of stereoscopic imaging techniques in the detection of glaucoma. Cardiff University, PhD

Sheen, N. J. L., Morgan, J. E., Poulsen, J. L. & North, R. V. (2004). Digital stereoscopic analysis of the optic disc - evaluation of a teaching program. *Ophthalmology* 111, 1873-1879

Sherry, L. M., Wang, J. J., Rochtchina, E., Wong, T. Y., Klein, R., *et al.* (2002). Reliability of computer-assisted retinal vessel measurement in a population. *Clinical and Experimental Ophthalmology* 30, 179-182

Shields, M. B. (1980). Gray crescent in the optic nerve head. *American Journal of Ophthalmology* 89, 238-244

Shiose, Y. (1990). Intraocular-pressure - new perspectives. *Survey of Ophthalmology* 34, 413-435

Shuttleworth, G. N., Khong, C. H. & Diamond, J. P. (2000). A new digital optic disc stereo camera: Intraobserver and interobserver repeatability of optic disc measurements. *British Journal of Ophthalmology* 84, 403-407

Siik, S., Airaksinen, J., Tuulonen, A., Alanko, H. I. & Nieminen, H. (1991). Lens autofluorescence in normal individuals. *Acta Ophthalmologica* 69, 187-192

Soares, A. S., Artes, P. H., Andreou, P., Leblanc, R. P., Chauhan, B. C., *et al.* (2004). Factors associated with optic disc hemorrhages in glaucoma. *Ophthalmology* 111, 1653-1657

Soliman, M. A., van den Berg, T. J., Ismaeil, A. A., de Jong, L. A. & de Smet, M. D. (2002a). Retinal nerve fiber layer analysis: Relationship between optical coherence tomography and red-free photography. *American Journal of Ophthalmology* 133, 187-195

Soliman, M. A. E., de Jong, L., Ismaeil, A. A., van den Berg, T. & de Smet, M. D. (2002b). Standard achromatic perimetry, short wavelength automated perimetry, and frequency doubling technology for detection of glaucoma damage. *Ophthalmology* 109, 444-454

Somani, R., Tennant, M., Rudnisky, C., Weis, E., Ting, A., *et al.* (2005). Comparison of stereoscopic digital imaging and slide film photography in the

identification of macular degeneration. *Canadian Journal of Ophthalmology* 40, 293-302

Sommer, A., Tielsch, J. M., Katz, J., Quigley, H. A., Gottsch, J. D., *et al.* (1991). Relationship between intraocular pressure and primary open angle glaucoma among white and black Americans. *Archives of Ophthalmology* 109, 1090-1095

Sonnsjo, B. & Krakau, C. E. T. (1993). Arguments for a vascular glaucoma etiology. *Acta Ophthalmologica* 71, 433-444

Sowka, J. & Aoun, P. (1999). Tilted disc syndrome. *Optometry and Vision Science* 76, 618-623

Spaeth, G. L., Lucy, M. & Pereira, M. (2000). How does resetting intraocular pressure help optic nerve function? *Eye* 14, 476-487

Spalding, J. M., Litwak, A. B. & Shufelt, C. L. (2000). Optic nerve evaluation among optometrists. *Optometry and Vision Science* 77, 446-452

Spraul, C. W., Lang, G. E., Lang, G. K. & Grossniklaus, H. E. (2002). Morphometric changes of the choriocapillaris and the choroidal vasculature in eyes with advanced glaucomatous changes. *Vision Research* 42, 923-932

Spry, P. G. D., Spencer, I. C., Sparrow, J. M., Peters, T. J., Brookes, S. T., *et al.* (1999). The Bristol Shared Care Glaucoma Study: Reliability of community optometric and hospital eye service test measures. *Briitish Journal of Ophthalmology* 83, 707-712

Stefansson, E., Landers, M. B., 3rd & Wolbarsht, M. (2005). Retinal vessel caliber and diabetic retinopathy. *Archives of Ophthalmology* 123, 709

Stewart, W. C., Connor, A. B. & Wang, X. H. (1995). Anatomic features of the optic disc and risk of progression in ocular hypertension. *Acta Ophthalmologica Scandinavica* 73, 237-241

Stiles, W. (1939). The directional sensitivity of the retina and the spectral sensitivities of the rods and cones. *Proceedings of the Royal Society, London - Series B* 127, 64 - 105

Sugiyama, K., Tomita, G., Kawase, H., Onda, E., Hayakawa, T., *et al.* (1997a). The prevalence of disc hemorrhage and peripapillary atrophy in subjects at the time of health check-up. *Investigative Ophthalmology & Visual Science* 38, 3835-3835

Sugiyama, K., Tomita, G., Kitazawa, Y., Onda, E. & Shimohara, H. (1997b). The associations of optic disc hemorrhage with retinal nerve fiber layer defect and peripapillary atrophy in normal-tension glaucoma. *Ophthalmology* 104, 1926-1933

Sugiyama, K., Tomita, G., Kawase, K., Onda, E., Shinohara, H., *et al.* (1999). Disc hemorrhage and peripapillary atrophy in apparently healthy subjects. *Acta Ophthalmologica Scandinavica* 77, 139-142

Sung, V. C. T., Bhan, A. & Vernon, S. A. (2002). Agreement in assessing optic discs with a digital stereoscopic optic disc camera (Discam) and Heidelberg Retina Tomograph. *British Journal of Ophthalmology* 86, 196-202

Suzuki, Y. (1995). Direct measurement of retinal vessel diameter - comparison with microdensitometric methods based on fundus photographs. *Survey of Ophthalmology* 39, S57-S65

Swindale, N. V., Stjepanovic, G., Chin, A. & Mikelberg, F. S. (2000). Automated analysis of normal and glaucomatous optic nerve head topography images. *Investigative Ophthalmology & Visual Science* 41, 1730-1742

Takamoto, T. & Schwartz, B. (1985). Reproducibility of photogrammetric optic disc cup measurements. *Investigative Ophthalmology & Visual Science* 26, 814-817

Tan, J. C., White, E., Poinoosawmy, D. & Hitchings, R. A. (2004). Validity of rim area measurements by different reference planes. *Journal of Glaucoma* 13, 245-250

Tay, E., Seah, S. K., Chan, S. P., Lim, A. T., Chew, S. J., *et al.* (2005). Optic disc ovality as an index of tilt and its relationship to myopia and perimetry. *American Journal of Ophthalmology* 139, 247-252

Taylor, S., Srinivasan, B., Wordinger, R. J. & Roque, R. S. (2003). Glutamate stimulates neurotrophin expression in cultured muller cells. *Molecular Brain Research* 111, 189-197

Terman, A. & Brunk, U. T. (2004). Molecules in focus: Lipofuscin. *The International Journal of Biochemistry & Cell Biology* 36, 1400-1404

Tezel, G., Kolker, A. E., Kass, M. A., Wax, M. B., Gordon, M., *et al.* (1997a). Parapapillary chorioretinal atrophy in patients with ocular hypertension. 1. An evaluation as a predictive factor for the development of glaucomatous damage. *Archives of Ophthalmology* 115, 1503-1508

Tezel, G., Kolker, A. E., Wax, M. B., Kass, M. A., Gordon, M., *et al.* (1997b). Parapapillary chorioretinal atrophy in patients with ocular hypertension. 2. An evaluation of progressive changes. *Archives of Ophthalmology* 115, 1509-1514

Tezel, G., Dorr, D., Kolker, A. E., Wax, M. B. & Kass, M. A. (2000). Concordance of parapapillary chorioretinal atrophy in ocular hypertension with visual field defects that accompany glaucoma development1*1. *Ophthalmology* 107, 1194-1199

Tezel, G., Siegmund, K. D., Trinkaus, K., Wax, M. B., Kass, M. A., *et al.* (2001). Clinical factors associated with progression of glaucomatous optic disc damage in treated patients. *Archives of Ophthalmology* 119, 813-818

Tezel, G., Trinkaus, K. & Wax, M. B. (2004). Alterations in the morphology of lamina cribrosa pores in glaucomatous eyes. *British Journal of Ophthalmology* 88, 251-256

Tezel, G. & Wax, M. B. (2004). Hypoxia-inducible factor 1 alpha in the glaucomatous retina and optic nerve head. *Archives of Ophthalmology* 122, 1348-1356

Thanos, S., Mey, J. & Wild, M. (1993). Treatment of the adult retina with microglia-suppressing factors retards axotomy-induced neuronal degradation and enhances axonal regeneration in vivo and in vitro. *Journal of Neuroscience* 13, 455-466

The European Glaucoma Prevention Study Group (2003). Reproducibility of evaluation of optic disc change for glaucoma with stereo optic disc photographs. *Ophthalmology* 110, 340-344

Theodossjades, J. & Murdoch, I. (2001). What optic disc parameters are most accurate assessed using the direct ophthalmoscope. *Eye* 15, 283-287

Tielsch, J. M., Katz, J., Quigley, H. A., Miller, N. R. & Sommer, A. (1988). Intraobserver and interobserver agreement in measurement of optic disc characteristics. *Ophthalmology* 95, 350-356

Tielsch, J. M., Katz, J., Singh, K., Quigley, H. A., Gottsch, J. D., *et al.* (1991). A population-based evaluation of glaucoma screening: The Baltimore Eye Survey. *American Journal of Epidemiology* 134, 1102-1111

Tokunaga, T., Kashiwagi, K., Tsumura, T., Taguchi, K. & Tsukahara, S. (2004). Association between nocturnal blood pressure reduction and progression of visual field defect in patients with primary open-angle glaucoma or normal-tension glaucoma. *Japanese Journal of Ophthalmology* 48, 380-385

Tout, S., Dreher, Z., Chan-Ling, T. & Stone, J. (1993). Contact-spacing among astrocytes is independent of neighbouring structures: In vivo and in vitro evidence. *Journal of Comparative Neurology* 332, 433-443

Trew, D. R. & Smith, S. E. (1991). Postural studies in pulsatile ocular blood flow: II. Chronic open angle glaucoma. *British Journal of Ophthalmology* 75, 71-75

Tuulonen, A. & Airaksinen, P. J. (1991). Initial glaucomatous optic disc and retinal nerve-fiber layer abnormalities and their progression. *American Journal of Ophthalmology* 111, 485-490

Tuulonen, A., Jonas, J. B., Valimaki, S., Alanko, H. I. & Airaksinen, P. J. (1996). Interobserver variation in the measurements of peripapillary atrophy in glaucoma. *Ophthalmology* 103, 535-541

Uchida, H., Ugurlu, S. & Caprioli, J. (1997). Peripapillary atrophy in glaucoma: A risk factor for progression. *Investigative Ophthalmology & Visual Science* 38, A3888

Uchida, H., Ugurlu, S. & Caprioli, J. (1998). Increasing peripapillary atrophy is associated with progressive glaucoma. *Ophthalmology* 105, 1541-1545.

Uchida, H., Yamamoto, T., Tomita, G. & Kitazawa, Y. (1999). Peripapillary atrophy in primary angle-closure glaucoma: A comparative study with primary open-angle glaucoma. *American Journal of Ophthalmology* 127, 121-128

Uhm, K. B., Lee, D. Y., Kim, J. T. & Hong, C. (1998). Peripapillary atrophy in normal and primary open-angle glaucoma. *Korean Journal of Ophthalmology* 12, 37-50.

Van Norren, D. & Van Meel, G. J. (1985). Density of human cone photopigments as a function of age. *Investigative Ophthalmology and Visual Science* 26, 1014-1016

Varma, R., Douglas, G. R., Steinmann, W. C., Wijsman, K., Mawson, D., *et al.* (1989a). A comparative-evaluation of 3 methods of analyzing optic disc topography. *Ophthalmic Surgery and Lasers* 20, 813-819

Varma, R., Spaeth, G. L., Steinmann, W. C. & Katz, L. J. (1989b). Agreement between clinicians and an image analyser estimating cup-to-disc ratios. *Archives of Ophthalmology* 107, 526-529

Varma, R., Quigley, H. A. & Pease, M. E. (1992a). Changes in optic disc characteristics and the number of nerve-fibers in experimental glaucoma. *American Journal of Ophthalmology* 114, 554-559

Varma, R., Steinmann, W. C. & Scott, I. U. (1992b). Expert agreement in evaluating the optic disc for glaucoma. *Ophthalmology* 99, 215-221

Varma, R., Tielsch, J. M., Quigley, H. A., Hilton, S. C., Katz, J., *et al.* (1994). Race-related, age-related, gender-related, and refractive error-related differences in the normal optic disc. *Archives of Ophthalmology* 112, 1068-1076

Varma, R., Skaf, M. & Barron, E. (1996). Retinal nerve fiber layer thickness in normal human eyes. *Ophthalmology* 103, 2114-2119

Ventura, L. M. & Porciatti, V. (2005). Restoration of retinal ganglion cell function in early glaucoma after intraocular pressure reduction: A pilot study. *Ophthalmology* 112, 20-27

Vernon, S. A. (1991). Screening siblings for glaucoma in the UK. *Journal of the Royal Society of Medicine* 84, 545-546

Vetrugno, M., Quaranta, G. M., Maino, A., Mossa, F. & Cardia, L. (2000). Contrast sensitivity measured by 2 methods after photorefractive keratectomy. *Journal of Cataract and Refractive Surgery* 26, 847-852

Vickers, J. C., Schumer, R. A., Podos, S. M., Wang, R. F., Riederer, B. M., *et al.* (1995). Differential vulnerability of neurochemically identified subpopulations of retinal neurons in a monkey model of glaucoma. *Brain Research* 680, 23-35

Vickers, J. C., Hof, P. R., Schumer, R. A., Wang, R. F., Podos, S. M., *et al.* (1997). Magnocellular and parvocellular visual pathways are both affected in a macaque monkey model of glaucoma. *Australian and New Zealand Journal of Ophthalmology* 25, 239-243

Vittitow, J. L. & Borras, T. (2002). Expression of optineurin, a glaucoma-linked gene, is influenced by elevated intraocular pressure. *Biochemical and Biophysical Research Communications* 298, 67-74

Volbrecht, V. J., Nerger, J. L., Imhoff, S. M. & Ayde, C. J. (2000). Effect of the short-wavelength-sensitive-cone mosaic and rods on the locus of unique green. *Journal of the Optical Society of America A - Optics Image Science and Vision* 17, 628-634

Vorwerk, C. K., Gorla, M. S. R. & Dreyer, E. B. (1999a). An experimental basis for implicating excitotoxicity in glaucomatous optic neuropathy. *Survey of Ophthalmology* 43, S142-S150

Vorwerk, C. K., Naskar, R. & Dreyer, E. B. (1999b). Excitotoxicity and glaucoma. *Klinische Monatsblätter für Augenheilkunde* 214, 2-11

Wang, J. J., Mitchell, P., Rochtchina, E., Tan, A. G., Wong, T. Y., *et al.* (2004). Retinal vessel wall signs and the 5 year incidence of age related maculopathy: The Blue Mountains Eye Study. *British Journal of Ophthalmology* 88, 104-109

Wang, L., Damji, K. F., Munger, R., Jonasson, F., Arnarsson, A., *et al.* (2003). Increased disc size in glaucomatous eyes vs normal eyes in the Reykjavik Eye Study. *American Journal of Ophthalmology* 135, 226-228

Watkins, R., Panchal, L., Uddin, J. & Gunvant, P. (2003). Vertical cup-to-disc ratio: Agreement between direct ophthalmoscopic estimation, fundus biomicroscopic estimation, and scanning laser ophthalmoscopic measurement. *Optometry and Vision Science* 80, 454-459

Wax, M. B. & Tezel, G. (2002). Neurobiology of glaucomatous optic neuropathy: Diverse cellular events in neurodegeneration and neuroprotection. *Molecular Neurobiology* 26, 45 - 55

Weber, A. J., Kaufman, P. L. & Hubbard, W. C. (1998). Morphology of single ganglion cells in the glaucomatous primate retina. *Investigative Ophthalmology & Visual Science* 39, 2304-2320

Weber, J., Dannheim, F. & Dannheim, D. (1990). The topographical relationship between optic disc and visual field in glaucoma. *Acta Ophthalmologica* 68, 568-569

Weber, J. & Klimaschka, T. (1995). Test time and efficiency of the dynamic strategy in glaucoma perimetry. *German Journal of Ophthalmology* 4, 25-31

Wehrwein, E., Thompson, S. A., Coulibaly, S. F., Linn, D. M. & Linn, C. L. (2004). Acetylcholine protection of adult pig retinal ganglion cells from glutamate-induced excitotoxicity. *Investigative Ophthalmology & Visual Science* 45, 1531-1543

Weih, L. M., Mukesh, B. N., McCarty, C. A. & Taylor, H. R. (2001a). Association of demographic, familial, medical, and ocular factors with intraocular pressure. *Archives of Ophthalmology* 119, 875-880

Weih, L. M., Nanjan, M., McCarty, C. A. & Taylor, H. R. (2001b). Prevalence and predictors of open-angle glaucoma: Results from the visual impairment project. *Ophthalmology* 108, 1966-1972

Weinreb, R. N., Lusky, M., Bartsch, D. U. & Morsman, D. (1993). Effect of repetitive imaging on topographic measurements of the optic nerve head. *Archives of Ophthalmology* 111, 636-638

Weinreb, R. N., Shakiba, S. & Zangwill, L. (1995). Scanning laser polarimetry to measure the nerve fiber layer of normal and glaucomatous eyes. *Am J Ophthalmol* 119, 627-636

Weinreb, R. N. & Levin, L. A. (1999). Is neuroprotection a viable therapy for glaucoma? *Arch Ophthalmol* 117, 1540-1544

Whitaker, D., Steen, R. & Elliott, D. B. (1993). Light scatter in the normal young, elderly, and cataractous eye demonstrates little wavelength dependecy. *Optometry and Vision Science* 70, 963-968

Wild, J., Moss, I. D., Whitaker, D. & O'Neill, E. C. (1995). The statistical interpretation of blue-on-yellow visual field loss. *Investigative Ophthalmology & Visual Science* 36, 1398-1410

Wild, J. M., Dengler-Harles, M., Searle, A. E. T., O'Neill, E. C. & Crews, S. J. (1989). The influence of the learning effect on automated perimetry in patients with suspected glaucoma. *Acta Opthalmologica* 67, 537-545

Wild, J. M., Searle, A. E. T., Dengler-Harles, M. & O'Neill, E. C. (1991). Long-term follow-up of baseline learning and fatigue effects in the automated perimetry of glaucoma and ocular hypertensive patients. *Acta Ophthalmologica* 69, 210-216

Wild, J. M. & Hudson, C. (1995). The attenuation of blue-on-yellow perimetry by the macular pigment. *Ophthalmology* 102, 911-917

Wild, J. M. & Moss, I. D. (1996). Base-line alterations in blue-on-yellow normal perimetric sensitivity. *Graefe's Archive for Clinical and Experimental Ophthalmology* 234, 141-149

Wild, J. M. (1997). SITA - a new outlook for visual field examination primary and shared care. *Optician* 213, 35-39

Wild, J. M., Hutchings, N., Hussey, M. K., Flanagan, J. G. & Trope, G. (1997). Pointwise univariate linear regression of perimetric sensitivity against follow-up time in glaucoma. *Ophthalmology* 104, 808-815

Wild, J. M., Cubbidge, R. P., Pacey, I. E. & Robinson, R. (1998). Statistical aspects of the normal visual field in short-wavelength automated perimetry. *Investigative Ophthalmology & Visual Science* 39, 54-63

Wild, J. M., Pacey, I. E., O'Neill, E. C. & Cunliffe, I. A. (1999). The SITA perimetric threshold algorithms in glaucoma. *Investigative Ophthalmology and Visual Science* 40, 1998-2009

Wild, J. M. (2001). Short-wavelength automated perimetry. *Acta Ophthalmologica Scandinavica* 79, 546-559

Wolfs, R. C. W., Ramrattan, R. S., Hofman, A. & de Jong, P. T. V. M. (1999). Cup-to-disc ratio: Ophthalmoscopy versus automated measurement in a general population. *Ophthalmolgy* 106, 1597-1601

Wollstein, G., Garway-Heath, D. F. & Hitchings, R. A. (1998). Identification of early glaucoma cases with the scanning laser ophthalmoscope. *Ophthalmology* 105, 1557-1563

Wollstein, G., Garway-Heath, D. F., Fontana, L. & Hitchings, R. A. (2000a). Identifying early glaucomatous changes. Comparison between expert clinical assessment of optic disc photographs and confocal scanning ophthalmoscopy. *Ophthalmology* 107, 2272-2277

Wollstein, G., Garway-heath, D. F., Poinoosawmy, D. & Hitchings, R. A. (2000b). Glaucomatous optic disc changes in the contralateral eye of unilateral normal pressure glaucoma patients. *Ophthalmology* 107, 2267-2271

Wong, T. Y., Klein, R., Sharrett, A. R., Duncan, B. B., Couper, D. J., *et al.* (2004). Retinal arteriolar diameter and risk for hypertension. *Annals of Internal Medicine* 140, 248-255

Wood, J. M., Wild, J. M., Smerdon, D. L. & Crews, S. J. (1989). Alterations in the shape of the automated perimetric profile arising from cataract. *Graefe's Archive for Clinical and Experimental Ophthalmology* 227, 157-161

Wormald, R. P., Basauri, E., Wright, L. A. & Evans, J. R. (1994). The African Caribbean Eye Survey: Risk factors for glaucoma in a sample of African Caribbean people living in London. *Eye* 8, 315-320

Wyllie, A. H. (1992). Apoptosis and the regulation of cell numbers in normal and neoplastic tissues: An overview. *Cancer Metastasis Review* 11, 95-103

Yamamoto, S., Kamiyama, M., Nitta, K., Yamada, T. & Hayasaka, S. (1996). Selective reduction of the s cone electroretinogram in diabetes. *British Journal of Ophthalmology* 80, 973 - 975

Yamazaki, Y. & Drance, S. M. (1997). The relationship between progression of visual field defects and retrobulbar circulation in patients with glaucoma. *American Journal of Ophthalmology* 124, 287-295

Yasuzumi, K., Ohno-Matsui, K., Yoshida, T., Kojima, A., Shimada, N., *et al.* (2003). Peripapillary crescent enlargement in highly myopic eyes evaluated by fluorescein and indocyanine green angiography. *British Journal of Ophthalmology* 87, 1088-1090

Yogesan, K., Barry, C. J., Jitskaia, L., Eikelboom, R. H., Morgan, W. H., *et al.* (1999a). Software for 3-D visualization/analysis of optic-disc images. *IEEE Engineering in Medicine and Biology Magazine* 18, 43-49

Yogesan, K., Constable, I. J., Barry, C. J., Eikelboom, R. H., Morgan, W., *et al.* (1999b). Evaluation of a portable fundus camera for use in the teleophthalmologic diagnosis of glaucoma. *Journal of Glaucoma* 8, 297-301

Yucel, Y. H., Zhang, Q., Weinreb, R. N., Kaufman, P. L. & Gupta, N. (2003). Effects of retinal ganglion cell loss on magno-, parvo-, koniocellular pathways in the lateral geniculate nucleus and visual cortex in glaucoma. *Progress in Retinal and Eye Research* 22, 465-481

Zangwill, L., Shakiba, S., Caprioli, J. & Weinreb, R. N. (1995). Agreement between clinician and a confocal scanning laser ophthalmoscope in estimating cup/disc ratios. *American Journal of Ophthalmology* 119, 415-421

Zangwill, L., Berry, C. A., Garden, V. S. & Weinreb, R. N. (1997). Reproducibility of retardation measurements with the nerve fiber analyzer II. *Journal of Glaucoma* 6, 384-389

Zangwill, L. M., Weinreb, R. N., Berry, C. C., Smith, A. R., Dirkes, K. A., *et al.* (2004a). Racial differences in optic disc topography. *Archives of Ophthalmology* 122, 22-28

Zangwill, L. M., Weinreb, R. N., Berry, C. C., Smith, A. R., Dirkes, K. A., *et al.* (2004b). The confocal scanning laser ophthalmoscopy ancillary study to the ocular hypertension treatment study: Study design and baseline factors. *American Journal of Ophthalmology* 137, 219-227

Zeyen, T. G., Raymond, M. & Caprioli, J. (1992). Disc and field damage in patients with unilateral visual-field loss from primary open-angle glaucoma. *Documenta Ophthalmologica* 82, 279-286

Zhang, Y. F. & Stone, J. (1997). Role of astrocytes in the control of developing retinal vessels. *Investigative Ophthalmology & Visual Science* 38, 1653-1666

Zhao, G. L. & Xu, M. Y. (1987). A model of capillary networks for the exchange of substances. *Scientia Sinica. Series B: Chemical, biological, agricultural, medical and earth sciences* 30, 1043-1051

Zhao, Y. & Li, F. M. (1987). Microangioarchitecture of optic papilla. *Japanese Journal of Ophthalmology* 31, 147-159

Zulauf, M., Caprioli, J., Hoffman, D. C. & Tressler, C. S. (1991). Fluctuation of the differential light sensitivity in clinically stable glaucoma patients In: *Perimetry Update*, (Eds. Mills, R. P. & Heijl, A.) Kugler and Ghedini Publishers, Amsterdam, 183-188